Università degli Studi di Milano

Facoltà di Scienze e Tecnologie

Dipartimento di Chimica

Doctorate School in Chemical Sciences and Technologies

Doctorate in Chemical Sciences

XXVIII cycle

COPPER AND RUTHENIUM COMPLEXES IN SENSITIZED SOLAR CELLS AND OPTOELECTRONICS

Mirko Magni

R10034

Supervisor: Prof. Dominique Marie Roberto

Co-supervisors: Prof. Patrizia Romana Mussini

Dr. Claudia Dragonetti

A. Y. 2014/2015

[…] non aveva letto Agatha Christie.

Non importa se uno scienziato non conosce la spiegazione di una coincidenza:

essa può essere indicativa di qualcosa di più profondo

che al momento può non avere spiegazione:

dopotutto, questo è la scienza.

Arthur Eddington una volta sottolineò che

l'uomo sta a metà strada fra un atomo e una stella.

ci sono uno-seguito-da-ventisette zeri di atomi in un essere umano,

e uno-seguito-da-ventotto zeri di essere umani comporrebbero una stella.

[Davide Whitehouse, *Il sole. Una biografia*, Mondadori, 2007]

La nobiltà dell'Uomo […] era consistita nel farsi signore della materia

[…] vincere la materia è comprenderla,

e comprendere la materia è necessario per comprendere l'Universo e noi stessi.

[Primo Levi, *Il sistema periodico*, Einaudi, 2009]

In ricordo di Ambrogina,
che ci ha lasciato prematuramente

Index:

Overview of the Thesis and Its Contextualization

The thesis has been entirely centered on the concept of *Light* involving both the development of transition metal complexes for the conversion of light into electric energy through dye-sensitized solar cells and, conversely, the production of light starting from electricity by fabrication of electroluminescent devices. The importance of Light for the Earth and the mankind, and the actuality of all researches devoted to present and future technologies around light matters was officially recognized on the end of 2013 by the General Assembly of the United Nations with the proclamation of the present year 2015 "International Year of Light (IYL 2015) and Light-Based Technologies".

Since millions of years sunlight is the source of life, being the needful source of energy for any plant and animal species on our Planet, and (in principle) it will continue to allow life for more millions of years. At the same time since the beginning of the appearance of humans on Earth, people have found out ways to produce "artificial" light with increasingly sophisticated methods, starting from a simple fire obtained burning woods by cave men to the efficient light-emitting diodes exploiting electricity by current metropolitan men.

This historical *excursus* shows very well, from my point of view, how the humankind was, is and will be strictly and indissoluble jointed with Light whether it is from the Sun or is artificially generated on Earth. In this context the thesis work has taken place sharing the efforts between two diametrically opposed goals. One task was the sunlight harvesting and its exploitation for electric energy production; the second aim was the antithetic light production employing electricity.

The main part of the thesis has been devoted to the *sunlight-to-electricity conversion*, a target that is well contextualized within the global commitment for the progressive increase of the percentage of electric energy produced by renewable resources. In this context dye-sensitized solar cells, DSSCs, are promising devices alternative to the well established technology of silicon photovoltaics for energy production from the abundant and ubiquitous solar light. DSSCs are devices able to harvest solar light and convert it into electricity employing a sensitizer (adsorbed on a semiconductor) and a redox couple properly chosen. The project concerned the design, synthesis and characterization of both sensitizers and redox mediators constituted by ruthenium and copper-based complexes respectively, together with their assembly into laboratory-type DSSCs to evaluate their performance. In this way an all-round study was carried out, starting from molecules on paper to test benches, passing through laboratory counters.

The second, minor part of the thesis was focused on the diametrically opposed task, *the generation of light*. In this context some luminescent heteroleptic complexes based on the cheap and quite

abundant copper element were proposed. The final aim was the synthesis of efficient luminophores for fabrication of devices able to generate light applying an electric potential across two electrodes, such as in organic light-emitting diodes, OLEDs, or in analogue light-emitting electrochemical cells, LECs. In these devices the active component (*i.e.* chromophore) is excited by an external potential and emits light at a certain wavelength during the radiative decay to its ground state; the phenomenon is named electroluminescence. The light production in LED-type devices is very efficient especially compared with other traditional artificial light sources like incandescent bulbs (both filled with inert or halogen gas) and fluorescent lamps, and so in line with the international policy of reducing energy consumption.

In conclusion the thesis project can be schematically depicted (see below) as a circular pathway that joints together two opposite but strictly interconnected concepts (*i.e.* light and electricity) mutually corresponding to the task and the mean, the start and the end.

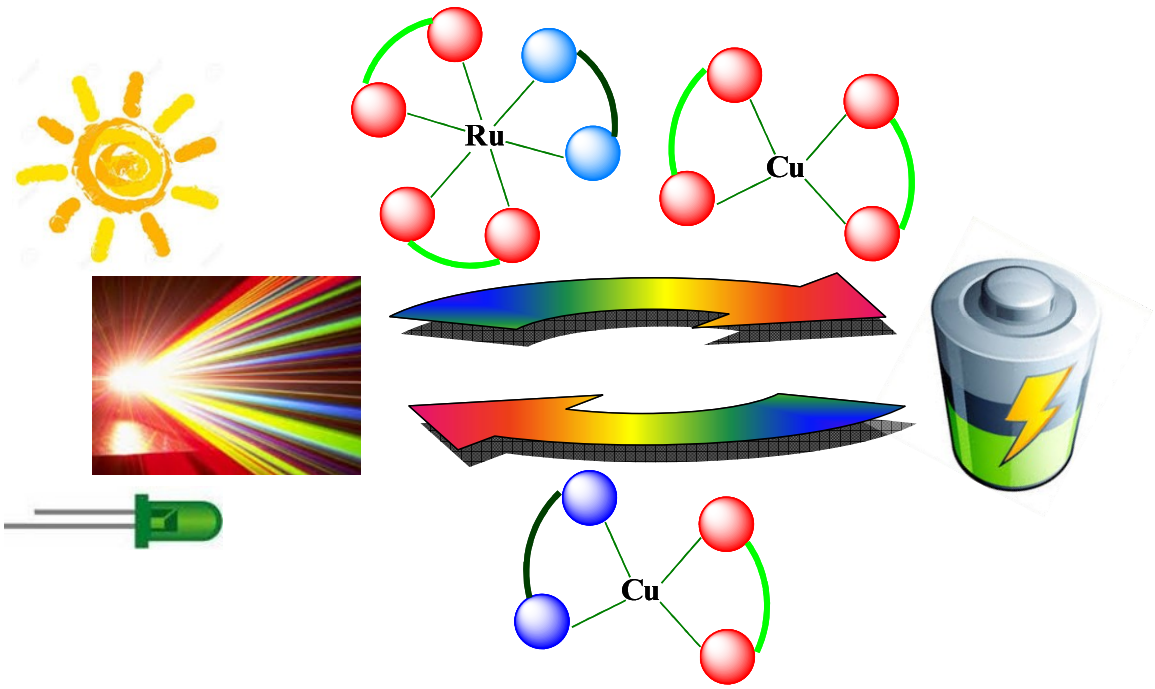

According to this double-route nature, the thesis will be divided into two big chapters entitled *dye-sensitized solar cells* and *(electro)luminescent copper complexes*, each ones focused on one arches of the "cyclic pathway" involving the sunlight-to-electricity conversion and the production of light, respectively.

Dye-Sensitized Solar Cells, DSSCs

Introduction

State of the art for light-to-electricity conversion devices

Since the XVIII century, with the occurrence of Industrial Revolution, the technological evolution and the social, economic and political history of humanity have always been connected (and strictly dependent) to the need of finding energy sources capable to convert internal energy (stored into their chemical bonds) into work (*i.e.* ordered and directional energy) exploitable to reduce manual efforts and to increase and speed up production of assets. The ultimate goal has been to achieve an ever greater wellbeing. To date, fossil fuels have surely been the most exploited energy source starting from the first steam engines (fuelled by coal) to modern auto vehicles and industries (directly or indirectly supplied with oil or hydrocarbon gas). Unfortunately the exploitation of fossil fuels suffers of a lot of problems and risks concerning all stages of the supply chain, from the extraction from subsoil to the processing and the final use. To name one, ignoring any conflicts related to control deposits, it is well-established that the combustion of fuels (and similar derivates) produce the so called greenhouse gases that account for the anthropogenic global warming which in turn result in widespread environmental damage [1].

By the way, beyond the social and environmental issues the principal and practically insurmountable limit of fossil fuels is their non-renewable nature. This means that humanity in order to maintain the today lifestyle has to direct toward other, possibly renewable, energy sources which should be more “ethic” and have a less anthropogenic impact on the Earth. This is practically mandatory also considering that the worldwide demand of energy is expected to increase drastically in the following decades according to the population increase. Therefore the fossil fuels depletion puts an hard double challenge to humanity for the near future, that is the choice of the best candidate(s) among renewable resources to gradually accompany and eventually supplant fossil fuels, and the development of the relative technologies that make them exploitable in a competitive way. In this competition the sunlight is probably the optimal task being ubiquitous, abundant, and practically inexhaustible. In fact photovoltaic systems can be located practically in any place of the world respect for example to both wind farms and hydroelectric plants that can be built only in specific sites where from one hand wind is constant in time and sufficiently intense and from the other one in proximity of rivers, lakes or artificial reservoirs. As said just before, other advantages of the use of sunlight are the huge amount of radiant power that reaches the surface of our Earth (*ca.* 1000 W m^{-2}, in a sunny day with the Sun at its zenith) and its constancy evaluated over a very and very long period (in the order of millions of years!). In order to give a more realistic idea of the

power that every day the Sun offers to us, and that without photovoltaics systems goes to waste, the average irradiance in Italy considering alternation day/night, winter/summer, sunny/cloudy is 180 W m^{-2}.

Sunlight is a polyhedral energy source exploitable to simply capture thermal energy through so called solar thermal plants, or produce electric energy through more complex systems like solar thermodynamic and photovoltaic ones. In the first case energy of sunlight is firstly captured as heat and then the last is converted into electricity; on the other hand photovoltaic devices are able to directly convert electromagnetic energy coming from Sun into electric one, exploiting the homonym photovoltaic effect. This effect, firstly observed by A. E. Becquerel in the first half of XIX, is directly connected with photoelectric effect the study of which earned A. Einstein the Nobel prize in physics in 1921. When a p-n junction in a semiconductor material is illuminated by photons with energy equal or higher than the band gap of the material electrons, e^-, from low-lying valence band of p-doped site are excited to the conduction band where they are free to move into the n-doped part driven by built-in potential. This motion (balanced by diffusion of positively charged holes, h^+, in the opposed direction) generates an electromotive force, so converting light energy into electric one; electron/hole recombination processes inevitably occur limiting the light-to-electricity conversion efficiency of the device. This is what happens in each single silicon cell constituting the building block of commonly named solar panel; it is a module constituted by various cells electrically connected in series. Modules can be connected in turn forming an array to produce a useful output voltage (Figure 1).

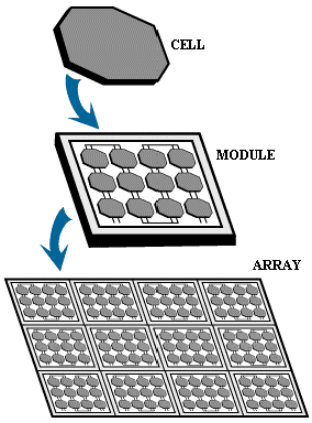

Figure 1 Schematic representation of common silica-based photovoltaic panel assembling. From NASA web site (http://science.nasa.gov).

The silicon-based photovoltaic panels was the first technology developed to exploit sunlight for a direct production of electricity. The first photovoltaic module (actually a solar battery) was built by Bell Laboratories in 1954, but it was still too expensive to gain a widespread use. This was possible starting from 1970 when photovoltaic technology began sufficiently mature to ensure more affordable costs (thanks also to the researches done through the NASA space programs). Crystalline

silicon (or germanium)-doped photovoltaic panels are quite efficient (around 21% [2]) and robust but they require high pure materials and high vacuum lines for cells assembling; the energy-demanding procedures make high the price for these so called "first generation" solar cells.

To make photovoltaics, PV, a really competitive technology able to supplant hydrocarbon one, low-coast and environmentally sustainable approaches (*i.e.* based on quite abundant and non-toxic raw materials) have to be developed. In an attempt to achieve this goal over the years new generations of photovoltaics devices have been developed. The "second generation" employs a thin-film technology in order to significantly reduces amount of photovoltaic material (and cost), reducing thickness from few nanometers to tens of micrometers (in comparison with *ca.* 100-200 μm of bulk crystalline silicon cells); it includes amorphous silicon cells, copper indium gallium selenide (CIGS), cadmium telluride (CdTe) and cadmium indium diselenide ($CdInSe_2$). Even if they guarantee a lower production cost, unfortunately they exhibit efficiency a bit lower than bulk silicon devices; moreover the last two examples suffer of the high toxicity of their components. The "third generation" cells included very different types of devices; in the very last decades emerging photovoltaics includes organic solar cells (such as bulk-heterojunction devices), quantum dot solar cells, dye-sensitized solar cells (DSSCs) and perovskite solar cells.

Despite the young age of perovskite solar cells (first report was published in 2009, but only since 2012 they caught significant attention by scientific community) very interesting results have been already obtained by these solid-state devices. Even if the main topic of this thesis are DSSCs it seems right to dedicate a subchapter to perovskite-based solar cells that catalyzed the almost undivided attention of the research groups involved in the field of solar energy, making DSSCs a sort of "marginal" topic.

Perovskite solar cells

Virtually in parallel with the start of this thesis a new type of sunlight-to-electricity devices named perovskite solar cells has become particularly attracting being able to increase its conversion efficiency from an unpromising 3.8% in 2009 [3] to a certified 20.1% in 2014[1], making this the fastest-advancing solar technology to date. In other word, in only 3-5 years (mostly from 2012 to today) this new class of third generation solar cells was able to pass from performances significantly lower than those of the most performing DSSCs ($\eta > 10\%$) to efficiency comparable to commercially available bulk silicon based photovoltage devices.

[1] A device by researchers from Korea University of Science and Technology, from National Renewable Energy Laboratory, *Best Research-Cell Efficiencies chart*.

Perovskite solar cell is solar cell which includes a perovskite structured compound (general formula ABX_3) as the light-harvesting active component. Most commonly the absorber material is a hybrid organic-inorganic lead or tin halide material such as methylammonium lead trihalide ($CH_3NH_3PbX_3$, with $X^- = I^-$, Br^-, Cl^-; Figure 2), methylammonium tin trihalide ($CH_3NH_3SnX_3$) and formamidinum lead trihalide ($H_2NCH_3NH_3PbX_3$).

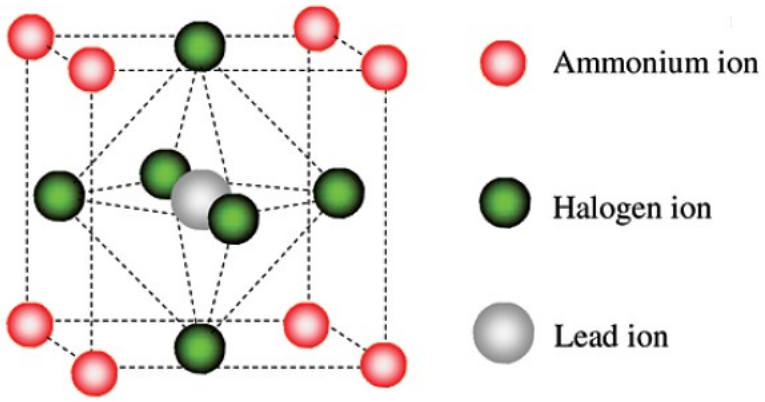

Figure 2 Unit cell of methylammonium lead trihalide, $CH_3NH_3PbX_3$, the most commonly employed perovskite absorber in solar cells. From [3].

These active materials have the same type of crystal structure as calcium titanium oxide, $CaTiO_3$, known as Perovskite mineral. In perovskite compounds ABX_3:

- 'A' and 'B' are two cations of very different sizes, with 'A' larger than 'B';
- 'X' is an anion that bonds to both cations;
- the ideal structure is a cubic-symmetry cell where 'B' is in 6-fold coordination, surrounded by an octahedron of 'X' anions, and the 'A' is in 12-fold cuboctahedral coordination (Figure 2).

Perovskite materials have found great and proficient application in solar energy devices due to some desirable physical and chemical characteristics. One of these features is surely their narrow optical band gap, tunable varying the halide content [4], [5]. For example the band gap of one the most studied absorber methylammonium lead trihalide is between 2.3 eV and 1.6 eV to be compared with that of titanium dioxide (3.2 eV, for anatase mineral form) employed in typical DSSCs. This allows to harvest directly the sunlight acting itself, as already described, as an absorber; contrary to TiO_2 semiconductor which must be sensitized (see next chapter for more details). Another very interesting property of perovskite is that diffusion length for both holes and electrons is over one micrometer [6]; this means that charges can be transported in the perovskite itself over long distances (if compared with common thickness employed in thin-film architecture, see below). Moreover perovskite can be easily manufactured with a variety of solvent or vapor deposition techniques commonly employed in traditional laboratory and that can be scaled up with relative

feasibility if compared with the multi-step processes involved in the fabrication of silicon solar devices.

Perovskite solar cells work efficiently in a number of somewhat different architectures. For example depending on the role of the perovskite material, devices can be divided into so called *sensitized* and (planar) *thin-film* cells (Figure 3).

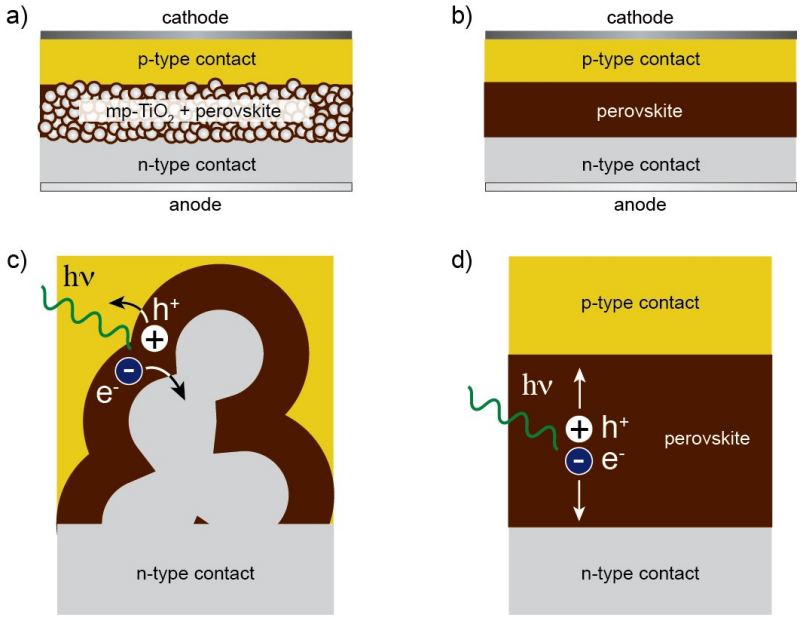

Figure 3 Schematic representation of a sensitized-perovskite solar cell (left) and a thin-film perovskite solar (right). On the top schemes of the two architectures (a and b, respectively) and on the bottom a schematic picture of the charge generation and extraction in the two situations (c and d, respectively). From http://commons.wikimedia.org/wiki/File:Perovskite_solar_cell_architectures_1.png

Perovskite-sensitized solar cells are very similar to conventional dye-sensitized devices; the difference is that the function played by the organic/organometallic dye in a DSSC is replaced by the perovskite material. So similarly to sensitization in DSSC, the perovskite is coated onto a charge-conducting scaffold (mesoporous TiO_2) and the photogenerated electrons are transferred from the perovskite layer to the TiO_2 sensitized layer through which they are transported to the underlying electrode (anode) and then into the external circuit. So, similarly to DSSCs, in this architecture perovskite material acts simply as a light absorber leaving to another component of the cell the role of transporting charges.

On the contrary, in thin-film solar cells perovskite plays a double role acting both as photoactive component and as charge transport material exploiting the just mentioned finding that perovskite materials can also act as highly efficient, ambipolar charge-conductor [6]. From this point of view in thin-film architecture perovskite acts in a way similar to silicon-based PV systems, performing simultaneously both absorption and charge-carrier transport. In this case a flat layer of perovskite, pristine or formed on a mesoporous inert scaffold (*e.g.* Al_2O_3), is sandwiched between two selective contacts (p-type and n-type); after light absorption and the subsequent charge-generation, both

negative and positive charge carriers are transported through the perovskite to charge selective contacts.

Due to the great similarity with the well-studied DSSCs, perovskite-sensitized solar cells was the first architecture employed [3], [7-9]. Nevertheless over the time researchers have realized that thin-film architecture functions well [10-12].

Notwithstanding the promising performances obtained in very few years, the main limitation to transfer perovskite solar cells from the laboratory to industry, and to their actual commercialization, are linked mainly to two drawbacks, the stability and the quite high toxicity of the photovoltaic material. Lead perovskites suffer of humidity and moisture sensitivity which bring to degradation of the material with consequent breakdown of cell performances [13]. Such sensitivity forces to work in very restrictive conditions (*e.g.* glove boxes filled with inert gas) to limit contact of active photovoltaic material with oxygen and moisture, which implies high cost of production on large scale plants. The second limit to the direct scale up of lead perovskite solar cells is the presence of lead in their network. Works are in progress in order to develop efficient lead-free devices with efficiencies as comparable as lead-containing ones, substituting indicted lead with less toxic tin.

Dye-sensitized solar cells

As anticipated the main object of this first part of the thesis are dye-sensitized solar cells, shortly DSSCs. When talking about them is impossible not to mention the paper of O'Regan and Graetzel [14] which represents a milestone with more than 14400 citations that, probably, make it the most famous work in the field of photovoltaics in the last quarter of century. Nevertheless it is important to cite in view of a correct historical contextualization other previous works, significant because they reported the first observation and explanation of the main mechanism that makes DSSCs unique among photovoltaic devices; it is the *sensitization* of a semiconductor employed as photoelectrode. The first report dates back to 1887 [15] while the accepted operating mechanism of sensitization (described in detail few lines below) of ZnO crystals was elucidated in '60 of last century [16]. The next steps that led to the successive development of DSSCs were done during the subsequent twenty years when the idea to chemisorbe dyes on dispersed particles to improve interface area was presented to scientific committee [17, [18].

As in somehow suggested by the term "dye-sensitized", in this type of solar cells absorption of light and the concomitant photogeneration of charge carriers (*i.e.* electron-hole pairs) does not occur directly in the semiconductor as in all conventional PV devices but through a new component, the molecular sensitizer (also simply named dye). In this sense DSSCs are unique, being able to separate the two functions of light harvesting and charge transport. The aforementioned separation

is at the same time, the innovation and one of the key point of DSSC technology aimed at lowering cost of productions and to a better environmental sustainability. In fact it brings advantages including possibility to employ materials with less stringent demands upon both optical and electronic properties (which in turn demand for very high purity material and so high treatment cost) and so potentially greatly enlarging the choice of semiconductors pointing to reduce costs of both raw materials (*e.g.* TiO_2 and ZnO) and their processing.

In the most common n-type DSSCs the just mentioned separation of optical and electrical processes is realized by placing molecular sensitizer at the interface between an electron conducting material (mostly TiO_2) and a p-type conductor constituted by a redox electrolyte or a hole-transporting material (Figure 4). Light harvesting can be improved working on chemical modification of the sensitizer while in parallel, but at the same time in independent way, optimization of the electrolyte/hole-transporting material allows enhancement of charge-carrier transport. Thanks to this architecture the incident photons of appropriate energy are harnessed by the sensitizer molecules chemisorbed on the mesoporous semiconductor; resulting photoexcited dyes inject electrons, e^-, in the underlying conduction band of semiconductor and the resulting oxidized dye is regenerated by hole, h^+, injection in the electrolyte/hole-transporting material (*i.e.* reduction reaction by electron transfer from a reduced species in the electrolyte to oxidized dye molecules). Electron/hole recombination can occurs very rapidly by recapture of injected electrons by oxidized dyes since the charge space effects, that drives separation of photogenerated e^-/h^+ couple in silicon-based devices, are usually negligible in nanostructured systems, like TiO_2 substrate. Relatively long life charge separation is only guaranteed by intrinsic kinetic properties of the electrolyte/p-type conductor which indirectly avoids (or better, slows down) recombination process by recovery the dye in its recombination-inactive reduced form. A more detailed description of the role of redox electrolyte is postponed to the related subchapter.

The cycling of the aforementioned process, mandatory to make operational the device, is allowed by the regeneration of the redox species in the electrolyte/hole-transporting material occurring through an electron transfer at the interface with a second electrode, named cathode (Figure 4). It is typically a transparent conducting oxide, TCO, covered with a suitable catalyst able to reduce overpotential of the regeneration reaction. In this way the galvanic chain representing a DSSC is completed, (–)TCO|n-type conductor|dye|p-type conductor|catalyst|TCO(+).

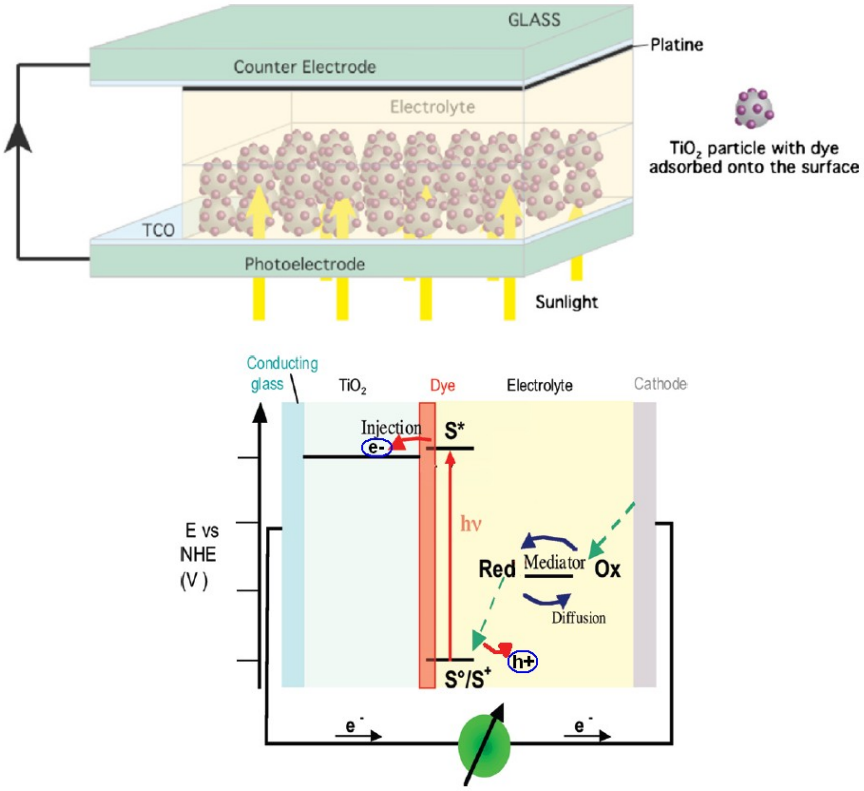

Figure 4 Top: schematic representation of the components of a dye-sensitized solar cell (from ref. 19). Bottom: main processes occurring during "perfect" DSSC operation (adapted from ref. 20).

Notwithstanding the good purposes offered by DSSC architecture pointing to develop low-cost devices, implementing natural abundant and non-toxic materials, to date their validated efficiencies (which means under standard air mass 1.5, AM 1.5, reporting conditions) are significantly lower than those reached by first and second generation solar cells, like crystalline silicon and CIGS devices. Nevertheless DSSCs already outperforms its competitors in ambient light and indoor conditions [21]. A 12.3% remarkable efficiency was published at the end of 2011 [22] but it has been exceeded three years later by a record 13% both obtained by Graetzel and co-workers [23] who constructed porphyrin-sensitized cells combined with a $Co^{III/II}$ tris(bipyridyl)-based redox electrolyte[2].

The proper choice of dye/redox mediator couple is mandatory to obtain efficiently working cells, and it can even make the difference between a functioning cell or not. Even if results discussed later in this thesis clearly confirm the enormous influence of a (sometimes purely fortuitous) guessed dye/mediator coupling, an exhaustive example is outlined in reference [22]. A positive 58% gain in

[2] Actually immediately after the first writing of this introduction a new extraordinary record (even over 14 %) was published on 14th September 2015. [K. Kakiage, Y. Aoyama, T. Yano, K. Oya, J. Fujisawab, M. Hanaya, *Chem. Comm.* (2015) DOI: 10.1039/c5cc06759f]

photon-to-current efficiency was recorded holding steady the sensitizer and simply changing the redox mediators, passing from common I_3^-/I^- to $Co^{III/II}$ tris(bipyridyl) couple.

DSSC classification

DSSCs can be divided into three big families on account of the physical state of the electrolyte, used here with the general meaning of hole-transport mediator. Electrolyte (discussed later in more detail) plays crucial role both on the photon-to-current conversion efficiency and on stability of the cell, this last of primary importance for the industrialization and commercialization on large scale of these photovoltaic devices. Its relevance justifies a classification of DSSCs according to the nature and composition of the electrolyte. The three categories are liquid DSSCs, quasi-solid-state DSSCs (qss-DSSCs) and solid-state DSSCs (ss-DSSCs) [24].

Liquid DSSCs are the most widespread devices and they are the most studied. They can be further distinguished in cells employing organic solvents and ionic liquids. The description of electrolytes based on traditional solvents is postponed to next dedicated chapter. Due to their nature (room-temperature) ionic liquids, ILs, are particular organic-inorganic salts that are at the same time solvent and supporting electrolyte, being composed entirely of ions; they are characterized by very low vapour pressure, low flammability and toxicity, but generally higher viscosity respect to common volatile organic solvents. This features is the main responsible for general lower efficiency of IL-based DSSC respect to devices employing traditional organic solvent (like acetonitrile, valeronitrile, etc.), limiting the mass-transport phenomena. At the same time the high viscosity make easier the enclosure of IL-DSSCs reducing problems of leakage of the electrolyte and volatilization of solvent that are the most important drawbacks for commercialization of traditional liquid DSSCs. A further differentiation can be done according to the nature of the redox mediators dissolved, but this point will be analyzed in next dedicated chapter.

Even if to date liquid DSSCs recorded the best performances, in the last years many efforts have been done by different groups all over the world to develop competitive *solid* or *quasi-solid electrolytes*. The objective is to significantly increase the long term stability of DSSCs especially for outdoor applications, where so high temperature, intense UV radiation and weathering put a strain on the devices. The main durability problems are accentuated by the presence of liquid electrolytes and they concern the aforementioned leakage and volatilization of solvent due to ineffective sealing of the sandwiched cells, the desorption of dye mediated by liquid component and corrosion of counter electrode (especially in presence of iodine-based electrolytes). The hope of researchers is that solid transport mediators or quasi-solid electrolytes, due to their own physical nature, should reduce these drawbacks. Unfortunatly, the same (quasi)-solid nature brings some

disadvantages such as *in primis* the bad interfacial contact properties with semiconductor/dye which can significantly hamper dye regeneration reaction and so break down the efficiency of the device.
A good compromise could be the *quasi-solid electrolytes* which have properties intermediate between liquid and solid ones due to the special nature of its physical state. This causes the quasi-solid electrolytes simultaneously posses both cohesive properties of solid state (desired to limit leakage and volatilization) and the diffusive properties of liquid one (favouring mass transport, conductivity and the aforementioned interfacial contact). In any case performances of qss-DSSCs are often lower than those of liquid ones; at best of my knowledge the record performance was a 9.5% efficiency obtained in 2011 [25]. The intermediate physical state of quasi-solid electrolytes is guaranteed by the presence of a small percentage of solvents, that still cause on long term instability of the electrolyte.
The natural next step of research devoted to "solidification process" of electrolyte to increase first of all stability of devices for their actual application has been the development of *all-solid transport materials*. Two families have been studied, ionic conductors and inorganic or organic hole transport materials. The last family includes the quite famous p-type semiconducing polymers like polypyrrole, polyaniline and polythiophene but also molecular hole-transport materials like spiro-MeOTAD, a quite expensive molecule largely employed also in perovskite solar cells that are in turns all-solid state devices. Main drawback of solid-state transport materials is the low interfacial contact with TiO_2/dye limiting dye regeneration and so increasing potential loose due to dye recombination reaction. The best performances are around 4-6% with peaks up to 7.2% [26].
In conclusion in the last decade a lot of work has been done pointing to stabilization of electrolyte for long term actual application of DSSCs; the guideline has been the "solidification" of the p-type transport material according to the intrinsic properties of solid state materials. Unfortunatly to date the dichotomy stability/efficiency is still insurmountable forcing to decide on which of the two features pointing, even if interesting results have been obtained both with semi-solid and all-solid devices. Considering that semi-solid electrolytes can be obtained by "gelification" of liquid electrolytes using both polymers or inorganic specie (like TiO_2 nanoparticles) [24] it seems, from my point of view, a good choice pointing to study and develop liquid electrolytes, easier to characterize, knowing that it will be possible to convert them into analogue semi-solid ones which would exhibit a good compromise between stability and efficiency. This consideration prompts me to restrict the thesis work to liquid DSSCs.

Liquid DSSCs: dye

General overview

One of the main component of a DSSC is the sensitizer (or simply the dye). It is a coloured molecule deputed to absorb light kicking off the photovoltaic process that converts a flux of photons into a flux of electrons (*i.e.* electricity) which can be accumulated and stored, or directly employed by an external load connected to the cell electrodes. The dye is the actual element that makes DSSC unique in the field of photovoltaic devices; as already anticipated the key point is the *sensitization* phenomenon that not only allows separation of the light harvesting from the charge-carrier transport process (with the advantages already described in the above introduction section) but it seems to make exploitable for photovoltage generation photons with nominal energy lower than the band gap of the semiconductor. Obviously a trick exists: the sensitization involves a third species over the semiconductor and the sensitizer that is an electronically excited state of the sensitizer of sufficiently high energy able to inject electrons into the conduction band of the n-type semiconductor with a downhill process (Figure 4). In this way sensitization of a wide band gap semiconductor (*e.g.* anatase TiO_2, with a band gap about 3.2 eV requiring $\lambda < 390$ nm) is possible by an appropriate choice of the dye which has an accessible photoexcited state higher in energy than the conduction band of the semiconductor to which the dye is adsorbed. Moreover solar radiation spectrum (Figure 5) can be more efficiently exploited than using direct photoexcitation of titania.

The advantages offered by sensitization go well beyond the implementation in light-to-electricity conversion devices. It is efficiently employed in other fields such as in the solar fuel production with dye-sensitized photoelectrochemical cells, DS-PECs, through which sun driven water splitting produces hydrogen [27] or in artificial leafs mimicking photosynthesis of the plants to convert light energy in chemical one [28].

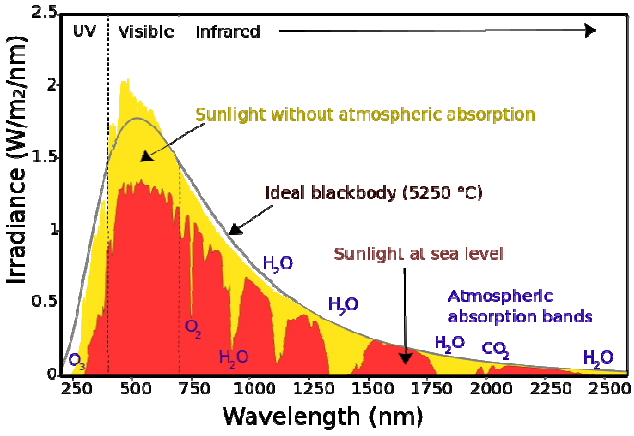

Figure 5 Solar radiation spectrum at upper zone of atmosphere and at sea level. From https://commons.wikimedia.org/wiki/File:Solar_spectrum_en.svg.

The dye molecules not only start the photovoltaic conversion but they are involved in other steps of the chain process (Figure 6) that, virtually, ends with the conversion of each photon in an electron. As just described after light harvesting the downhill injection of electrons in the conduction band of the mesoporous TiO_2 by the excited sensitizer molecules, S^*, occurs (step 1) with their concomitant conversion into oxidized form, S^+. The ideal pathway provides only another process involving the dye S^+, that is the dye regeneration (step 3) by electron transfer with the reduced form of the mediator presents into the electrolyte that permeates the TiO_2 porous. Among parasitic reactions that reduce the overall cell efficiency two of them directly involve the dye. The first is the decay of the excited state S^* to ground before electron injection occurs; it is typically a quite fast process occurring in the nanosecond time scale, but thousand times slower than electron injection (Figure 6). A much slower parasitic reaction (with rate constant of 10^3-10^6 s^{-1}) involves the recapture by oxidized S^+ species of the injected electrons from titania; such charge recombination is generally favoured by presence of intra-band surface states in the semiconductor and it is the more evident the more inefficient is the dye regeneration by redox mediator [29] which is the only process favouring the e^-/h^+ separation. In fact, as already mentioned, in nanostructured semiconductors charge space effect is practically inexistent unlike classical silicon-based photovoltaic devices.

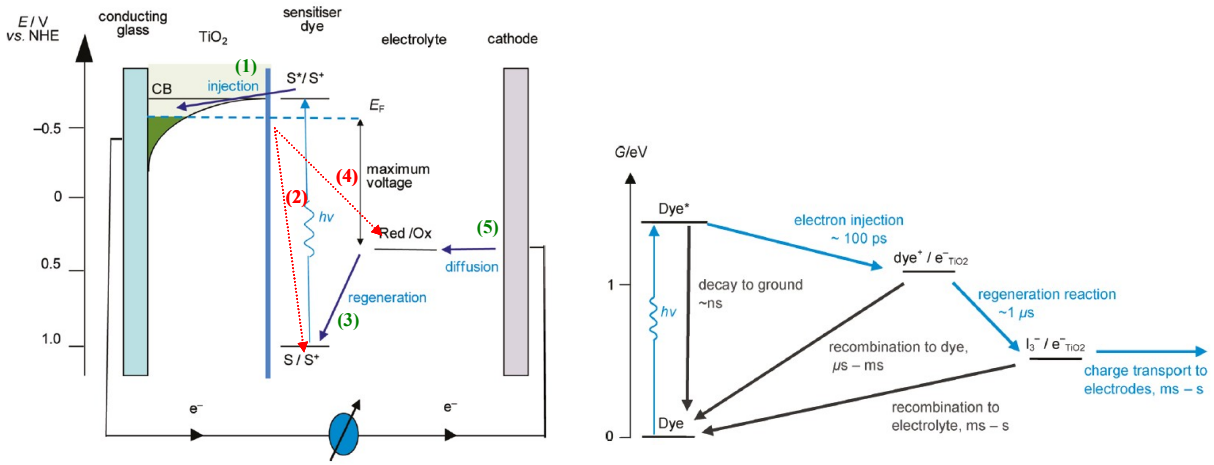

Figure 6 Left: energetics of operations of DSSCs. Right: state diagram representation of the kinetics of DSSC function. Adapted from ref. [29].

According to the mechanism of action of the dye described just above and the results from a lot of works carried out in the last 25-years on hundreds of chemically different sensitizers it has been possible to determine some common features that an efficient dye has to fulfil. They comprehend both optical, energetic and structural requirements.

Apart from the quite obvious chemical and photochemical *stability* of the dye in its ground and excited state (as well as in the oxidized one), a *molar absorption coefficient*, ε, that is as high as possible is one of the most desired characteristics for an efficient sensitizer in order to increase its light harvesting capability, but it is not enough. A *bathochromic extension* of the absorption

spectrum of the dye is well accepted with the aim of making exploitable the considerable near-infrared portion of the solar radiation spectrum (region around 600-900 nm). It is possible to calculate that the maximum short-circuit current density, j_{sc}, for a dye with an absorption onset of 900 nm is more than 30 mA cm^{-2} in comparison with a theoretical value of *ca.* 15 mA cm^{-2} for a dye with an onset of 600 nm, with about 7 mA cm^{-2} increment of maximal current by a red-shifting of 100 nm of the absorption onset in the aforementioned 600-900 nm range [30].

Another important property requested to a sensitizer concern the *energetic levels* of the ground, as well as of the excited state, that have to be positive enough to allow the electron transfer with redox active component of the electrolyte and negative enough to make possible the electron injection into the conduction band of the semiconductor respectively, minimizing potential looses. This means that both redox potential, evaluated in term of half-wave potential $E_{1/2}^{(S+/S)}$, and the energy of the photogenerated S^* species have to be such as to ensure only minimal driving force for dye regeneration and electron injection respectively. The minimum driving force required for a near-quantitative regeneration of common Ru dyes by iodide is about 0.2 to 0.3 eV [30] (the quite high value respect to the thermodynamic 60 mV requested for a electrochemically reversible monoelectronic electron transfer results from the two-electron and low reversibility character of the I^- to I_3^- reaction; this aspect will be reconsidered in the successive chapter dedicated to the redox mediators); while 0.15-0.20 eV are considered sufficient for electron injection [31]. Higher driving force results only in energy looses.

In order to increase electron injection (and also dye regeneration) the *structure of the sensitizer* can play a key role. Dyes with a "directional" architecture which exhibits a dipole moment (originated by the sum of coherently oriented single components) pointing toward anchoring groups and the semiconductor can give raise to a fast and efficient electron injection into TiO_2 band, reducing the probability of decay to ground too. Moreover the structure of the dye can retard the parasitic charge recombination reaction by oxidized form of the mediator (discussed in detail in the subsequent chapter) favouring the formation of a compact monolayer of sensitizer molecules that passivates the underlying semiconductor surface acting as an insulator that impairs back-electron transfers.

Since the publication of the milestone article by O'Regan and Graetzel [14] a lot of efforts have been devoted to overcome the reported 7-8 % efficiency focusing almost exclusively on the molecular engineering of sensitizer. Among this wide ensemble two big families of compounds can be identified, this is dyes based on transition metal complexes and full organic sensitizers (Figure 7). A common and essential structural element to both families of dyes is the anchoring group. As suggested by the "seafaring" term, it enables absorption of the dye onto the mesoporous surface of the metal oxide semiconductor allowing its sensitization and so the operation of the DSSC. The role

of the anchoring group is of fundamental importance influencing not only the efficiency of electron injection in the semiconductor conduction band but also the temporal stability of the device because it controls the sorption/desorption equilibrium of the dye. The two traditional anchoring groups are carboxylic acid and cyanoacrylic acid functions but in recent years novel anchor groups have emerged [32] which make a larger pool of materials available for designing new DSSC sensitizers offering potentially interest effects at the dye/TiO_2 interface.

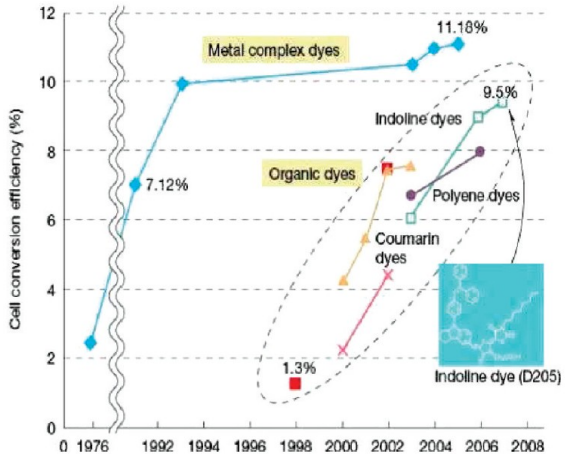

Figure 7 Snapshot of the more relevant steps of the evolution until 2008 of light-to-electricity conversion efficiency (standard AM 1.5) for DSSCs based on metal complex dyes (mainly Ru-based) and organic ones. From ref. [30].

Transition metal complex dyes

Many of the best photon-to-electron conversion efficiencies have been achieved with metal-containing dyes. Even if the 12.3% and 13% record efficiencies for DSSCs were reached with the zinc porphyrins **YD2-*o*-C8** [22] and **SM315** [23] respectively (Figure 8), ruthenium(II) polypyridyl sensitizers are surely the family that gave the more promising results in terms of both stability and photovoltaic performances, with best efficiencies ranging from 8 to 12% [20], [33]. These dyes are characterized by generally intense metal-to-ligand charge transfer, MLCT, bands in the visible and near-IR region with energetics favourable to the electron injection into TiO_2 conduction band. Optical onset in the 600-900 nm region takes advantage of the increase in photocurrent. Generally speaking Ru-dyes have structure that facilitates the e^-/h^+ separation especially in thiocyanate, NCS, derivatives; in this latter case the monodentate ligand acts as hole delocalizing group which makes easier the electron transfer with the reduced species of electron shuttle in the electrolyte.

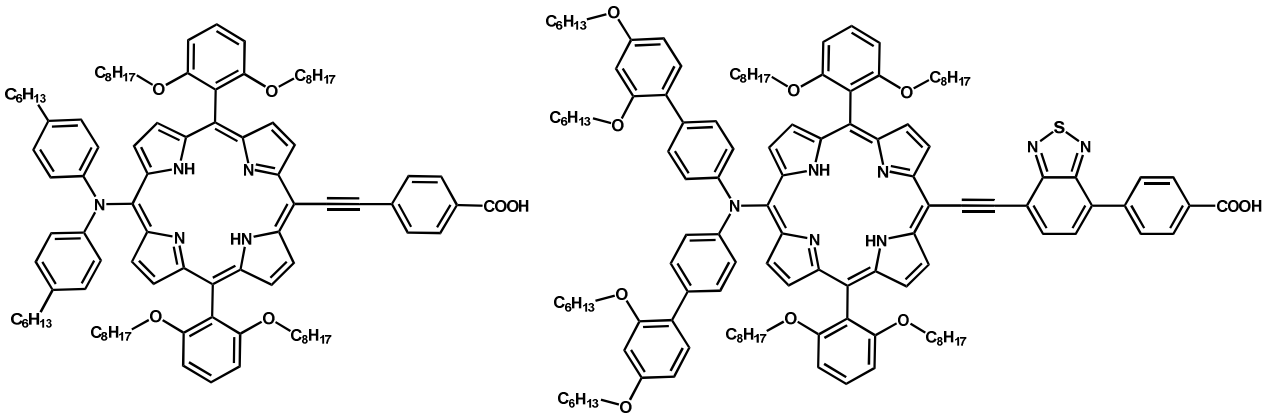

Figure 8 Structures of the record zinc porphyrins YD2-*o*-C8 (left) and SM315 (right).

A brief historical panoramic will now be presented citing the most important and performing Ru(II) sensitizers developed since 1993 with the aim to retrace their main evolution steps [33]. For my choice precise efficiencies will not reported since they depend from too much factors many of which go beyond the pure chemical features of the analysed dyes but reside largely on the dexterity in the cell assembly and the know-how own of each single laboratories. The first developed family of Ru(II) dyes (and perhaps fortuitously already very promising) is constituted by *homoleptic bis-bipyridyl* complexes with two thiocyanates ligands, of which **N3** and its semi deprotoned form **N719** are the forefathers (Figure 9). They were firstly reported by Graetzel and co-workers in 1993 [34] and exhibited efficiency higher that 10% thanks to a light harvesting extended up to about 800 nm. Few years later the same group published the terpyridyl analogue of **N3** and **N719** named "**black dye**"; it is a panchromatic sensitizer able to extent its absorption onset up to 920 nm allowing to reach j_{sc} higher than **N3** even if its has a lower molar absorption coefficient [35], [36].

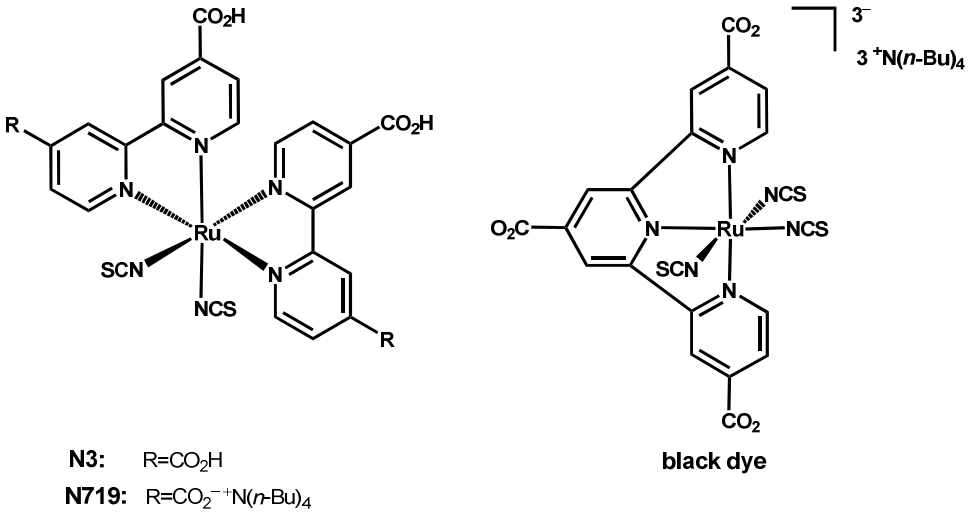

Figure 9 Structures of N3 and related N719 (left) and of black dye (right).

A successive generation of bis-bipyridyl complexes of bis-thiocyanate Ru(II) was proposed firstly in 2006. It consisted in amphiphilic and/or π-extended *heteroleptic complexes* (Figure 10) with increased tolerance against water attach (and so increase stability of the cell) and improved light

harvesting through an increase of the molar absorption coefficient and a bathochromic shift of the spectral response.

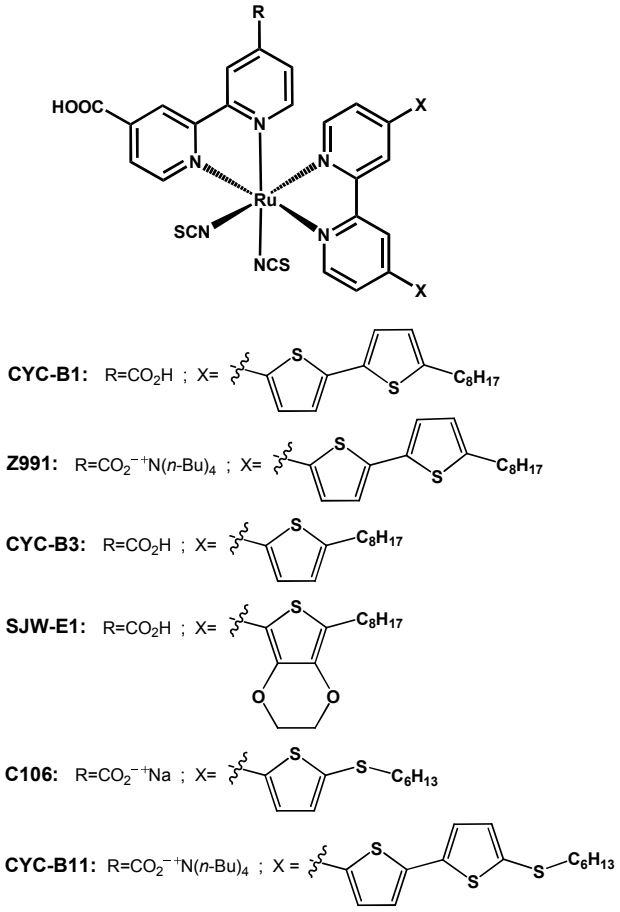

Figure 10 Structures of some important heteroleptic bis-pyridyl Ru(II) complexes.

This series of heteroleptic sensitizers, which includes among others **CYC-B1**, **SJW-E1** and **CYC-B3** dyes, was obtained functionalizing the 4,4' positions of one bipyridyl ligand of **N3** dye with π-conjugated "antenna" systems like thiophene-based pendants exhibiting a long alkyl chain. These hydrophobic chains (also containing a sulphur atom as in **CYC-B11** and **C106** dyes) increase water tolerance and stability of the device but, at the same time, can contribute to minimize charge recombination by mediator. It is interesting that among these heteroleptic Ru(II) dyes, **Z991** (the mono tetrabutyl ammonium salt of the just mentioned **CYC-B1**) obtained a 12.3% efficiency which was for some times a record value for DSSCs [37].

An important ramification along the linear evolution of NCS-based Ru(II) sensitizers took off by the replacement of the two thiocyanates with a chelating C^N or N^N ligand. The modification of the coordination sphere was driven by the consideration that NCS can be the weakest part of the complex from the chemical stability point of view. In fact evidences of NCS ligand substitution by other components of the cell like 4-*tert*-butylpyridine (employed commonly as an electrolyte additive) was reported for **N719** [38].

According to this idea a new generation of *thiocyanate-free* dyes were synthesized developing cyclometalated (C^N) and tris-bipyridyl (N^N) complexes (Figure 11).

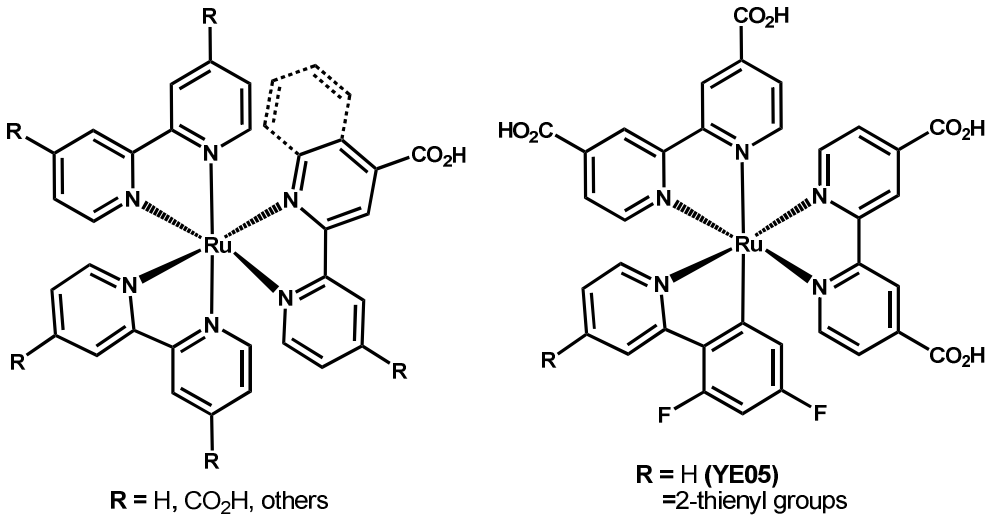

Figure 11 General structures of tris-bipyridyl complexes (left) and of cyclometalated dyes (right).

The first remarkable example of *cyclometalated dye*, **YE05**, was proposed in 2009 by Graetzel and co-workers [39] by the replacement of NCS donating groups with 2-(2,4-difluorophenyl)pyridine ligand which resulted a stronger electron donor then thiocyanates; the panchromatic sensitizer **YE05** exhibited an efficiency around 10% also thanks to an absorption onset around 780-800 nm. The red-shifted optical response respect to analogue **N719** results from the stronger electron donor nature of the cyclometalated ligand than thiocyanate groups. Less encouraging was the first results obtained with *thiocyanate-free N^N sensitizers*, especially when the chelating ligand used to replace the two NCS were pyridine-based scaffold. Up to 2011 efficiencies less or around 1% were obtained for many complexes of general formula $Ru[(bpy)_2L]^{2+}$ and $Ru[(H_2dcbpy)_2L]^{2+}$ [33] where bpy stands for 2,2'-bipyridine and H_2dcbpy for 2,2'-bipyridine-4,4'-dicarboxylic acid. Possible explanation for such poor performances was attributed to the absence of donating NCS ligands with their capability to stabilize t_{2g} molecular orbitals, lowering the dye energy levels and causing an important red shift to the corresponding MLCT absorption bands. Moreover the importance of H_2dcbpy anchoring groups were evident.

Before going on to briefly describe full-organic dye families, a citation on the studies carried out on copper(I) complexes as possible alternatives to Ru(II)-based sensitizers is useful [40], [41], 42]. The reason of this branch of research, in which also our group gave its small contribution [43], is quite obvious and concern the development of low-cost sensitizers exploiting the more abundant and cheaper copper element than ruthenium; moreover generally speaking purification of many Ru-dyes is quite difficult and time-consuming. To date efficiencies reported for the few known Cu(I) dyes

are three or four times lower than the best Ru(II) analogues, but it is a quite unexplored field. So it can be envisaged that great improvements are yet to come [44].

Organic dyes

Even if metal-based sensitizers hold the record performances (Figure 7) and are generally considered more stable than corresponding full-organic dyes, in the last years the latter have attracted more and more attention reaching AM 1.5 efficiencies just below 10% [45], [46], [47]. Possible explanations for this surge of interest in organic dyes can be recognized in the potential abatement of production costs respect to Ru(II) sensitizers, on which rest the high cost of raw metal and, as anticipated above, the time-consuming protocol needed to obtain sufficiently pure complexes. From my point of view another reason for such a fast diffusion of organic dyes can be correlated with the concomitant growth of researches aimed to development of alternative iodine-free electrolytes (for more details see the subsequent chapter). In fact it seems that organic sensitizers exhibit better performances than Ru(II) ones when combined with iodine-free electron shuttles, as verified also in this thesis.

Almost all full-organic sensitizers (often named metal-free dyes) have in common the so called "donor-π(spacer)-acceptor, D-π-A, architecture" (Figure 12). It is a very efficient structure that generate a well ordered and directional dipole momentum in the photoexcited state due to its charge transfer character. It results in a quite efficient e^{-}/h^{+} separation. In fact the architecture facilitates both the electron injection into the TiO_2 conduction band through the acceptor group (in which anchoring element is integrated) and the dye regeneration localizing the positively charged hole on the other hand of the molecule (far from the semiconductor surface) where a donor functionality is present. The two opposed functions A and D are linked by a π -conjugated bridge, which constitutes the third and last common element in the architecture of organic dyes.

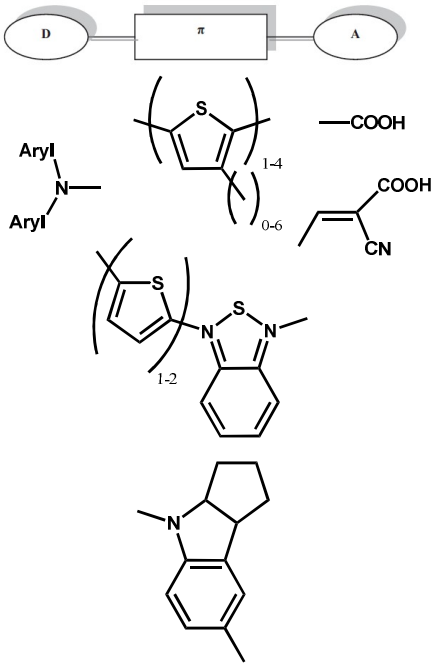

Figure 12 Top: schematic representation of the donor-π(spacer)-acceptor architecture of fully-organic dyes. Below: examples of the most common moieties employed as D, π -linker and A component.

Different moieties have been proposed in literature for the three components of the dye. Carboxilic acid and cyanoacrylic acid are the most employed acceptor/anchoring functionalities; triarylamine moiety, especially if functionalized with long and branched alkyl chains to prevent recombination by redox mediator, are the best performing donor group. A lot of chemically different moieties have been proposed as π-linker including benzothiadiazole units, thiophene chains (with and without hexyl chains, that reduce aggregation of the adsorbed molecules) like in **MK**-dye series [48], and the indoline unit which showed very excellent performances [45], [46].

In conclusion notwithstanding the efforts of many research groups, the organic sensitizers are not fully competitive in term of stability and performances with Ru(II)-based dyes. Despite the higher molar absorption coefficient of organic dyes than ruthenium ones, cells sensitized with the first exhibit lower efficiencies. A possible explanation can be the insufficient absorption of full-organic dyes in the red and near-IR region, below 700 nm. In fact, as already discussed, in the region between 600 and 900 nm the maximum photocurrent could in theory increases of 7 mA cm^{-2} units for a 100 nm red shift of the optical onset of the dye. Considerable increase in cell performances can be expected with new organic dyes having enhanced spectral response in the red and near-IR regions.

Liquid DSSCs: redox mediator

General overview

For almost fifteen years the research in the field of DSSCs was almost entirely monopolized by designing and synthesis of new sensitizers always as efficient as possible, considering this element as the only one capable to make cells competitive with silicon-based photovoltaics. Only in the last decade a relatively small number of scientists change route identifying in the redox mediator the possible turning point to move the stalemate in which the research gotten into (Figure 13), and since than always a greater number of papers has appeared in the literature, pointing that redox mediators is now a hot topics in the DSSC research field. For sake of curiosity the number of articles on new redox shuttles in 2010 and 2011 was more than the sum of all those published earlier [24].

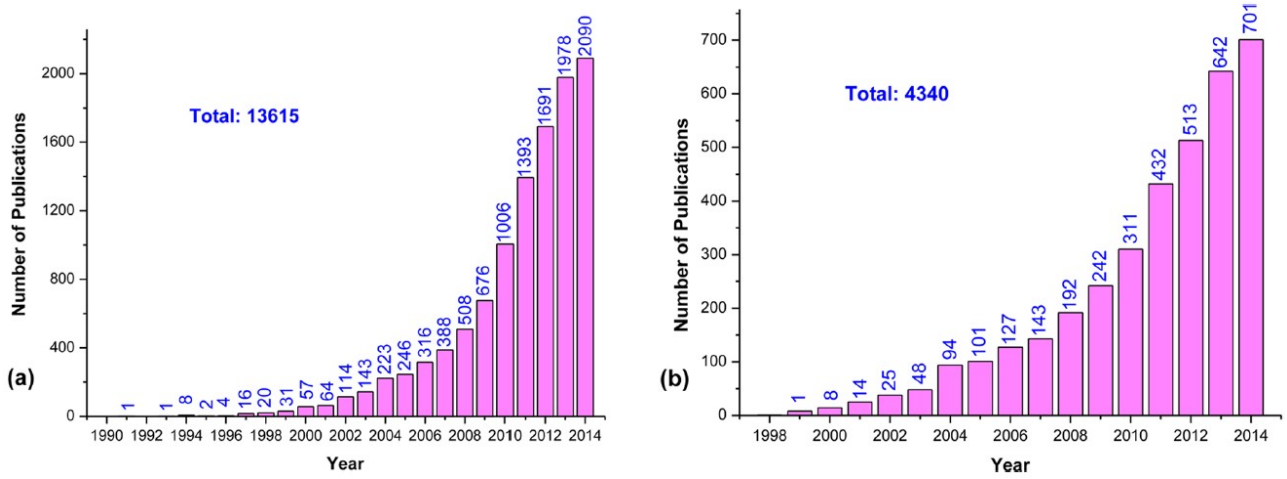

Figure 13 Number of articles published per year obtained from a literature search using the keywords "dye-sensitized solar cell" (a) and "dye-sensitized solar cell" and "electrolyte" (b). From ref. [24].

Redox mediator is the electrochemically active component of a liquid electrolyte, that permeates the pores of the sintered nanoparticles network constituting the metal oxide photoanode. It is actually constituted by an optimized mixture of oxidized and reduced form of a given electrochemically active molecule. In addition to the redox mediator the formulation of an electrolyte generally also includes a supporting electrolyte and some additives. The supporting electrolyte (*i.e.* a very soluble salt) increases the ionic conductivity of the liquid medium minimizing ohmic drop across the two electrodes of the cell. Additives are generally added to improve the operation of the device playing different role; a common additive is the aforementioned 4-*tert*-butylpyridine (added also in quite high concentration) that improves the open circuit photovoltage, V_{oc}, interacting with the acid sites of TiO_2 generating an up-banding of the conduction band edge of the semiconductor [49]. Other possible additive can be de-aggregating agents such as chenodeoxycholic acid, directly added in the

electrolyte to establish an equilibrium that avoid a net desorbtion of the same agent previously loaded onto the photoanode together with the dye during the sensitization period [50].

Turning back to the main object of this chapter, the redox mediator plays a role as important as that of the sensitizer; in fact it is true that the photovoltaic process is started by the dye through the light absorption and electron injection, but it is ultimately made exploitable by the redox mediator. Without an electrochemically active component able to restore the initial state of the dye the generation of electricity by photovoltaic process would be impossible. In fact the electron injected into the semiconductor immediately recombines with the acceptor state constituted by the oxidized dye due to negligible space charge effects in the nanoscaled TiO_2 particles. This would vanish any possible conversion of light into electricity resulting only in useless thermal energy dissipation. Long lived charge separation occurs mainly by virtue of the intrinsic kinetic properties of the redox mediator, which must ensure a fast dye recovery (sufficiently fast to compete with charge recombination), without undergoing substantial electron recombination at the photoanode. Apart dye regeneration the redox mediator is also involved in the heterogeneous electron transfer occurring at the other side of the cell, at the cathode interface, where the reduced form of the mediator is regenerated to complete the electrochemical circuit. Considering the ubiquitous role of the mediator inside the cell it is also commonly named “electron shuttle” highlighting its motion as a “cop” between the two opposite ends of a DSSC to guarantee the correct operation of the device.

As a consequence of the detailed description just provides it is simple to understand how the electron shuttle affects many energetic parameters of the cell. First of all it directly determines the V_{oc} of the device that is equal to the difference of the electrochemical potential, $\overline{\mu}$, of electrons in the semiconductor (corresponding to the energy of its quasi-Fermi level) and in the solution (corresponding to its Nernstian potential, to which it equals the $\overline{\mu}$ of electrons of the cathode). In a quite-direct way the features of redox mediator influence also the fill factor, *FF*, an integral parameter ranging from 0 to 1 that quantifies the degree of ideality of cell operation on the basis of the shape of the current *versus* potential, *JV*, curve of the device under illumination[3]. In other words it gives an idea of the importance of dissipative processes acting during the operation of the photovoltaic device, the higher the value the lower the overall potential drop in the cell. As mentioned it is an integral parameters which reflects the extent of any possible losses in the cell, ohmic and non-ohmic (*i.e.* electron transfer overpotential, mass transport overpotential and so on).

---

[3] Fill factor, *FF*, is properly defined as $\frac{J_{W,\max}V_{W,\max}}{J_{sc}V_{oc}}$, where $J_{W,max}$ and $V_{W,max}$ are photocurrent and photovoltage at the voltage where the power output of the cell is maximal, respectively.

In detail redox mediator affects the *FF* mainly in terms of the electron transfer overpotential at cathode and of the mass transport overpotential, in the last case especially in a quite viscous solvent and for a bulky mediator.

A quite complicated picture is depicted for the redox mediator. Not only it has to regenerate quickly the dye without recombine with electrons in the photoanode (this seems a contradiction) but at the same time it has to be regenerated at the cathode with an overpotential as low as possible to minimize potential losses. So it is the careful choice of the redox mediator and its cautious combination with the dye that allows development of ever more efficient DSSCs, taking into account the quite complicated and subtle balances that harmonize the numerous processes that finally result in the electric energy production. The "perfect" redox mediators would posses a lot of features including *i*) chemical and photochemical *stability* of both reduced and oxidized form; *ii*) *transparency* in the visible and near-IR region, in order to not compete with sensitizer for light harvesting; *iii*) *suitable half-wave potential*, sufficiently negative to allow dye regeneration and at the same time sufficiently positive to increase V_{oc}; *iv*) *suitable electron transfer rates* as fast as possible to allow an efficient dye regeneration and to minimize overpotential of the cathodic process, and on the other hand as slow as possible to reduce occurrence of e^-/h^+ recombination on both TiO_2 and underlying SnO_2; *v*) *very high solubility* of both reduced and oxidized species in common organic solvents (or ionic liquids) to allow an efficient mass transport in bulk solution and into the TiO_2 mesopores; *vi*) *not corrosive*.

The most (and unique, for almost ten years) employed redox mediator has been I_3^-/I^- couple. However, as discussed in more detail in the underlying subchapter, it is far from being counted an ideal electron shuttle neither from an applicative point of view or from purely academic one (*i.e.* as a reference couple due to the complexity and peculiarity of its mechanism, see below). For both reasons, especially from 2000, development of alternative electron shuttles have caught attention of more and more research groups viewing in these mediators a possibility to go deeper in the understanding of the dye regeneration process and to increase the cell performances by reaching the challenging dichotomy of the fast regeneration and the slow recombination.

I_3^-/I^- couple

Triiodide/iodide couple was the undisputed redox mediator in DSSCs from 1993 to the beginning of the new millennium and it is responsible for most of the record performances obtained in last years with DSSCs. However, as just anticipated, I_3^-/I^- is far from fulfilling all the features requested to an "ideal" redox couple [51]. Surely a first big advantage of iodide-based electrolyte is the high solubility of I^- salts which allows very high dye regeneration rates and low mass transport

overpotential; this advantage is in somehow counterbalanced by the volatility and the corrosiveness of iodine that results in problem of stability of the devices. Moreover I_3^-/I^- electron shuttle well resolved the challenging kinetics requested for a slow back-electron transfer from TiO_2 and a fast dye regeneration (at least with ruthenium-based sensitizers like **N3** and analogue **N719**); even if the $S^+ \rightarrow S$ process is efficient it seems to be restricted to high-driving force reactions due to complicated inner-sphere multi-electron-transfer steps which were, only partially, clarified after fifteen years of researches showing that specific structural features of the dye are requested [52], [53]. In fact the same iodine-based electrolyte resulted in some cases inefficient in presence of high absorbance and highly-polarizable organic dyes due to the aforementioned complicated mechanism of the regeneration; the specificity of dye/I^- interaction necessary limits alternative dyes which can be used effectively with I_3^-/I^- electrolyte and it makes it difficult to directly transfer that what was learnt to develop electrolytes based on alternative redox couples. The demand for high driving force regeneration combined with the too negative redox potential of the couple for many dyes ($E_{1/2}^{(I3-/I-)}$ ≈ 0.35 V *vs* NHE) are the main aspects that limit the V_{oc}. Typical DSSCs exhibit V_{oc} that are in the range 0.75-0.85 V thus wasting about half of the 1.8 eV optical gap potentially exploitable for **N3**, many of which is spent in the overpotential necessary to drive regeneration at an acceptable rate. Moreover reduction of I_3^- to iodide at counter electrode needs for platinized surfaces that catalyzed the reaction; however it seems that even platinum is attached by I_3^-/I^- mixture giving raise to problems of stability on long period of time.

Iodine-free electrolytes

Generality

Two reasons gave the inputs to researches in the field of new redox mediators alternative to the common I_3^-/I^- couple. The first reason was the finding that the quite slow increase of cell efficiency in twenty years in spite of the extraordinary efforts of many groups could be charged to the not optimal features of I_3^-/I^- couple. The second was a sort of "academic" reason, it is the necessity to identify new electron shuttles characterized by simpler electron transfer mechanism able to increase knowledge of the interfacial charge separation processes and to carry out structure-reactivity studies which results can be transfer to other analogue systems with the aim to increase the photovoltaic performances of the cells developing more and more efficient electron shuttles. In this context *outer-sphere redox mediators* can be the optimal choice. They are species, usually coordination complexes, in with the electron transfer, ET, occurs without any direct participation of coordinated ligands or without any particular arrangement of the systems before the redox process. Similarly from a purely electrochemical point of view [54] outer-sphere ET refers to a redox event that occurs

between species (in our case dye and mediator) that remain separate and intact before, during and after the ET process. No particular approach or pre-association is needed in this family of redox mediators, exactly opposed to what happens with I^- species. The kinetics of outer-sphere ET mediators is described by the so called "Marcus theory" for which Rudolph A. Marcus won the Nobel prize in 1992; according to this theory ET rate is primarily governed by a thermodynamic driving-force dictated by the difference in energy of the two reacting species; moreover ET rate strongly depends on any possible structural rearrangements in the structure of the species (the so called outer reorganization, at which it is associated an outer reorganization energy) and/or of their surrounding medium molecules (inner reorganization, with the correlated inner reorganization energy) that occur during the switching of their oxidation states.

Apart from Br_3^-/Br^- [55] and pseudohalogen mediators such as $(SCN)_2/SCN^-$ [56] and $(SeCN)_2/SeCN^-$, the most part of literature inherent to alternative mediators deals with *outer-sphere first-row transition metal complexes* due to the relatively easy tunability of their redox potential and of their ET kinetics by a proper choice of the ligands and of the metal atom. Anyway particularly instructive was the case of $(SCN)_2/SCN^-$ [56] because it clearly illustrated that the study for developing efficient redox mediators is not a simple matter. In fact pointing to a new electron shuttle with a more positive potential (oxidative potential of $(SCN)_2/SCN^- > (SeCN)_2/SeCN^- > I_3^-/I^-$) does not necessary translate to the theoretically expected increase of V_{oc} because of the already repeatedly cited criteria of fast dye regeneration and low back-electron interception.

Considering metal complex mediators, first raw metals have captured the attention thanks to their low cost and abundance. These are two important criteria considering the large quantity of mediators requested into a single DSSC (*e.g.* common concentration ranges are 0.25-0.10 M for reduced form and a tenth for the oxidized one). *Iron* was employed as ferrocene and ferrocenium salt in combination with common Ru(II)-dyes with relatively pour results; main limitations are related with the instability of oxidized form (in presence of O_2 and also 4-*tert*-butylpyridine) and with the too fast electron transfer process that efficiently regenerates dye but at the same time gives raise to effective charge recombination creating loss of both photovoltage and photocurrent. The breakthrough was reached with the 7.5% efficiency obtained in combination with a bulky push-pull organic dye [57]. *Nickel* [58] and very recently *manganese* [59] were also used to synthesized electron shuttle for DSSCs without no exceptional results.

Much more interesting are the complexes based on *cobalt* and *copper*.

Cobalt-based complexes

To date, octahedral Co(II)/(III) polypyridyl complexes represent the most successful examples of electron transfer mediators in iodine-free DSSCs. The first report was in 2001; in the subsequent

years only one article per years (on average) had as object cobalt-redox redox mediators until 2010 which can be considered a breakthrough point. At the end of that year [60], and in the next one [22], [61], [62], thanks to the works of different research groups was demonstrated the feasibility of using outer-sphere electron shuttles based on Co(II)/(III) diimine complexes to produce high efficient DSSCs up to 12% under 1000 W m^{-2} AM1.5 G illumination.

Possible explanation accounting for the very good performances of cobalt mediators resides in both its optical and electrochemical features. The higher transparency in the visible region respect to I_3^- /I^- (which exhibits a broad absorption in the 350-450 nm region) allows a less competitive light harvesting. More important it is the high inner reorganization energy associated to the spin-forbidden electron transfer (from high spin Co(II) to low spin Co(III)) which slows down self-exchanging kinetics reducing significantly the back-electron transfer at photoanode. Other interesting feature is the easy tunability common to other metal complexes that makes possible an *ad hoc* choice of the couple dye/mediator.

Copper-based complexes

Very few number of papers (around a dozen) have been published dealing with transition metal complexes as electron shuttles based on copper atoms. A net advantage respect to cobalt is the quite low toxicity of copper, but on the other hand, copper complexes suffer for some drawbacks respect to Co analogues *in primis* their colour. In fact generally speaking copper complexes of aromatic diimines (*e.g.* 2,2'-bipyridydes and 1,10-phenanthrolines) are red which means they have a relative intense maximum absorption around 450 nm with ε values of some thousands units, a window that should be as transparent as possible to limit the competition with the dye for the light harvesting. Moreover, $Cu^{(II)/(I)}$ redox switch is generally accompanied by significant variation in the geometry of the central atom (and so an high inner reorganization energy) due to the different preferred geometries assumed by copper in the two oxidation states. Cu(I) having a d^{10} electronic configuration prefers a tetrahedral disposition of the surrounding ligands while Cu(II) mainly prefers a tetragonal geometry which minimized the energy of electronic configuration, with the possibility to expand its coordination sphere from four to up to six. This intrinsic characteristic slows down the ET rates reducing the undesired charge recombination but at the same time hampering the dye regeneration which has to be as fast as possible to minimize the recombination by dye^+ species.

As often happens, Nature provides the inspiration to solve problems. It is know that in natural systems copper is involved in very efficient electron transfer processes like in the blue copper proteins. The specific chemical environment around the copper atom makes ET so fast and efficient. In fact the coordination geometry of the Cu is essentially blocked by the protein folding (Figure 14),

hampering any significant variation from the distorted tetragonal geometry that represents a compromise between the two preferred ones. Starting from this observation Fukuzumi *et al.* reported for the first time in 2005 [63] two blue copper model complexes as mediators for DSSCs; the [(–)-sparteine-N,N'](maleonitriledithiolato-S,S')copper mimics the spectral and electrochemical features in blue copper centres, while bis(2,9-dimethyl-1,10-phenanthroline)copper, **[Cu(dmp)$_2$]$^{+/2+}$**, represented the sterically hindered analogue of bis(1,10-phenanthroline)copper (Figure 14). The reported efficiencies could not rival with that of Co polypyridyl complexes but with this pioneering work authors opened the way to a new class of potentially efficient electron shuttles clearly demonstrating the possibility to increase the too slow ET kinetics of the simple bis(1,10-phenanthroline) copper$^{(II)/(I)}$ couple (and hence increase the cell efficiency) by simply introducing methyl groups in the positions adjacent the two nitrogen atoms. Methyl groups in **[Cu(dmp)$_2$]$^{+/2+}$** made the complex structure more rigid reducing variation of geometry during the ET process, so minimizing its energy barrier.

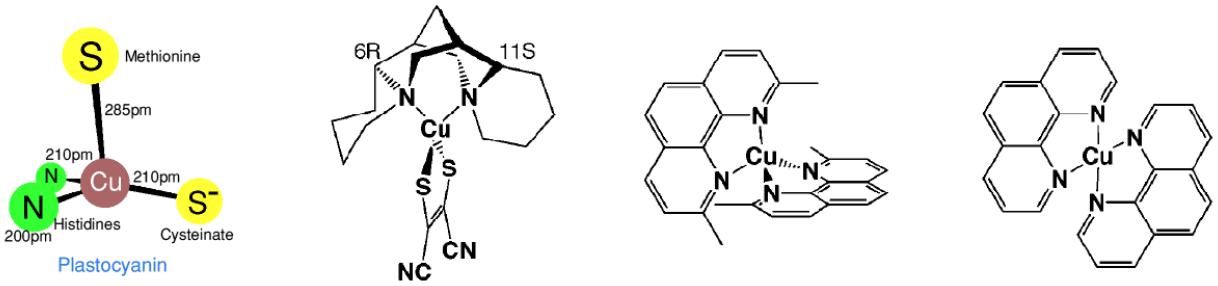

Figure 14 Schematic picture of the active site of a blue copper protein (*i.e.* plastocyanin) in which copper atom is forced into a distorted tetragonal geometry by protein environment (left). Chemical structures from left to right of sparteine-based copper complex, bis(neocuproine)copper and bis(phenanthroline)copper employed as first redox mediators in DSSCs [63].

Even if few other copper complexes have been proposed employing bipyridine, pyridyl-quinoline and biquinoline as ligands [64], the neocuproine-based copper mediator **[Cu(dmp)$_2$]$^{+/2+}$** resulted the most promising and the most employed in subsequent works. Just before the starting of this thesis in 2011 Wang and co-workers [65] reported a record efficiency of 7.0% obtained coupling **[Cu(dmp)$_2$]$^{+/2+}$** redox mediator with a sterically hindered D-π-A organic dye named **C218**. Moreover in 2015 the same electron shuttle couple was employed in an all-solid DSSC exhibiting interesting performances [66].

Approaches for limiting charge recombination

Notwithstanding the high inner reorganization energy of cobalt complexes the rate of recombination is not quite low enough to allow for quantitative charge collection (*i.e.* ideally one electron for each absorbed photon). This is a limitation shared by almost all outer-sphere electron shuttles, including copper-based redox mediators that have been the object of this thesis. So it is interesting to analyzed

the methodologies designed to bridge the problem of electron recapture from TiO_2 (or from the underlying SnO_2) by oxidized form of the redox couple. Many of the approaches described below have been thought and tested with cobalt-based mediators but results can be easily transferred to other analogue metal-based electron shuttles, including copper ones.

A first idea was to create an actual *physical barrier* to block mediators from electrode surface hampering/reducing the electronic coupling and so increasing the energy barrier of the electron transfer. Such methodology implies the deposition of an ultrathin alumina coating through atomic layer deposition on the TiO_2 nanoparticles of the photoanode [67], or the passivation of the underlying SnO_2 by deposition and sintering of a compact TiO_2 layer at the bottom of the mesoporous nano-TiO_2 layer (Figure 15). Drawback of these methods is that charge injection also has to cross the physical insulating barrier and it is not ideal.

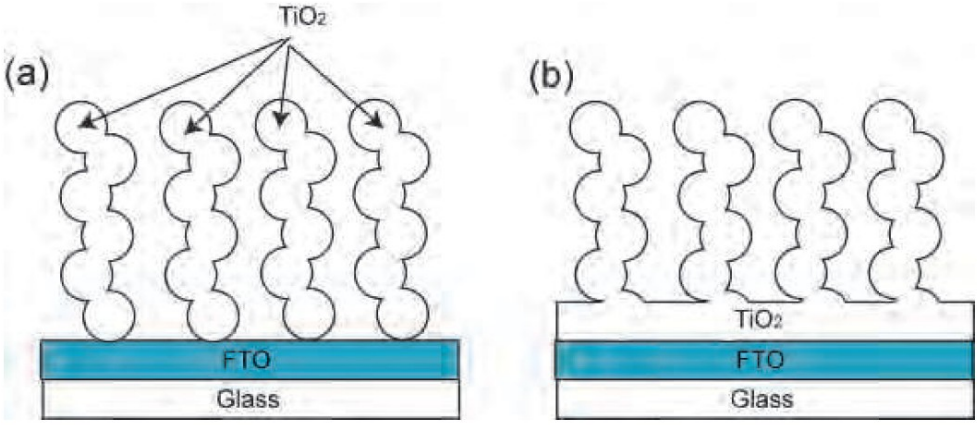

Figure 15 Picture of a simple photoanode constituted by porous TiO_2 nanoparticles sintered on an FTO-covered glass (lift) and of a passivated electrode through the deposition of a compact TiO_2 underlayer (right). From ref. [68].

Clever methods to build a "unidirectional" electron blocking layer that do not affect the electron injection regard the introduction of *steric hindrance* through bulky or long aliphatic chain attached on the mediator or on the dye molecules, acting as spacers that limit the proximity of the oxidized mediators to the surface of the photoanode and, as a consequence, exponentially minimizing the electron transfer probability occurring through tunneling effect. The beneficial effect of bulky *tert*-butyl groups respect to hydrogen or simple methyl substituents in positions *para* to the nitrogen atoms of bipyridyl-type ligands had been proved for cobalt complexes [69]. However increment of bulkiness of redox mediators brought inevitably to a decrease of the diffusion coefficient of the species in solution making more difficult the mass transport process in the DSSCs both through sintered TiO_2 nanoparticles and through bulk electrolyte between the two electrodes. To avoid the drawback of a slower diffusion the sterical hindrance was created on the sensitizer molecules which are immobilized on the metal oxide surface, as already mentioned in the previous section dedicated to dyes; this approach was adopted to develop both Ru(II) and organic sensitizers obtaining very

interesting results. The already cited work of Yella [22] can be an extraordinary proof of the effectiveness of the "steric hindrance on dye" approach in which authors combined a non-hindered mediator (the $Co^{(III)/(II)}$ tris(bipyridyl) redox couple) with a porphyrin functionalized with long octoxyl chains obtaining efficiency up to 12%.

A border line methodology that can be classified between the "physical barrier" methods and the "steric hindrance" approaches is the silanization. Unlike other "physical barrier" approaches it is a post-sensitization method (*i.e* it is performed after the sensitization of the photoanode) that employs silanes with a long insulating aliphatic chain [70]. Silanes anchor to any possible zones of the TiO_2 nanoparticles not covered by dye molecules (or to the uncovered underlying SnO_2 surface) reducing the recombination on the sensitized layer acting as sterically hindered barrier that limits the electronic coupling with d orbitals of oxide surfaces. In this way a physical barrier is created but, unlike aforementioned Al_2O_3 monolayer or compact TiO_2 underlayer, it acts as a "monodirectional" barrier that does not influence the injection of electrons.

From literature to thesis: aims of the work

The first and bigger part of the PhD thesis object of this chapter entitled "Dye-sensitized solar cells" was dedicated to the study of new and effective families of *dyes* and *redox mediators* which are two of the most important components in a DSSC responsible, as largely discussed in the "Introduction" session, of the light harvesting and of the actual cyclic operation of the device respectively. A close synergy has to occur between these two elements if an effective light-to-electricity conversion is desired. In fact if it is true that the molecular sensitizer is an essential component to begin the photovoltaic process, it is equally true that it is the electron shuttle (constituting the active part of the electrolyte) that makes effective the electric energy production.
In particular efforts were aimed to the development of new and effective families of *thiocyanate-free Ru(II) dyes* and of *copper-based redox mediators*.

Ru(II) polypyridyl sensitizers

The aim of this part of the thesis was devoted to synthesize, characterize from spectroscopic and electrochemical point of view, and finally test in laboratory-type dye-sensitized solar cells two new families of *polypyridyl thiocyanate-free Ru(II) sensitizers*. The main reason concerning the choice to focus on dyes that contain a costly transition metal was dictated by the literature; as already discussed to date some of the best promising and stable DSSCs are based on Ru(II) molecular sensitizers. The need to have sufficiently robust dyes from both chemical and photochemical point of view for actual long term application is mandatory to make the third generation photovoltaics competitive with the well mature silicon panels. In this context the choice to point to NCS-free light harvesters can be understood, being the ancillary ligands one of the most reliable sources of the long term instability exhibited by DSSCs. The general formula reported in Figure 16 evidence the common feature to both families of the new *thiocyanate-free* Ru(II) sensitizers, in which the two monodentate NCS of the analogue **N3** dye are replaced by one N^X chelating ligand. In particular the proposed sensitizers comprehend:

- *two identical 2,2'-bipyridyl ligands* bringing a total of four carboxylic functions to anchor the molecule to the TiO_2 surface and to allow the electron injection from the photoexcited state of the dye into the conduction band of the semiconductor,
- the third ligand is a *N^X chelating aromatic anion* responsible of the peculiar optical and electrochemical properties of each single molecules. In the first family we proposed the N^O *8-oxyquinolate* ligand while in the second case we chose the N^N *5-pyrid-2-yl tetrazolate* ligand.

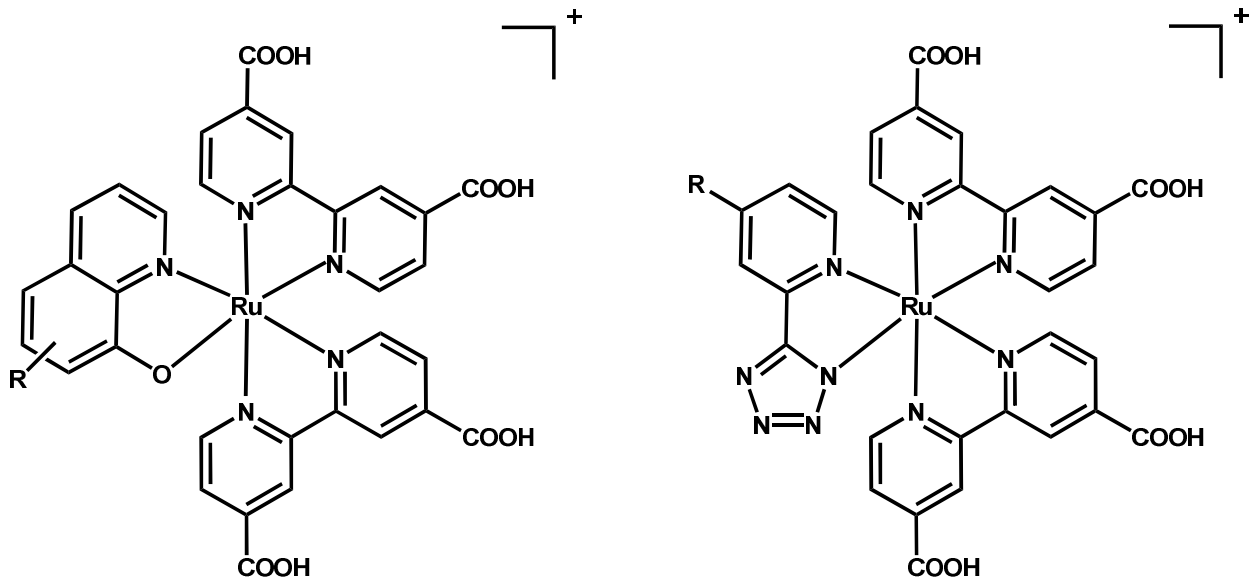

Figure 16 General structures for the two series of thiocyanate-free cationic dyes proposed in this thesis. On the left the 8-oxyquinolate Ru(II) family, and on the right the 5-pyrid-2-yl tetrazolate Ru(II) one.

The common design was dictated by combining literature evidences pointing to the importance of *two identical bipyridine dicarboxylic acid ligands* (respect to analogue systems bringing only one bipyridine anchor) [33] and the promising performances of bidentate cyclometalated ligands [39], [71], [72], [73] which can be considered an *anionic ligand* (*i.e.* a carbanion ligand). The novelty of the proposed complexes resides in the investigation of new N^X anionic chelating moieties (with X ≠ C) that could maintain the well desired strong electron deficiency nature of the cyclometalated ligands and the chemical stability of the related Ru(II) complexes. Two X heteroatoms have been chosen (Figure 16):

- X = *oxygen* when *8-oxyquinolate* scaffold was employed,
- X = *nitrogen* with *5-pyrid-2-yl tetrazolate* scaffold

with the aim to analyze how the nature of the formally negative charged atom of the electron withdrawing chelating ligand (*i.e.* oxygen or nitrogen) and the structure of the ligand itself affect the optical and electrochemical properties of the resulting Ru(II) polypyridine sensitizers and hence the performances in DSSCs.

The choice of pyrid-2-yl tetrazolate ligand had a second interesting connection with the recent literature. Among the families of NCS-free Ru(II) dyes N^N chelating ligands based on pyrid-2-yl azolate ligands resulted particularly promising [74]. A couple of months after the beginning of the PhD thesis an interesting paper of Graetzel and co-workers [75] demonstrated that changing a pryridyl-pyrazole with a pyridyl-triazole ligand in a heteroleptic Ru(II) dye an increase in the cell efficiency of about 20% occurred. In other words the study seemed to suggest that the increasing the number of nitrogen atoms of the heterocyclic five-member ring an increase in cell efficiency was obtained. Starting from this consideration we decide to synthesis a N^N chelating ligand in

which a pyridine is coupled with the *tetrazole* (the most nitrogen enriched five-atom heteroaromatic ring) hoping to further increase the photovoltaic performance or, at least, to propose a new family of promising thiocyanate-free sensitizers.

For the development of both classes of sensitizers one of the guideline was the "applicability" of the synthetic procedures. In other words the minimization of the synthetic steps was always kept in mind in order to maximize as much as possible the yields of the final complexes and, at the same time, to limit the cost of the sensitizers. This means that we focused on moieties of relatively simple structures and low molecular mass, and on related ligands that did not require too many synthetic efforts. The second guideline was the modification of the bare scaffold of the ligand with functionalities that could extend π-conjugation and/or increase the oxidation potential of the resulting dyes in order to improve light harvesting (keeping in mind that a 100 nm red shift in the optical onset of the sensitizers in the region 700-900 nm could leave to about 7 mA cm^{-2} increase in the photocurrent) and/or to increase the driving-force for the dye regeneration process (or to allow the employment of redox mediators more oxidizing than iodide).

Copper-based redox mediators

As already mentioned, in the quite young research field of iodine-free electrolytes for DSSCs the feasibility of employing copper complexes as redox mediators alternative to the common I_3^-/I^- couple has been only marginally considered. A very small number of complexes were proposed at the beginning of my thesis [63], [64], [65] (an only few others have appeared in the meantime, also thanks to our contribution [76]) and, moreover, a number of studies ever more limited was devoted to deep understanding the dependence of the electrochemical features of the copper complexes by the ligand structures [77].

The development of new alternative electron shuttles were driven by two key points. An ideal redox mediator for DSSCs have to posses well defined *optical* and *electrochemical features* that allow to minimize the interference with the dye molecules for the light harvesting and satisfy at the best the quite insurmountable dichotomy of a fast dye regeneration and a slow charge recombination, respectively. Keeping in mind both these aspects a series of copper-based complexes having two identical *1,10-phenanthrolines* as ligands were developed (Figure 17).

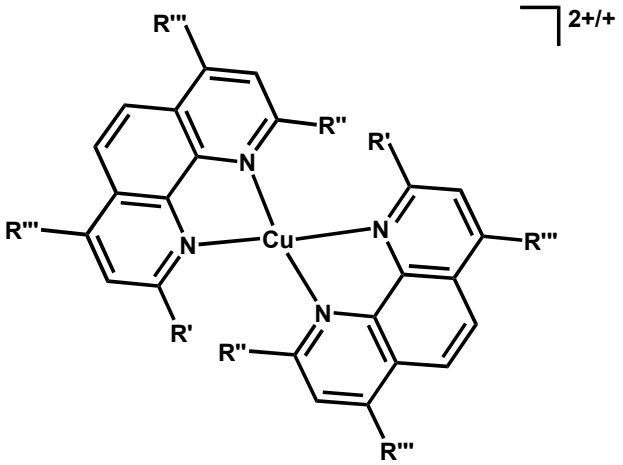

Figure 17 General structure for the family of bis(1,10-phenanthroline)copper complexes.

The choice of the nature of the ligands was dictated by some strongholds:

- the *simplicity* that is mandatory considering that a potentially marketable mediator has to be as cheap as possible due to the huge quantity presents in the device;
- the *chemical modulability* of the scaffold that has to easily allow variation of the steric hindrance of the ligand.

Last point is of fundamental importance because the turning point to develop efficient redox mediators seems to be the capability to modulate the *geometrical rigidity* of copper complexes influencing the ET energy barrier [63] (and not only) by the choice of appropriate ligands. Moreover some proofs suggest that the molar absorption coefficient of copper complexes can be partially modulated by tailoring the ligands with specific substituents [78], so allowing to design complexes with less intense visible absorption.

Due to the lake of a rational interpretation of the electrochemical behavior of copper complexes object of this work, the first goal was the clarification of the dependence of both thermodynamical (*i.e.* $E_{1/2}$) and kinetic ET parameters by chemical nature of the ligands and the reaction medium. After the acquisition of these mandatory information the second step was started. It was the direct tests in laboratory-type DSSCs performed on the most promising complexes to evaluate their actual performances. The final aim was obviously to reach the highest efficiency but the possibility to correlate the cell performance with basic electrochemical parameters of the mediators was also taken in high regard. The characterization plan finally included the evaluation of the stability of complexes that were monitored for a quite long period of time.

Results and discussion: Ru(II)-based sensitizers

8-Oxyquinolate dye family

Synthesis

In parallel to our work Graetzel *et al.* [79] published a paper reporting the performances obtained by $[Ru(quin)(dcbpy)_2]^+$ dye in which Ru(II) atom was combined with one 8-hydroxyquinoline, **quinH**, ligand with two 2,2'-bipyridine-4,4'-dicarboxylic acid molecules, **dcbpy**. The proposed synthesis implied long reaction time (*i.e.* 18 hours) and tedious work-up, including purification of the alkalinized crude mixture by Sephadex chromatography. Our group developed a new efficient synthetic protocol (Scheme 1) exploiting microwave irradiation which allowed to drastically reduce the reaction time (from 18 hours to only 5 minutes) and, at the same time, to limit the work up procedure to a simple precipitation of the desired product from the reaction mixture [80].

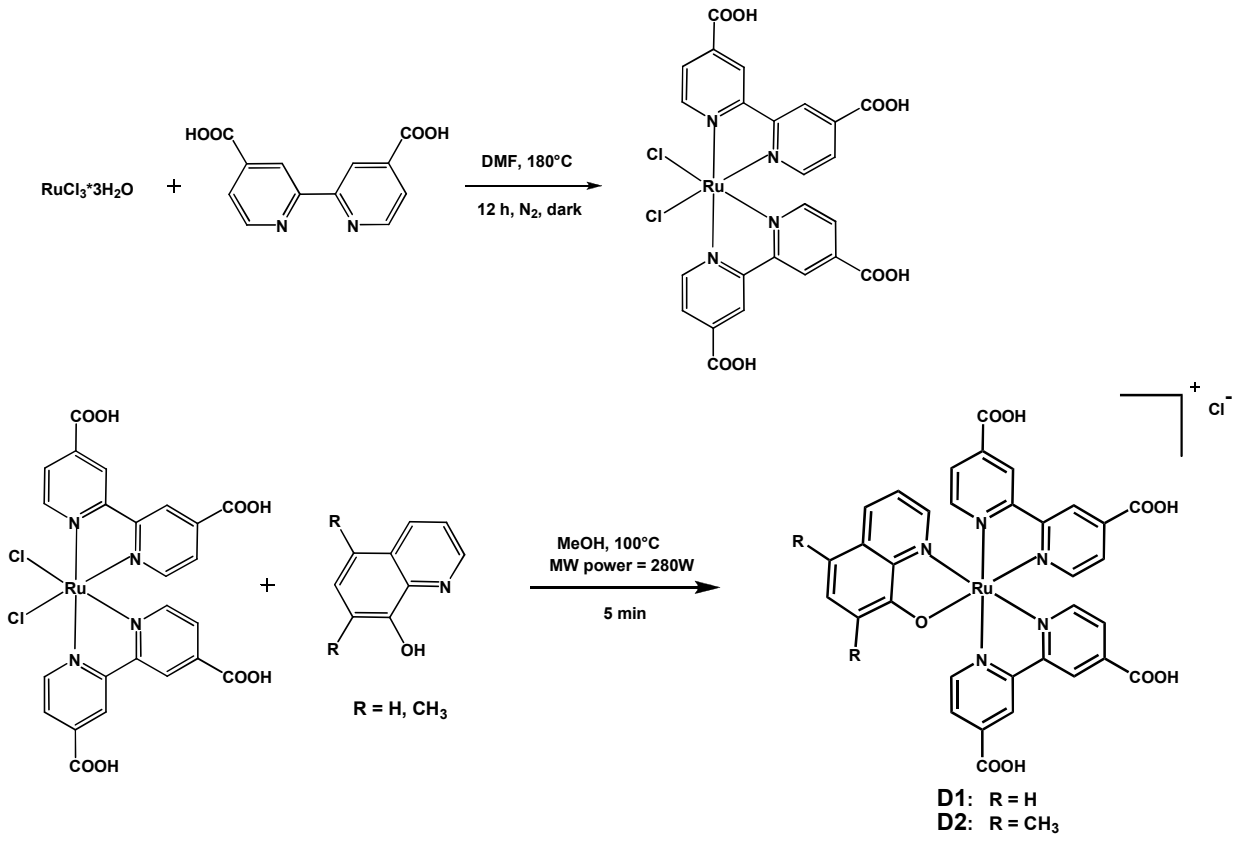

Scheme 1 Synthetic pathway for the preparation of dyes D1 and D2. A microwave (MW) reactor was employed to improve the efficiency of the chloride substitution step.

This protocol was successfully employed to synthesize the already mentioned dye $[Ru(quin)(dcbpy)_2]Cl$, **D1**, and the dimethyl analogue $[Ru(Me_2\text{-}quin)(dcbpy)_2]Cl$, **D2**, where **$Me_2$-quinH** was 5,7-dimethylqinoline, via a two-step procedure, involving the preparation of the *cis*-

$[RuCl_2(dcbpy)_2]$ precursor according to literature [81], and the subsequent chloride ions substitution with the corresponding chelating quinoline ligand performed in a microwave reactor. Both ligands are commercially available. See experimental section for more detailed procedure and identification of the products.

Characterization

Electronic UV-visible spectra

The optical properties of the **D1** and **D2** were studied [80] recording UV-visible spectra in ethanol (Figure 18). The sharp intense UV absorption band centred at 310 nm was superimposable in both spectra; the electronic transition was attributed to a singlet ligand centred π-π^* excitation localized on the dcbpy ligands. Generally speaking Ru(II) polypyridyl complexes exhibit intense electronic transitions in the visible region ascribable to two closely spaced singlet metal-to-ligand charge transfer, MLCT, excitations. Introduction of electron rich ligands, such as NCS anion or in our case the bidentate oxyquinolate, into the coordination sphere of the metal causes potentially large modification in the energetic structure of the complex. As expected the absorption patterns of **D1** and **D2** are comparable. Two neat electronic transitions were observed centred at 388 nm and 523 nm for **D1**, with molar extinction coefficients, ε, around 10^4 M^{-1} cm^{-1}, in agreement with value reported by Graetzel for the chemisorbed dye [79]. The low energy transition is blue shifted respect to the corresponding **N3** band (λ_{max}=534 nm, in ethanol) [34]. A quite remarkable red-shift between 10-30 nm was observed for the methylated complex **D2** according to the electron donating nature of the two alkyl groups on the quinoline moiety (*i.e.* 399 and 548 nm respectively); in this complex the transition at 548 nm occurred at a low energy than in **N3**. An intermediate electronic transition was also observed as a shoulder for complex **D1**, around 470 nm, in a region where **N3** shows a valley; in **D2** such transition seems to disappear or, more likely, to shift toward higher energy as an almost unperceivable shoulder at about 420 nm. Unfortunately the non optimal coverage of the visible and near-IR region (onset at 700-750 nm) combined with the relatively low ε values are two not ideal properties for assuring satisfactory sunlight harvesting.

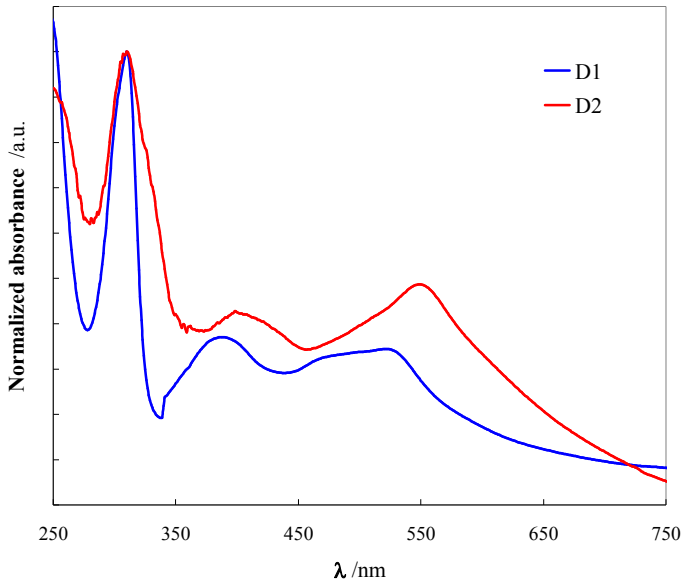

Figure 18 Normalized electronic absorption UV-vis spectra for oxyquinolate-based dye D1 (blue line) and D2 (red line) in ethanol. Concentration *ca.* $5 \cdot 10^{-5}$ M.

Of particular relevance is the similarity of **D1** and **D2** spectra (including the intermediate band at 420-470 nm) with those of structurally and electronically analogue cyclometalated **YE05** dye [39]. Both quinolate and phenylpyridyl ligands respectively introduce substantial contribution to the highest occupied molecular orbital HOMO [79] involving d atomic orbitals of Ru. The metal-ligand interaction makes easier the stabilization of the oxidized dye generated after electron injection into TiO_2 conduction band allowing a broader delocalization of the resulting positive charge between the metal centre and the π orbitals of the anionic ligands. According to the theoretical explanation proposed for **YE05** dye, the intermediate electronic transition around 450 nm in our complexes could be attributable to the just mentioned sizable hole delocalization onto the anionic N^O ligand.

Voltammetric study

Before starting with the description of the voltammetric characterization I would like to make a clarification regarding the common way of referring electrochemical potentials of sensitizers. Many literature data concerning the standard potential, E^0, or similarly the half-wave potential, $E_{1/2}$, of the dyes are referred to the standard hydrogen electrode (SHE). From my point of view this common method is not perfectly correct because a systematic error is invariably included into the reported potential value. The error comes from including into the potential value the so called *liquid junction potential*; in few words it is the potential (negative or positive) that is invariably generated at the interphase between two different electrolytes (*i.e.* different solvents, or same solvent with different supporting electrolytes). Considering that almost all dyes are insoluble in water (the solvent employed as internal reference solution of SHE and of the more common operational reference electrodes like saturated calomel electrode, SCE, or silver/silver chloride electrode, AgCl|Ag) and

that measurements for the determination of the standard potential for $dye^+|dye$ couple are performed in organic solvents (usually the same employed in the DSSC) the aforementioned junction potential is invariably present. The correct way to report a redox potential, especially when employing non-aqueous solvents, was suggested many years ago by IUPAC (International Union of Pure and Applied Chemistry) and implies the employment of a *intersolvental redox reference* [82]. This species is considered to have an ET barrier practically independent from the reaction medium; so it is possible to purge the liquid junction potential from the value of the potential obtained experimentally, which is referred to an (aqueous) operational reference electrode, simply referring such potential to the potential of one of the intersolvental redox refences (e.g. ferrocene and decamethylferrocene) determined in the same experimental conditions.

According to the IUPAC recommendation, which makes easier, immediate and, most of all, correct the comparison of potential values recorded in different conditions, in this thesis *all potentials* (unless otherwise stated) will be *referred* to the *reference redox couple ferrocenium|ferrocene*, $Fc^+|Fc$, whose half-wave potential was determined daily in a blank solution equal to that employed for the measurements of the analytes. The only exceptions were done for the E^0 of the dyes to agree with the common use in this field so as to make easier the comparison of our results with literature data.

The non-innocent nature of the oxyquinolate ligands was supported by voltammetric measurements performed not only for the two dyes but also on the constituting neutral free-ligands **quinH**, **Me_2-quinH** and **dcbpy** in order to better clarify the electrochemical properties of this new class of hydroxyquinoline-based sensitizers [80]. Voltammetric signals recorded in N,N-dimethylformamide, DMF, (Figure 19) revealed electroactivity for the free-ligand quinolines in both the anodic and cathodic potential window, unlike **dcbpy** molecule that was electro-oxidative stable.

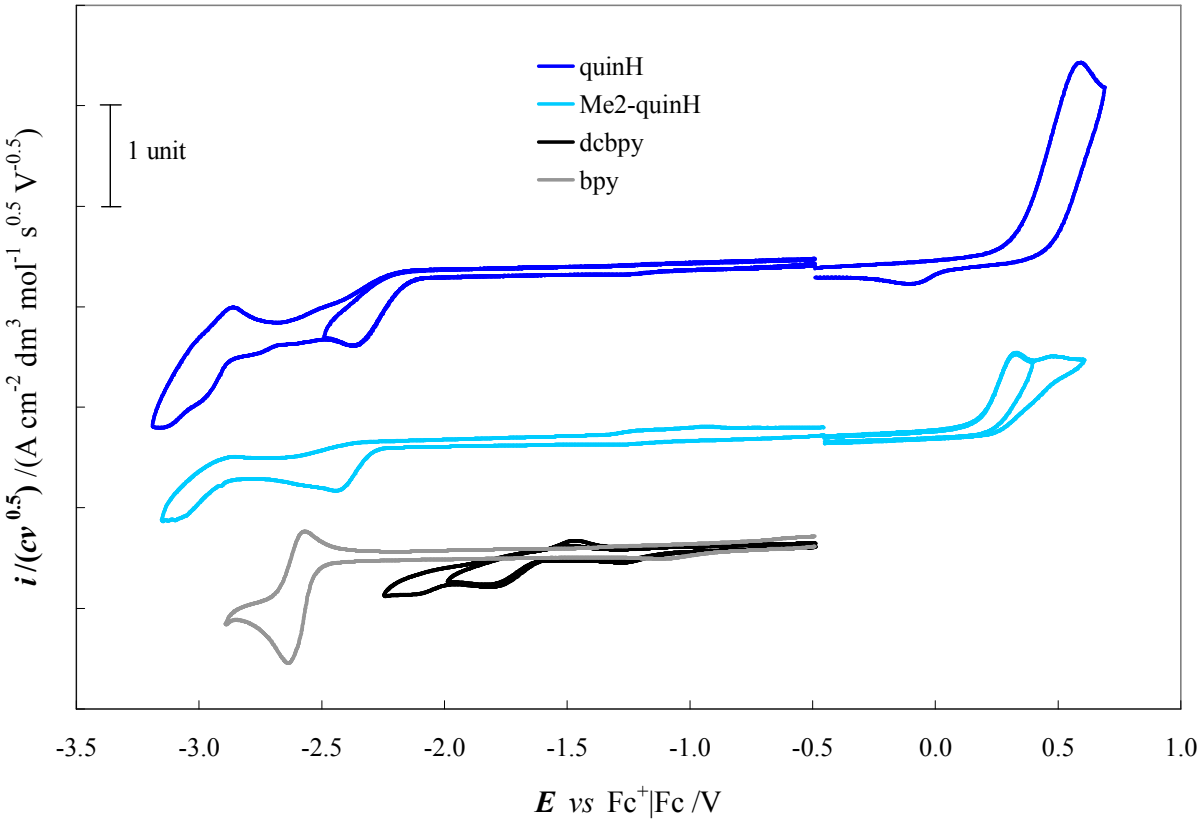

Figure 19 Normalized cyclovoltammograms for the free ligands quinH, Me_2-quinH and dcbpy. For sake of comparison the CV of 2,2'-bpy is also reported (grey line). Concentration *ca.* 0.001 M in DMF and $TBAPF_6$ 0.1 M, scan rate potential 0.05 V s^{-1}, GC electrode.

In particular a neat diffusive ($\partial \log I_p / \partial \log \nu \approx 0.5$, where a slope of 0.5 indicated a diffusion controlled process [54]), chemically and electrochemically irreversible oxidation process was invariably observed in cyclic voltammograms, CVs, for both **quinH** and **Me_2-quinH** even if some differences have to be noted. The last molecule, **Me_2-quinH**, was actually characterized by a monoelectronic peak couple. The study of the CVs recorded at different scan rate potentials (between 0.02 and 2 V s^{-1}) suggested the existence of a chemical step involving the species electrogenerated at the potential corresponding to the first oxidation peak. However no further experiments were done, being out of the scope of this study a deep mechanistic interpretation of the voltammograms. On the other hand the unique anodic peak recorded for **quinH** was indicative of a two-electron oxidation process (for comparison with the current intensity of the monoelectronic reduction peak, see below); the CV shape was in good agreement with literature data also considering the difference in the proticity (and hence proton availability) of the reaction medium (DMF in our situation *versus* acqueous [83] or H_2O/methanol mixture [84] for the works reported in literature) being known that protons play a direct role in the electrooxidation mechanism that involved formation of free-radical intermediates and quinonoid-type compounds. The *ca.* 0.3 V negative shift in the position of the oxidation peak for the pristine methylated hydroxyquinoline

respect to the pristine 8-hydroxyquinoline was in agreement with the electro releasing nature of the two alkyl substituents (Table 1).

Table 1 Main cyclovoltammetric parameters for three free ligands and the two complexes. Concentration *ca.* $1 \cdot 10^{-3}$M, in DMF with tetrabutylammonium hexafluorophosphate, $TBAPF_6$. 0.1M. Glassy carbon electrode; scan rate potential 0.05 V s^{-1}; positive feedback 210-220Ω.

	Oxidation		Reduction	
	E_p *vs* Fc^+|Fc /V	$E_p - E_{p/2}$ /V	$E_{p,IRed}$ *vs* Fc^+|Fc /V	$E_{p,IRed} - E_{p/2}$ /V
quinH	0.59	0.145	– 2.37	0.121
Me_2-quinH	0.33	0.084	– 2.44	0.090
dcbpy			– 1.82	0.115
D1[a]	0.29	–	– 1.72	–
D2[a]	0.18	0.064	– 1.71	0.060

[a] Average of two independent measurements.

As expected from the inductive effect an inversion in the relative position of the first cathodic peak of the two free-ligands occurred respect to the anodic counterparts (Figure 19). Interestingly the electronic effect of alkyl groups was significantly attenuated for the reduction process; this would point to the first oxidation site being closer to the methyl groups than the first reduction one, the last tentatively attributed to the formation of a radical anion located mainly on the pyridine side of the condensed moiety, while the oxidation process should involve the phenolic side of the molecule.

As anticipated the **dcbpy** free ligand is oxidatively stable but presents some reduction processes, the first of which was recorded at a potential more positive than in the quinoline ligands probably due to the electron withdrawing effect of the two carboxylic units probably directly involved in the electron transfer. The key role played by –COOH functionalities was supported by the neat different CV pattern recorded for the simple **bpy** (*i.e.* 2,2'-bipyridine) taken as a reference molecule (Figure 19). In fact not only a shift of 0.8 V in positive direction was observed for the dicarboxy derivate respect to the pristine **bpy** but at the same time the nature of the ET clearly change from a chemically and electrochemically reversible process for **bpy** to a multi-step chemical irreversible one in **dcbpy**. The presence of –COOH that act as internal proton sources can significantly influence the follow-up reaction explaining the peculiar morphology of the pattern of **dcbpy**.

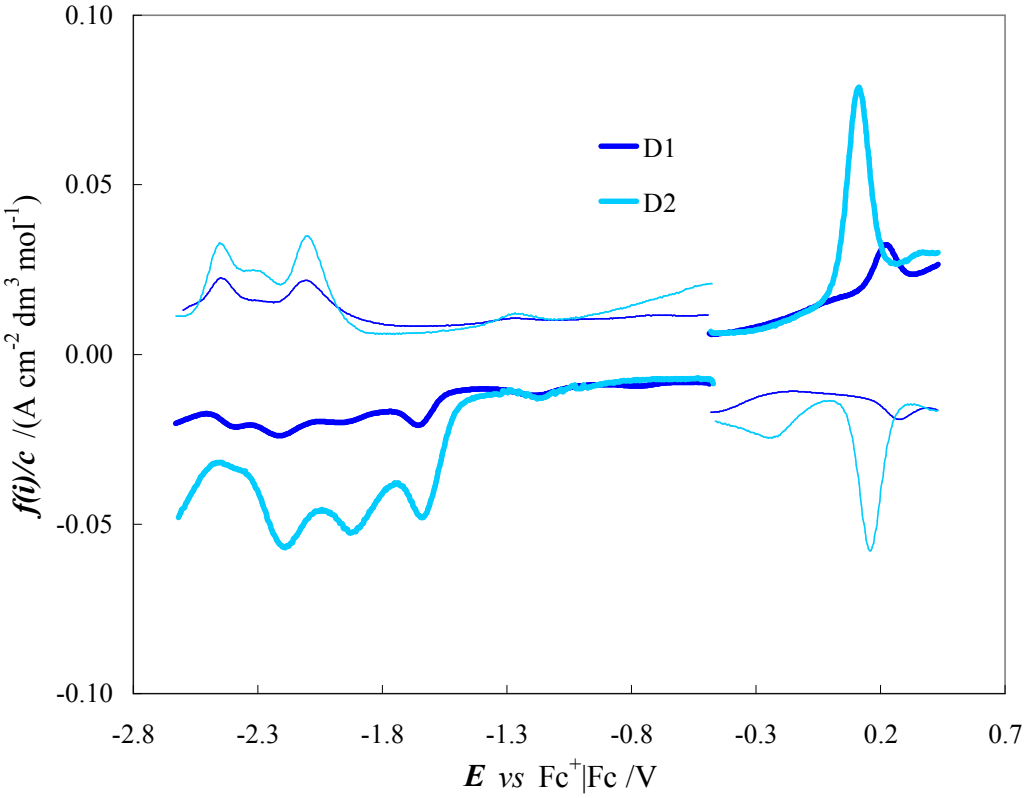

Figure 20 Forward (thick lines) and backward (thin lines) normalized differential pulse voltammograms for D1 (dark blue) and D2 (light blue). Complex concentration was 0.001 M in DMF and TBAPF$_6$ 0.1 M; GC electrode; scan rate potential 0.05 V s^{-1}. Lower peak intensity for D1 was attributed to a non complete dissolution of the weighted sample.

CV pattern of **D1** was not very clear probably due to its lower solubility respect to **D2** which in turns was characterized by an increased solubility attributable to the two methyl units. For this reason differential pulse voltammograms, DPV, will be reported for a direct comparison of the two dyes (Figure 20). Similarly to the free ligands, voltammograms of the two complexes exhibited features that can be explained involving electronic effects of the ligands (Table 1). The cathodic window was characterized by a complicated series of *ligand-centred reductions*; the first two peaks were attributed to an ET localized on each of two **dcbpy** ligands, being the easier reducible components of the system. However the complicated pattern was not further analyzed; I underline only that for both **D1** and **D2** the first reduction process was shifted at a slightly positive potential respect to the corresponding free-ligand **dcbpy** according to the decrease of the electron density on the bipyridyl moiety as a consequence of the metal coordination.

More interesting is the analysis of the anodic window being the dye/dye$^+$ ET the active process during the operation of a DSSC. Both complexes showed a diffusive, monoelectronic oxidation process which was chemical and also electrochemical reversible (considering the substantial invariance of E_p with the potential scan rate as well as the half-peak width, E_p-$E_{p/2}$, and the forward-backward peak distance); in **D2** it took place at a more negative value than in D**1** due to the electro donating effect of methyl groups, with standard potentials, $E^{0(dye+|dye)}$, equal to 0.86 and 0.96 V *vs*

SHE[4] respectively (Table 2). Although the peaks of the complexes maintain the same relative position of the corresponding free ligands their potential difference is three-times smaller consistently with the first oxidation site being significantly farer away from the electron donating groups, and thus perceiving significantly smoothed inductive effects. As in similar Ru(II) complexes, the *oxidation* is attributable to a *metal-centred* process but in these systems oxyquinolate ligand can be significantly involved considering the similar oxidation potential of $Ru^{3+}|Ru^{2+}$ and **quinH**$^{+}$|**quinH** (or then again **Me$_2$-quinH** $^{+}$| **Me$_2$-quinH**) couple.

Thus the electrochemical characterization just discussed seems to confirm the non-innocent role of the oxyquinolate moiety [79] that is, in turn, significantly involved in the oxidation process and, consequently, in the definition of the HOMO energy. Accordingly oxidation could be best described as a $[Ru(R\text{-}quin)]^{2+/+}$ couple (Figure 21) than a simpler $Ru^{3+/2+}$ couple like in **N3** or similar dyes; this is justified by the increased delocalization of the positive charge offered by the electron-rich oxyquinolate moiety, which would be more favoured in **D2** thanks to the presence of electro releasing methyl groups. Actually the smaller negative shift of the oxidation peak going from ligand **Me$_2$-quinH** to corresponding complex **D2** respect to the non-methylated couple (*i.e.* 0.15 V *vs* 0.3 V, respectively) could also be regarded as the HOMO being in this case more similar to the ligand one, *i.e.* with a higher ligand contribution, with respect to the parent compound **D1**. Even if we did not perform quantum calculations on our complexes, thanks to the voltammetric results we can also argue that LUMO was mainly localized on the **dcbpy** similarly to practically all other polypyridyl Ru-based dyes; in this way a quite good polarized donor-acceptor structure was created in the complexes, potentially improving the electron injection into TiO_2 and, at the same time, limiting the parasitic back-electron transfer due to the good capability of oxyquinolate moiety to attract and stabilize the resulting positive charge.

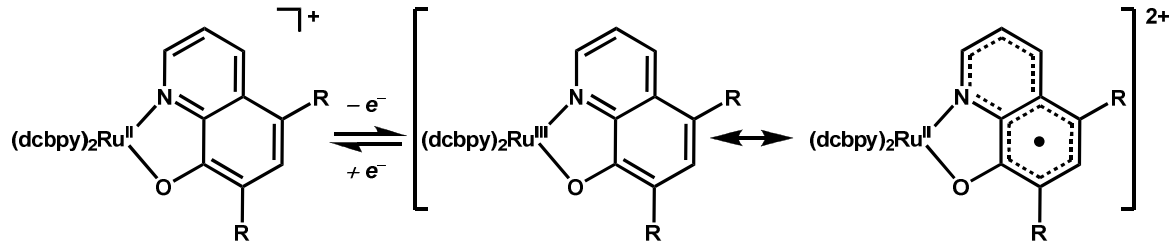

Figure 21 Anodic conversion (backward and forward reaction) of D1 and D2 dyes; resonance forms involving oxyquinolate moiety for the dye^{+} species are depicted.

[4] Evaluated from DPV patterns; $E^{0(dye+|dye)} \approx E_{p,anodic} + \Delta E/2$, where ΔE is the modulation amplitude equal to 0.05 V in this case [57]. The value referred to SHE was obtained as $E^{0(dye+|dye)}$ (*vs* SHE)=$E^{0(dye+|dye)}$ (*vs* SCE)+E_{SCE} (*vs* SHE), with E_{SCE} (*vs* SHE)=0.244 V *vs* SHE [57]. For sake of comparison with CV shown in Figure 20, in our experimental conditions $E_{1/2}^{Fc+|Fc}$ was *ca.* 0.47 V *vs* SCE, in DMF.

Concluding this electrochemical discussion it is interesting to note that the metal-centred ET is characterized by a higher electrochemical reversibility than in parent **N3** dye; this observation confirmed the similarity of our **D1** and **D2** dyes to cyclometalated **YE05** sensitizer from both an optical and electrochemical point of view. Oxyquinolate-based **D1** and **D2** complexes are slightly more oxidizable than both analogue NCS-free **YE05** and thiocyanate-based **N3** probably due to the higher stabilization of dye^+ species offered by oxyquinolate moiety (Table 2). In some how the increased stabilization of oxidized form could derive from the more stable 5-member cycle Ru-N-C-C-O resulting from the coordination of the metal atom with the N^O terminals of the oxyquinolate moieties respect to the 4-member cycle resulting from the cyclometalated phenylpyridine in **YE05**.

Table 2 Standard potentials, E^0, of the sensitizers discussed in the text above.

dye	E^0 *vs* SHE /V	reference
D1	0.96	this work
D2	0.86	this work
YE05	1.08	39
N3	1.10	34

DSSC tests

Acquired the basic spectroscopic and electrochemical information for **D1** and **D2** complexes we tested them as sensitizer for TiO_2 photoanode then assembled in a sandwich-type DSSC together with a platinised fluorine tin oxide, FTO, electrode acting as cathode. The assembling and tests were performed by professor Alessandro Abbotto (Università degli Studi di Milano-Bicocca) and his colleagues at MIB-Solar Center (Solar Energy Research Center, Milano). For these measurements a classical double layer screen printed photoanode were employed; it consisted of a first transparent layer (10 μm) of TiO_2 nanoparticles covered with a scattering layer (4 μm) constituted by TiO_2 particles with a diameter of 20 nm and 150-250 nm respectively. See experimental section or reference [80] for other details.

Dyes were tested with electrolytes containing the common I_3^-/I^- redox couple; different compositions were formulated varying the nature and the quantity of some common additives employed to optimize cell performances. Before reporting the results of DSSC tests I will briefly summarize the effects of more common additives. As just mentioned in the introduction, one of the most famous additive is 4-*tert*-butylpyridine, tbpy, which commonly brings to an increase in V_{oc} ascribed to an elevation of the flatband potential of TiO_2 film [49], or to a decrease of the charge recombination kinetics by a simpler passivation effect of the adsorbed heteroaromatic base [34], or to a synergic effect between them. In both cases the less negative energy of the Fermi level or the

"physical barrier" can bring to a decrease of the efficiency in the electron injection from dye^+ species. Other useful additives employed in our experiments are two cations, lithium and guanidinium ions respectively. Their have a common effect, in some how opposite to that of tbpy; in fact these cations generally bring to an increase of photogenerated current, mainly improving the electron injection (due to the conduction band edge shift toward lower energies, especially for Li^+) [85] or hampering charge recombination at the TiO_2 interface (by creation of a self-assembled monolayer with dye molecules, especially for the bulkier guanidinium ion) [86]. In any case many experimental results demonstrated that a suitable combination of N-containing Lewis basis and cations allow to obtained very interesting cell performances, probably due to a synergic effect.

Coming back to our tests, the best performing electrolytes was formulated mixing in a acetonitrile/valeronitrile 85:15 (v/v) solution the following components: 0.6 M N-butyl-N-methyl imidazolium iodide, 0.03 M I_2, 0.10 M guanidinium thiocyanate and 0.5 M tbpy. Moreover the effect of another common additive was also checked named chenodeoxycholic acid, CDCA. It is a de-aggregating agent that was co-adsorbed with the dye onto the metal oxide surface of the photoanode during the sensitization step (some authors suggested that higher stability of the photoanode can be obtained directly adding the acid into the electrolyte solution [50]).

Unfortunately no extraordinary results (Figure 22) were obtained with neither **D1** (accordingly to the parallel but independent work of Graetzel [79]) nor **D2**, even if a neat increase in both V_{oc} and *FF* where obtained in our measurements respect to the value reported by Graetzel for **D1**. Photon-to-current efficiency, PCE, recorded in our experiments were around 1% under 100 mW cm^{-2} AM1.5 G simulated illumination, with a maximum of 1.2% and a j_{sc}=3.5 mA cm^{-2} recorded with a photoanode sensitized by **D1** with CDCA as co-absorbent (CDCA:**D1** molar ratio 1:1 in the sensitization solution). For sake of comparison in the same virtually identical cell equipped with the same electrolyte but sensitized with **N719** dye reached a PCE of *ca.* 7% (Table 3).

Table 3 Main photovoltaic parameters for solar cells sensitized with D1 and D2.

Entry	dye[a]	additive	i_{sc} /mA cm^{-2}	FF	V_{oc} /V	PCE %
1	D1	–	3.1	0.66	0.48	1.0
2	D1	CDCA[b]	3.5	0.67	0.50	1.2
3	D2	–	2.8	0.70	0.51	1.0
4	D2	CDCA[b]	1.4	0.65	0.49	0.4

[a] Dye solution $2 \cdot 10^{-4}$ M in ethanol. [b]Added directly into the dye solution in 1:1 molar ratio (CDCA/dye).

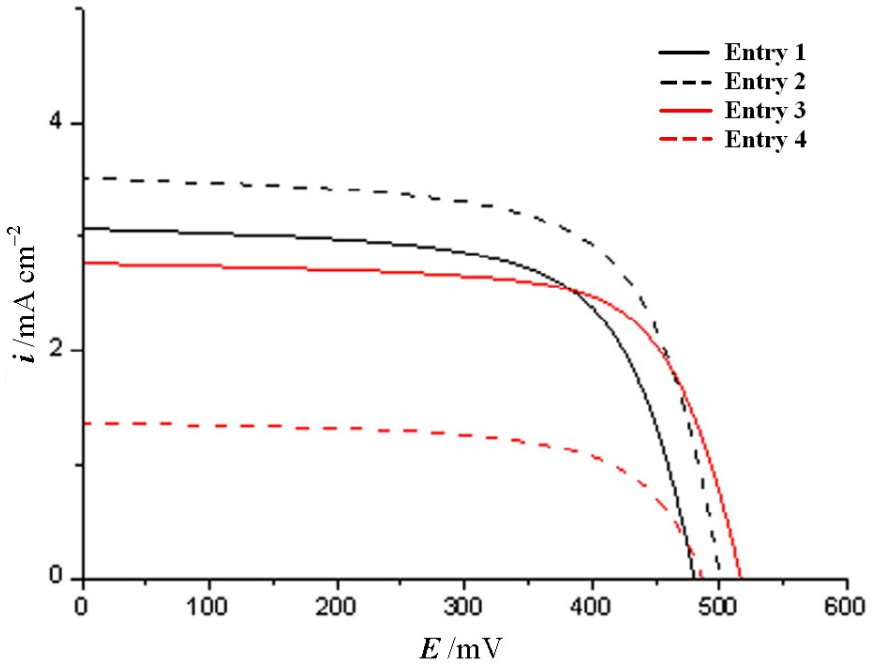

Figure 22 Synopsis of *iE* characteristics of the DSSCs reported in Table 3. Modified from ref. [80].

In all cases V_{oc} ranged between 480 and 515 mV for cell with **D1** and **D2**. The quite low photovoltages can be explained by a fast recombination process both through the same dye^+ specie or through the oxidized form of the redox mediator. Data that can in some extent recognize in the $e^-_{(TiO2)}$ + dye^+ recombination process the main potential responsible for the low efficiency it could be the significantly higher reversibility of both oxyquinolate-base dyes respect to **N3** (and **N719**) that could play a negative effect reducing the energy barrier of the parasitic electron transfer. At the same time the higher stabilization of the oxidized dye offered by oxyquinolate scaffold respect to thiocyanate-analogue **N3** and **N719** (Table 2) can limit the rate of dye regeneration reducing of *ca.* 150 mV the still considerable driving force, promoting the undesired e^-/h^+ recombination. On the other hand the poor photogenerated currents could not be attributed to a non perfect balance between the energy level of the semiconductor conduction band and that of the photoexcited charge-transfer state of the dye. Assuming that the excited state energy can be approximately described by the LUMO level, on the basis of $E_{p,Ired}$ values our dyes have LUMO levels higher in energy of *ca.* 0.1 eV than **N3**, resulting in an increased driving force for the electron injection. Possible explanation could be found in a non uniform distribution of dye molecules on the TiO_2 surface; in fact, at least with **D1**, co-adsorption of CDCA slightly increased the photocurrent generated by the device (entry 2 *vs* entry 1, Table 3). Unfortunately clear and easy explanation for the worst performance of **D2** dye were not found. In fact, contrary to expectations, cell sensitized with this dye showed higher V_{oc} (notwithstanding the lower driving force for dye regeneration) and better *FF*, but a (slightly) lower photocurrent even if both maximum absorbance and optical onset of **D2** were red shifted respect to **D1** analogue.

In conclusion much more work has to be performed to better elucidate the behavior of this new class of sensitizers, including for example electrochemical impedance spectroscopy measurements able to give information on the actual extent of recombination by oxidized form of mediator and transient absorption spectroscopy study through laser photolysis measurements to analyze the dye regeneration kinetics. Concerning the potential chemical modification of the quite simple hydroxyquinoline ligands employed in this first screening, improvements may result from extending their π-conjugation system in order to increase the optical properties; the functionalization with electron rich scaffold such as thiophene units will be encouraged in order to maintain the directional dipolar structure just described (*i.e.* LUMO on the anchoring **dcbpy** ligands and HOMO on the mixed Ru-oxiquinolate scaffold pointing away from the TiO_2 surface toward the electrolyte).

Pyrid-2-yl tetrazolate dye family

Synthesis

Inspired by the already mentioned work [75] showing the beneficial effect of increasing the number of nitrogen atoms in the five-member ring of (pyrid-2-yl)azolate ligands in Ru(II)-dyes we decided to design a new family of polypyridyl thiocyanate-free Ru(II) sensitizers substituting the labile monodentate NCS ligands with a N^N anionic *5-(4'-R-pyrid-2'-yl)tetrazolate*. These chelating ligands link to a pyridine the most nitrogen enriched heteroaromatic five-member ring, the tetrazole. According to the just mentioned sequence of nitrogen-enriched azole the best performance should be expected combining pyridine with pentazole, the five-member "heterocyclic" ring fully constituted by nitrogen atoms. Unfortunatly this "exotic" pentazoles (including its derivates) are very unstable and often highly explosive compounds, much more than tetrazoles. So we decided to limit to four the number of nitrogen atoms in the azole ring, preparing for the first time in literature Ru(II) sensitizers bringing 5-(4'-R-pyrid-2'-yl)tetrazolate ligands.

Tetrazoles are unknown compound in nature; they were prepared in laboratory for the first time [87] at the beginning of XXI century thanks to the synthesis of 5-aminotetrazole (used many years later as one the components in automobile airbag). The pristine heterocycle tetrazole was firstly prepared only nine years later, in 1910. In both cases quite hazardous reactions were carried out, employing the toxic, explosive and volatile hydrazoic acid in combination with the appropriate cyanide (also toxic). Nowadays tetrazoles are largely diffused in medicinal chemistry (being metabolically stable surrogates, *i.e.* bioisosteres, for a carboxylic acid unit) [88], in material sciences (as specialty explosives), in metallurgy (as corrosion inhibitor agents) [89], and in coordination chemistry (as ligands). In the challenge for the development of easier, cheaper and safer synthetic procedures for the synthesis of tetrazole derivates the paper of Sharpless and co-workers [90] can be considered a milestone work. It implied the addition of an inorganic azide, *i.e.* sodium azide, to an aqueous solution (or suspension) of an organic nitrile in presence of stoichiometric amounts of low-cost Zn(II) salt. It is a quite robust procedure, which allows to use a great variety of aryl and alkyl nitrile substrates. Interestingly is also the possibility to substitute the inorganic azide with trimethylsilyl azide, $TMSN_3$, working in presence of a catalytic amount of tetraalkylammonium fluoride salt [91] avoiding the use of metal and allowing solventless conditions. Other papers reported possibility to employ MW to increase reaction yields working with high boiling organic solvents like dimethylsulphoxide or dimethylformamide.

Among dipolarophiles proposed by Sharpless [90] for the [2+3] *dipolar cycloaddition reaction* the electron-poor 2-cyanopyridine was of particular relevance for our scopes; it reacted quite fast at

refluxing condition. Moreover authors verified that no (or, at most, a minimum amount) toxic and volatile hydrazoic acid was produced in the optimized conditions involving 1 eq. of $ZnBr_2$ and 1.1 eq. of NaN_3 respect to the reacting nitrile. The basic pH of the working medium helped to limit the volatile acid production. In similar experimental condition but employing DMF as solvent (one of the more common way of carrying out the tetrazole synthesis) authors verified a huger production of hydrazoic acid.

In the tetrazole synthesis, according to the general mechanism of a 1,3-dipolar cycloaddition reaction, the pyridinecarbonitrile acts as the dipolarophile while the azide is the 1,3 dipole which shares four electrons in the π-systems over its three nitrogen atoms. Actually the exact mechanism of the addition of the azide ion to the organic nitrile is still under debates [90] with evidences supporting both a two-step and a [2+3] concerted pericyclic mechanism (Figure 23).

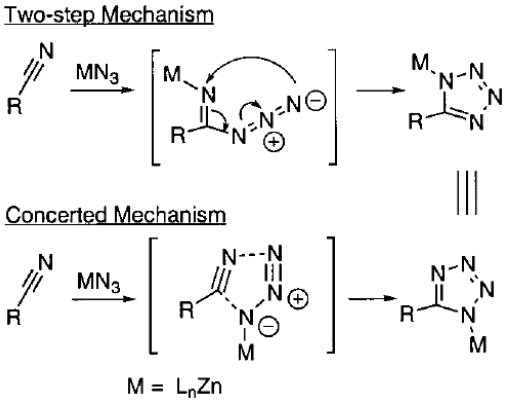

Figure 23 Schematic representation of the two proposals describing the tetrazole synthesis by addition of an azide to a nitrile: two-step mechanism (top) and concerted pericyclic mechanism (bottom). Adapted from ref. [90].

For all these reasons we decided to exploit the safe and optimized protocol developed by Sharpless for our aims: the synthesis of a series of 5-(*p*-substituted-pyrid-2'-yl)-1*H*-tetrazole, then employed for the preparation of new NCS-free Ru(II) sensitizers to be tested in DSSCs. For completeness the 5-(6'-mesityl-pyrid-2'-yl)-1*H*-tetrazole, **6-Mes-TetraH**, (entry 7 of Table 4) is also reported in the scheme below, but it is a ligand designed and employed for the second part of the thesis dealing with luminescent copper(I) neutral complexes; in any case its discussion will be postpone to the second part of this thesis, entitled "Heteroleptic luminescent Cu(I) complexes".

In Table 4 have been listed only molecules actually isolated and characterized. (See experimental section for more details and for characterization data). Concerning the 4-substituted tetrazoles the functionality introduced can be classified into two distinct families, electron withdrawing halogen groups (characterized also by π-donating ability), and aromatic π-delocalizing and/or electron releasing substituents. Tetrazoles in Table 4 have been assembled according to this classification to

make clear the rationalization of the chemical modification of the common 5-(pyrid-2-yl)tetrazole scaffold.

Table 4 Synthetic pathway for the preparation of *para*- (and *orto*-) substituted 5-(R-pyrid-2'-yl)-1*H*-tetrazoles.

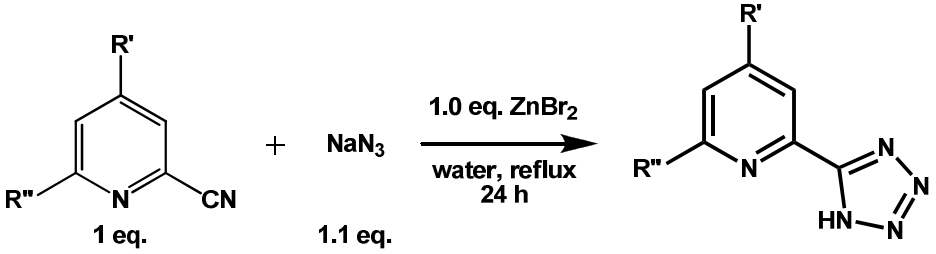

TetraH: R'=H, R''=H
Cl-TetraH: R'=Cl, R''=H
I-TetraH: R'=I, R''=H
Ph-TetraH: R'=Ph, R''=H
(*p*-Me$_2$N)Ph-TetraH: R'=(*p*-Me$_2$N)phenyl, R''=H
Th-TetraH: R'=2-thienyl, R''=H
6-Mes-TetraH: R'=H, R''=mesityl

entry	R'	R''	yield[a]
1	H	H	76%
2	Cl	H	82%
3	I	H	37%
4	Ph	H	75%
5	*p*-(Me$_2$N)Ph	H	10%[b]
6	thien-2-yl	H	40%
7	H	Mesityl	44%[c]

[a]Averaged values, on the isolated product. [b]Some difficulties were encountered during the precipitation, probably for the presence of the second basic site. [c]Reaction does not go to completeness and some reagent was recovered. Yield was calculated on the actual reacted cyanopyridine.

Other two tetrazoles were studied but to date we have been not able to isolate them; they will be discussed below after the description of the syntheses of carbonitrile intermediates, **I-1** – **I-5**.

4-R-2-cyanopyridine intermediates

Only three cyanopyridines employed as precursors to construct the tetrazole ring were commercially available; they were the pristine 2-cyanopyridine and its 4-chloro and 4-phenyl derivates. In other cases suitable reactions have been performed starting from the just mentioned 2-cyano-4-chloropyridine by a direct one-step reaction (in only one case) or, more often, by a two-step pathway that passed through the 2-cyano-4-iodopyridine, **I-1**, intermediate. In the following pages the syntheses of these carbonitrile scaffolds will be reported; except for the common intermediate **I-1** reported as first, other molecules were assembled according to their expected properties in order to make clearer the rationality that driven their chemical design.

2-cyano-4-iodopyridine, ***I-1***

It was an unknown compound in literature excepts for few medicinal patents (only ten up to 2012) containing the molecule in question as potential intermediate of the final biologically active compound; however no information regarding its synthesis or characterization have been found. Pyridinecarbonitrile **I-1** revealed a very useful and polyhedral intermediate; in fact the more labile C-I bond (respect to C-Cl bond of the starting chloro-analogue) allows an increased reactivity in reaction involving C-C bond formation such as Sonogashira, Stille and Suzuki cross-coupling (see below). **I-1** was synthesised through a microwave-assisted literature protocol (Scheme 2) developed for the trans-halogenation of various chloro-, bromo- and pseudohalogen-substituted quinolines, isoquinolines and pyridines [92].

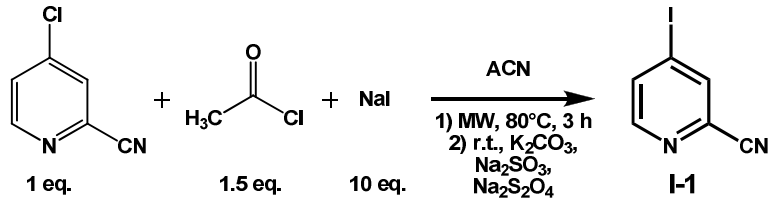

Scheme 2 Trans-halogenation reaction for the synthesis of I-1.

The reaction proceeds through an aromatic nucleophilic substitution reaction, S_NAr, facilitated by the acylation of the ring nitrogen of pyridine through. The resulting acetyl-pyridinium cation makes the C-Cl bond breaking easier by the nucleophile iodide deriving from inorganic salt NaI added in large excess (*i.e.* 10-fold excess) in order to ensure a much higher iodide than chloride ion concentration in the reaction mixture. Experimental conditions require the heating at 80°C through MW of the acetonitrile-based reaction solution for 3 hours; so the protocol ensure milder condition and shorter reaction time than those employed in other trans-halogenation protocols (*e.g.* T>100°C, strongly acidic conditions such as presence of hydroiodic acid, and reaction time longer than 24 hours). The MW-assisted reaction was scaled without problems from 100 mg up to *ca.* 400 mg of the starting chloro-derivate. The synthetic pathway was completed by a simple and fast work-up involving few liquid-liquid separation steps, and by a fast purification of the crude mixture through SiO_2 flash-column which gave the pure desired **I-1** product with a 52% average yield. (See experimental section for more details and for characterization data)

2-cyano-4-(ethynylphenyl)pyridine, ***I-2***

The cyano intermediate **I-2** was prepared with the aim of studying the effect of an (alkyl) spacer between the pyridine and the phenyl rings on the π-delocalization character of the resulting tetrazole derivate and its influence on the optical and light harvesting properties of Ru(II) dye, to be compared with the sensitizer bringing the **Ph-TetraH** ligand in which the two aromatic rings are directly linked.

First syntheses were carried out via Sonogashira cross-coupling reaction directly performed on the commercially available 4-chloropyridinecarbonitrile following a literature procedure [93]. It was proposed as an efficient Cu-free MW-assisted procedure for the coupling of a terminal alkynes (such as phenyl acetylene) with a great variety of electron-rich, electro-neutral and electron-poor aryl chlorides, a quite hard task due to the poor reactivity of C-Cl bond. Among the tested aryl chlorides 3-chloropyridine was the species more similar to our substrates, and it gave raised a quite high conversion. Unfortunatly working both in exactly identical conditions (except for the substitution of P(*t*-Bu)$_3$ phosphine with the quite similar electron-rich PCy$_3$), entry 1, and slightly changing reaction conditions (*i.e.* temperature and reaction time), entry 2, we were not able to isolate the desired product (Table 5).

Table 5 Different pathways proposed for the synthesis of I-2 intermediate.

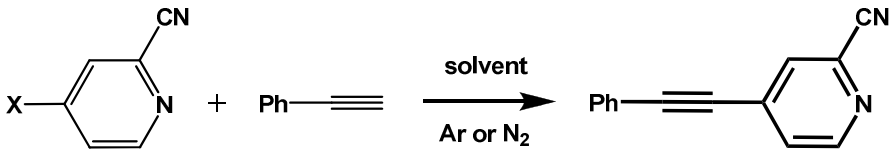

I-2

entry	X	solvent	catalyst	phosphine	base	time and temp.	yield[a]
1	Cl	DMF	$PdCl_2(PPh_3)_2$ + DBU	PCy_3	Cs_2CO_3	10 min 150°C (P_{MW} = 250W)	–
2	Cl	DMF	$PdCl_2(PPh_3)_2$ + DBU	PCy_3	Cs_2CO_3	15 min 160°C (P_{MW} = 250W)	–
3	I	TEA/THF 2:1	$PdCl_2(PPh_3)_2$ + CuI	PPh_3	(TEA as co-solvent)	24 h reflux	< 10%
4	I	H_2O	$Pd(PPh_3)_4$ + CuI	–	DIPEA	24 h r.t.	71%

[a] On the isolated product.

We also tried to obtained the final desired product 5-[4-(ethynylphenyl)pyrid-2yl]-1*H*-tetrazole directly starting from **Cl-TetraH** as substrate and applying both the same aforementioned experimental protocol and a classical Cu(I)-catalyzed Sonogashira reaction. In both cases no interesting results were obtained.

Having the possibility to substitute the low reactive -Cl with the much more interesting -I in sufficiently good yield (Scheme 2), we decided to perform the desired alkyne/arene cross coupling on the more reactive **I-1** intermediate. Also in this case two different procedures (Table 5) were adopted giving raise in both cases to the desired pure product, but with a great difference in term of

time requested for the purification and of final yields. In fact the crude mixture obtained by entry 3 was very complex with at least five or six UV visible TLC spots, many of which with very similar retention factors hardly separable through chromatographic column; this difficulty forced to search for a more feasible synthesis that was reported in entry 4 of Table 5. It was found out in a quite innovative Cu(I)-assisted Sonogashira reaction that employs water as the reaction solvent, so avoiding toxic and also usually more expensive organic solvents. As underlined by same authors [94] it was the first efficient procedure reported for the palladium-catalyzed cross coupling reaction of π-deficient iodoheteroaromatics in water. Applying this reported procedure the synthesis of **I-2** were carried out with quite high yield (the average value on pure isolated product was 71%) after a liquid-liquid extraction and a very easy and fast purification of the crude via SiO_2 flash chromatography. (See experimental section for more details and for characterization data)

2-cyano-4-(1'-ethynylpyrenyl)pyridine, ***I-3***

As a natural prosecution of the π-conjugation extension started with ethynylphenyl-derivate **I-2**, the cyanopyridine **I-3** was designed by substituting the simple phenyl ring with the highly conjugated tetra-ring fused analogue pyrene. In collaboration with the colleague Dr. Filippo Nisic **I-3** was obtained through a three-step procedure starting from the commercially available 1-Br-pyrene(Scheme 3).

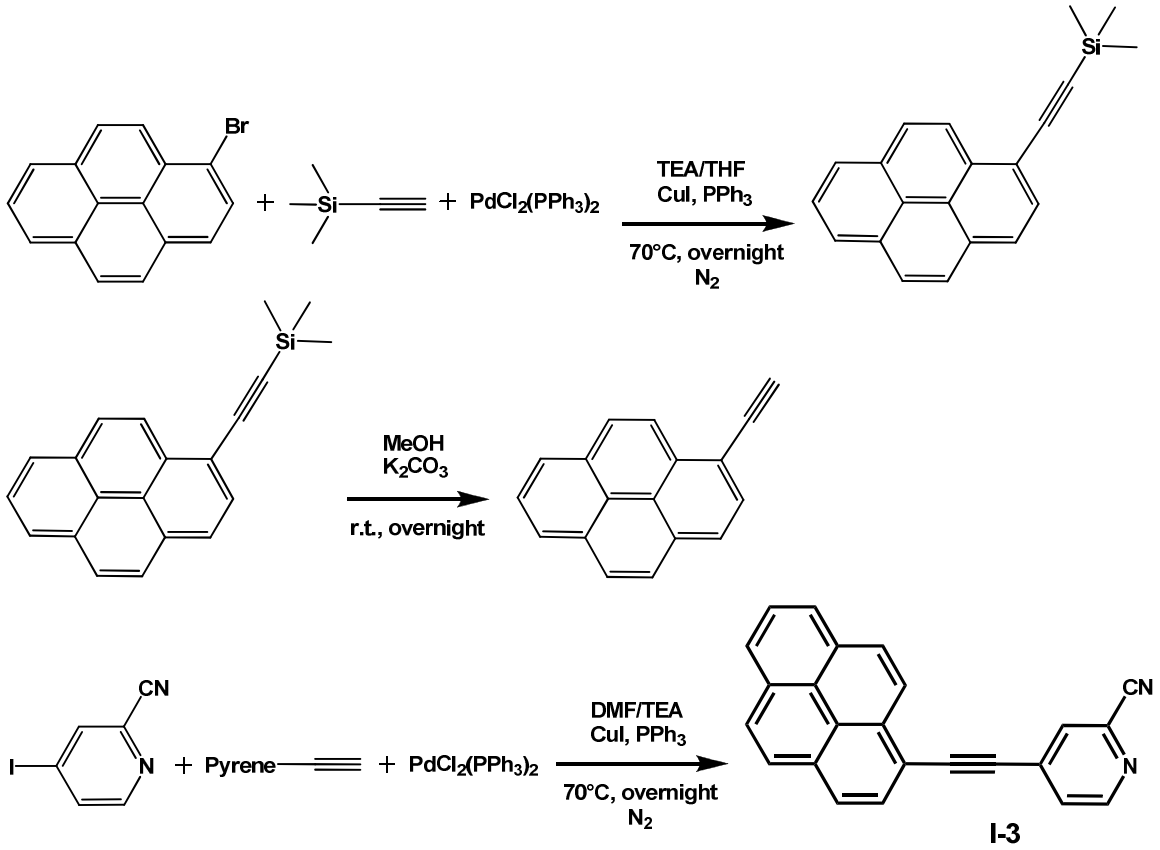

Scheme 3 Three-step pathways followed for the synthesis of I-3 intermediate.

In the first step alkynylation of bromopyrene was obtained by reacting it with ethynyltrimethylsilane in presence of Pd catalyst, followed by the deprotection of the alkynyl group by treatment with K_2CO_3 in methanol. Finally cross-coupling via Sonogashira reaction was performed to obtain the desired cyanopyridine **I-3**.

2-cyano-4-(4'-(N,N-dimethylamino)phen-1'-yl)pyridine, ***I-4***

Similarly to the **I-2** and **I-3** cases the intermediate **I-4** was designed to study the combination of the increased delocalization with the electron richness by means of the addition of the well-known electron releasing dialkylamino substituent on a phenyl ring.

In this case a Suzuki cross-coupling reaction was chosen to combine through a C-C bond the boronic derivate of the electro releasing *p*-dimethylaniline with the haloheteroaromatic scaffold (Scheme 4); in this case the commercially available chlorinated pyridinecarbonitrile was direcly employed as starting reagent due to the significantly higher reactivity of the C-Cl bond toward such type of cross-coupling respect to the analogue Sonogashira reaction. Experimental condition was inspired from a literature procedure [95] without a deep optimization of the conditions; **I-4** was isolated after chromatographic purification of the crude mixture in a quite low yields (*ca.* 20%) because 24 hours of reaction was not sufficient to completely convert the reagents. (See experimental section for more details and for characterization data)

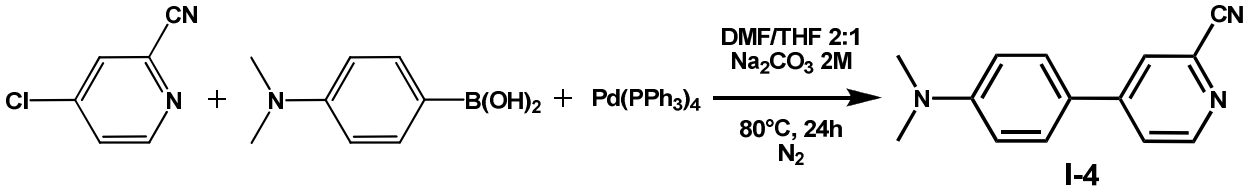

Scheme 4 Schematic procedure for the synthesis of I-4 intermediate.

2-cyano-4-(thien-2'-yl)pyridine, ***I-5***

Coherently with the route started with the three immediately preceding intermediates devoted to develop pyridyl-tetrazoles with π-extended and electron-rich structures, the intermediate **I-5** was synthesized by directly attaching through a C-C bond the electron-rich thienyl ring to the pyridine scaffold in order to combine in an unique substituent both the wanted properties (*i.e.* π-delocalization ability and electron releasing nature).

I-5 was obtained by means of a third type of cross-coupling reaction, the Stille reaction, which allows the C-C bond formation between an organic electrophile and an organotin compound via palladium-catalyzed reaction. Generally speaking the reaction involved a sp^2-hybridized carbon atom of an halo- (or pseudohalo-) allyl, alkenyl or aryl compound, which acts as electrophile, with a sp^2- (or in some specific cases sp^3-) hybridized carbon of a trialkylstannane. In the specific case of under examination **I-5** product was obtained through a synthetic procedure commonly used in our

laboratory (Scheme 5) combining the more reactive iodo-pyridinecarbonitrile **I-1** and the tributylstannilthiophene in presence of bis(triphenylphosphine)palladium(II) dichloride as catalyst. The desired cyanopyridine was isolated in a quite reasonable yields (*i.e.* average value 68%) after a classical extraction step followed by a very simple purification via SiO_2 flash chromatography. (See experimental section for more details and for characterization data.)

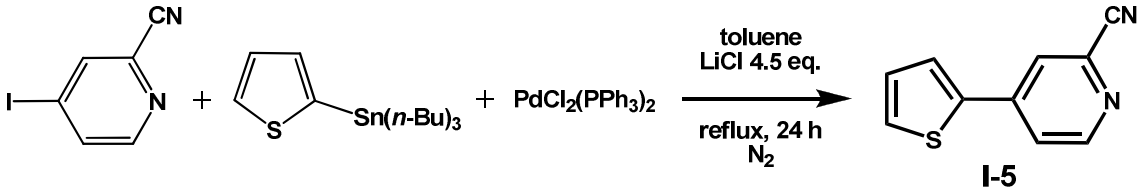

Scheme 5 Schematic procedure for the synthesis of thiophene-containing I-5 intermediate.

5-(4'-R-pyrid-2'-yl)-1*H*-tetrazoles

The just concluded subchapter presented the series of five 4-substituted pyridinecarbonitrile platforms on which (together with other three purchased substrates) the related 5-substituted-1*H*-tetrazoles were constructed as described in Table 4. To date, as well described below, only in two cases we have not been able to isolate the desired product; in fact the main limitation and problem of the water-based tetrazole synthesis followed here was the pour solubility (or even complete insolubility) of the starting cyanopyridine, especially when a lipophilic portion was added to the basic 2-cyanopyridine scaffold.

Moreover an isoquinoline-based tetrazole was also synthesised with the aim of further increasing the π-delocalization ability of the ligand and hence potentially increase the light harvesting of the resulting Ru(II) dye.

5-(4'-(ethynylphenyl)pyrid-2'-yl)-1H-tetrazole

Unfortunately the step of formation of the titled tetrazole ring on the cyano **I-2** precursor through Sharpless' procedure [90] failed. Possible explanation can be the complete insolubility of the intermediate in water. In the future we will try to modify the reaction medium, adding for example a small aliquot of organic solvent (possibly highly volatile) than can be evaporated before the final basification-acidification step.

5-(4'-(1''-ethynylpyrenyl)pyrid-2'-yl)-1H-tetrazole

In this case reaction medium was a mixture 2:1 acetone/water in order to increase the solubility of the lipophilic **I-3** and hence its potential conversion in the product. The work-up was also slightly modified because no precipitation was observed after the classic basification/acidification step. Even if to date we have not been able to isolate the desired tetrazole we obtained experimental proof of its formation through both ^{1}H-NMR and, first of all, mass spectrometry technique (working

in cation chemical ionization, CI^+, mode the peak at *m*/*z*=371 was recorded). Future work will be focused on the isolation of the desired product.

5-(isoquinol-1'-yl)-1H-tetrazole

The product **TetraH-Isoquin** was synthesised in good yield applying the same identical procedure employed for analogue pyrid-2-yl derivates starting from the commercially available 1-isoquinolinecarbonitrile (Scheme 6).

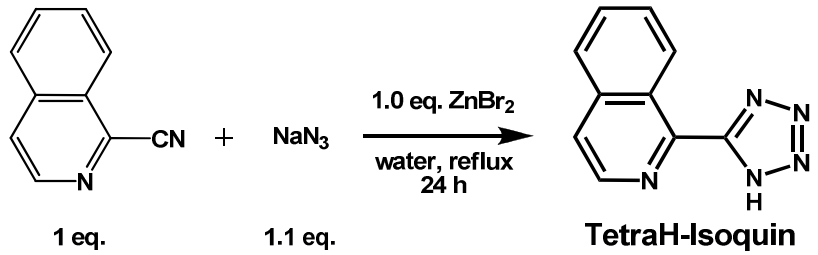

Scheme 6 Synthetic pathway for the synthesis of 5-(isoquinol-1'-yl)-1*H*-tetrazole.

[Ru(dcbpy)$_2$(4-R-Tetra)]Cl complexes

Tetrazolate complexes were synthesised employing the same two-step strategy developed for the oxyquinolate family. The *cis*-[$RuCl_2(dcbpy)_2$] precursor (obtained with an averaged yield of 45%) was subjected to chloride substitution with the appropriate tetrazole chelating ligand in refluxing methanol [96] (Table 6).

See the experimental part for the characterization of the complexes. To date not all the prepared tetrazoles were complexed with Ru(II), but the work will be surely continued in the very next future considering the quite promising results obtained in DSSC tests with the simpler Ru(II) sensitizers, **D1**-**D3**; in fact these data, which will be discussed in the following section, suggested that the introduction of π-delocalizing electron rich substituents (like **I-4** and **I-5**) could be the right way to increase cell efficiencies.

Table 6 The two-step pathway employed for the synthesis of tetrazolate-based Ru(II) sensitizers, D3-D6.

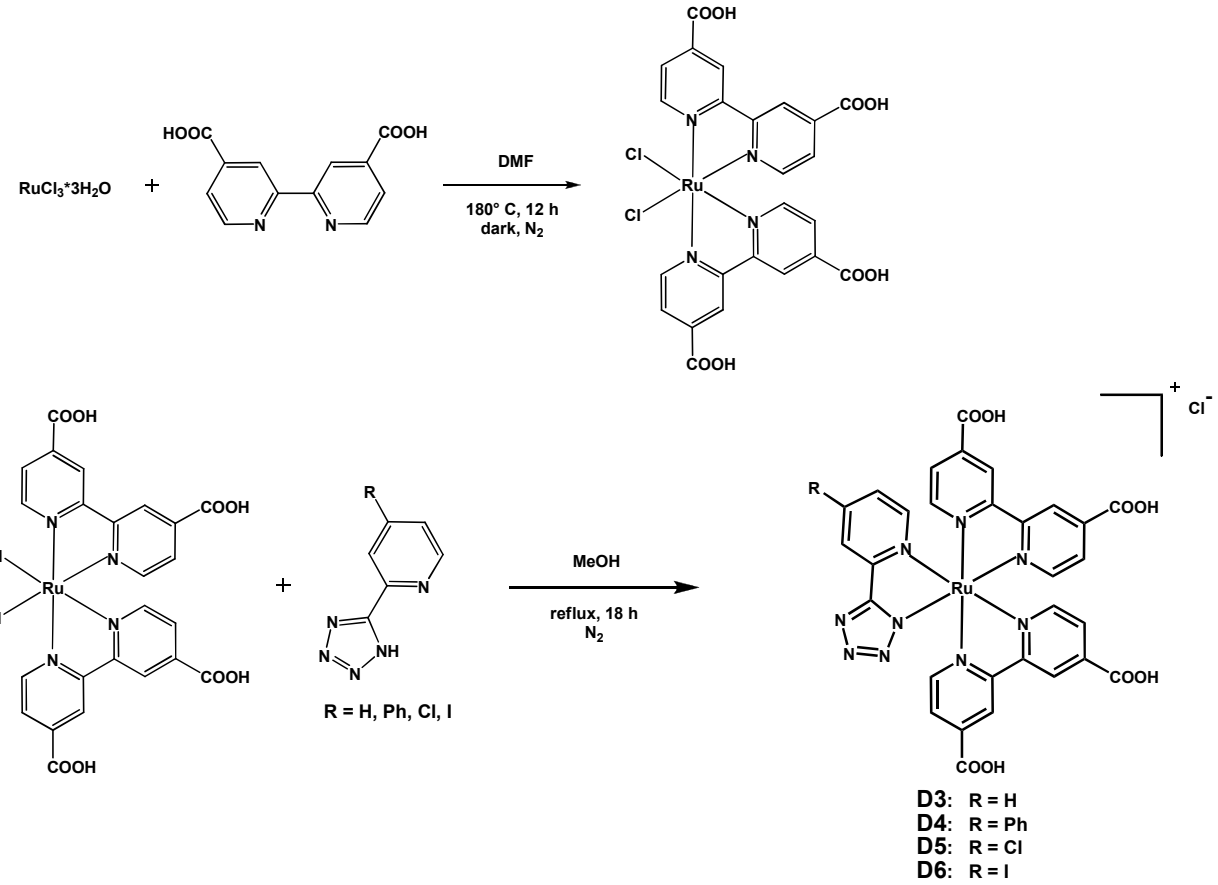

entry	tetrazole ligand	dye product	yield[a]
1	TetraH (R=H)	D3	51%
2	Ph-TetraH (R=Ph)	D4	48%
3	Cl-TetraH (R=Cl)	D5	45%
4	I-TetraH (R=I)	D6	12%[b]

[a]Yields are referred to the final tetrazole coordination step. [b]The quite low yield was attributed to the quite low amount of starting material that made the final precipitation a low efficient step.

Characterization

Electronic UV-visible spectra

The optical properties of **D3**-**D6** dyes were studied recording UV-visible spectra in ethanol (Figure 24). Similarly to oxyquinolate sensitizers a sharp intense electronic transition around 310 nm attributable to a singlet ligand-centred π-π^* excitation localized on the dcbpy ligands characterized the UV region of the spectra of tetrazole-based dyes. Strong analogies between the two families of Ru(II) complexes can be observed also for the visible part of the electronic spectra that showed two intense broad bands together with a third less intense transition all attributable to metal-to-ligand charge transfer processes. This last transition could contribute to a more efficient light-harvesting in

the region 350-500 nm respect to N3 dye, even if the absorption onset of the tetrazolate dyes resulted blue-shifted respect to the just mentioned NCS-based sensitizer. Theoretical calculations performed on **D3**, **D4** and **D5** dyes by the group of Dr. Filippo De Angelis (Computational Laboratory for Hybrid/Organic Photovoltaics, Istituto CNR di Scienze e Tecnologie Molecolari, Perugia) evidenced HOMOs with slightly differences in energy level upon variation of the substituents on the pyridyl ring and LUMOs levels practically isoenergetic [97]. In all cases (and probably also for **D6** analogue) HOMOs mainly involved the Ru atom and the tetrazole scaffold which contributes to stabilize the molecular orbital energy due to its mesomeric properties; on the contrary, as usual, LUMOs were centered on the carboxylated bipyridine ligands (Figure 24).

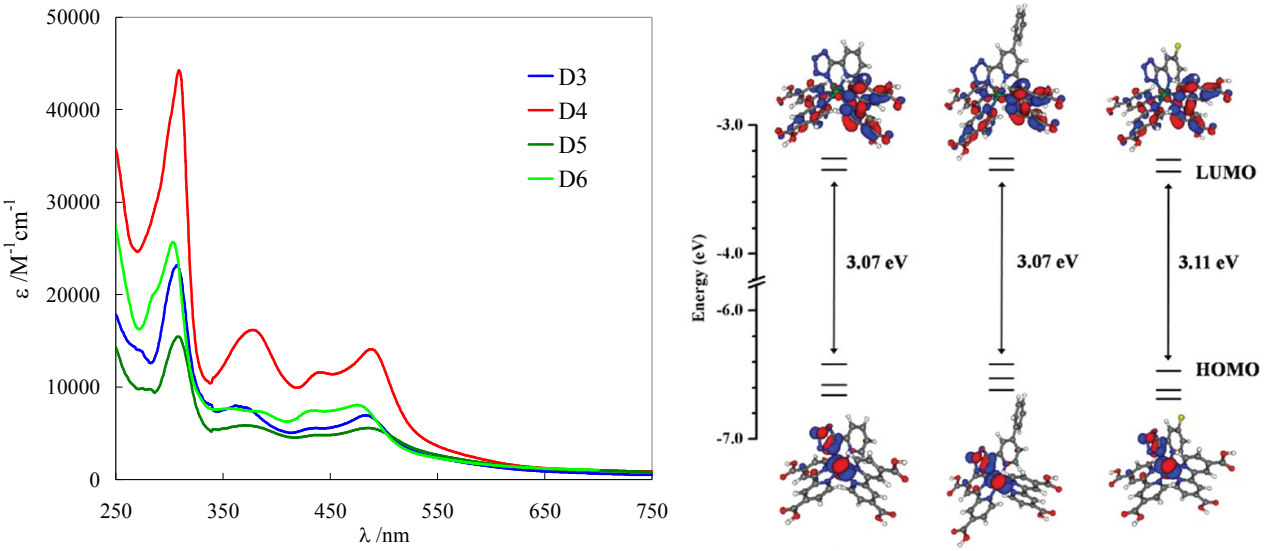

Figure 24 Left: UV-visible spectra of tetrazolate-based Ru(II) dyes in ethanol (left) and a schematic representation of the energy levels for in order D3, D4 and D5 with isodensity surface plots of their HOMO and LUMO molecular orbitals (right).

Voltammetric study

Similarly to the work carried out for the family of the oxyquinolate sensitizers **D1** and **D2** before characterizing the electrochemical behavior of complexes **D3-D6** a voltammetric study was performed in order to clarify the main electron transfer properties of tetrazole free ligands. This first step not only was necessary to better understand the electrochemical responses of the related complexes but it also contributed to enlarge the quite poor literature data on this family of heteroaromatic molecules [98], [99].

Voltammetric patterns recorded in DMF (Figure 25) revealed a quite high stability of the free ligands toward electrooxidation being absent any signals in the accessible anodic window. On the contrary the potential scan in the cathodic window exhibited only one monoelectronic reduction process except for **Ph-TetraH** which showed an additional neat monoelectronic, chemically irreversible and electrochemically quasi-reversible electron transfer process at a more negative potential ($E_{p,IIc}$ = –2.69 V *vs* $Fc^+|Fc$). The second reduction peak can be tentatively attributed to the

injection of a second electron on the phenyl pendant able to easily delocalized and stabilized the incoming negative charge. Respect to both 8-hydroxyquinolines tetrazole ligands revealed much more easily reducible species according to the higher electron withdrawing character of the five-member ring. Tetrazoles exhibited reduction potentials slightly more negative than that of 2,2'-bipyridine-4,4'-dicarboxylic acid except for **Ph-TetraH** species for which a comparable value was recorded.

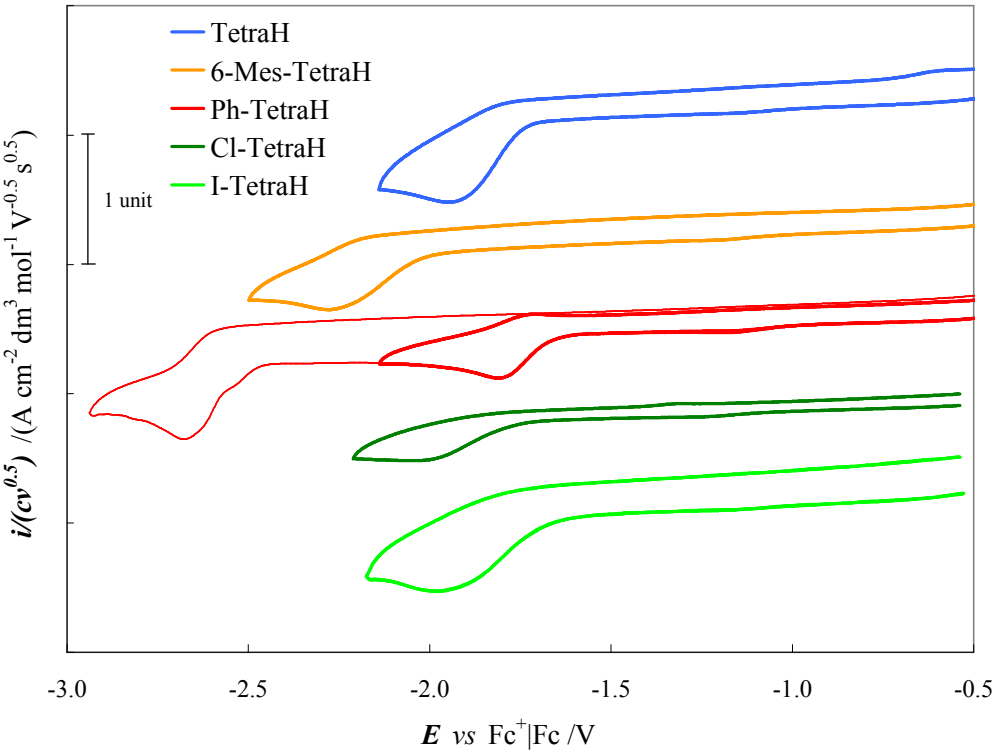

Figure 25 Synopsis of normalized cyclovoltammograms of the free-ligand tetrazoles. Concentration *ca.* 0.001 M in DMF and $TBAPF_6$ 0.1 M, scan rate potential 0.2 V s^{-1}, GC electrode.

The potential of the unique cathodic peak (or of the first one for **Ph-TetraH**) for all the 4-substituted tetrazoles was slightly modulated by chemical modification of the pyridyl ring and they ranged in a window narrower than 0.25 V, with **Ph-TetraH** and **Cl-TetraH** the easier and harder reducible species respectively. The quite low spread of peak potentials suggested that the sites involved in the reduction were far away from the pyridine moiety probably localized on the tetrazole ring itself. **Ph-TetraH** was the unique species which exhibited a slightly chemically reversible process due probably to the stabilization effect allowed by the π-delocalizing phenyl substituent. Similarly the 6-mesityl derivate was characterized by a reduction process with a similar level of chemical reversibility despite its quite negative potential ($E_{p,c}$ = –2.28 V *vs* $Fc^+|Fc$). In all cases the peak potential was shifted to more negative value respect to the *ca.* –1.4 V *vs* $Fc^+|Fc$[5] of

[5] The original value has been referred to the $Fc^+|Fc$ potential scale using as conversion constant $E_{1/2}^{(Fc+|Fc)}$ = 0.39 V *vs* SCE.

the forefather 1*H*-tetrazole [99].

A quite detailed study employing different electrode materials and working conditions was performed to elucidate in detail the nature of first electron transfer. Electrochemistry of tetrazoles is an almost unexplored research field especially for 5-(pyrid-2-yl) derivates. Partial information concerning the electrochemical properties of pristine tetrazole and of its 5-phenyl derivate can be obtained by a quite interesting work that correlated the potential of the backward anodic peak (associated to the oxidation of the anion electrogenerated during the forward cathodic scan from the corresponding protonated neutral species) with the nucleophilicity of the anion species [100]. Literature suggested that the electroreduction process involves an electron transfer that breaks the N-H bond with the concomitant formation of the nucleophilic anion and the liberation of H_2 gas (Figure 26).

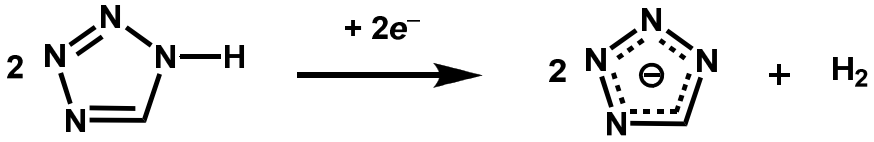

Figure 26 Schematic representation of the proposed electroreduction process for 1*H*-tetrazole.

To confirm this hypothesis two approaches were followed: *i*) the addition of a base able to deprotonate the tetrazole ring and *ii*) the study of the electron transfer process on a surface catalytic toward evolution of hydrogen. In the first case the progressive addition of NaOH solution (in DMF) to the pristine **TetraH** resulted in a progressive decrease and finally a complete disappearance of the cathodic signal coherently with the deprotonation of the species (see Gallery, Figure G 1). The voltammetric patterns recorded with different waiting time after each spiked aliquot suggested that the deprotonation reaction was kinetically slow; stable and superimposable signals were obtained only *ca.* 20-30 seconds after the addition. Same kind of measurements were also performed on **Ph-TetraH** (Figure 27) but no significant variation was induced to the second cathodic peak confirming that the effect of spiked NaOH was strictly confined to the ET process involving the acid site of the tetrazole.

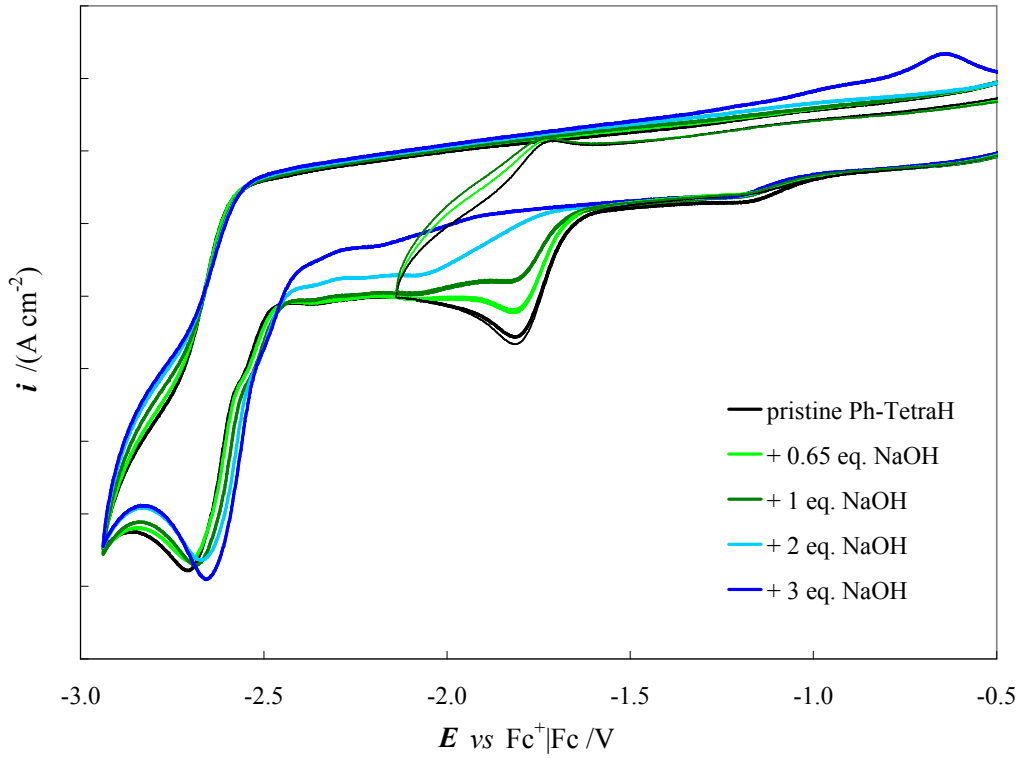

Figure 27 Synopsis of cyclovoltammograms of Ph-TetraH ligand (black lines) during subsequent additions of NaOH solution (in DMF). Concentration *ca.* 0.001 M in DMF and $TBAPF_6$ 0.1 M, scan rate potential 0.2 V s^{-1}. GC electrode.

For the second approach a series of representative tetrazoles were chosen and their voltammetric patterns were recorded on a platinum, Pt, electrode which is a well known catalytic material for the hydrogen evolution. The cathodic peak potentials were then compared with those obtained on a GC electrode taken as an inert reference electrode material in order to estimate the catalytic effect, C.E., computed as C.E. = $E_{p,c,Pt} - E_{p,c,GC}$. Considerable catalytic effects of about 0.5-0.6 V was calculated for the representative 5-(4-R-pyrid-2-yl)tetrazoles (Figure 28) suggesting the actual involvement of H atom abstraction and H_2 generation. As a further confirmation a catalytic effect was also observed with silver electrode, Ag (Figure 29); in this case a smaller positive shift of the peak potential was observed (*ca.* 0.1 V) according to the lower efficiency of silver as hydrogen evolution electrocatalyst. As explained just below the behavior of **I-TetraH** has not to be considered here due to a peculiar electrode/substrate interaction.

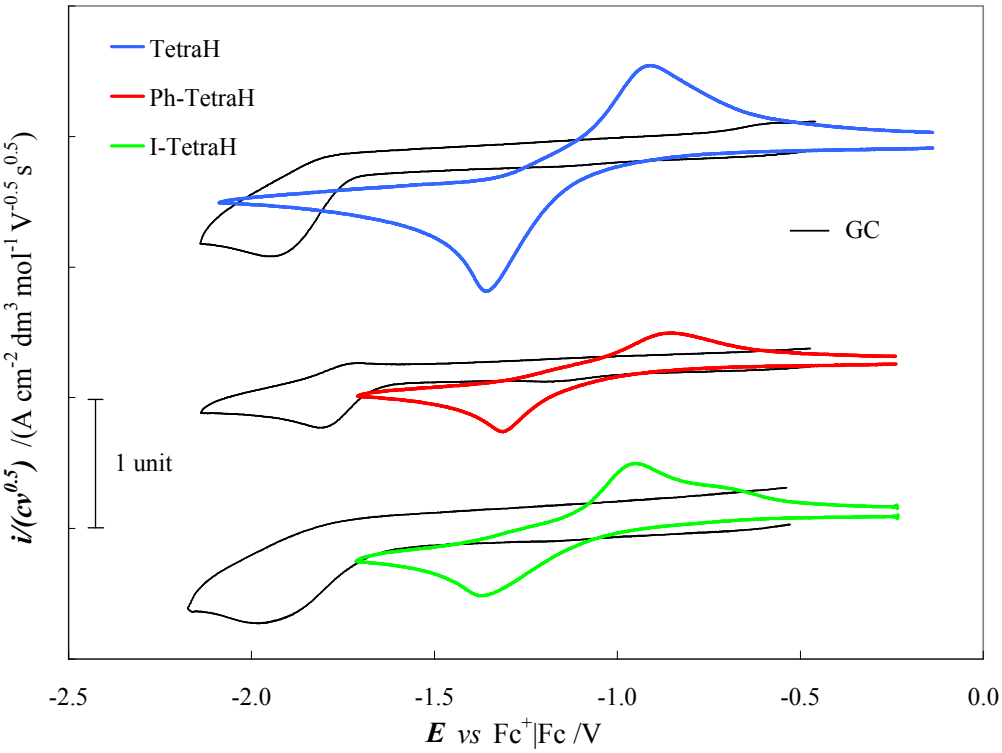

Figure 28 Normalized cyclovoltammograms of three representative tetrazoles recorded on Pt electrode (coloured thick lines). Concentration *ca.* 0.001 M in DMF and $TBAPF_6$ 0.1 M, scan rate potential 0.2 V s^{-1}. For sake of comparison the corresponding patterns recorded on GC electrode are also reported (thin black lines).

For sake of curiosity I wanted to verify if the carbon-halogen, C-X, bond in **Cl-TetraH** and **I-TetraH** was also electroactive. As just said on GC electrode the unique signal for both halo-tetrazole derivates were attributable to N-H electrocleavage and no peak attributable to a C-X was seen in the accessible potential window; the implementation of silver electrode, Ag, could be extremely useful due to its high catalytic behavior toward electrocleavage of C-X bond in organic compounds as well known in our research group [101] ,[102]. Moreover exploitation of Ag surface could be a very smart approach for the identification of the target bond due to the high selectivity of Ag for C-X bonds. **I-TetraH** was chosen as the best reference molecule considering not only the intrinsic weaker nature of C-I respect to C-Cl bond but also the increasing of Ag catalytic effect in the order Cl < Br < I according to the relative adsorption affinity of Ag for the halogen ion. The CVs (Figure 29) clearly showed a net variation in the peak height and morphology resembling peaks recorded in our laboratory for halo-aromatic compounds. Moreover the positive shift (respect to the same molecule recorded on GC) was significantly higher than that observed for halogen-free tetrazoles. Both proofs could suggest that on Ag the more favoured reaction is the dissociative electron transfer process resulting in the C-I cleavage instead of the N-H bond breaking.

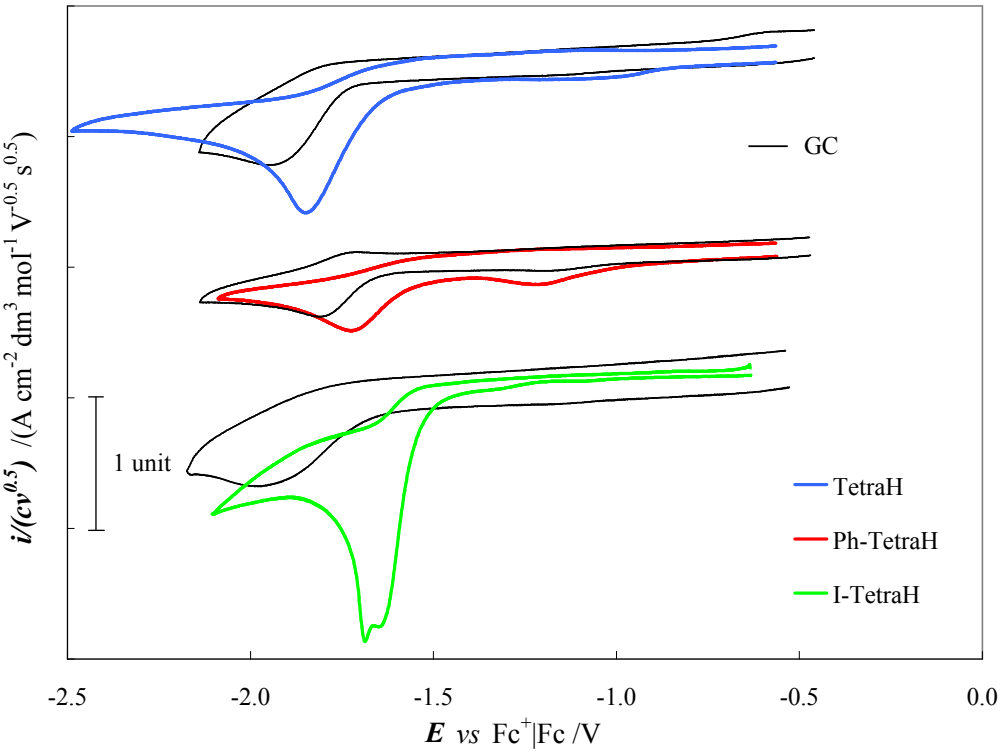

Figure 29 Normalized cyclovoltammograms of the three representative tetrazoles recorded on Ag electrode (coloured thick lines). Concentration *ca.* 0.001 M in DMF and $TBAPF_6$ 0.1 M, scan rate potential 0.2 V s^{-1}. For sake of comparison the corresponding patterns recorded on GC electrode are also reported (thin black lines).

Electrochemical behavior of **6-Mes-TetraH** differed significantly from that of its 4-R-pyrid-2-yl analogues; in fact not only the reduction process was significantly hampered (Figure 25) but it did not reveal any catalytic behavior when recorded on Pt electrode (see gallery, Figure G 2). In any case the reduction process occurred at a potential *ca.* 0.1 V more positive than that of the carbonitrile precursor according to the more electron rich nature of the tetrazole ring.

After this detailed study of the free-ligands the next part of the subchapter will be dedicated to the electrochemical characterization of the related Ru(II) complexes [96], [97]. As in the case of the oxyquinolate sensitizers only DPV patterns will be reported being resulted clearer than corresponding CVs.

The anodic potential window was characterized by a quite intense first oxidation peak (*ca.* 0.5 V *vs* $Fc^+|Fc$) followed by a less intense one at more positive potential. The remarkable difference of peak intensities suggested the possibility that the two ETs could involve two independent chemical entities with different diffusion coefficients (and hence, probably diverse bulkiness). Considering the invariant potential of the first oxidation peak along the series of complexes and the nature of the counteranion of the Ru(II) complexes addition of Cl^- as both internal (see gallery, Figure G 3) and external standard (Figure 30) were performed. This revealed that the first anodic peak was attributable to the electrooxidation of chloride ions while the second at more extreme potentials was

actually related to the electron transfer involving the cation complex. Moreover the perfectly comparable peak current of the equimolar solution of chloride (*i.e.* tetrabutylammonium chloride salt, TBACl) with that of the first anodic peak of all Ru-containing samples confirmed the anionic nature of the tetrazole-based ligand, otherwise a peak with a height equal to half the intensity of the first anodic peak in the complex sample should be recorded.

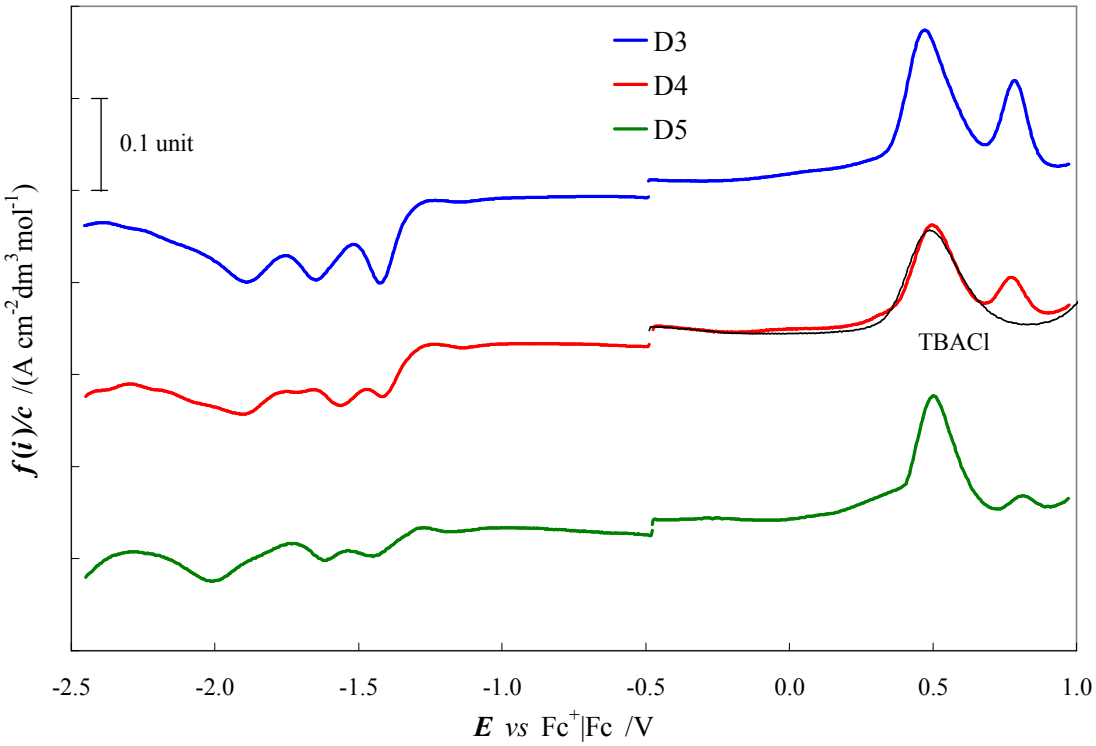

Figure 30 Normalized DPV patterns of the tetrazolate-based complexes D3-D5 (coloured lines) dissolved in DMF with TBAPF$_6$ 0.1 M on GC electrode. Sample concentration *ca.* 0.001 M. Potential scan rate 0.05 V s^{-1}. For sake of comparison the anodic scan of an equimolar solution of TBACl was reported (black thin line).

The second anodic signal was a chemically reversible process with a peak potential slightly modulated by the chemical modification introduced through the pyridyltetrazolate ligand. The quite high oxidation potentials respect to oxyquinolate-based complexes **D1** and **D2**, and even to cyclometalated **YE05** and NCS-based **N3** dyes (at least 0.6 V and 0.4 V more positive potential respectively; compare Table 2 with Table 7) were attributed to the electron withdrawing nature of the nitrogen enriched *tetrazole-containing ligands* which could *influence* the electron transfer tentatively attributed to a *Ru-centred process* according with theoretical calculations. Moreover in qualitative good agreement with HOMO levels from quantum mechanics the standard potentials of complex **D3** and **D4** were quite invariant, E^0 = 1.50 V *vs* SHE, while the presence of the halogen atom brought to a small but perceivable positive shift of the oxidation potential of **D5**, E^0 = 1.53 V *vs* SHE (Table 7). The inductive effect of the Cl atom on complex **D5** is significantly soften with respect to the that produced by the same substitution on a ferrocene molecule (0.03 V *vs* 0.14 V respectively) [97]. This datum together with the limited tunability of the oxidation process

involving cation complex can point to a substantial distance between the substitution site and the actual redox centre corroborating the theoretical results that described HOMO as an orbital mainly delocalized on Ru and the tetrazole ring portion of the ligand.

Table 7 Standard potential for the Ru(II)-centred process (*i.e.* the second anodic peak) for D3-D5 dyes.

dye	E^0 *vs* SHE /V [a]
D3	1.50
D4	1.50
D5	1.53

[a] See footnote number 4 (pag. 43) and the first paragraphs of "Voltammetric study" in "8-Oxyquinolate dye family" chapter for details on the conversion.

The cathodic scan showed three subsequent reduction processes. Similarly to oxyquinolate **D1** and **D2** dyes they can be attributable to *ligand-based processes*, the first of which occurred at more positive potentials than in the corresponding free-ligands due to the complexation effect. A neat difference between our two families of NCS-free dyes was observed for the first ET that occurred invariably at almost 0.3 V more positive potential ($E_{p,Ic} \approx -1.44$ V *vs* $Fc^+|Fc$) in the series of tetrazolate-based complexes; moreover it was positively shifted respect to **N3** dye too [79]. Similarly to the anodic behavior the remarkable anticipated reduction can be attributed to the electron withdrawing character of the tetrazolate ligands. An unambiguous more accurate attribution of the first reduction process was not proposed yet but for comparison with other structural and electronic $[Ru(X)(dcbpy)_2]^{n-}$ analogues, and combining information coming from the electrochemical study of free-ligands and from the theoretical calculations of LUMO the electron transfer could be tentatively ascribed to a reduction localized on one of the dcbpy moieties, even if implication of pyridyltetrazolate could not be excluded considering electrochemical results. In fact especially in **D4** complex its Ph-Tetra anionic ligand could compete with the bipyridines as the site for the reduction due to the quite identical E_p recorded for their corresponding free-ligands.

DSSC tests

Final step of the work was the sensitization of TiO_2 photoanode with the tetrazolate-based Ru(II) dyes **D3**-**D5** (**D6** complex will be tested as soon as possible in combination with other potential dyes containing the already synthesised **Th-TetraH** and **(*p*-Me$_2$N)Ph-TetraH**). Device assembling and their tests were carried out in collaboration with the research tem of Dr. Filippo De Angelis; experimental details were reported in related published papers and in their electronic supporting information [96], [97].

One of the task of this part of the project was the development of robust dyes which limited their photodegradation and/or chemical modification in presence of potentially coordinating species (*e.g.*

tbupy) respect to NCS-based sensitizers [38]. This first goal was efficiently reached, as demonstrated by the absence of any substitution product in the mass spectra recorded after stress tests during which dyes **D4** and **D5** were refluxed in acetonitrile at 82°C for 24h in presence of a large excess of *tert*-butylpyridine (100:1 tbupy/dye molar ratio). As depicted in Figure 31 only the molecular peak of pristine complexes (*i.e.* *m*/*z*=812 and *m*/*z*=770 for **D4** and **D5** respectively) was revealed in FAB^+ spectra (*i.e.* cation detection through fast atom bombardment ionization protocol) after the treatment, while no traces of the mono- (or eventually di-) substituted tbupy derivates were observed at *m*/*z*=889 (or 966) and *m*/*z*=847 (or 924) for **D4** and **D5** respectively.

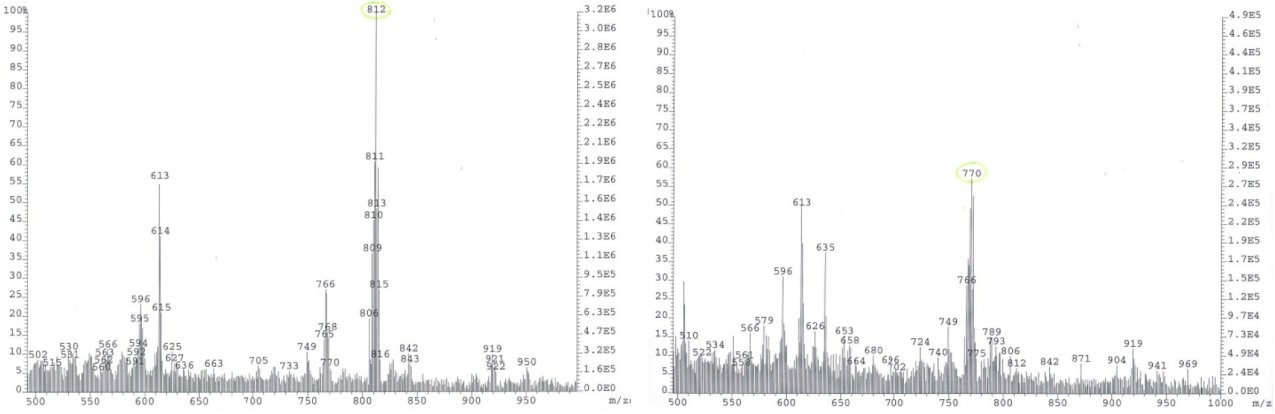

Figure 31 FAB^+ spectra acquired after the stress test on D4 (left) and D5 (right) in refluxing acetonitrile for 24h in 100:1 molar excess of *tert*-butylpyridine. Molecular peak for the pristine complexes have been underlined.

To properly judge the sensitization properties of this new family of tetrazolate-based dyes a first screening was performed on the forefather **D3** to identify its best working condition [96] in combination with a commercially available iodide-based electrolytes. Additives such as LiI and co-adsorbent species like CDCA were tested, and their results are summarized in Table 8 together with the related *iE* characteristics in Figure 32. Chenodeoxycholic acid (entry 2 *vs* entry 1 of Table 8) brought to a small increase in i_{sc} coupled with a remarkable growth of the open circuit potential; moreover the practically superimposable visible spectra of **D3** adsorbed on TiO_2 photoanode with and without CDCA (see gallery, Figure G 4) suggested the presence of only weak aggregation issues. As a consequence the improvement of the photovoltaic parameters should be related to the hampering of parasitic charge recapture processes between I^- species in solution and electrons into TiO_2. Entry 3 of Table 8 clearly evidenced the expected rise of photogenerated current (and the related slightly decrease of V_{oc}) attributable to the downshift of TiO_2 conduction band edge induced by Li^+ ions that improved electron injection from excited dye* species. However the best 3.0% photon-to-current conversion efficiency, PCE, (entry 4, Table 8) was obtained combining the easier electron injection coming from the addition of LiI into the electrolyte with the passivation effect attributed to CDCA. The main responsible for the remarkable improvement of efficiency was surely the photocurrent, which increased of about 30% respect to the unmodified control cell, entry 1.

Table 8 Photovoltaic parameters for D3-sensitized solar cells (active area 0.2 cm^2) with different additives. Simulated AM1.5 G sun illumination.

Entry	additive [a]	i_{sc} /mA cm^{-2}	V_{oc} /V	*FF*	PCE %
1	–	5.6	0.63	0.68	2.4
2	0.01 M CDCA	5.9	0.66	0.70	2.7
3	0.1 M LiI	6.4	0.60	0.67	2.6
4	0.01 M CDCA + 0.1 M LiI	7.6	0.61	0.65	3.0

[a] Iolitech ES-0004 HP electrolyte (containing 1-butyl-3methylimidiazolium iodide, iodine, guanidinium thiocyanate and *tert*-butylpyridine, in a mixture of valeronitrile and acetonitrile). CDCA was directly added in the sensitizer solution (0.2 mM in EtOH).

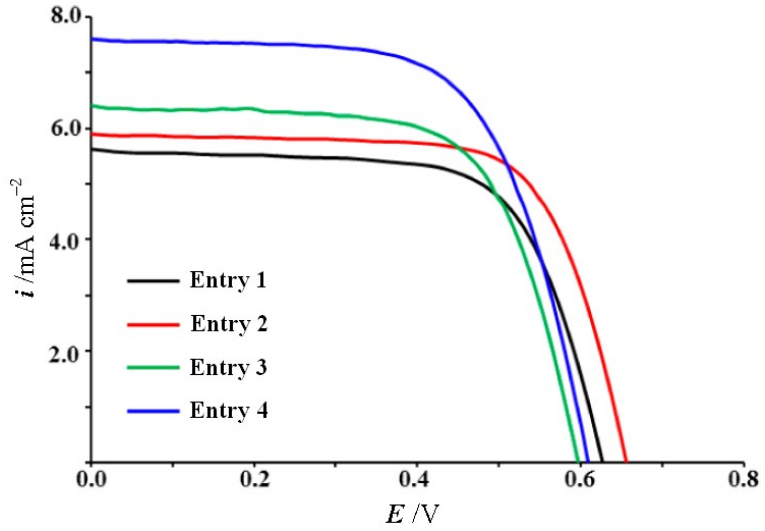

Figure 32 Synopsis of *iE* characteristics of the D3-sensitized solar cells reported in Table 8 for cell optimization. Modified from ref. [96].

Employing the best working conditions found during cross-tests on **D3**, solar cells sensitized with **D4** and **D5** (with CDCA as co-adsorbent) and filled with the same iodide-based electrolyte (with addition of 0.1 M LiI) were assembled and tested (Figure 33). They exhibited photon-to-current conversion efficiency ranging from 3% up to 3.4% to be compared with a 6.5% PCE of a control cell sensitized with N719 (Table 9); moreover all tetrazolate-based sensitizers had more than tripled the overall cell efficiencies of oxyquinolate analogues **D1** and **D2** increasing both photocurrent (50% more, notwithstanding their blue-shifted optical spectra) and photovoltage (20% more). These results can be considered quite interesting especially considering the extremely simplicity of the tetrazolate ligands synthesised through a one-step reaction from commercially available cianopyridines of reasonable price (from 5 €/g to 100 €/g).

Table 9 Photovoltaic data of solar cells (active area 0.2 cm^2) sensitized with tetrazolate-based dyes D3-D5[a].

Entry	dye	i_{sc} /mA cm^{-2}	V_{oc} /V	*FF*	PCE %
1	D3	7.8	0.62	0.64	3.1
2	D4	8.2	0.64	0.65	3.4
3	D5	7.2	0.65	0.65	3.0
4	N719	13.9	0.75	0.62	6.5

[a] Iolitech ES-0004 HP electrolyte (containing 1-butyl-3methylimidiazolium iodide, iodine, guanidinium thiocyanate and *tert*-butylpyridine, in a mixture of valeronitrile and acetonitrile); 0.1 M LiI was added. A 20:1 molar ratio CDCA/dye was directly added in the sensitizer solution (0.2 mM in EtOH).

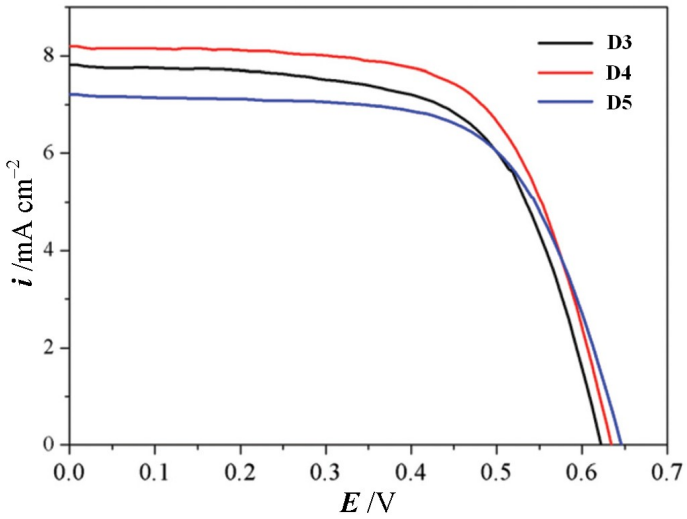

Figure 33 *iE* characteristics of the solar cells reported in Table 9 sensitized with D3-D5. Modified from ref. [97].

According to expectation the best 3.4% efficiency was recorded with the more π-delocalized **D4** dye mainly due to the higher molar extinction coefficient (see the above UV-vis spectroscopic characterization) that could bring to a better light harvesting capability. Confirming the crucial role played by the absorption features of **D4** in determine its better performance, the only cell parameters significantly modified along the series of nominally identical cells (expect for obviously the dye) was the generated photocurrent which experienced a 14% maximum variation compared to 4% and 1% for V_{oc} and *FF* respectively. Moreover computational results showed that **D3**-**D5** dyes have essentially isoenergetic LUMOs mainly localized on the carboxylated bipyridine moiety which is directly involved in the anchoring process to the photoanode surface. This allowed to tentatively consider comparable the efficiency of the electron injection process occurring from the excited dyes to the TiO_2 conduction band, being induced by the same thermodynamic driving force. So even in absence of incident photon-to-current graph, all these data confirmed that the high photocurrent generated by **D4**-sensitized cell could be reasonably attributed to the better optical properties of the sensitizers respect to its two analogues.

Unfortunately all tetrazolate-based dyes exhibited PCE equal to approximately half of the value recorded with the control N719-sensitized cell mainly due to the poor photogenerated currents which were about 40% lower than N719-based device. The neat discrepancy could be attributable to the different coverage of visible window between NCS-based benchmark and NCS-free dyes (see gallery, Figure G 4). In fact the comparison clearly evidenced a red-shift in both maximum (around 520 nm) and onset (around 650 nm) of the optical absorption of N719 respect to tetrazolate sensitizers that resulted in a better light harvesting and hence, probably, in the higher i_{sc} notwithstanding the comparable or even greater dye loading evaluated for **D3** (5.1×10^{-8} mol cm^{-2}) with respect to N719 (4.1×10^{-8} mol cm^{-2}).

Summarizing

In conclusion the family of NCS-free Ru(II) sensitizers based on the anionic N^N pyrid-2-yl-tetrazolate chelating scaffold proposed here for the first time showed remarkable results reaching performances three-times higher than those obtained with 8-oxyquinolate analogues, simply employing easy-to-prepare ligands. Nevertheless PCEs were certainly far away from the conversion obtained with well established N719 dye, reaching values at the best only slightly higher than half of the value with the NCS-based control cell. However I think that this last new family is well promising for the development of stable and efficient sensitizers through a rational engineering of the tetrazolate scaffold, considering that a remarkable 10% increase of the overall cell efficiency was obtained by simply appending a phenyl ring to the pryrid-2-yl-tetrazole building block (from 3.1% with **D3** to 3.4% with **D4**).

The immediate hope will be to further increase the current PCE, possibly exceeding the target of 4%, employing the already synthesized **(*p*-Me$_2$N)Ph-TetraH** and **Th-TetraH** ligands exploiting the electron donating features of the aniline-functionalized tetrazole and the π-conjugative and electron rich nature of the thienyl ring respectively. This can be an effective way to shift the absorption spectrum of the resulting dyes toward higher wavelengths and to increase their dipolar structure favouring the h^+/e^- separation and also the dye regeneration kinetics. Furthermore the employment of 3-hexyl-thiophene unit instead of the simpler unsubstituted thiophene core like in **Th-TetraH** could also open the way to the exploitation of tetrazolate-Ru(II) sensitizers in combination with iodine-free electrolytes based on fast outer-sphere electron couples which generally needed long/branched alkyl chains to hamper charge recombination between oxidized form of the electron shuttle and the photoanode surface.

Results and discussion: $Cu^{(I)/(II)}$-based redox mediators

Synthesis

Starting from the pioneering work of Fukuzumi *et al.* [63] showing the dramatic effect that substituents in 2 and 9 positions of 1,10-phenanthroline had on the photovoltaic performance of DSSCs filled with an electrolyte based on phenanthroline-based copper complexes, I started a project centred on the design, synthesis and characterization of a series of homoleptic bis(1,10-phenanthroline)copper complexes studying in detail how first of all electrochemical but also spectroscopic features are related to the substituents on the condensed heteroaromatic scaffold.

The first step was the research of synthetic procedures for the introduction of different alkyl and aryl substituents with various steric hindrance in specific positions of 1,10-phenanthroline. Suitable way was identified in the nucleophilic aromatic substitution reactions through lithium chemistry considering that different kind of lithium-derivates are commercially available avoiding their preparation. A modification of literature procedures [103], [104] was applied for the synthesis of almost all the below phenanthrolines; it involved the addition of the alkyl/aryl nucleophile followed by the hydrolysis and re-aromatization with manganese dioxide of the intermediate to give the final product. The only exception was the synthesis of 2-methyl-1,10-phenanthroline, **Me-phe**, for which a condensation between 8-aminoquinoline and the proper α,β-unsaturated aldehyde (*i.e.* crotonic aldehyde) was performed in H_2SO_4 as solvent and in presence of NaI as catalyst [105]. Yields are summarized in Table 10. For entries 5, 6, 8-11 of Table 10 preparation of the lithium derivates, R-Li, was mandatory. They were synthesised (and then directly added under inert atmosphere to the desired phenanthroline solution) reacting *tert*-butyllithium with the proper bromo-arene at –78°C (*i.e.* 2-bromotoluene or bromomesitylene). More detailed procedures have been reported in the experimental section.

Table 10 Synthetic pathways for the preparation of asymmetric and symmetric 1,10-phenanthroline ligands.

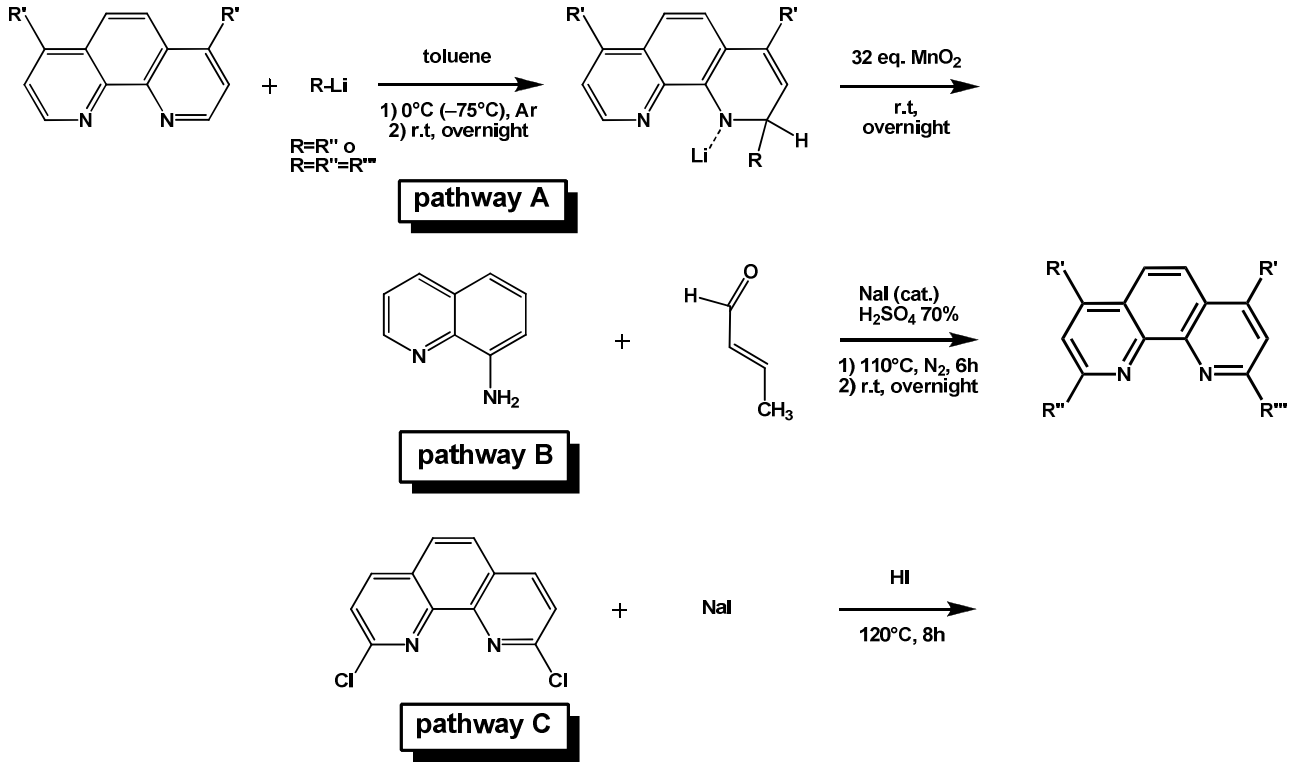

entry	ligand name	R'	R''	R'''	pathway	yield[a]
1	Me-phe	H	H	CH_3	B	62%
2	*n*-Bu-phe	H	H	*n*-Bu	A	31%
3	*t*-Bu-phe	H	H	*t*-Bu	A	40%
4	Ph-phe	H	H	Ph	A	36%
5	Tol-phe	H	H	*o*-Tolyl	A	29%
6	Mes-phe	H	H	Mesityl	A	25%
7	Ph-4,7-$Form_2$-phe	CHO	H	Ph	A	20%
8	Mes-4,7-Me_2-phe	CH_3	H	Mesityl	A	70%
9	Mes-4,7-(*p*-Tol)-phe	*p*-Tol	H	Mesityl	A	19%
10	Tol_2-phe	H	*o*-Tolyl	*o*-Tolyl	A	33%[b]
11	Mes_2-phe	H	Mesityl	Mesityl	A	21%[b]
12	I_2-phe	H	I	I	C	71%

[a] On the isolated product. [b] Isolated by the same reaction mixture from which mono-substituted product was obtained.

In general from lithium-mediated procedure (pathway A) both symmetric and asymmetric substituted phenanthrolines were obtained and they were then separated through flash-chromatography on neutral Al_2O_3; the symmetric species was the first eluted species probably due to the higher steric hindrance of the substituents that limit interaction of nitrogen atoms with the stationary phase. On the other hand the condensation reaction (pathway B) revealed obviously more

selective and the desired **Me-phe** was obtained with a sufficiently high purity after a faster liquid-liquid separation/extraction and acidification/basification step.
Two symmetric phenanthrolines with halogen units (*i.e.* -Cl e -I) were also included in the structural screening to study the effect of electron withdrawing substituents. Starting from the commercially available 2,9-dichoro-1,10-phenanthroline, **Cl-Phe**, the corresponding di-iodo derivate, **I-Phe**, was synthesised with moderate yield by a nucleophilic substitution reaction according to the procedure firstly reported by Siegel, Benaglia *et al.* [106].

Copper complexes were prepared in high yields through an easy and fast procedure starting from Cu(I) or Cu(II) inorganic salts, and isolating the product in pure form by simple recrystallization/precipitation. The syntheses of some complexes were carried out in the context of the bachelor degree theses of Rachele Ossola and Marta Trifilò.
Tetrakis(acetonitrile)copper(I) was chosen as the precursor for the preparation of bis(R-phenanthroline)Cu(I) complexes through a two-step protocol. Firstly $[Cu(ACN)_4]^+$ was prepared adding a proper HX acid to a solution of Cu_2O [107] (pathway A, Table 11) or, equivalently, to a mixture of $Cu(CO_3)_2Cu(OH)_2$ salt and metallic copper (pathway B, Table 11) dissolved/suspended in acetonitrile. Due to the air sensitivity of Cu_2O it was employed mainly for bulky preparation of the Cu(I) precursor reacting one-pot all the content of the sealed ampoule (*i.e.* 5 g); on the contrary the second pathway was chosen for the preparation of also moderate quantities of $[Cu(ACN)_4]^+$ coupled with different counterions (*i.e.* BF_4^-, PF_6^-, ClO_4^-) in order to employ them in the electrochemical study to clarify the effect on anions on the metal-centred electron transfer properties (see the electrochemical section). In the second step (Table 11) the solution of the desired phenanthroline was added dropwise to the solution of Cu(I) precursor which immediately turned red/dark orange.

Table 11 Synthetic pathways for the preparation of homoleptic phenanthroline-based Cu(I) complexes, 1-16.

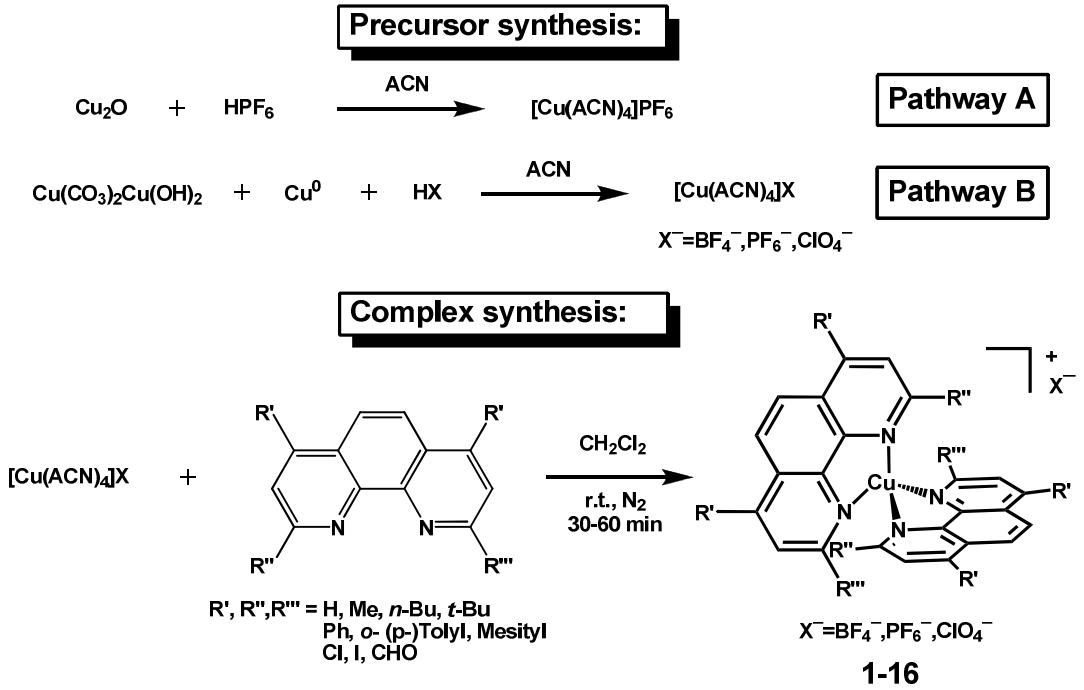

entry	complex name[a]	R'	R''	R'''	yield[b]
13	1	H	H	H	68%
14	2	H	H	CH_3	51%
15	3	H	H	*n*-Bu	60%
16	4	H	H	*t*-Bu	75%
17	5	H	H	Ph	74%
18	6	H	H	*o*-Tolyl	82%
19	7	H	H	Mesityl	70%
20	8	CH_3	H	H	54%
21	9	CH_3	H	Mesityl	86%
22	10	CHO	H	Ph	68%
23	11	*p*-Tol	H	Mesityl	74%
24	12	H	CH_3	CH_3	82%
25	13	H	*o*-Tolyl	*o*-Tolyl	58%
26	14	H	Cl	Cl	57%
27	15	H	I	I	54%
28	16	Ph	CH_3	CH_3	84%

[a] All complexes here reported have the hexafluorophosphate anion. [b] On the isolated product.

On the other hand the starting materials for the synthesis of the oxidized form of redox mediator were two simple commercially available inorganic salts, $CuSO_4 \cdot 5H_2O$ and $CuCl_2 \cdot 2H_2O$. The first salt was employed for the synthesis of tetra-coordinated complexes (pathway C, Scheme 7).

Considering the relatively low stability of some Cu(II) complexes in solution (which increased increasing their oxidation half-wave potential) a second synthetic strategy starting from $CuCl_2$ was developed (pathway D, Scheme 7) to prepare penta-coordinated species in which the chloride ion directly entered into the coordination sphere of the central atom resulted in much more stable Cu(II) complexes. In both cases the desired product was obtained performing an anion exchange adding to a water (or water/ethanol) solution an excess of $NaPF_6$ which caused precipitation of the complex. For a more accurate description of the general protocol for the synthesis of the cuprous and cupric complexes and for details on their characterization please refer to experimental section.

Scheme 7 Synthetic pathways for the preparation of phenanthroline-based Cu(II) complexes, 17-22.

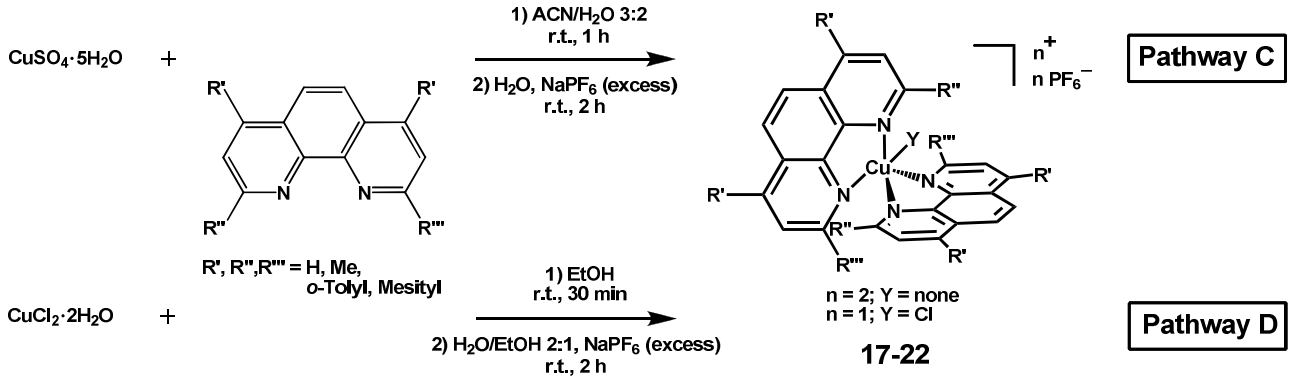

entry	complex name	R'	R''	R'''	Y	pathway	yield[a]
29	17	H	H	*o*-Tolyl	none	C	60%
30	18[b]	H	H	*o*-Tolyl	Cl	D	25%
31	19	H	H	Mesityl	none	C	50%
32	20	H	H	Mesityl	Cl	D	76%
33	21	CH_3	H	Mesityl	none	C	53%
34	22	H	CH_3	CH_3	Cl	D	49%

[a] On the isolated product. [b] Cyclovoltammogram revealed the co-presence of **17** as impurity (<25%).

Characterization

Electronic UV-visible spectra

UV-visible spectroscopy allowed not only to add a new information useful for the characterization of the products but first of all to study the effects that the complex geometry and the ligand substituents induce on both distribution of the electronic energy levels and intensity of electron transitions in the complexes, so monitoring how the colour and the molar absorption coefficient could be modulated. Taking into account the role thought for these complexes (*i.e.* redox mediators in DSSCs) the possibility to reduce their competition with sensitizer molecules for light harvesting is of primarily importance. This can be performed both reducing the absolute light absorption of the

two species constituting the redox couple and minimizing the overlap between their optical spectra and that of the dye. Moreover as discussed more in detail in the following lines, visible absorption spectroscopy was also employed as a fast and easy method to check the time stability (*i.e.* from hours up to months) of Cu(I) and Cu(II) complexes when dissolved in a organic solvent. In fact long-term stability is another mandatory ideal feature requested to a redox mediator and hence identification of any chemical modifications in the coordination environment of the copper that could allow to satisfy this feature would be extremely useful.

All subsequent discussion will be entirely centred on the visible and near-IR part of the electronic absorption spectra (being the more interesting for the application in DSSCs) comparing how electronic transitions were modified along the series of the Cu(I) and Cu(II) complexes in order to find any possible general rules that can help to synthesise complexes with the optical features requested for a redox mediator. Generally speaking the visible region of the spectra showed two neatly different behavior for cuprous and cupric complexes, according to the different electronic population of the d atomic orbital of metal core (d^{10} configuration for **1-16**, and d^9 for **17-22**). On the other hand the UV region of the spectra were characterized by sharp and intense peaks attributable to π-π^* intraligand electronic transitions.

Cu(I)-complexes

In Cu(I)-complexes the spectra were characterized by a broad absorption band with a maximum ranging between 433 nm and 492 nm (corresponding to **4** and **10** respectively, Table 12) exhibiting a very small, or even absent, solvatochromism[6] (see Figure G 5 for example complex **9**). Nevertheless a neat different spectrum was recorded for complex **4** passing from dichloromethane to acetonitrile; similar variation were observed also for the two halo-derivates **14** and **15** in both ACN e DMF. Analogue peculiarities were also detected in the electrochemical behavior of these last three complexes as discussed in more detailed in the relative section (see below).

According to literature [108] the main visible transition is commonly denoted *band II* and corresponds to a symmetry allowed electronic transition from a 3d orbital of the copper atom to a low-lying anti-bonding π^* orbital localized on the phenanthroline moiety (*i.e.* a MLCT process).

[6] More details have been reported in the bachelor thesis of Rachele Ossola (academic year 2013-2014).

Table 12 Maximum absorption wavelengths, λ_{max}, for selected Cu(I) complexes in dichloromethane.

complex	R'	R''	R'''	λ_{max} /nm[a]
1	H	H	H	442
2	H	H	CH_3	454
3	H	H	*n*-Bu	455
4	H	H	*t*-Bu	433
5	H	H	Ph	443
6	H	H	*o*-Tolyl	459
8	CH_3	H	H	440
9	CH_3	H	Mesityl	447
10	CHO	H	Ph	492
12	H	CH_3	CH_3	457
14	H	Cl	Cl	479
15	H	I	I	440
16	Ph	CH_3	CH_3	477

[a] ±1 nm.

The other two predicted bands for a general $Cu(N\hat{}N)_2^+$ complex of D_{2d} symmetry (namely *band I* and *band III*, at decreasing wavelengths respectively) can be partially identified as shoulders in some of our systems. The assumption of a metal-to-ligand charge transfer was corroborated also by theoretical calculations that I performed only on a restricted number of complexes. Results steadily evidenced that HOMOs were firmly localized on the copper atom while LUMOs were delocalized across the two phenanthrolines (see as an example Figure 34 for **3**). A partial exception was found for LUMO in complex **4** (see below).

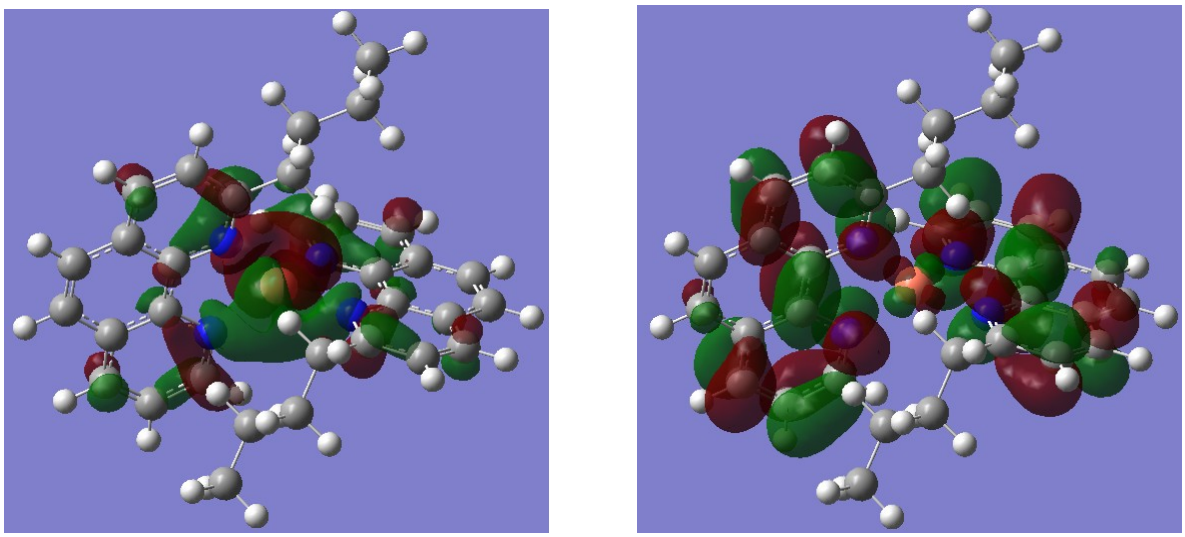

Figure 34 Isodensity surface plots (isodensity contour: 0.02) of HOMO (left) and LUMO (right) molecular orbitals for complex 3.

Interesting for our purpose would be the possibility to correlate the variation of the maximum absorption wavelength, λ_{max}, and of the intensity of MLCT with the *position*, the *number*, the *size* and the *chemical nature* of substituents on the chelating phenanthrolines. Even if the spectra were recorded in different solvents the influence of substituents on the position of the MLCT band for a selected series of Cu(I) complexes (Table 12) was studied in dichloromethane, DCM, considered an inert solvent, according also to the electrochemical results, due to its low coordination capability. According to literature [78] finding a clear rationalization was not easy, even if some specific observations can be done possibly useful to enlarge the knowledge on the optical properties of $Cu(N\hat{}N)_2^+$ complexes.

The wavelength of the absorption seemed to be mainly affected by the "external" 4 and 7 positions of the phenanthroline ligands. Particular eloquent was the comparison between the insertion of –Ph group in the "internal" position 2 and the "external" 4 and 7 ones. While the first substitution brought to a negligible shift (**1** *vs* **5**) the second one caused a 20 nm red shift in the absorption (**12** *vs* **16**) tentatively attributed to the higher stabilization of LUMO deriving from the unconstrained external –Ph able to assume a configuration that resulted in a more efficient conjugation with phenanthroline than that of the internal substituent forced to assume a less favourable higher dihedral angle. Even more remarkable was the *ca.* 50 nm bathochromic shift induced by the introduction of two formyl groups in complex **10** (respect to **5**).

Interesting all the substituted complexes of Table 12 exhibited λ_{max} mainly red-shifted than the pristine $[Cu(phe)_2]^+$ complex, **1**, or in few cases comparable to it. This means that the asymmetric substitution of the two internal positions of phenanthrolines invariably generated a red-shift of the absorption maximum, contrary to the literature results showing that a blue-shift occurred when an asymmetric substitution in the external 4 and 7 positions is performed.. The only exception was the remarkable blue shift (*ca.* 10 nm) of the complex **4** which brought the bulky *tert*-butyl group in the internal position. It is possible to note that the aforementioned red-shift occurred independently by the electronic character of the phenanthroline substituents (compare for example complexes **12** and **14**, respect to reference **1**). All these observations suggested that the electronic transitions are mainly influenced by the geometry around the central atom induced by the internal substituents. As a confirmation the two electronegative substituents, like chloride and iodide, induced diametrically opposite shift of the λ_{max}; in fact the introduction of the smaller but more electronegative chloride ions caused a red shift of more than 35 nm (**14** respect to the reference compound **1**) while the presence of iodides, **15**, induced only an opposite slight ipsochromic shift.

Considering the importance assumed by the geometry I tried to correlate the spectroscopic data both with results obtained by theoretical calculations and with the crystal structures obtained through X-

ray diffraction (the last performed by Prof. Francesco Demartin, Università degli Studi di Milano). Unfortunatly in both cases no additional information useful to rationalize the λ_{max} trend were atteined. In particular no interesting correlations were extrapolated by X-ray structures of the complexes useful for this comparison (**4**-**6**, **9** and **14**; see experimental section) in fact in all these systems the dihedral angle between the two phenanthrolines was very similar, ranging in a very narrow range around 75° suggesting only a distortion of the complexes from the ideal D_{2d} symmetry. Similarly poor results were obtained by the comparison of spectroscopic results with HOMO-LUMO for the optimized complexes obtained by theoretical calculations. The only albeit week correlation was found between the discrepancy observed in the visible spectrum of **4** and the neatly different LUMO distribution. Probably in agreement with the higher interligand angle respect to its analogues, LUMO was localized quite exclusively on only one phenanthroline resulting in a more destabilized molecular orbital (Figure 35).

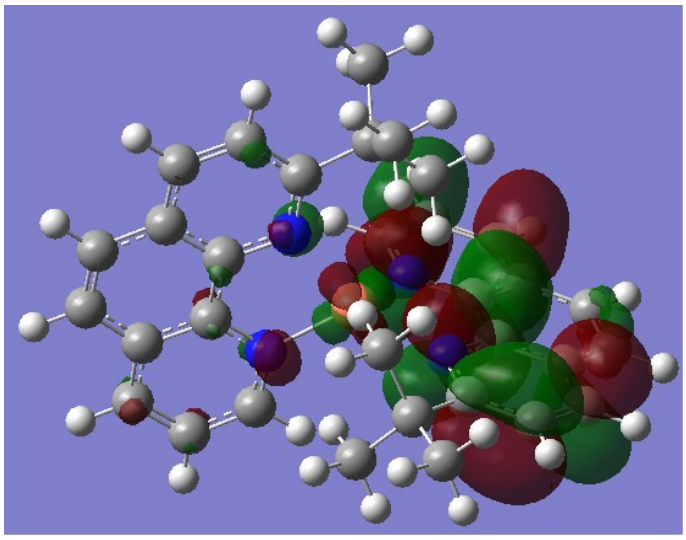

Figure 35 Isodensity surface plots (isodensity contour: 0.02) of LUMO molecular orbital for complex 4.

Quite instructive was the spectrum of complex **5** (Figure 36); its main MLCT band at 443 nm was followed by a lower intense tail around 550 nm that can be ascribed to the so called *band I* (see above). The same morphology can be find also in analogue complex **6** even if it was much more attenuated than in **5**, while the band completely disappears in the complex **9**. A similar low-energy band was already cited in literature but it was identified as a sort of fingerprint for Cu(I) complexes with 2,9-diaryl-phenathroline ligands [78]. The results here discussed showed that this shoulder band can also identify complexes with mono-aryl-phenanthrolines and that its presence is not a "necessary condition" for this class of Cu(I) complexes (*i.e.* it is absent in complex **9**) in good agreement with a previous literature observation [109].

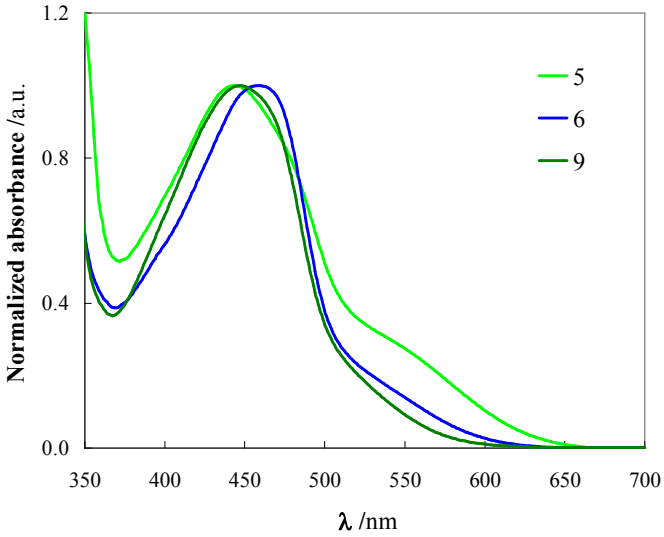

Figure 36 Synopsis of visible spectra for complexes 5, 6 and 9 showing the characteristic shoulder at *ca.* 550 nm.

Attention was also pointed to the evaluation of the intensity of the MLCT transitions as a function of phenanthroline substituents to develop Cu(I) complexes with a molar absorption coefficient as low as possible, so to reduce the light-harvesting competition with dye when they employed as active component of the electrolyte in DSSCs. In view of their application the intensity *vs* structure study was carried out in acetonitrile, ACN, a more suitable solvent than dichloromethane for laboratory-type solar cell due to its low viscosity and acceptable boiling point (over 80°C) to limit its evaporation during irradiation of the cell.

Similarly to λ_{max} also in this case literature already evidenced the difficulty of depicting a unique simple picture for the MLCT intensities of bis-phenanthroline Cu(I) complexes, but some interesting observation came out from this analysis (Table 13). In agreement with both the above discussion and the literature [78] the intensity of MLCT band was extremely sensitive to the presence of substituents in the two "external" 4 and 7 positions of the phenanthrolines; addition of methyls enhanced the ε (**8** *vs* **9**) but this phenomenon was greatly amplified by insertion of π-delocalized phenyl groups that resulted in a three-fold increase of the molar absorption, passing from **12** to **16**. Quite instructive is the comparison of complexes with 2-substituted and 2,9-disubstituted phenanthrolines.

Table 13 Molar absorption coefficient, ε, at λ_{max} of MLCT band for selected Cu(I) complexes in acetonitrile.

complex	R'	R''	R'''	λ_{max} /nm[a]	10^3 ε /dm^3 mol^{-1} cm^{-1}
2	H	H	CH_3	447	6.4
3	H	H	*n*-Bu	452	6.2
4	H	H	*t*-Bu	426	2.2
				356	2.1
5	H	H	Ph	437	4.6
6	H	H	*o*-Tolyl	455	4.6
8	H	H	Mesityl	451	4.2
9	CH_3	H	Mesityl	445	4.4
12	H	CH_3	CH_3	455	8.0
13	H	*o*-Tolyl	*o*-Tolyl	470	4.5
16	Ph	CH_3	CH_3	475	24

[a] ± 1 nm.

The mono-functionalized species **2**-**6** and **8**, **9** exhibited an absorption which was invariably lower than the value of 2,9-dimethyl complex **12**. In particular the presence of aryl groups in the internal positions significantly decreased the molar absorption of the complexes as clearly elucidated by comparing mono-aryl **5**, **6**, **8** and **9** with mono-alkyl **2** and **3** species (**4** showed a peculiar behavior). The scarce impact of aryl groups on the absorption of complexes was univocally shown by the identical ε values recorded for complex **6** and **13**.

As anticipated ACN seemed to significantly modified the optical properties of complex **4**; the unique MLCT band observed in DCM appeared splitted into two less intense bands of comparable molar absorptions in the higher polar and greater coordinating ACN solvent. A similar anomaly was also detected in its electrochemical behaviour (see below) passing from DMC to ACN but surprisingly the chemical shifts of all its protons remained practically identical when ^{1}H-NMR spectra were recorded in deuterated solvents of different polarity and proticity (*e.g.* CD_2Cl_2, CD_3CN and CD_3OH). Unfortunately an exhaustive explaination able to take into account all these experimental data was not formulated yet.

Apart from the unexplained anomaly of complex **4** the spectroscopic study just discussed has given some important guidelines for the synthesis of future complexes but it has also shown interesting features useful for the choice of the more suitable complexes as redox mediators among those already prepared. These information can be summarized here in few lines: *i*) functionalization of phenanthroline scaffold invariably results in complexes with red-shifted visible spectra respect to the reference compound $[Cu(phe)_2]^+$, confirming the key role played by the structure surrounding

the metal center; *ii*) substituents in the external 4 and 7 positions of the phenanthrolines red shift and increase the intensity of the MLCT band (especially π-delocalized units); *iii*) presence of only one substituent in the internal positions of the ligands reduces, also significantly, the intensity of the absorption respect to the "prototype" complex with 2,9-dimethyl-phenanthrolines; *iv*) aryl groups in the internal positions significantly decrease the molar absorption coefficient of complexes respect to analogue mono-alkyl species (contraty to the effect induces when they are used to functionalize the external positions, see the previous point two); *v*) an easy relationship between λ_{max} and the alkyl/aryl nature of the internal substituents has not been found yet.

So in conclusion the complexes with 2-monosubstituted phenanthrolines (especially with aryl groups) should be an optimal choice in term of at least optical properties, because they should have a red-shifted and relatively low intense visible absorption that minimize the competition with the dye for the light harvesting.

Cu(II)-complexes

The visible spectrum of all phenanthroline-based Cu(II) complexes **17-22** exhibited a broad band followed by a less intense one at higher wavelengths remarkably red shifted respect to the MLCT band of Cu(I) counterparts. According to the partial occupation of the d orbitals of Cu atom the band at shorter wavelength was attributed to a ligand field transition exclusively involving the central atom. The d-d electronic excitations (Table 14) were located around 690-750 nm and characterized by at least one order of magnitude less intense absorption than the charge transfer processes occurring in Cu(I) complexes.

Table 14 λ_{max} and related ε for Cu(II) complexes in acetonitrile.

complex	R'	R''	R'''	Y	λ_{max} /nm[a]	ε /dm^3 mol^{-1} cm^{-1}
17	H	H	*o*-Tolyl	none	688	79
18	H	H	*o*-Tolyl	Cl	692	112
19	H	H	Mesityl	none	695	124
20	H	H	Mesityl	Cl	696	157
21	CH_3	H	Mesityl	none	696	106
22	H	CH_3	CH_3	Cl	741	226

[a] ± 2 nm.

The low absorption intensity (around 100 and 200 dm^3 mol^{-1} cm^{-1}) and the relatively high λ_{max} made negligible the overlap of these optical spectra with that of the sensitizers. So differently from the reduced counterpart, the study and the optimization of the oxidized form of the redox mediators

was focused to increase its stability. In fact due to the quite high oxidation potential of the complexes the Cu(II) forms tended to convert into its more stable reduced one.

Time stability

The stability of Cu(II) complexes became clearly evident trying to synthesize the species [Cu(2,9-dimethylphenanthroline)$_2$]$^{2+}$ starting from $CuSO_4$ precursor (pathway C, Scheme 7). When at the end of the reaction the mixture was slightly heated to evaporate co-solvent ACN the solution turned from green to red; characterization via UV-vis spectroscopy of the isolated red powder revealed a spectrum perfectly superimposable to that of the species **12**, the reduced form of the desired product. Such kind of transformation occurred also for the other synthesized Cu(II) complexes **17**, **19**, **21** even if the conversion was significantly slower as monitored recording visible spectra after different periods of time, that spread from some hours to days and even months. As an example Figure 37 reproduces the time evolution of a sample of **17** dissolved in ACN stored in a close vessel (opened only for the measurements), at room temperature and away from direct light to avoid possible concomitant photodegradation processes.

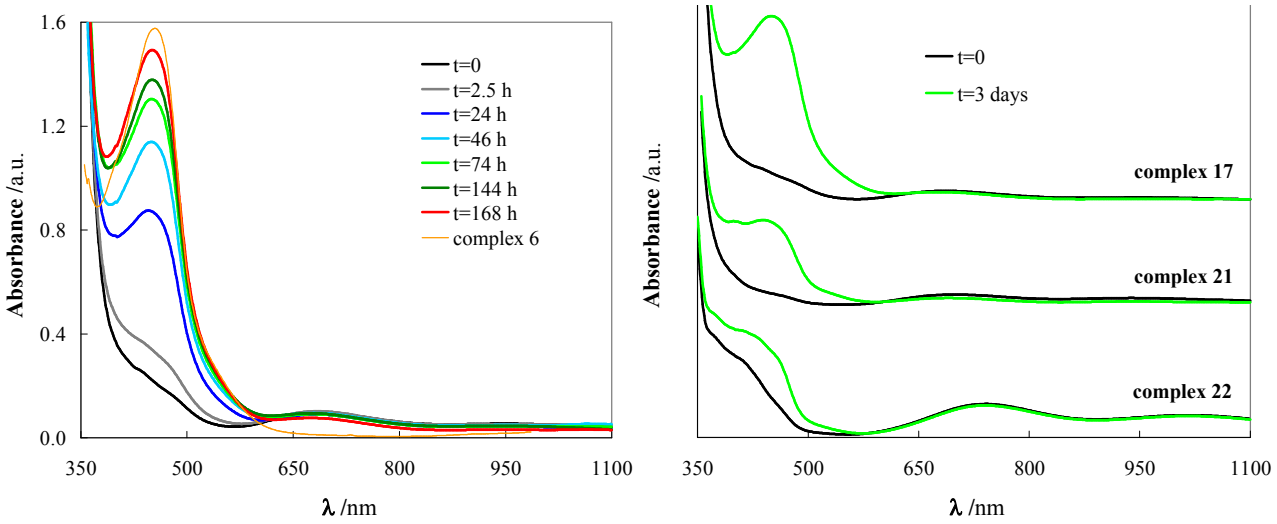

Figure 37 Left: effect of time (up to one week) on the visible spectrum of Cu(II) complex 17 (thick lines). For sake of comparison the spectrum of its Cu(I) analogue, 6, is also reported (orange thick line). Right: comparison at fixed time of the spectra for complex 17, 21 and 22. Sample concentrations *ca.* 0.001 M in ACN.

A possible explanation for the slower interconversion of **17**, **19**, **21** into their corresponding Cu(I) complexes **6**, **8** and **9** respect to the just mentioned case of [Cu(2,9-dimethylphenanthroline)$_2$]$^{2+}$ was found in the more negative potential of their half-wave potentials (see electrochemical section below, for farther information); this seemed to suggest that the possible turning point toward the enhancement of the chemical stability of Cu(II) species could be the stabilization of the cupric state of the complex metal. Moreover, as shown in Figure 37, the presence of the fifth chloride ligand in complex **22** (as clearly confirmed by mass spectrometry analysis, surprisingly never reported in literature before, see gallery Figure G 6) resulted in a slower interconversion of the complex respect

to both tetra-coordinated species **17** and **21**. Their relative stability has been estimated by the intensity of the MLCT band at shorter wavelength (around 450 nm) that raises during time taking also into account the ε of each Cu(I) counterparts (ε ≈ 4.5 dm^3 mol^{-1} cm^{-1} for both **17** and **21**, and 8.0 dm^3 mol^{-1} cm^{-1} for **22**, Table 13).

Starting from these hypotheses and considering that no literature evidences was found for [Cu(2,9-dimethylphenanthroline)$_2$]$^{2+}$ but only for its penta-coordinated analogue [CuCl(2,9-dimethylphenanthroline)$_2$]$^+$, **22**, I tried to synthesize Cu(II) complexes **18** and **20** bringing a chloride ion as the ancillary ligand, according to the pathway D of Scheme 7. Omitting the case of the species **18** (due to the undesired partially co-presence of species **17** in the isolated sample) the introduction of Cl^- ancillary ligand gave rise to a very stable complex **20** which remarkably enhanced the stability of its tetra-coordinated analogue **19** as confirmed by the perfectly superimposable optical spectra recorded even after two months since its dissolution in ACN (Figure 38). The improvement of stability achieved by ancillary ligand was attributed, as hypothesized, to the stabilization of the cupric state of the central atom as deeply studied by cyclic voltammetry (see relative section for more details).

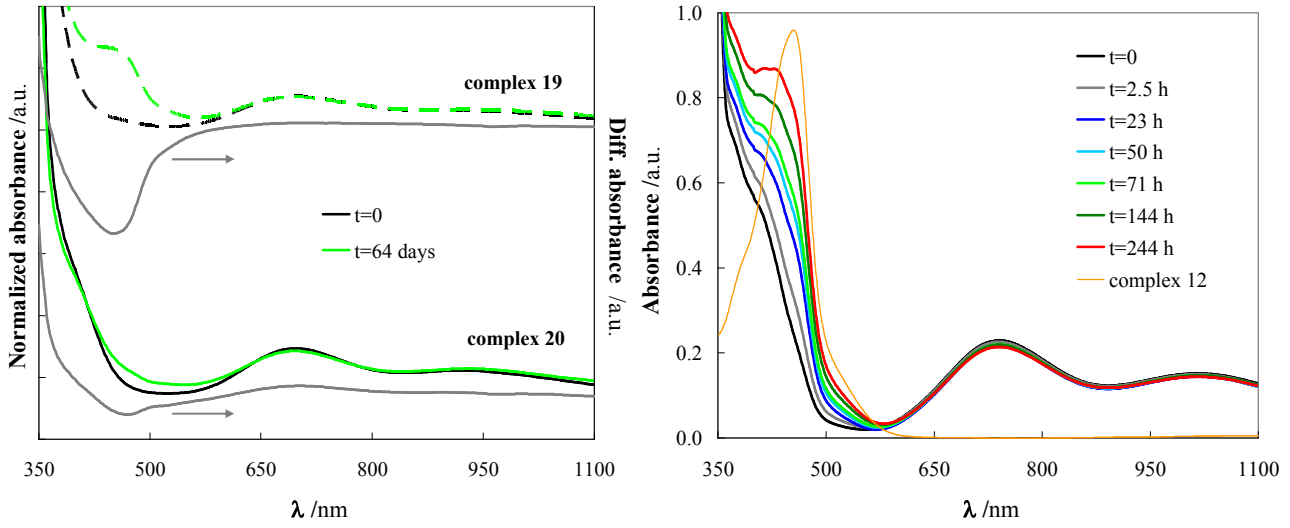

Figure 38 Left: comparison of the visible spectra of complexes 19 (up) and 20 (down) after two months. Differential spectra (gray lines) are also reported $\Delta A = A_{t=0} - A_{t=64\ days}$. Right: time evolution of complex 22 (thick lines) and, for comparison, the spectrum of complex 12 (orange thin line). Cu(II) concentrations *ca.* 0.001 M in ACN.

It is mandatory to highlight that in any case the interconversion process observed does not significantly modify the composition of an electrolyte of a DSSC formulated with these copper-based mediators, first of all because the process progressively slows down in time reaching an equilibrium and in second instance the composition of an actual electrolyte generally presents a quite large excess of reduced species respect to its oxidized one (in our studies 10:1 or even higher). Moreover the high intensity of the MLCT band respect to the ligand field one misleads; in fact this difference is mainly attributable to the more than ten-fold higher molar absorption coefficient of the

cupric species respect to the cuprous one. For example in the case of species **17** shown in Figure 37 only around 10% of the original Cu(II) species was converted after one week; considering a longer time period, after two months only less than 5 % of the species **19** (Figure 38) was converted.
In conclusion the introduction of ancillary ligand (possibly even different from chloride) seemed to be a possible and feasible method to improve the stability of Cu(II) species and so to improve their interest for a future large scale application.

Electrochemical study

Similarly to the previous section dedicated to optical study, this important part of the project was devoted not only to study the general electrochemical behaviour of our homoleptic copper complexes but also to understand how the substituents on the phenanthroline ligands influence the thermodynamic (*i.e.* half-wave potential, $E_{1/2}$) and the kinetics (*i.e.* heterogeneous rate constant, k_{het}) of their metal-centred electron transfer directly involved in the operation of a DSSC. The possibility to draw a sort of "activity *versus* structure" map not only allows a rationalisation of the electrochemistry of these compounds that surprisingly have not been object of a comprehensive study yet, but it has also been of fundamental importance for the interpretation and also prediction of the photovoltaic results obtained by DSSC tests that will be reported in a following chapter. In fact many photovoltaic parameters of solar cells are strictly related to the electrochemical properties of the redox mediators. For example the $E_{1/2}$ of the electrolyte (equal to the $E_{1/2}$ of the redox couple) defines the maximum photovoltage potentially generated by an ideal photon-to-current device, being equal to the difference in energy between the chemical potential of electrons in solution and that in the TiO_2 semiconductor. Moreover the $E_{1/2}$ can also significantly affect the thermodynamic aspect (the driving force) of both the efficiency of dye regeneration process and the extent of the parasitic dark current. Similarly the electron transfer rate constant remarkably affects in the first instance the mediator regeneration occurring at the cathode interface which in turns contributes in defining the fill factor, *FF*, parameter of the cell.
In the following pages will be reported the results of the electrochemical studies that have been classified into three subchapters including respectively the thermodynamic aspects of the electron transfer, the observations on the ET kinetics and, finally, the study concerning the effect of the cathode material on the ET of a cupric species chosen as example. It is necessary to underline that in some cases the boundary between thermodynamic and kinetics is quite thin, so possible interconnection between this subchapter will be possible.

Aspects affecting the redox potential of complexes

Notwithstanding the rich literature concerning electron transfer at copper centres extensively reviewed by Rorabacher [77] few years ago, a comprehensive study on the electrochemical properties of bis(phenanthroline)copper complex family is completely absent to my knowledge. As anticipated one of the objective of this part of thesis has been to try to fill this gap analysing how electrochemical features of phenanthroline-based copper complexes are affected by ligand substituents and by other experimental conditions such as solvent, supporting electrolyte and coordinating agents. To do this a relatively large and variegated ensemble of Cu(I) analogues was investigated, see Table 11. Many of these results have been collected and published in a paper [110].

Substituent effect

A first screening was performed on six complexes (Figure 39) properly chosen to have different substituents in both internal and external positions (*i.e.* 2 an 9, and 4 and 7 positions respectively) on the phenanthroline scaffold, in order to elucidate the general features of the complexes (also comparing their patterns with that of free-ligands) and to clarify the role played by the substituents.

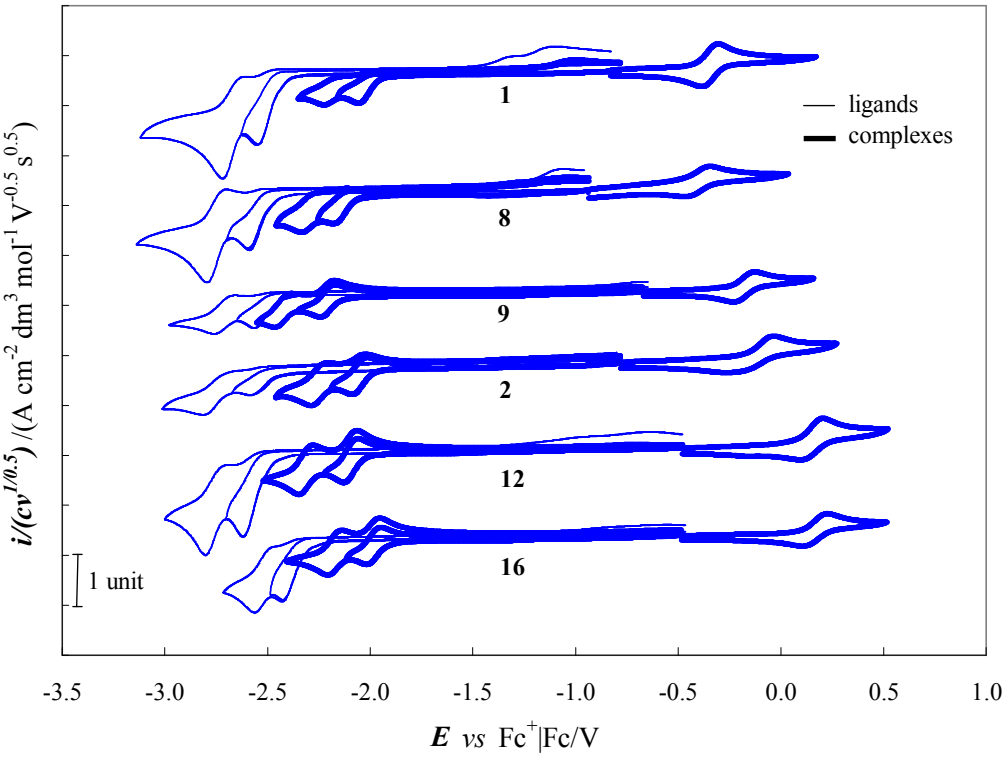

Figure 39 Synopsis of normalized CVs on GC electrode for a representative ensemble of Cu(I) complexes (thick lines) and of their related phenanthrolines as free-ligands (thin lines). The number of substituents in 2 and 9 positions of the phenanthrolines progressively increased from top to bottom. Sample concentration around $1 \cdot 10^{-3}$ M in DMF and $TBAPF_6$ 0.1 M. Ohmic drop compensated by positive feedback.

All six phenanthrolines were oxidatively stable but they presented two subsequent reduction peaks; the first one was monoelectronic, electrochemically quasi-reversible and chemically irreversible

that can be tentatively attributed to the formation of a radical anion species as suggested in some literature works [111]. The second, more negatively shifted, peak was more chemical reversible. The relative peak positions along the series can be explained simply in term of the inductive or mesomeric electronic effect of the substituents. Substituents in the internal positions had more pronounced effects than analogue ones placed in 4 and 7 positions, suggesting a greater distance of the latter from the reduction redox site (compare the peak shift of **2** and **12** *vs* **1**, and **2** *vs* **1** respectively). The positive shift of the peak potential induced by the mesomeric effect of two analogue aromatic substituents (*i.e.* a phenyl in **L16**, and a mesityl in **L9**) revealed to be significantly affected by the position of the functionalization (compare the peak distance between **L16** and **L12**, with that between **L9** and **L8**). The particularly smoothed effect induced by mesityl ring could be indicative of a hampered π-conjugation between the aromatic ring and the condensed heteroaromatic scaffold.

Contrary to the free-ligand cases, the complexes exhibited a monoelectronic chemically reversible peak (Figure 39) attributable to a metal-centred electron transfer in addition to the two reduction peaks assigned to ligand-centred processes according to the localization of the computed HOMO and LUMO (see Figure 34, and Figure 40).

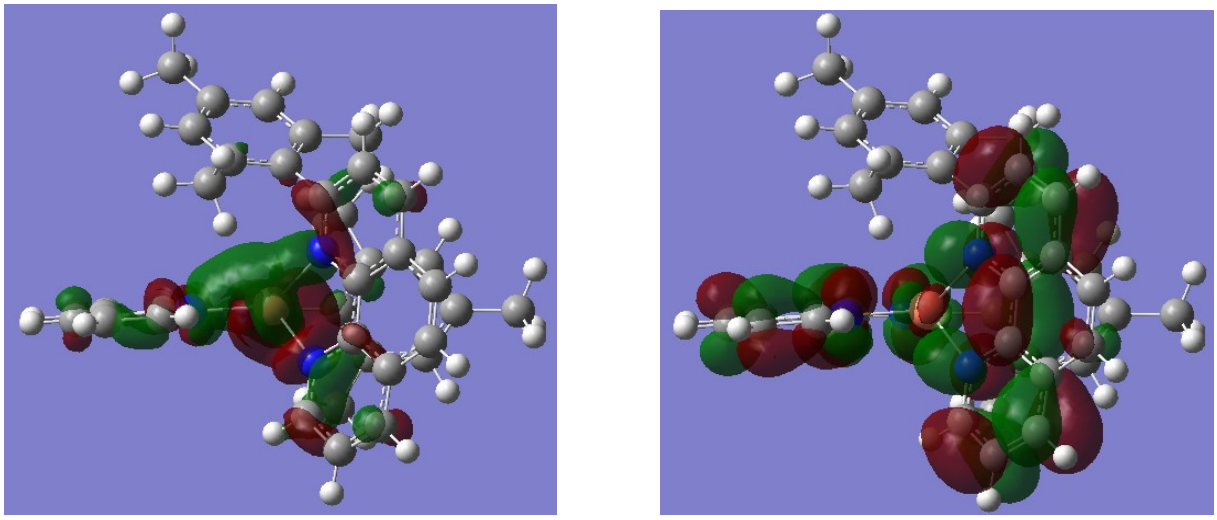

Figure 40 Isodensity surface plots of HOMO (left) and LUMO (right) for complex 9. Isodensity contour: 0.02.

Comparison of convoluted currents allowed to establish that the reduction processes involved the exchange of one electron per complex molecule; for comparison with free-ligands, the two reduction peaks of complexes should correspond to the formation of two stable radical anions on each phenanthroline group, behaving as equivalent but reciprocally interacting redox sites. The net increase of the stability of the species electrogenerated during the reduction and the positive shift of the peaks respect to the corresponding free-ligands are both coherent with the metal complexation that reduces the electron density on the phenanthroline core.

Much more interesting was the analysis of the anodic window, and the study of the just anticipated Cu^{2+}/Cu^{+} ET which is directly involved when the complexes are employed as redox mediator in DSSC. It is a monoelectronic, chemically reversible, and quasi-electrochemically reversible process that differently from the ligand-based reactions is mainly influenced by steric effects of the chelating ligands, overshadowing electronic ones. In fact the expected negative shift of the peak potential upon introduction of electron releasing methyls was observed only in the case of complex **8** in which the substituents are placed in the external position of the phenanthrolines (**8** *vs* **1**). Instead substituents placed in the internal 2 and 9 phenanthroline positions chiefly influence the behaviour of the Cu^{2+}/Cu^{+} redox couple through their steric hindrance, affecting the geometry around the metal centre.

Actually similar experimental observation have already been cited in literature [112], [113] but they were highly fragmented and never combined organically in a rational way. The novelty introduced here was essentially the inclusion in the electrochemical study of bis(2-substituted-phenanthroline)copper complexes (**9** and **2** of the investigated series) that allowed to clearly and univocally demonstrate that the energetics of the electron transfer occurring at the metal core is strictly proportional to the number of occupied internal positions. In particular higher the number of substituents adjacent to the two nitrogen atoms of the chelating ligand more positive the half-wave potential, $E_{1/2}$, of the corresponding copper complex. In fact the six complexes appear clearly partitioned in three distinct groups (Figure 39): **1** and **8** (no internal substituent), **9** and **2** (one internal substituent), **12** and **16** (two internal substituents). In more detail comparing **1**, **2** and **12** complexes, the subsequent addition of methyl groups in the 2 and 9 positions regularly shifts the anodic peak at more positive potentials by *ca.* 0.25 V per each substituent, in a direction opposite to that virtually induced by their electron releasing nature.

This rationalization allowed us to forecast one of the main important electrochemical parameter (*i.e.* $E_{1/2}$) of a new designed complex even before it is synthesized and tested; in other word the just discovered strictly correlation between the internal substituents and the oxidation potential made possible both the preparation of copper complexes with $E_{1/2}$ both spread over a wide potential gap and fine modulated combining the steric effect of substituents with the electronic ones. This is a remarkable result of this project because it allowed the development of copper complexes as redox mediators for DSSC with oxidation ability optimized for each specific dye. In this way useless loss of exploitable potential can be limited for example minimizing the driving force necessary for dye regeneration process. Incidentally this is exactly one of the main drawback of the common I_3^-/I^- redox couple that makes it far away from being ideal mediators.

The modulation of $E_{1/2}$ by the internal substituents has been not only a powerful tool for the synthesis of copper complexes with desired oxidative ability but also a diagnostic parameter to confirm the metal-centred nature of the redox process occurring in the anodic window. Generally speaking complexes in which copper is in one of its two more common Cu(I) or Cu(II) oxidation states assumed preferentially a tetrahedral geometry with a 4-coordinate environment and a distorted tetragonal one with 5- (or even 6-) coordinate environment respectively [77], [114], [115]. The presence of substituents adjacent to the two chelating nitrogens should interfere with the geometry rearrangement that accompanies the ET process. This can explain the remarkable half-wave potential dependence from the internal substituents. The steric effect exerted by 2,9 substituents can be compared with the operation of a *kiss-lock enclosure* employed in some women's handbags; increasing the number of internal substituents the geometry modification induced by ET is progressively hampered forcing the electrogenerated product (*i.e.* cupric complex) to maintain an environment around the central copper atom similar to the original one preferred by Cu(I) species. This would result in destabilization of the Cu(II) product, and therefore in a less thermodynamically favoured ET that accounts for the positive shift of the Cu^{2+}/Cu^{+} reversible process observed moving from top to bottom in the Figure 39.

Solvent effect

Considering the unsaturated coordination sphere of the species generated cycling the potential around the metal-centred reversible peak the electron transfer process could be potentially affected by coordinating species, including molecules of donating solvent[7].

Accordingly with this hypothesis the solvent appeared to be selectively non-innocent for the Cu^{2+}/Cu^{+} ET process while it did not affect significantly the ligand-based reduction processes (Figure 41). A progressive negative shift of the metal-centred process was recorded for complex **9** (taken here as an example) with the increasing of the donating ability (or, equivalently, polarity) of the solvent going from less polar DCM to DMF, passing through intermediate donating ACN. Same trend was recorded for all the six complexes previously discussed (Figure 42).

[7] The quantity *donor number*, DN, was defined to quantify the Lewis basicity (*i.e.* "coordination ability") of a chemical species including solvents.

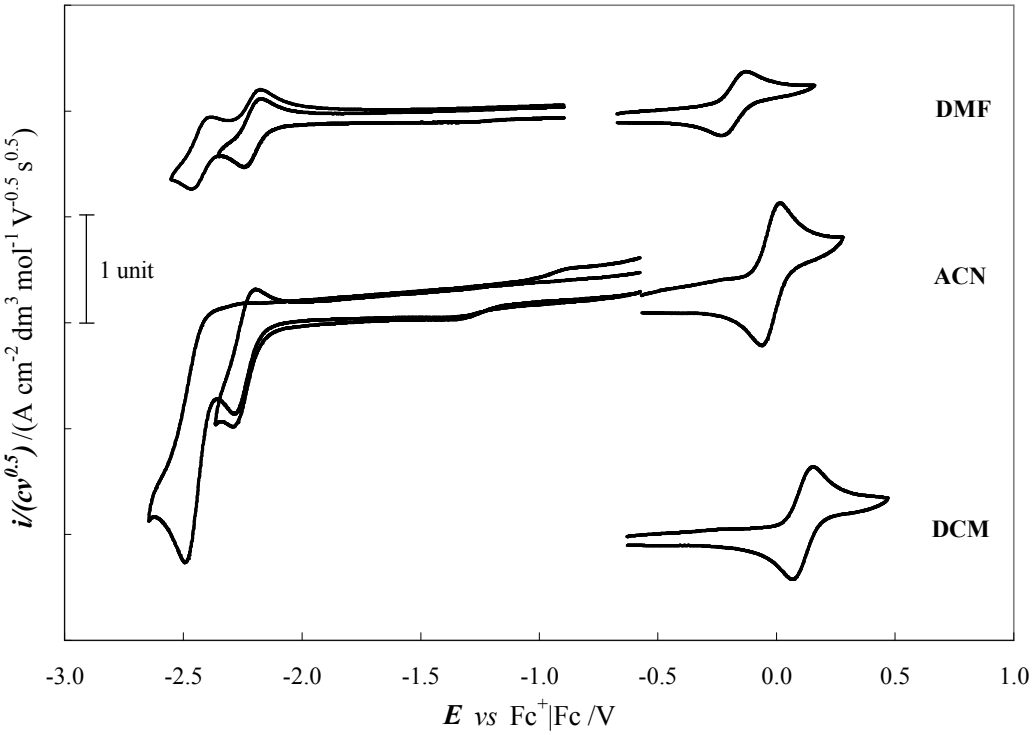

Figure 41 Synopsis of normalized cyclovoltammograms of complex 9 dissolved in solvents of different donating ability (from top to bottom in decreasing order: DMF, ACN and DCM). The supporting electrolyte was $TBAPF_6$ 0.1 M in al three cases; GC electrode. Compensation of the ohmic drop by positive feedback technique. (Cathodic pattern in DCM was not reported to due a specific interaction of solvent with the sample.)

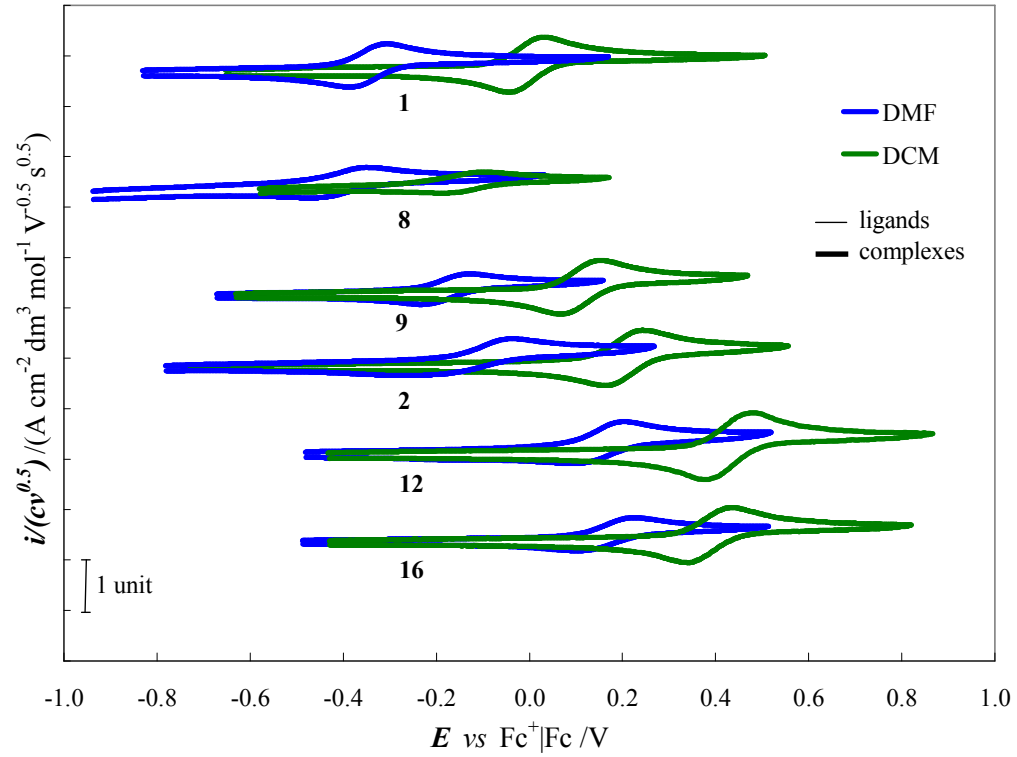

Figure 42 Synopsis of normalized cyclovoltammograms of the six sample complexes recorded in DMF and DCM. In both cases the supporting electrolyte was $TBAPF_6$ 0.1 M; GC electrode. Compensation of the ohmic drop by positive feedback technique.

The selectivity of the solvent-induced phenomenon points to a direct interaction between solvent and the central metal, as reported also in former literature [77], [114], [115], which results in a

thermodynamic stabilization of the electrogenerated Cu(II) complex. It is interesting to not that the conspicuous negative shifts of peak potential from the low polar DCM to much donating DMF was of *ca.* 0.28 V except for **1** and **16** corresponding to the least and most hindered complexes (due to the 4,7 phenyl rings) which showed the higher and the lower displacement respectively.

Thank to this work, for the first time, a direct observation of the involvement of solvent molecules in the inner coordination sphere of copper complexes was obtained by a pure electrochemical method, avoiding the employment of more complicated and sophisticated spectroelectrochemical combined-techniques. In more detail an adapted protocol was developed starting from a polarographic method originally proposed in 50's by Kolthoff and Lingane [116] to study the "sequestration" phenomenon of diverse metal cations dissolved in water by coordinating molecules following the negative shift of their half-wave reduction potentials upon increasing ligand, L, concentrations, accounting for increasing reagent ion stabilization. In fact for electro-chemically reversible systems, exchanging n electrons per wave, the following linear relationship holds:

$$\Delta E_{1/2} = -(k/n)\log K_f - p(k/n)\log c_L \qquad \text{(eq. 1)}$$

where $\Delta E_{1/2} = E_{1/2,\text{complexed ion}} - E_{1/2,\text{metal ion}}$, k = Nernst parameter, n = number of exchanged electrons (per mole of sample), K_f = complex formation constant, p = complexation number.

In the present study the role originally played by metal cations was taken by the cationic copper complexes, while the coordinating ligand became the donating DMF molecules. However similarly to original protocol the negative potential shift was followed of the Cu^{2+}/Cu^{+} oxidation peak potential of the complexes dissolved in low polar DCM, upon small additions of polar DMF which promoted the oxidation process providing an auxiliary ligand for the preferred 5-coordinate geometry of the Cu(II) complex product. Thus, according to previous equation, plotting $\Delta E_{1/2}/(k/n)$ *vs* $\log c_{DMF}$ should yield a straight line which slope accounts for the DMF complexation number and its intercept accounts for the formation constant of the DMF: complex adduct. In this case $\Delta E_{1/2}$ in the equation was define as followed: $\Delta E_{1/2} = E_{1/2,\text{ copper complex, with DMF}} - E_{1/2,\text{ copper complex, in pure DCM}}$.

It is worthwhile noticing that results of the subsequent DMF additions gave raise to straight lines in $\Delta E_{1/2}/(k/n)$ *vs* $\log c_{DMF}$ plots with quite unitary slopes, hence evidencing that the DMF complexation number resulted in all cases *ca.* 1. Figure 43 below reports as an example the plots obtained for complexes **1** and **9**, together with the related linear regression parameters.

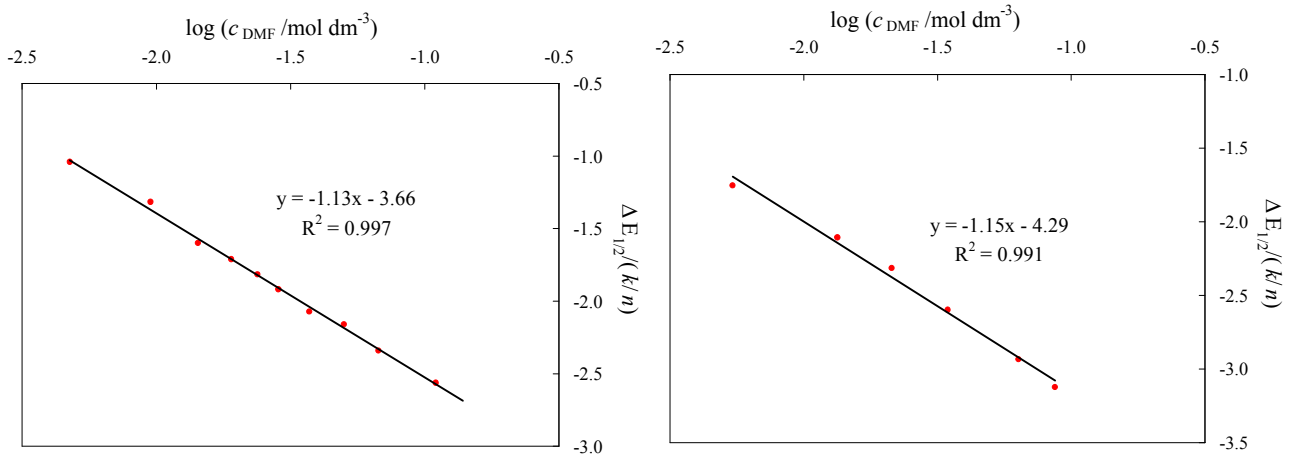

Figure 43 Oxidation half-wave potential shift, $\Delta E_{1/2}$, for the complexes 1 (left) and 9 (right) upon progressive additions of small volume of DMF ligand starting from a pure DCM solution of the complex.

As anticipated the study just described represents the first example in literature of the application of a purely electrochemical method to prove the direct interaction of coordinating solvents with the central metal of complexes, and to even quantify the number of these interacting solvent molecules per molecule of complex. The results supports the original hypothesis developed starting from the simple qualitative observation of the net negative shift of the oxidation peak potential of the complexes when recorded in DMF respect to DCM (Figure 42); in particular it was proven that a molecule of donating DMF (and, considering the trend of the potentials in Figure 41 and Table 15, of ACN too) could easily provide the ancillary ligand required for the 5-coordinate geometry preferred by Cu(II), resulting in a more thermodynamic favoured oxidation process.

Even if the metal-centred ET was significantly modulated by the nature of the working medium the relative peak positions along the reference series of the six complexes were maintained independently by the solvent polarity (Figure 42); this means that the substituent effect already described for sample dissolved in DMF remains invariably valid also in other solvents. The study of the effects of ligand substituents and of the solvent was also extended to a larger, and so more representative, ensemble (Table 15) to confirm or disprove the conclusion just formulated above. Considering the huge impact of the solvent on the energetics of Cu^{2+}/Cu^{+} process the study on this second larger ensemble was performed using a more suitable solvent for the subsequent tests in DSSCs (*i.e.* acetonitrile) to have more realistic picture of the energetics in the photovoltaic devices.

Table 15 summarizes the $E_{1/2}$ value of complexes potentially exploitable as redox mediators in DSSC, so characterized from a relatively high oxidation potential; for sake of comparison the completely unsubstituted complexes has been also included.

Table 15 Main electrochemical parameters for some Cu(I) and tetra-coordinate Cu(II) complexes in ACN and DCM on GC electrode. Half-wave potential, $E_{1/2}$, are referred to the intersolvental reference couple $Fc^+|Fc$. Potential scan rate 0.2 V s^{-1}.

complex	R'	R''	R'''	ACN	DCM
				$E_{1/2}$ /V	$E_{1/2}$ /V
1	H	H	H	–0.38	–0.01
2	H	H	CH_3	0.02	0.20
3	H	H	*n*-Bu	0.11	0.32
4	H	H	*t*-Bu	0.34	0.38
5	H	H	Ph	0.10	0.23
6 and 17[a]	H	H	*o*-Tolyl	0.09	0.25
7	H	H	Mesityl	0.06	–
9 and 21[a]	CH_3	H	Mesityl	–0.02	0.11
11	*p*-Tol	H	Mesityl	0.05	0.23
12	H	CH_3	CH_3	0.30	0.43
14	H	Cl	Cl	0.55	0.75
15	H	I	I	0.60	0.81
16	Ph	CH_3	CH_3	0.29	0.39

[a] Cu(II) complexes **17**, **21** were measured only in ACN.

As a result the hypothesis of the *kiss lock* effect by 2,9 substituents was confirmed, being all complexes with monosubstituted ligands more easily oxidized than disubstituted derivates; the only exception was found for the *tert*-butyl substituted complex **4** which confirmed its peculiar character already evidenced during the spectroscopic analysis performed in ACN. The clear anomaly of complex **4** detected along the series of $E_{1/2}$ recorded in ACN was quite difficult to interpret considering that the peculiar behaviour was observed only with same kind of characterizations (*i.e.* in the optical and electrochemical properties, but not in the nuclear features as confirmed by ^{1}H-NMR). However considering its quite high oxidation potential in ACN and the too small negative shift respect to DCM medium, I tentatively attribute at least the electrochemical anomaly to the high 3-D character of *tert*-bu groups that can prevent (or better hamper) the coordination of the donating ACN molecule with the central copper atom resulting in a lower stabilization of the Cu(II) product.

It is interesting to note that in this second ensemble have been included also complexes bringing electron withdrawing halogen groups in the two internal positions of phenanthrolines (*i.e.* **14** and **15**). Their extremely high $E_{1/2}$ were explained considering the additive nature of the electronic effect of substituents that summed to that exercised by the steric hindrance of the halogen. However the more positive $E_{1/2}$ of di-iodo derivate respect to the di-chloro analogue was a further confirmation of the predominant effect of steric factors over the electronic one for substituents adjacent to chelating

nitrogens; in fact accounting for pure electronic effect (*e.g.* polarity) an inversion in the potential value should be expected. Similar conclusion could be obtained for the increasing half-wave potential value in the series **2**<**3**<**4** evaluated in DCM, in order to avoid the just described peculiarity of **4** in ACN (Table 15). This order could be explained in term of increasing bulkiness of alkyl chains (Me<*n*-Bu<*t*-Bu) while the exactly opposite order should be recorded if the electron releasing nature of the substituents (*t*-Bu>*n*-Bu>Me) was the predominant effect.

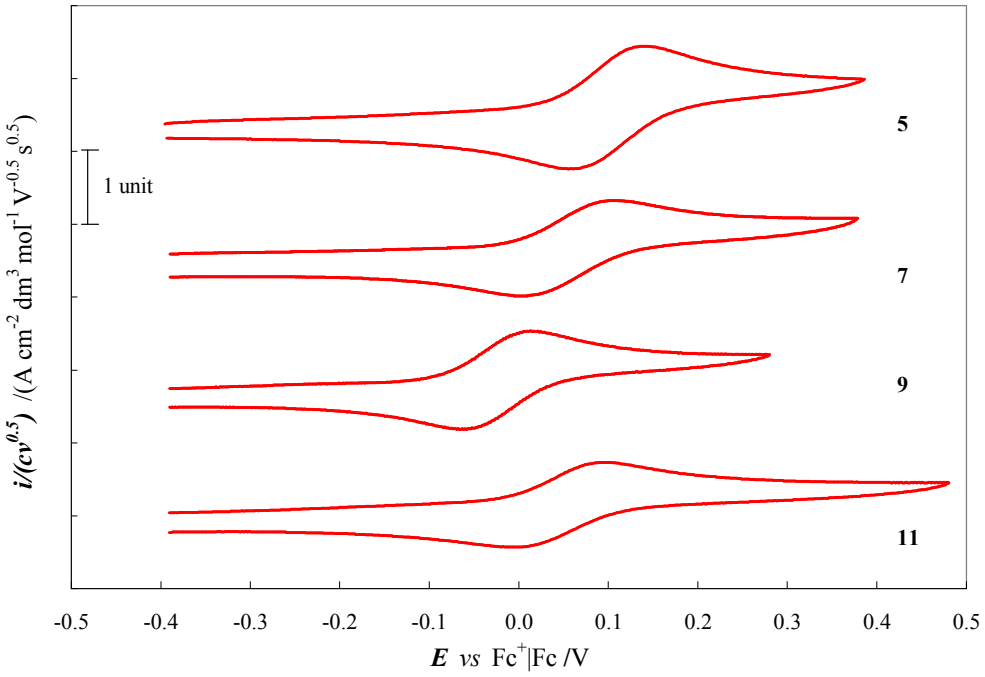

Figure 44 Comparison of CVs for complexes bearing 2-aryl-substituted-phenanthrolines (aryl = phenyl for 5, and mesityl for the other complexes) bringing also different substituents in their 4 and 7 positions (hydrogens for 5 and 7; methyls for 9; and *p*-tolyl for 11). Sample concentration 0.001 M in ACN with TBAPF$_6$ 0.1 M, on GC electrode.

On the contrary the half-wave potential of the metal-centred process is controlled by electronic effects if the substituents are placed in the external 4 and 7 positions of the phenanthrolines (**8** *vs* **9** *vs* **11**, Figure 44). According to the slightly electron attracting nature of a tolyl group respect to the electron releasing nature of a methyl (as demonstrated by Hammett constant values [117]) the complex **11** resulted more hardly oxidizable than **9**; the latter in turns had a $E_{1/2}$ negatively shifted of *ca.* 80 mV respect to the "reference" compound **8** unsubstituted in the external positions due to the electron releasing nature of –CH_3 groups.

The tetra-coordinate Cu(II) complexes **17** and **21** showed cathodic and anodic patterns perfectly superimposable to their corresponding Cu(I) species, **6** and **9** confirming that the *in situ* electro-generated species from **17** and **21** during potential cycle is actually **6** and **9** and vice versa. On the contrary an unexpected pattern was recorded for species **19**, differing from its Cu(I) counterpart **7**. Further analysis will be necessary to clarify this strangeness. Discussion of the penta-coordinate

Cu(II) species **18**, **20** and **22** will be addressed in the next subsection regarding the effect of chloride ions.

Summarizing the measurements performed on this second larger ensemble of Cu(I) complexes confirmed the hypothesis of *kiss lock* and hence the crucial role played by internal substituents on the phenanthrolines in determine the $E_{1/2}$ of the metal-centred process. Steric effect neatly prevails on the electronic one for internal substituents, while only electronic nature of the external groups are important in tuning the oxidation ability of complexes. Even if the number of substituents on 2- and 9-carbons allowed to spread the half-wave oxidation potential on a quite huge window (up to 1 V, combining also the additive effect of EWD groups), the employment of different alkyl and aryl groups can be exploited to finely tune the oxidation potential of the resulting complexes probably due to their effect on the geometry of the metal centre. For example the free rotation of internal substituents (such as in **5**, see figures G 7 and G 9) can induce a different geometry in the complex respect to similar "freezed" groups (like in **9** or **13**, see figures G 7, G 8 and G 10) resulting in different electrochemical properties (*i.e.* different $E_{1/2}$ but also diverse k_{heter}, see following chapter). Unfortunately combination of crystal structural information by X-ray diffraction analysis with electrochemical data did not help in defining a more general rule.

Anion effect: complex counterions and supporting electrolyte counteranion

The working medium can affect the metal-centred oxidation process not only through the just discussed interaction of a donating solvent with the inner coordination sphere of the copper atom but also through the anion of the supporting electrolyte (mandatory in any voltammetric measurements). In this case the interaction could occurred through coulomb forces exerted between the two species of opposite charge (*i.e.* the cationic complex and the anion of the supporting electrolyte) resulting in a ion pair formation that should be favoured in solvent with low relative permittivity. The result of the hypothetic ion pair formation should be similar, even if less pronounced, to the effect exerted by the aforementioned solvent:complex adduct formation, it is a selective negative potential shift of the Cu^{2+}/Cu^{+} ET process as a consequence of the thermodynamic stabilization of the electrogenerated Cu(II) product, while leaving unchanged the ligand-based processes.

Actually experimental proof for the non-innocent role of the anion of the supporting electrolyte in the electrochemical features of cuprous/cupric complex transitions was obtained. Such verification was achieved on complex **9** (Figure 45) considering solvents of decreasing relative permittivity (DMF >ACN>DCM) in combination with tetrabutylammonium supporting electrolytes with counteranions of increasing donating ability ($BPh_4^-<PF_6^-<ClO_4^-$) [118].

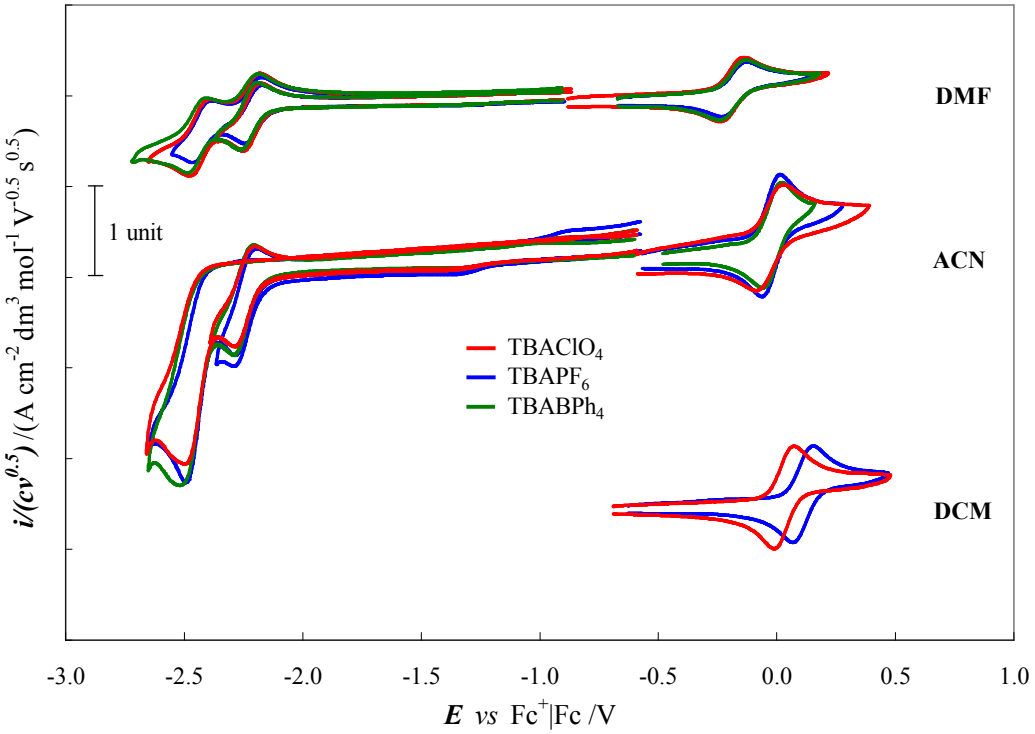

Figure 45 Synopsis of normalized cyclovoltammograms of complex 9 recorded in solvent of decreasing polarity (DMF, ACN, DCM) employing supporting electrolytes 0.1 M having anions of different donating ability ($TBAClO_4$> $TBAPF_6$>$TBABPh_4$). GC electrode; compensation of the ohmic drop by positive feedback technique.

As expected no significant variation of the $E_{1/2}$ was observed changing the supporting electrolyte anion in the two more polar solvents (*i.e.* DMF and ACN); on the contrary in the lower polar DCM a negative shift of *ca.* 0.1 V is observed substituting PF_6^- with the smaller, more donating ClO_4^- anion. The different behaviour of the electrolyte anions in the polar and low polar media could be ascribed to the polar solvent hampering the ionic couple formation both on account of its relative permittivity (as anticipated) and also of its completing the 5-coordinate geometry of Cu(II) complex.

Attempts to quantify the ion pairing was performed exploiting an experimental procedure analogue to that previously described for the study of the solvent effect but, unfortunately, no significant results were obtained probably to the too low electrostatic forces acting in this situation.

To analyze in more detail the effect of the counteranion and the ion pairing effect two analogues of complex **9**, named complex **9-BF_4** and **9-ClO_4** (Figure 46), were studied in DCM with the less donating $TBABF_4$ supporting electrolyte (see gallery, Figure G 11). Complex **9-BF_4** and **9-ClO_4** differ from **9** only for the counteranion; it is a low donating tetrafluoroborate, BF_4^-, and the more donating perchlorate, ClO_4^-, respectively.

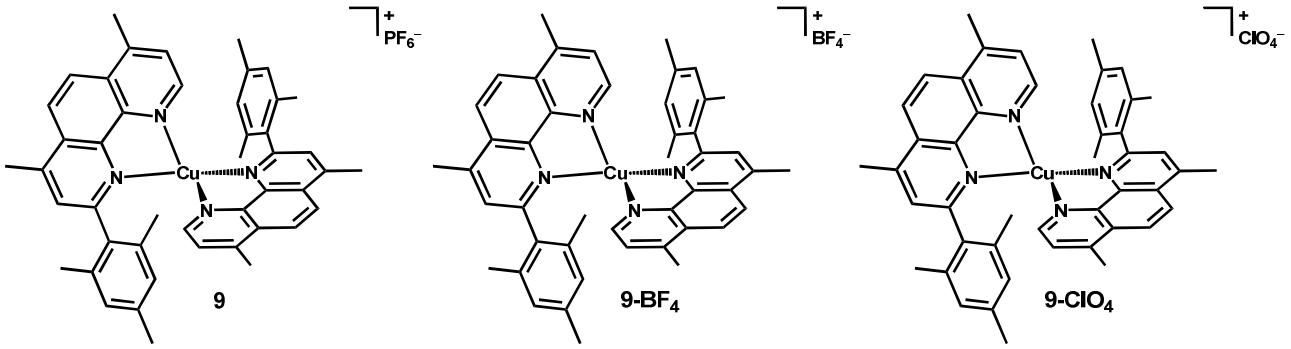

Figure 46 Structures of the analogue complexes 9, 9-BF_4 and 9-ClO_4 (from left to right).

In this case a quite absence of modulation of the $E_{1/2}$ of the metal-centred ET for the three analogue complexes was recorded; in fact all the half-wave potentials recorded fallen within a window of just 10 mV (*i.e.* $E_{1/2}$ = 0.080 , 0.074 and 0.069 V *vs* $Fc^+|Fc$ for **9**, **9-BF_4** and **9-ClO_4** respectively). This seemed to indicate that the cationic complex/counterion interaction involved quite weak forces and that only in presence of a significant excess of donating anions (*e.g.* ClO_4^-, when it was present as supporting electrolyte, 100-fold more concentrated than the sample) such interaction can modify through a mass-action phenomenon the energetic of the Cu^{2+}/Cu^+ ET process (Figure G 11).

Effect of coordinating species: chloride and tert-butylpyridine

Considering the capacity of a donating solvent to form an adduct with the coordinatively unsaturated Cu(II) species generated during the potential cycle around the reversible Cu^{2+}/Cu^+ peak couple, I also investigated by an electrochemical point of view what happened when other coordinating species (even more donating than solvent molecules) were added into a solution of the copper complexes. Attention was firstly focused on chloride ions that were employed in this work to stabilize Cu(II) complexes, as already discussed; the electrochemical study of the chloride interaction with copper complexes was employed to clarify the reason of the observed stabilization. *Tert*-butylpyridine, tbupy, was also investigated as a possible neutral and bulkier coordinating molecule considering its use as common additive in the formulation of DSSC electrolytes (as largely described in the previous sections).

The study of chloride effect was started comparing the CV patterns of Cu(I) complex $[Cu(neocuproine)_2]^+$, **12**, with that of its penta-coordinating Cu(II) counterpart $[Cu(neocuproine)_2Cl]^+$, **22**. Contrary to the perfect superposition of both cathodic and anodic patterns observed for **6**/**17** and **9**/**21** couples (Figure 47) for the couple **12**/**22** a net difference was detected for the metal-centred process despite the identical patterns for the two ligand-based ETs.

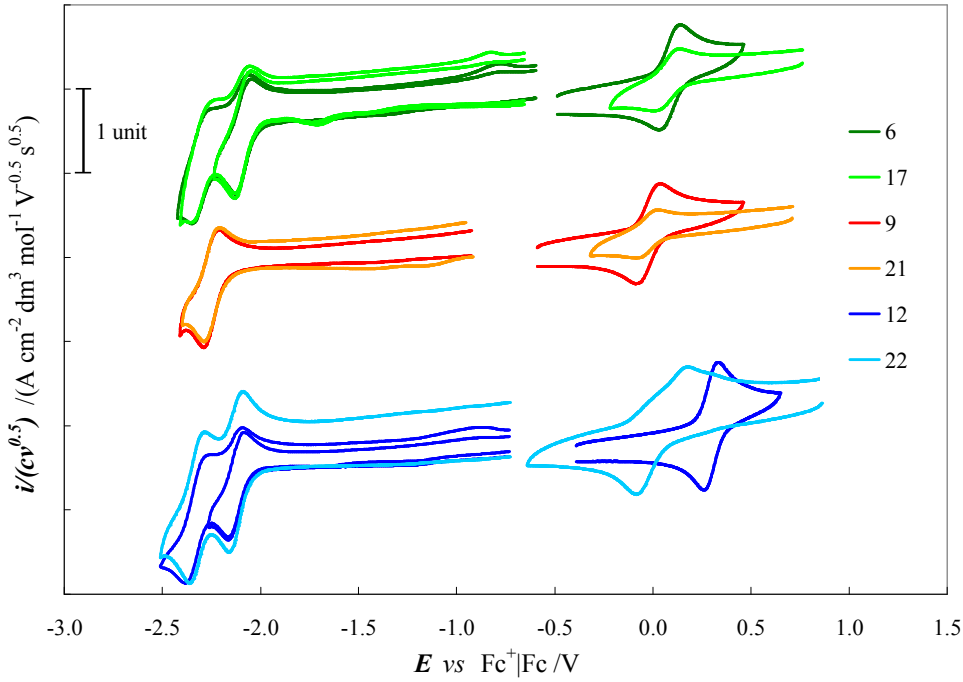

Figure 47 Synopsis of normalized cyclovoltammograms of Cu(I) complexes 6, 9, 12 and their related tetra-coordinate Cu(II) species 17 and 21, and penta-coordinate 22. Solvent ACN with $TBAPF_6$ 0.1 M on GC electrode; compensation of the ohmic drop by positive feedback technique.

Unexpectedly a net lower peak current was detected for the metal-centred process in both complexes **17** and **21** respect to their Cu(I) counterparts; on the contrary perfectly superimposable patterns were recorded for the two cathodic peaks. Moreover the intensity of the metal-centred oxidation process was observed to be dependent from the nature of supporting electrolyte (see gallery, Figure G 12), but the process was not further investigated.

Surprisingly no electrochemical information have been presented in previous works employing this complex as redox mediator [65], [66]; to the best of my knowledge the only paper is related to the characterization of the analogue complex $[Cu(neocuproine)_2Cl]Cl{\cdot}H_2O$ in absolute ethanol and in a 50% mixture ethanol/water, where a complicated electrochemical behaviour was observed [119]. The lake of data made the electrochemical characterization of complex **22** mandatory.

The Cu^{2+}/Cu^{+} ET of **22** was shifted toward more negative potential and exhibited a more pronounced electrochemical irreversibility than **12**. The half-wave potentials were 0.30 V *vs* $Fc^{+}|Fc$ for **12** (Table 15), and 0.04 V *vs* $Fc^{+}|Fc$ for **22**. These experimental observations were related to the additional chloride ligand that specifically modifies only the metal-centred process of species **22** making different the coordination sphere of copper atom in the two complexes **12** and **22** (tetra- and penta-coordinate geometry, respectively).

A dipper understanding of the chloride/complex interaction was obtained recording CVs at increasing concentration of chloride added as TBACl into the starting solution of complex **12**. The subsequent addition of sub-stoichiometric chloride ions to a solution of complex **12** (Figure 48)

showed the progressive raise of the negatively shifted peak couple related to complex **22** (*vide infra*), and the concomitant linear decrease of the peak couple attributed to the starting complex **12** (see gallery, Figure G 13) which disappeared when one equivalent of Cl^- was added; this clearly suggested the occurrence of Cl^- ions complexation by molecules of **12** which convert into a new species corresponding exactly to complex **22** (see also Figure 50).

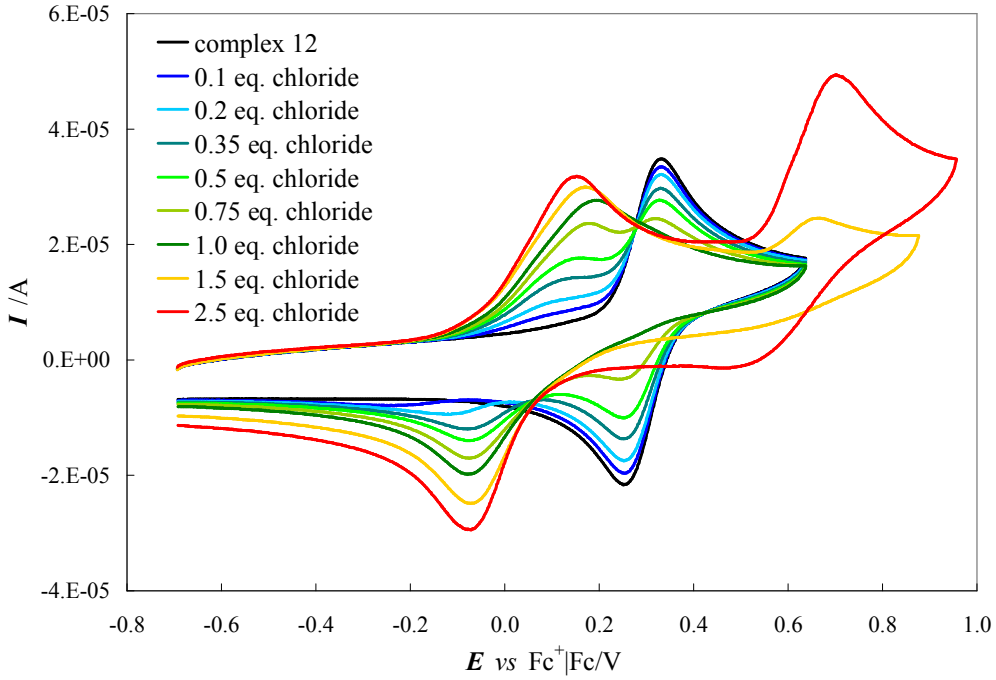

Figure 48 CVs of pristine complex 12 (black line) and at increasing amount of chloride ions spiked in the working medium as TBACl solution. Solvent ACN with $TBAPF_6$ 0.1 M on GC electrode; scan rate potential 0.2 V s^{-1}. Compensation of the ohmic drop by positive feedback technique.

The *ca.* 0.25 V potential shift in $E_{1/2}$ of **22** respect to **12** can be explained by the stabilization of the cupric state induced by the monodentate chloride ligand that forces the complex to assume a more energetically favorable tetragonal penta-coordinated geometry respect to the tetra-coordinated one of the cupric species resulting from the electrooxidation of **12**. In a similar way, the aforementioned increased electrochemical irreversibility of **22** can be attributable to a higher reorganization energy due to the significant variation of its coordination sphere occurring during the Cu^{2+}/Cu^+ ET which in turns means a higher energy barrier for complex **22** than for **12**.

Analysis of the morphology changes in the CV patterns of complex **22** recorded at different potential scan rate could give more information on its electron transfer process (Figure 49). If the scan rate was sufficiently high (*i.e.* higher than 1 V s^{-1}) an oxidation peak at less positive potential (peak A, in Figure 49) was progressively visible, suggesting the existence of a complicated electrochemical process. The electro-generated product, **22***, derived from the reduction of the starting species **22** can be subject to a follow-up chemical reaction characterized by a kinetics accessible in CV timescale; so the reoxidation of the electro-generated product can occur through

two different pathways corresponding to peak A and B in Figure 49. At low scan rates the backward ET (peak B, Figure 49) occurred on a chemically-modified species different from **22*** corresponding, probably, to complex **12** resulting from the dissociation of the chloride ancillary ligand; the difference of geometries between reagent, **22**, and product, **12**, supports the aforementioned high electrochemical irreversibility of this ET. On the other hand at high scan rates (*i.e.* when the scan rate potential is comparable with the rate of the follow-up reaction) the electro-generated cuprous species can be (even partially) directly reoxidized without undergoing to ligand dissociation reaction, resulting in the more electrochemically reversible process (peak A, Figure 49).

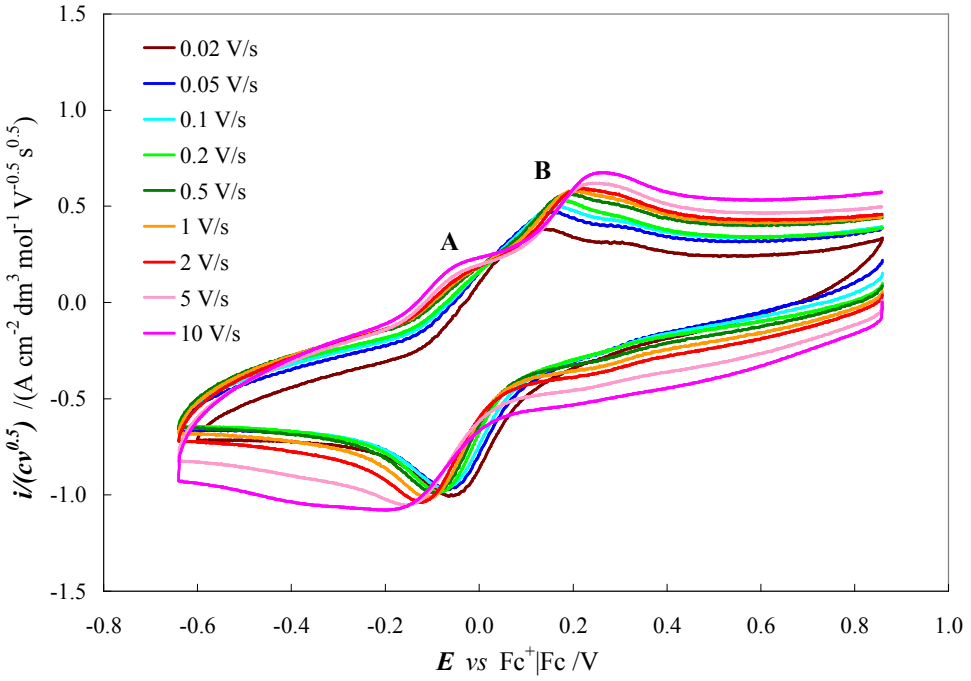

Figure 49 Normalized CVs of complex 22 recorded at different scan rate potentials (from 0.02 to 10 V s^{-1}) in ACN with $TBAPF_6$ 0.1M on GC electrode. Compensation of ohmic drop through instrumental positive-feedback method.

Experiments equivalent to those described just above for complex **22** involving the progressive addition of chlorides into the sample solution were performed starting from other Cu(I) and Cu(II) complexes and a similar complexation effect by chloride ions was observed (see figure G 14-15 for few examples); in particular the complete interconversion of the starting complex into its chloride analogue after addition of one equivalent of the halogenated ligand invariably characterized the measurements. As an example Figure 50 reports the results starting from **17** and **21** (besides the just described case of **12**). In all cases the coordination of Cl^- brought to a more electrochemical irreversible ET shifted toward more negative potentials respect to the starting condition, as deeply described for the complex **22**. As a consequence the resulting species was more easily oxidized than the starting species; in other words the coordination of chloride ion made the cupric species more

stable than the corresponding tetra-coordinate Cl-free Cu(II) one. This can be the reason for the better long-term stability observed via spectroscopic tests for penta-coordinated species like **22** and **20** (Figure 37 and Figure 38).

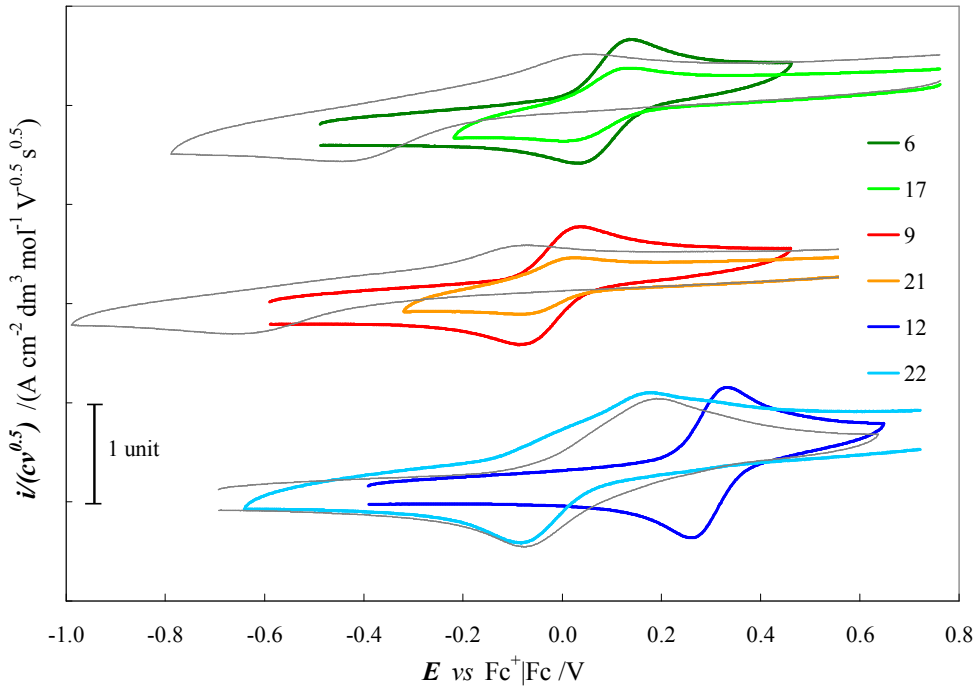

Figure 50 Synopsis of CVs of Cu(I) complexes 6, 9, 12, and Cu(II) complexes 17, 21, 22 (thick lines), and the pattern resulting from the addition of 1 eq. of chloride ions (thin grey lines) to a solution of 17, 21 and 12 respectively. Solvent ACN with $TBAPF_6$ 0.1 M on GC electrode; scan rate potential 0.2 V s^{-1}. Compensation of the ohmic drop by positive feedback technique.

The second coordinating species studied was tbupy, a Lewis base commonly added in electrolyte due to its capacity to adsorb onto TiO_2 photoanode of DSSCs resulting in a improved overall efficiency. The same electron lone pair of its nitrogen can make it a potential ligand for coordinatively unsaturated complexes (remembering that the same species was responsible of the NCS replacement in homoleptic and heteroleptic bis-bipyridyl Ru dyes). An investigation of how such interaction can modify the electrochemical behaviour of Cu(II) complexes could be of great interest to better understand the photovoltaic performances of devices fulfil with copper-based redox mediators.

Only one example was reported in literature for a similar electrochemical study performed on redox mediators; this paper, by Udo Bach and co-workers [120], analyzed the effect of two common DSSCs additives (*i.e.* tbupy and N-methylbenzimidazole) on the electrochemical behaviour of an unsaturated penta-coordinated cobalt complex and it evidenced a negative shift of $E_{1/2}$ as well as an increase in the electrochemical irreversibility of the ETs of the complex after the addition of an equimolar amount of each of the two additives. Coordination of the Lewis bases was invoked to explain such electrochemical modification and it was verified by X-ray analysis.

In the present work the redox species chosen for this study were the complex **21** and its cuprous partner, **9**, due to their remarkable performance as redox mediators (as described in the next section dedicated to DSSC tests). A protocol similar to that adopted for chloride addition was employed, it is the progressive increase of tbupy concentration in the working solution (ACN and $LiClO_4$ 0.1 M, the same electrolyte employed for DSSC tests), obtained by the subsequent addition of small volumes of a mother solution of the Lewis base, was monitored by recording CVs (Figure 51). Contrary to the addition of chloride ions the addition of up to equimolar amount of tbupy to the solutions of **9** or **21** did not bring to significant variation in either the $E_{1/2}$ nor the shape of the CVs; this is a proof that the heteroaromatic base did not induce a quantitative conversion of the pristine complexes contrary to chlorides. The "inactivity" of tbupy could be attributed to its neutral nature and to its quite demanding steric hindrance (compare to the chloride ions) that results in a weaker affinity for the positive charged copper atom [121].

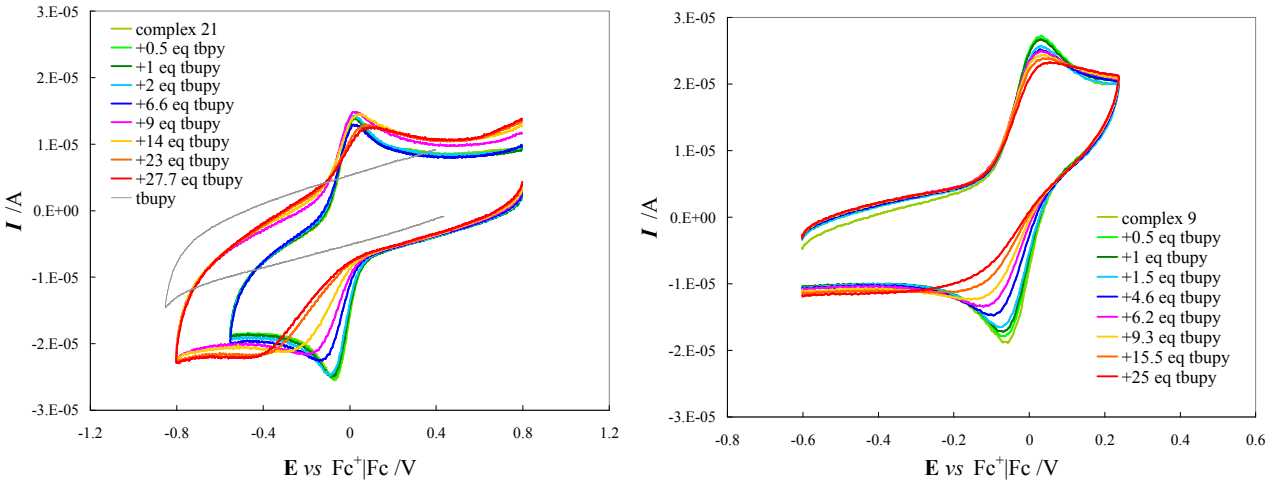

Figure 51 Synopsis of CVs for complex 21 (left) and 9 (right) in ACN with $LiClO_4$ 0.1 M on GC electrode after subsequent additions of tbupy from substochiometric quantity to a large excess (like that actually present in DSSC tests). GC electrode; potential scan rate 0.2 V s^{-1}.

To make the analyzed systems comparable to the conditions presented an actual DSSC, higher ratio of base were considered (up to *ca.* 25 eq.). In this situation a clear negative shift and a broadening of the cathodic peak occurred for complex **22** (Figure 51), suggesting a decrease of the electrochemical reversibility of the ET, while no significant variation in the position and height of the anodic peak was observed. Starting from a solution of the Cu(I) complex **12** the subsequent addition of tbupy caused a progressive disappearance of the cathodic peak (Figure 51) suggesting, also in this case, a direct action of the base on the oxidized form of the complex.

Similar experiment performed with a solution of **21** monitored by visible spectrophotometer (see gallery, Figure G 16) revealed the progressive raise of a band centred around 440-450 nm at increasing concentration of the base (not attributable to the latter); the maximum absorption

wavelength is very similar to that of the MLCT transition characterizing the optical spectrum of complex **9**.

Electron transfer kinetics of complexes

The next step in the electrochemical study of phenanthroline-based copper complexes has been the understanding of their electron transfer kinetics, being of fundamental importance to properly tune the rate constant to overcome the "kinetics dichotomy" of a fast dye (and mediator itself) regeneration reaction and a slow charge recombination.

To the best of my knowledge any previous study concerning this family of copper complexes has never been performed in literature; so this section of the thesis was also interesting from a "fundamental" point of view and not only for its successive implication in the development of redox mediator in DSSCs.

The plan of this study has been very similar to that adopted for the rationalization of the previous $E_{1/2}$ *vs* structure work; it is a series of complexes with phenanthrolines bringing different substituents in term of number and nature. Considering the crucial role of internal substituents in defining the oxidability of the compounds, the screening was focused only on complexes with substituent in these 2 and 9 positions.

The study was carried out employing two different electrochemical techniques: cyclic voltammograms and electrochemical impedance spectroscopy, EIS. The first approach required the subsequent recording of CVs at different potential scan rates and a quite long data processing; in fact it implied the identification of forward and backward peak potentials for each scan rate and their processing through the Nicholson method [122]. The method, developed originally in the 60's, correlates the forward-backward peak distance for a specific potential scan rate with the standard rate constant, k^0; but more reliable results could be obtained by averaging data obtained for each scan rates or by analyzing through the linear regression method the ensemble of values resulting from the different scan rates. In any case the resulted k^0 can significantly suffers from partially uncompensated resistance, giving raise to underestimated ET kinetics.

Considering the quite long procedure for both data recording and analysis we decided to put beside it a much faster method based on the analysis of impedance spectra [54], which in turn can give at the same time also over interesting information on the electrochemical system. A second big advantage is that possible interference by uncompensated resistance should be avoid considering the capacity of the technique to separate the different resistive elements active in an electrochemical process (*e.g.* ohmic resistance, charge transfer resistance, diffusion impedance, etc...). More in particular fitting through a complex nonlinear least square algorithm the experimental impedance spectrum with an appropriate so called equivalent circuit (constituted by series/parallel connections

of circuit elements, some of whose have no physical counterparts like Warburg element, that reproduce the impedance behaviour of the electrochemical system under study) it is possible to quantify the values of the circuit elements that minimize the deviation between the calculated data and the experimental ones. A deep description of the theoretical basis of EIS technique is far from the scope of the present thesis, so only information strictly requested by the study here presented will be given. Literature references can be for example [54], [123], [124], [125]; a reworked version can also be found in my master thesis [126].

For systems under investigation (*i.e.* the heterogeneous electron transfers at the interface of a bare solid electrode, GC) the *Randles equivalent circuit* [127] was commonly adopted (Figure 52). It is constituted by a series resistance, R_{sol}, joints to a two-line parallel: one branch contains a capacitance (or better a constant phase element, CPE, which takes into account for the non-ideality of the capacitive behaviour of the electrode), while the second one has a resistance which takes into account the energetic barrier of the electron transfer, R_{ct}, in series with a semi-infinite Warburg element which models the mass-transport resistance of reactants/products associated to each electrochemical process.

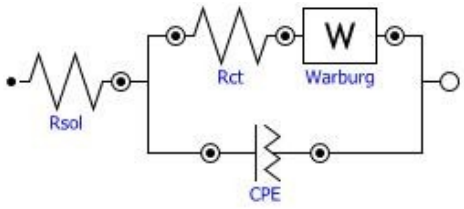

Figure 52 The Randles circuit.

For our aim the main important parameter that was analyzed was the charge transfer resistance being itself an important indicator of the facility of an ET but also of the velocity of the heterogeneous process. The equation $i_0 = \frac{I}{A} = \frac{RT}{FR_{ct}}$ makes possible the estimation of the exchange current density, i_0, of the ET starting from the fitted value of R_{ct} [54]; in the above equation A represents the electrode area and F the Faraday constant.

As we can see the equation does not take into account concentration of the electroactive species, as conversely k^0 does; this could lead to potential errors due to small differences in the concentration of the sample along the series of complexes. On the other hand for a correct estimation of the k^0 the bulk concentration of both reduced and oxidized species are necessary (and hence their co-presence into the working medium, contrary to our case where only the reduced for of the complex was added). In fact $k^0 = \frac{i_0}{FC}$, for the specific case in which reduced and oxidized species are at the same concentration, C.

Considering these two aspects and inspired by the k^0 *vs* i_0 correlation just above, the normalized rate constant parameter, generally named k_{heter}, was calculated as

$$k_{heter} = \frac{i_0}{FC_{Rd}} = \frac{RT}{F^2 R_{ct} C_{Rd}} \quad \text{(eq. 2)}$$

where C_{Rd} represents the concentration of the reduced form of the complex, the only one directly added into the solution. In this way the concentration-independent nature of R_{ct} (and hence of i_0) was avoided and, at the same time, the necessity of knowing the concentration of both species of the redox couple was overcome.

As for many previous tests acetonitrile was chosen as election solvent for this study, due to its satisfactory properties as solvent for the formulation of electrolytes for laboratory-type DSSCs. Considering the similarity of the recorded spectra, the case of the complex **3** was chosen as an example (Figure 53); it well showed the clear semi-circle corresponding to the R_{ct} process followed, at lower frequencies (points in the right part of the graph), by a linear trend with a unitary slope (*i.e.* inclination of 45°) associated to the Warburg mass-transport limitation phenomenon. The only partially resolved semi-circle at the highest frequencies (in the left part) is attributable to the so called *geometric capacitance* of the cell in parallel with the R_{sol} resistance of the solution, strictly correlated with the position and geometries of the three-electrode cell employed for the measurements [125].

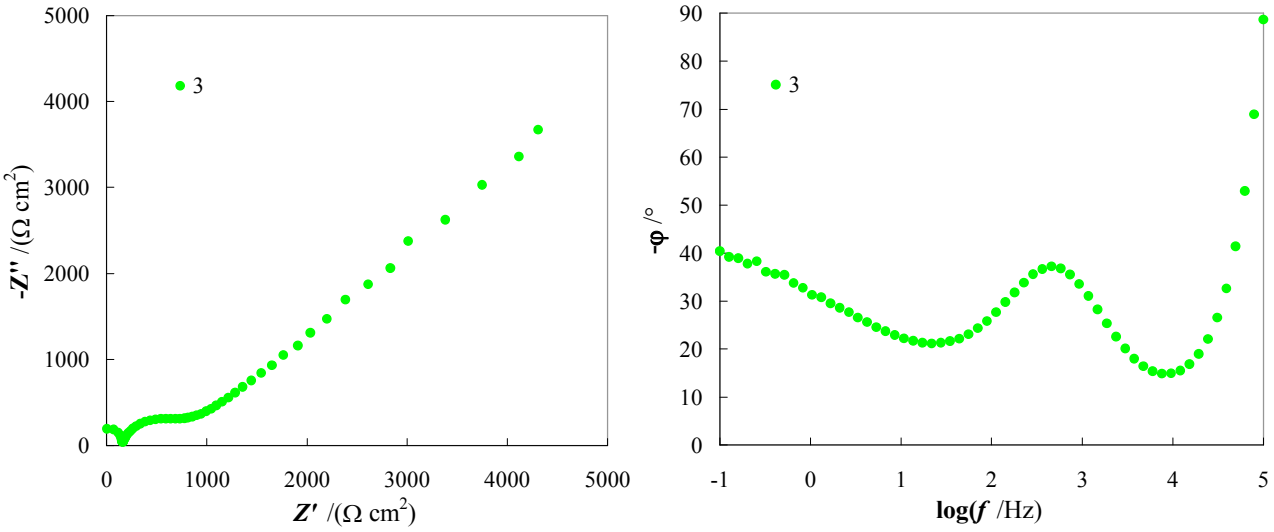

Figure 53 Nyquist diagram (left) and Bode phase plot (right) recorded for complex 3, in ACN with $TBAPF_6$ 0.1 M. Sample concentration 0.001 M; GC electrode.

To validate the EIS method the estimation of the constant rate was performed also through Nicholson method for the complex **5**; a good correspondence was obtained in this test, with the two values equal each other into the experimental error of 1σ (*i.e.* one standard deviation).

Table 16 summarized the values of kinetics parameters obtained by EIS, including approximate diffusion coefficients, D, of the complexes obtained as an average between data resulted by $i_{p,a}$ *vs*

$v^{0.5}$ plots and by the analysis of the limiting currents, i_{lim}, of the stationary CV signals obtained from the corresponding non-stationary ones through the semi-integral algorithm [54].

Table 16 Some kinetics parameters obtained for a selected ensemble of Cu(I) complexes at 0.001 M concentration in ACN with $TBAPF_6$ 0.1 M. For sake of comparison the corresponding $E_{1/2}$ values are also reported (from Table 15). GC electrode.

complex	R';R'';R'''	$E_{1/2}$ /V	R_{ct} (error) /Ω cm^{2} [a]	k_{heter} (error) /cm s^{-1} [b]	D /cm^2 s^{-1} [c]
1	H; H; H	–0.38	$5.3\cdot10^{2}$ ($1\cdot10^{1}$)	$4.9\cdot10^{-4}$ ($5\cdot10^{-5}$)	$4.1\cdot10^{-6}$
2	H; H; CH_3	0.02	$3.9\cdot10^{2}$ ($1\cdot10^{1}$)	$6.71\cdot10^{-4}$ ($9\cdot10^{-6}$)	$6\cdot10^{-6}$
3	H; H; *n*-Bu	0.11	$4.5\cdot10^{1}$ (5)	$4.7\cdot10^{-3}$ ($9\cdot10^{-4}$)	$1.0\cdot10^{-5}$
4	H; H; *t*-Bu	0.34	$2.4\cdot10^{1}$ (3)	$1.0\cdot10^{-2}$ ($3\cdot10^{-3}$)	$1.3\cdot10^{-5}$
5	H; H; Ph	0.10	$1.4\cdot10^{1}$ (4)	$1.9\cdot10^{-2}$ ($4\cdot10^{-3}$)	$1.0\cdot10^{-5}$
7	H; H; Mesityl	0.06	$1.12\cdot10^{2}$ (3)	$2.36\cdot10^{-3}$ ($7\cdot10^{-5}$)	$5.0\cdot10^{-6}$
9	CH_3; H; Mesityl	–0.02	$4\cdot10^{1}$ (6)	$6.9\cdot10^{-3}$ ($1\cdot10^{-3}$)	$6.6\cdot10^{-6}$
12	H; CH_3; CH_3	0.30	$1.35\cdot10^{1}$ ($7\cdot10^{-1}$)	$2.0\cdot10^{-2}$ ($2\cdot10^{-3}$)	$1.0\cdot10^{-5}$ ($1.1\cdot10^{-5}$ for **22**)
14	H; Cl; Cl	0.55	$2.4\cdot10^{2}$ ($5\cdot10^{1}$)	$1.1\cdot10^{-3}$ ($3\cdot10^{-4}$)	$7.7\cdot10^{-6}$

[a] From the fitting of the impedance spectrum with Randles circuit (Figure 52); average of two independent measurements. [b] Defined in eq. 2; from averaged R_{ct} value. [c] Average value from the two methods described in the text just before.

At first sight it is possible to easily distinguish the quite high charge transfer resistances (and hence the related slow ET kinetics) of the complex **1** and **2**, bringing no substituents in the internal positions of the ligands and one methyl respectively. These data, combined with the highest k_{heter} recorded for the neocuproine derivate **12**, seemed to suggest and confirm the crucial role played by the occupation of the internal positions not only in governing the oxidability but also in the kinetics features of the copper complexes. However a simple and general proportional relationship between the number of internal substituents and the k_{heter} (*i.e.* the higher the number of 2 and 9 substituents faster the ET rate) could not be defined beyond the general trend just described. In fact some

"anomalies" to this hypothetical can not be neglected (Figure 54) even between the similar aryl/alkyl substituted complexes (so excluding the more diverse dichloro complex, **14**, that in turn exhibited a quite low ET rate respect to its direct disubstituted counterpart **12**). The first, and maybe the more relevant, anomaly was obtained by comparing complexes **7** and **9**; even if they had the same identical chemical environment around the central copper atom (*i.e.* one mesityl ring) the two complexes exhibited R_{ct} values which differed of at least a factor of 3, clearly evidencing that a more complex explanation, which goes far beyond the similarity of the internal substituents, must be found to rationalize the kinetics features of complexes. Another interesting result concerned the quite high k_{heter} recorded for the complex **5**; it was comparable with that of the complex **12** bringing the disubstituted phenanthrolines and even one order of magnitude faster than its mono-aryl substituted analogue **7**. This suggested that neither a less demanding direct correlation between R_{ct} and the simple number of internal substituents is an hypothesis of general validity.

A possible explanation for the inverted ET rates for complex **5** *vs* **7** and **9** (considering the steric hindrance of the internal substituents as the key element) could be found in the free-rotation of the nominally less bulky phenyl rings respect to the blocked conformation of the mesityl ones (gallery, figures G9-10 and G 17), a feature already anticipated at the end of the subchapter entitled "Solvent effect". The rotation can make the phenyl rings more sterically demanding than the fixed mesityls, so resulting in a complex with a less flexible geometry around the metal centre and, hence, in a low ET energy barrier. Unfortunately this hypothesis can not explain the significant difference of k_{heter} recorded for the analogue **7** and **9**, which remains a big anomaly; in fact in both cases the mesityl rings are blocked as confirmed by their ^{1}H-NMR spectra.

In search of possible alternative explanations for the experimental trend in k_{heter} the hypotheses of a relationship with both half-wave potential (see Figure G 18) and structural features (see gallery, Table G 1) of the complexes had to be rejected, giving raise to worse correlations than with the aforementioned one. Contrary to expectation (considering the geometry modification occurring during the metal-centred ET) this "structural option" seemed to be the less promising, employing both experimental angles determined by single-crystal X-ray diffraction analysis and theoretical ones resulted by the optimized geometries (in vacuum, using a DFT-B3LYP level with a 6-31G* basis set). In fact, especially from diffraction data, a quite absent variability of the dihedral angle between the planes of the two phenanthrolines was detected.

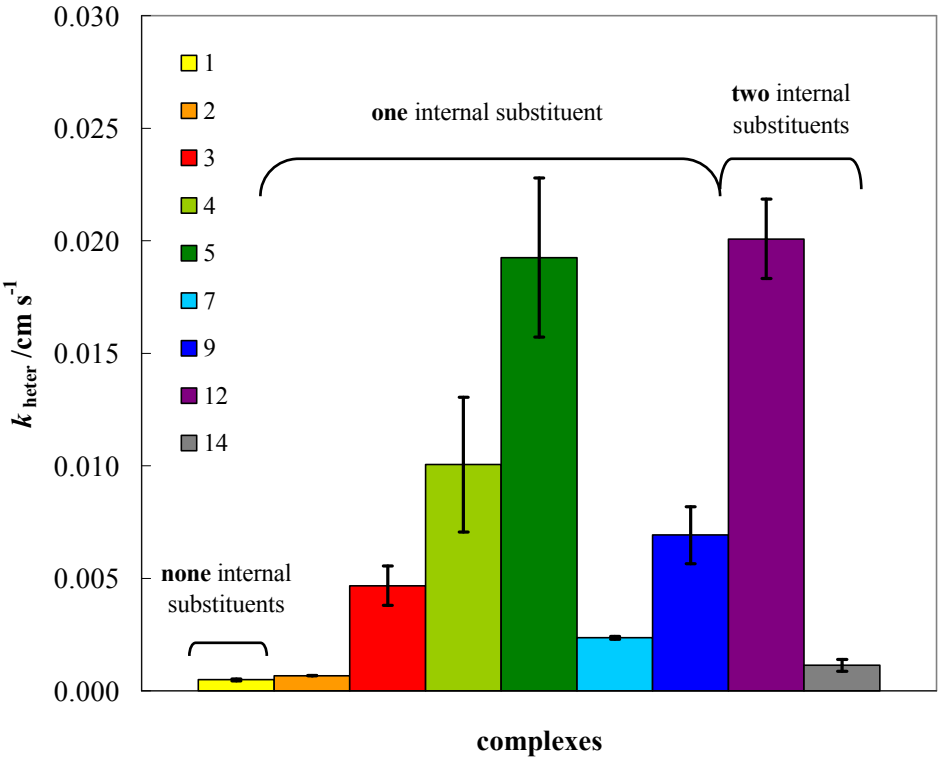

Figure 54 Bar chart reporting k_{heter} as a function of the number of increasing internal substituents (from left to right) on the two phenanthrolines ligands of the ensemble of Cu(I) complexes of Table 16.

So unfortunately, up to know a clear and comprehensive rationalization of the ET kinetics of bis(phenanthroline)copper complex family was not reached; among the possible hypotheses the more interesting seemed to derive from the correlation with the internal substituents even if a simple correlation with neither the number of substituents or the similarity of the central atom environment were not completely satisfactory. As a general trend, however, an increase of k_{heter} was observed when one and two substituents in 2 and 9 positions of the ligands are presented. In any case a good variety of ET rates were identified by changing the substituents in the internal positions on the phenanthroline moieties, and this could be of great interest in search of a good candidate as electron shuttle in DSSCs able to properly overcome the kinetic dichotomy of a fast dye regeneration reaction and a slow charge recombination process.

Cathode material to optimize the reduction of Cu(II) complexes

In view of the application of Cu-complexes as redox mediators in DSSCs a study devoted to find an electrode surface that could minimize the overpotential against the reduction of complexes was of great importance in order to increase the overall cell performances.

Considering the very promising behaviour exhibited by an electrolyte formulated with a mixture of complex **9** and **21** the study concerning the screening of some electrode surfaces as potential cathode material was performed on the Cu(II) complex **21** (dissolved in ACN with $LiClO_4$ as supporting electrolyte to reproduce the experimental conditions used during tests of the solar cells)

combining CV and EIS techniques. Two electrode surfaces have been tested, considering their large application in DSSCs and their relatively easy preparation methods: platinum, Pt, and poly(3,4-ethylendioxy)thiophene, PEDOT. Pt has been largely coupled with iodine-based electrolytes due to the catalytic behaviour of the metal toward reduction of I_3^- species to I^- [24]. PEDOT-modified electrodes, that can be easily prepared either by spin coating the polymer solution or by electrooxidative deposition from its monomer solution, are cheaper than platinum and have revealed very efficient in combination with iodine-free electrolytes [128], [129]. A third GC electrode has been also tested as reference material, ideally inert toward the Cu(II) species. In this study PEDOT-modified electrodes were obtained electrodepositing a thin film of the conducting polymer by cycling three times around the first oxidation peak of the monomer (at 0.01 M concentration) dissolved in ACN with $LiClO_4$ 0.1 M. Two different electrode substrates were employed (GC and Pt) to judge if the underlying substrate could affected the electrochemical response of complex **21**.

Voltammetric patterns (Figure 55) clearly showed a significantly higher ET barrier respect to the reference GC electrode according to the neatly lower electrochemical reversibility of the process that exhibited a $\partial E_p/\partial \log\nu \approx 130$ mV (gallery, Figure G 19). To confirm the worst performance of Pt respect to GC the fitting of the two corresponding impedance spectra recorded at the half-wave potential (Figure 56 and Figure G 20) with the Randles equivalent circuit showed a increase of one order of magnitude in the R_{ct} for the ET from GC to Pt electrode, going from *ca.* $1 \cdot 10^2$ Ω cm^2 to *ca.* $2 \cdot 10^3$ Ω cm^2 respectively.

On the other hand when the CV signal was recorded on PEDOT-modified electrode, independently by the nature of the electrode substrate below the polymeric coating (*i.e.* GC or Pt), the copper complex signal exhibited a diffusive, quasi-perfect electrochemical reversible ET very similar to the GC case (Figure 55). The results showed that PEDOT-modified electrodes allow a faster and easier regeneration of the copper-based mediators than Pt electrodes, so constituting a more efficient cathode material for solar cells.

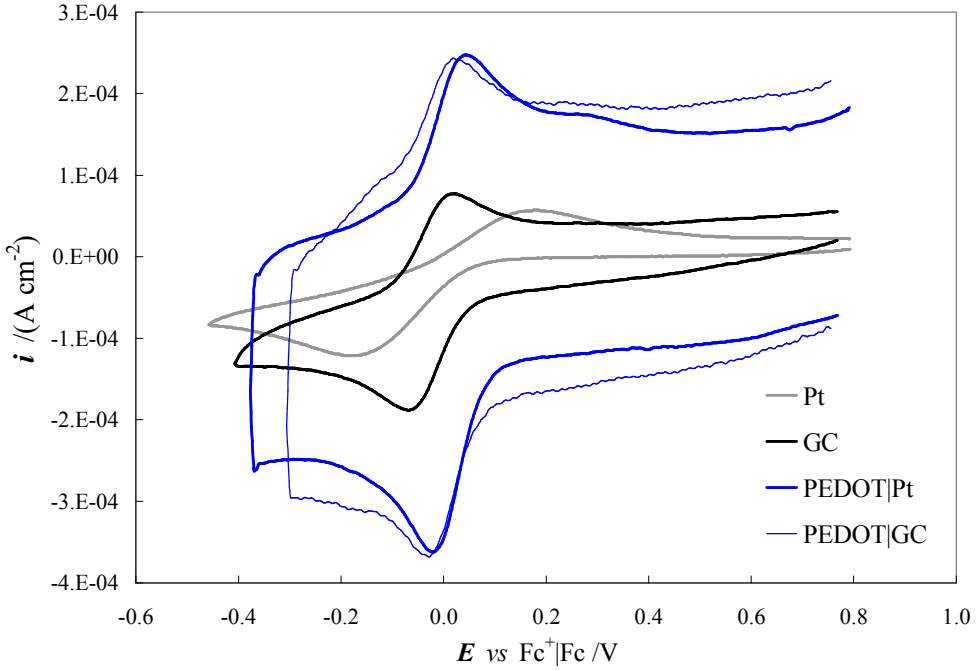

Figure 55 Normalized CVs of complex 21 in ACN with $LiClO_4$ 0.1 M recorded on different electrode supports: Pt (0.0341 cm^2, grey line), GC (0.071 cm^2, black line), PEDOT electrodeposited on Pt (blue line) and PEDOT electrodeposited on GC (blue thin line). Potential scan rate 0.05 V s^{-1}.

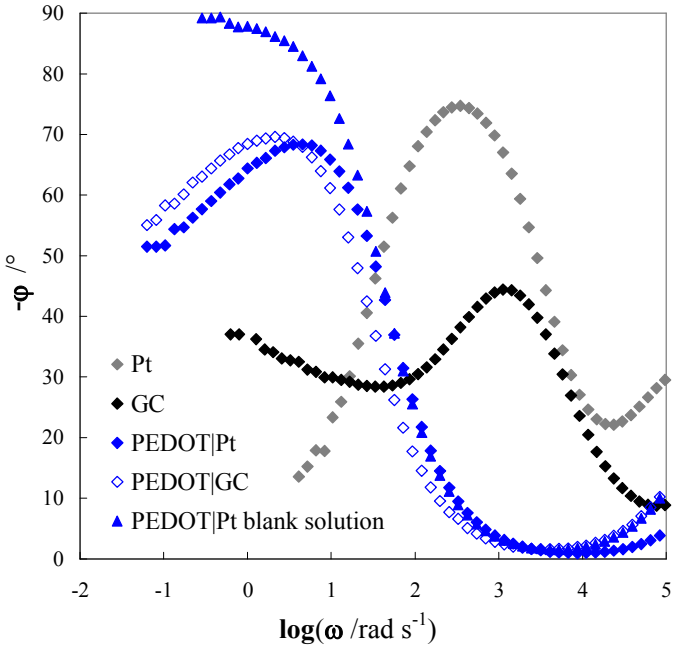

Figure 56 Synopsis of Bode phase diagrams of Figure 55. Bias potential set to the half-wave potential.

DSSC tests

First screening

This important chapter of the thesis deals with the direct exploitation of some copper complexes in dye-sensitized solar cells as redox mediators, allowing to make the most of the many information collected by all the previous deep investigations. In fact the spectroscopic and, mainly,

electrochemical data allowed to rationally identify into the quite large pool of synthesized copper complexes the most promising candidates to be tested in actual photovoltaic devices and then to better understand their performances.

To date only a limited number of available copper complexes has been tested and, an even smaller number was deeply studied in DSSCs. According to the cascade Scheme 8 below, the screening starts with a first "*aut aut*" barrier (*i.e.* in or out) and then it proceeded through two parallel evaluation steps that ranks the candidate according to their optical and electrochemical properties.

Scheme 8 The cascade process adopted to identify between the synthesized copper complexes the potential candidates to be tested in DSSCs.

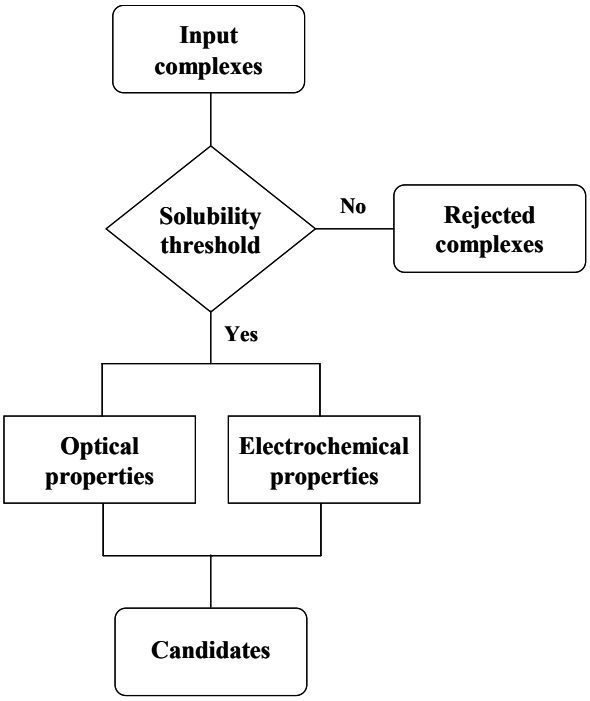

The first step was the evaluation the solubility of the candidates; in fact a sufficiently high solubility (able to reach at least a 0.1 M concentration) has been considered a mandatory feature for any effective redox mediators. This criterion was hence employed to perform a first skimming between potentially interesting complexes, that hence proceeded along the cascade process toward the ranking step, and the complexes that were rejected (and hence they immediately exited from the screening process).

Seven new Cu(I) complexes were subjected to the aforementioned screening; they were **2**, **5**, **9**, **10**, **14**, **15**, **16**; they were compared with the unique complex proposed in literature which exhibited satisfactory performances, the complex **12** that was chosen as the internal reference along all the study.

The "solubility" threshold of 0.1 M in ACN was not exceeded by complexes **10**, **14** and **15** that were so excluded by any subsequent study. The subsequent "score" step showed that the remaining

five candidates **2**, **5**, **9, 16** (and **12**) allowed a good sampling of both spectroscopic and electrochemical properties. For more clarity their main properties have been collected in Table 17.

Table 17 Summary of the main features of the complexes objected of the screening for DSSC application. Solvent ACN; for electrochemical data $TBAPF_6$ 0.1M was added as supporting electrolyte.

complex	R';R'';R'''	λ_{max} /nm (10^3 ε /dm^3 mol^{-1} cm^{-1}) [a]	$E_{1/2}$ *vs* Fc^+|Fc /V [b]	k_{heter} (error) /cm s^{-1} [c]
2	H; H; CH_3	447 (6.4)	0.02	$6.71\cdot10^{-4}$ ($9\cdot10^{-6}$)
5	H; H; Ph	437 (4.6)	0.10	$1.9\cdot10^{-2}$ ($4\cdot10^{-3}$)
9	CH_3; H; Mesityl	445 (4.4)	–0.02	$6.9\cdot10^{-3}$ ($1\cdot10^{-3}$)
12	H; CH_3; CH_3	455 (8.0)	0.30	$2.0\cdot10^{-2}$ ($2\cdot10^{-3}$)
16	Ph; CH_3; CH_3	475 (24)	0.29	–

[a] From Table 13. [b] From Table 15. [c] From Table 16.

Among the candidates there are complexes with very high molar absorption coefficient (*e.g.* **16**), with very fast and slow ET rate (*e.g.* **5** and **12**, *versus* **2** respectively), and also with quite different half-wave potentials. However in many case it is possible to identify couple that differs significantly only for a single parameters, and this could be particularly interesting to explain the photovoltaic performances of the corresponding devices. For example complexes **12** and **16** significantly differ in term of ε, while the couple **5** and **12** has comparable k_{heter} but quite different $E_{1/2}$, and so on. So the ensemble of Table 17 could allowed to track a lot of intercomparisons, even if to date only a partial comparison could be performed; however in the next future the characterization will be surely carried out also including other additional members from the pool of the already synthesized complexes.

A first preliminary test was performed in PEDOT-based symmetrical sandwich-type cells, in order to evaluate the limiting diffusion current (proportional to the maximum theoretical photocurrent generated by a DSSC with a comparable electrode-electrode distance) and any possible differences in term of exchange current between different electrolytes. PEDOT was chosen as electrode substrate accounting for its just mentioned catalytic activity toward the reduction of copper complexes. In these experiments the oxidized form of the mediator was directly generated *in-situ* through addition of a proper amount of $NOBF_4$ into the solution of Cu(I) complex dissolved in

ACN and $LiClO_4$ 0.1 M (considering a 1:1 stoichiometry). The study was carried out combining stationary linear scan voltammetry with EIS.

A selected ensemble of *i vs E* curves (or more simply *iE* curves) are reported in Figure 57. As expected by the high affinity of PEDOT electrode for copper complexes no R_{ct} resistance was detected in impedance spectra which conversely evidenced only one process at relatively low frequencies (lower for the thicker symmetric cells) attributed to the mass transport process. From the slop around E=0 it was possible to see that, from a qualitative point of view, the complex **9** seemed to have a higher exchange current density, i_0, not only than **2** but, unexpectedly, also than complex **5** which conversely showed the highest ET rate on GC electrode.

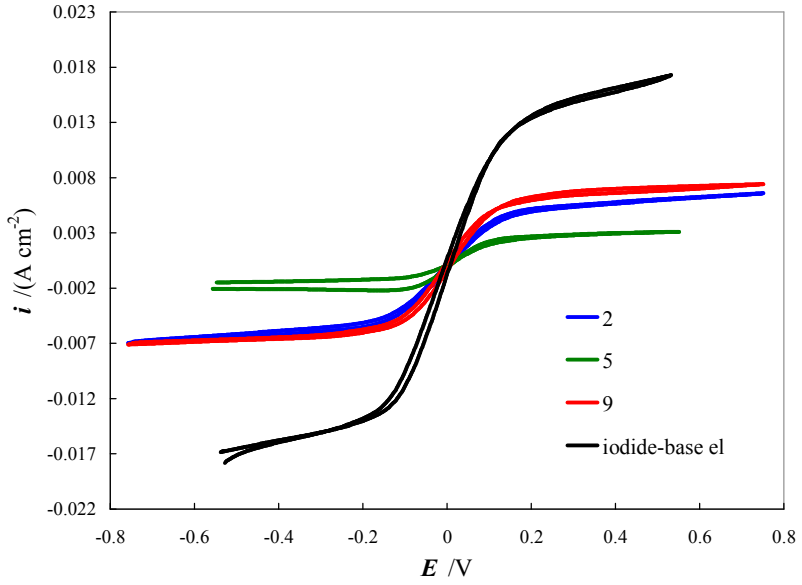

Figure 57 Left: normalized *iE* polarization curves of PEDOT-PEDOT symmetric cells (gasket 100 μm thick) for some Cu-based electrolytes (0.1 M concentration; Ox/Rd = 0.05; with $LiClO_4$ 0.1 M). For sake of comparison a iodide-base cell was also reported (black line). Solvent ACN.

Interestingly the limiting diffusion current of complex **5** was neatly lower than that recorded for the other analogues; this was an unexpected result considering its relatively good diffusion coefficient (double than that for both **2** and **9**, see Table 16). An explanation was not found except that in some how the quite high concentration of the sample (*ca.* 100-fold higher than in normal voltammetric measurements) induced a significant raise in the viscosity of the electrolyte; the occurring of a more hampered diffusion was also clearly evidenced by the higher $-Z''$ vs log(f) peak obtained by EIS measurements. Incidentally with the same **5** some troubles were encountered with concentrated solution prepared for the registration of ^{13}C-NMR spectrum due to a strange broadening of the proton signals (recorded to check the sample before starting the acquisition of carbon nuclei frequencies); the strangeness disappeared when the same sample was diluted.

In a second step the intrinsic dye regeneration capability of the Cu(I) complexes was preliminary studied through *transient absorption spectroscopy (TAS)* experiments (performed thanks to the

hospitality of Prof. Carlo A. Bignozzi e Prof. Stefano Caramori, at Università degli Studi di Ferrara). A tris-bipyridyl Ru(II) cationic complex was chosen as sensitizer (Figure 58) accounting for results from a fast screening of analogue metal-based and fully organic dyes (see gallery, Figure G 21). The dye is characterized by the absence of monodentate ligands (such as SCN^- or CN^-) potentially subjected to replacement reaction, and two long nonyl chains that could contribute to reduce the undesired charge recombination process by oxidized form of the mediator.

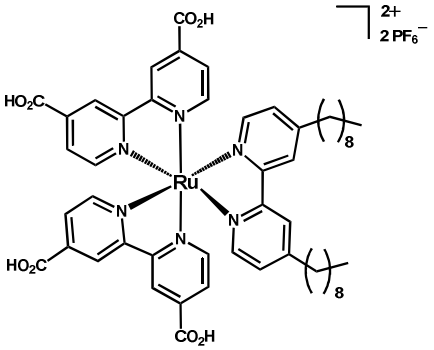

Figure 58 Chemical structure of $[Ru(dcbpy)_2(dnbpy)][PF_6]_2$ dye (dnbpy stands for 4,4'-dinonyl-2,2'-bipyridyl).

In few words TAS measurements allow to monitor the decay/growth of a signal at a chosen probe wavelength in a time scale from tens nanoseconds up to some microseconds after a laser excitation pulse. So two different light sources constituted the active set up for the TAS measurement: a white light probe source and a laser (in the specific case a nanosecond Nd:YAG laser, employing the 532 nm harmonic as excitation wavelength). The two light sources are orthogonally positioned (Figure 59) and they alternatively irradiate the sample that in the specific situation was a thin transparent sensitized TiO_2 photoanode oriented with an angle of 45° respect to both pulse and probe beams. The light coming from the continuum light source (*i.e.* the probe light) passes through the transparent sensitized TiO_2 matrix (deposited on FTO substrate) and finally reaches the detection system constituted by a photomultiplier and an oscilloscope. More detailed information can be found in our published work [76].

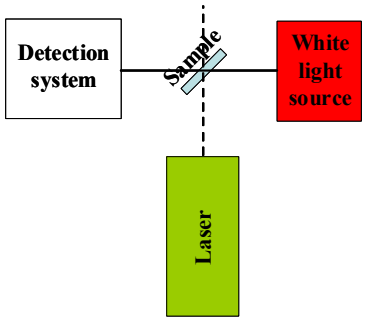

Figure 59 Simplified scheme of the experimental setup employed for TAS measurements.

The differential transient absorption spectrum of the dye loaded onto TiO_2 in an inert electrolyte (Figure 60) showed the bleach of the MLCT bands of the ground state, consistently with the

formation of Ru(III) species after the injection of electrons into the conduction band of the metal oxide (k_{inj} >10^8 s^{-1}, a process too fast to be observed with the experimental setup). The progressive disappearance of the bleaching with time (*i.e.* the progressive Ru(II) recovery) occurred solely by recapture of the photoinjected electrons, according to a multi-exponential kinetics reflecting the energy distribution of trap states within the TiO_2. The half-life time, $\tau_{1/2}$, for the faster component of the dye recovery was about 100 ns.

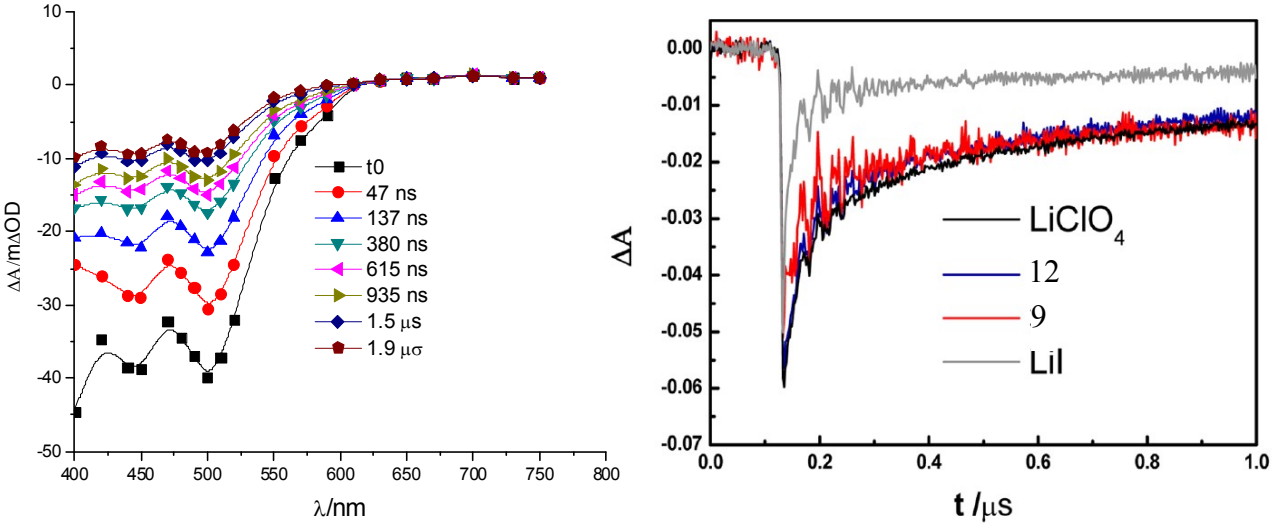

Figure 60 Left: TA spectrum of the dye $[Ru(dcbpy)_2(dnbpy)]^{2+}$ loaded onto transparent TiO_2 in a inert solution ($LiClO_4$ 0.1 M in ACN). Right: 490 nm recovery of Ru(II) dye in the presence of inert electrolyte (black line); 0.1 M Cu(I) + 0.1 M Li^+ (complex 9, red line, and complex 12, blue one); 0.1 M LiI (gray line). λ_{exc} = 532 nm (FWHM 7 ns laser pulse), excitation energies *ca.* 5 mJ cm^{-2} $pulse^{-1}$.

The dye regeneration kinetics for complexes **2**, **5**, **9** (compared with that of **12**, taken as reference, and an equimolar LiI solution, as benchmark) were evaluated monitoring the bleaching of Ru(III) species that should disappear faster than in the inert electrolyte due to the presence of the different electron donating species. The results clearly indicated a very slow dye regeneration kinetics for all copper complexes especially compared with that of I^- ions ($\tau_{1/2}$ *ca.* 15 ns). In fact the recovery of Ru(II) was only slightly faster than that recorded in a blank solution ($LiClO_4$ 0.1 M) for complex **9** and **12** (Figure 60); on the contrary for complex **2** and **5** the recovery seemed to be even slower than in the blank solution (see gallery, Figure G 22). This last apparent contradiction can be explained considering that the Cu(II) form generated at the initial part of the decay efficiently reacts with trapped electrons in TiO_2 so partially suppressing the direct electron recapture with Ru(III) unique responsible for the dye recovery in the inert solution. This could occur if the electron donation kinetics of Cu(I) species are comparable or slower than electron recapture. As a result the half-life of Ru(III) in presence of the Cu(I) species could paradoxically become even longer than that measured in the blank solution due to the resulting retarded dye recombination. This could be in agreement with the fast k_{heter} of complex **5** calculated in three-electrode configuration with GC

electrode (Table 17), but partially discordant with the slow ET rate of complex **2**. Another possible explanation for the unexpected longer half-life in presence of the two electron relays **2** and **5** could be attributable to a spectral contribution from the bleach of the intense coloured copper complexes (especially for **2**).

Apart the strange behaviour of these two complexes, a significantly slow dye regeneration rate invariably characterized the Cu(I) complexes under examination. Focusing on the complex **9** and the reference compound **12**, the *ca.* 300 mV larger driving force of **9** for the dye regeneration reaction seemed not to significantly improve the electron donating process (even if, actually, a slightly acceleration was observed in the first fast part of the decay trace, Figure 60). The ineffective larger driving force could be explained considering *i*) a sort of compensation effect by the larger inner reorganization energy associated to the ET of complex **9** than **12** (according to their relative k_{heter} that increase in the order **9**<**12**, Table 17), or *ii*) a not optimal electronic coupling between the Cu(I) complex and the Ru(III) species.

Considering the intrinsic features (both optical and electrochemical ones) and the results of the screenings just described two complexes have been chosen as candidates for the subsequent direct tests in DSSCs. The selected complexes were **9** and **16**; the first was chosen *i*) for its comparable dye regeneration kinetics respect to the already known complex **12**, *ii*) its lower molar absorption coefficient (about half the value of **12**) but also *iii*) for to the intermediate value of its k_{heter}. Conversely complex **16** was properly chosen for its high ε coefficient (in combination with its structural similarity and the quite identical $E_{1/2}$ with the complex **12**) to judge how an intense absorption by redox mediator could interfere with the light harvesting of the dye and, hence, with the photovoltaic performances of the cells.

As described in the following two chapters the redox mediators were tested in DSSCs with two different sensitizers: the just mentioned $[Ru(dcbpy)_2(dnbpy)][PF_6]_2$ (in the just below chapter) and the fully organic G3 dye (see the subsequent chapter).

Solar cells sensitized with cationic $[Ru(dcbpy)_2(dnbpy)][PF_6]_2$ complex

As already anticipated these series of measurements were performed using electrolytes in which the desired molar ratio between the oxidized and reduced form of the redox couple was obtained by the addition of a suitable amount of $NOBF_4$ [64] to a starting solution containing only the Cu(I) species. In all electrolytes $LiClO_4$ 0.1 M was also added as supporting electrolyte and as additive due to the beneficial effect of the alkaline cations to the cell performances [85]. The work described below was object of publication [76]; more details, especially for the experimental part, could be found in the paper.

Some preliminary tests were performed to optimize the photoanode. The employment of simple photoanodes, made by mesoporous TiO_2 deposited on FTO, was immediately rejected due to the completely absence of photocurrent attributable to an extremely fast charge recombination by Cu(II). The preparation of two-layer photoanodes (made by a mesoporous TiO_2 layer over an underlying compact one) only partially reduced the parasitic back-electron transfer, suggesting that it could efficiently occur on the exposed FTO surface according to the only modest overpotential to the ET offered by the conductive glass observed assembling FTO-FTO, TiO_2-TiO_2 symmetrical cells (Figure 61).

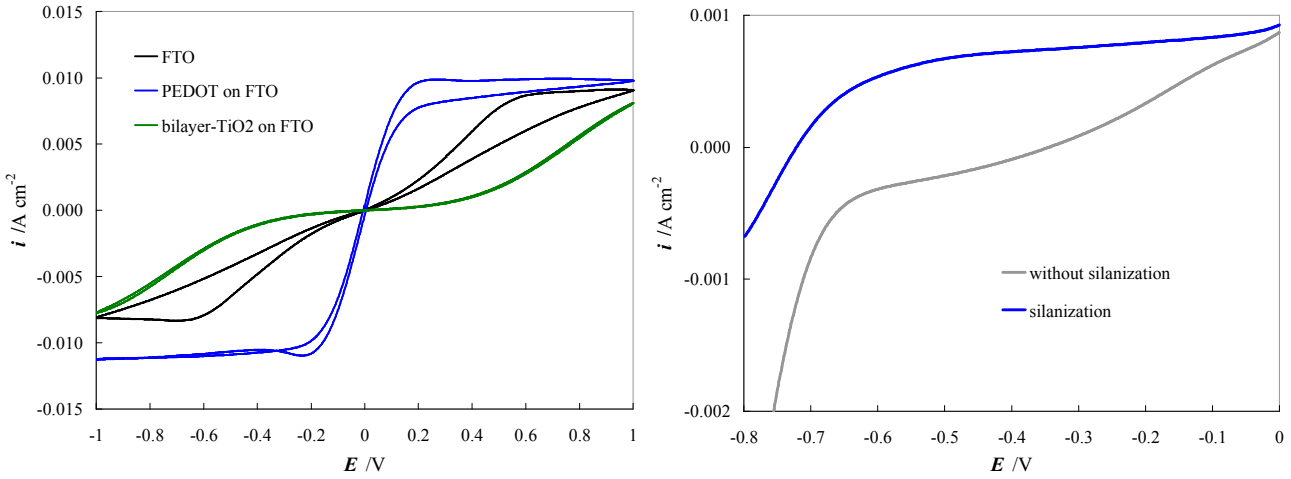

Figure 61 Left: normalized polarization curves of symmetric cells constituted by bare FTO, PEDOT-modified FTO and bilayer TiO_2 electrodes. Solution composition: 0.2 M total concentration of complex 12, Cu(II)/(Cu(I)+Cu(II)) = 0.01. Right: Normalized *iE* characteristics of sandwich-type DSSCs employing bilayer TiO_2 photoanode without silanization (gray line) and after silanization (blue line) sensitized with Ru(II) dye, under 90 mW cm^{-2} AM 1.5G illumination. Electrolyte composition: 0.1 M solution of mediator 12 (with 5% of Cu(II) form) in ACN with 0.1 M $LiClO_4$. Scan rate potential 0.005 V s^{-1}.

The third modification of the photoanode consisted in the silanization step; it is a post-sensitization treatment that employs silanes with a long insulating aliphatic chain [70]. As discussed in the "Introduction" section, silanes anchor to any possible zones of the TiO_2 nanoparticles not covered by dye molecules (or to the uncovered underlying SnO_2 surface) reducing the recombination on the sensitized layer acting as sterically hindered barrier that limits the electronic coupling between the oxide surfaces and the Cu(II) form in solution. In this way (*i.e.* silanized bilayer electrodes) sufficiently efficient photoanodes were obtained, increasing of *ca.* three-time of the cell efficiency (Figure 61).

Adopting the optimized photoanodes a comparative study between electrolytes based on complex **9**, **16** and the reference **12** were performed recording *iE* curves and impedance spectra under illumination and in the dark.

Polarization curves under illumination (Figure 62) and related photovoltaic cell parameters (Table 18) showed some interesting aspects that must be discussed taking into account also all the previous spectroscopic and electrochemical studies.

Table 18 Main photovoltaic parameters employing copper-based electrolytes in solar cells (active area 0.25 cm^2) sensitized with $[Ru(dcbpy)_2(dnbpy)][PF_6]_2$ dye [a], and sandwiched with a PEDOT-modified FTO cathode.

entry	electrolyte [b]	i_{sc} /mA cm^{-2}	*FF*	V_{oc} /V	*PCE*	$\tau_{e-(TiO2)}$ /ms [c]
1	complex **9** 0.15 M with 5% Cu(II)	2.4	0.58	0.58	0.9	5
2	complex **12** 0.15 M with 5% Cu(II)	1.1	0.50	0.73	0.4	1
3	complex **16** 0.15 M with 5% Cu(II)	1.1	0.49	0.71	0.4	2
4	I_3^-/I^- [d]	3.8	0.66	0.60	1.7	8

[a] Irradiation of 90 mW cm^{-2} simulated AM 1.5G sunlight. All data are averaged from two independent DSSCs under the same experimental conditions. [b] In all electrolytes was also added $LiClO_4$ 0.1 M, in ACN; for entries 1-3 the Cu(II) was generated *in-situ* by the addition of $NOBF_4$, in order to have [Cu(II)]/([Cu(I)]+[Cu(II)])=0.05. [c] From EIS measurements at V_{oc}. [d] EL-HSE electrolyte, purchased by Dyesol.

First of all a practically superimposable traces were obtained for the two structural analogue **12** and **16** (*i.e.* two methyls in 2,9 positions on each ligand) underlying the important role played by the internal substituents already largely stressed in previous sections. Interesting is the *ca.* 0.72 V open circuit potential, significantly better than the V_{oc} obtained with the iodide-based benchmark electrolyte; the remarkable photovoltages can be due to the high half-wave potential of the two complexes. Unfortunately both cells filled with **12** and **16** electrolytes presented a quite poor photocurrent, around 30% of that obtained by the benchmark electrolyte; this can be explained considering the quite slow dye regeneration rate evaluated by TAS measurements.

The similar performances obtained with **12** and **16** gives also a second interesting information; notwithstanding the quite different absorption coefficients (three-times higher for **16** than **12**) they seemed not to significantly affect the photovoltaic performances of the cells suggesting that a direct competition between adsorbed dye and the coloured redox mediator did not exist, or that it was not so crucial respect to the electrochemical features of the redox couple. This observation could be of fundamental importance also for future development of copper complexes (or even different outer-sphere electron shuttles) because it overshadows one of the main drawbacks generally counted for copper systems respect to cobalt ones, it is the intense colour.

Remarkable is the relative comparison between cells equipped with the electrolyte formulated with the new complex **9** and those based on the standard literature complex **12** (Table 18 and Figure 62). Our new asymmetric mesityl-architecture allowed to more than doubling the i_{sc}, the *FF* and also the

overall photon-to-current conversion efficiency, PCE, respect to **12**-based cells. Unfortunately it resulted below the performances of I_3^-/I^- reference electrolyte (commercially available EL-HSE "High Stability Electrolyte", Dyesol, Australia) which however contained a higher amount of I^- ions coming from a mixture of both inorganic and organic salts.

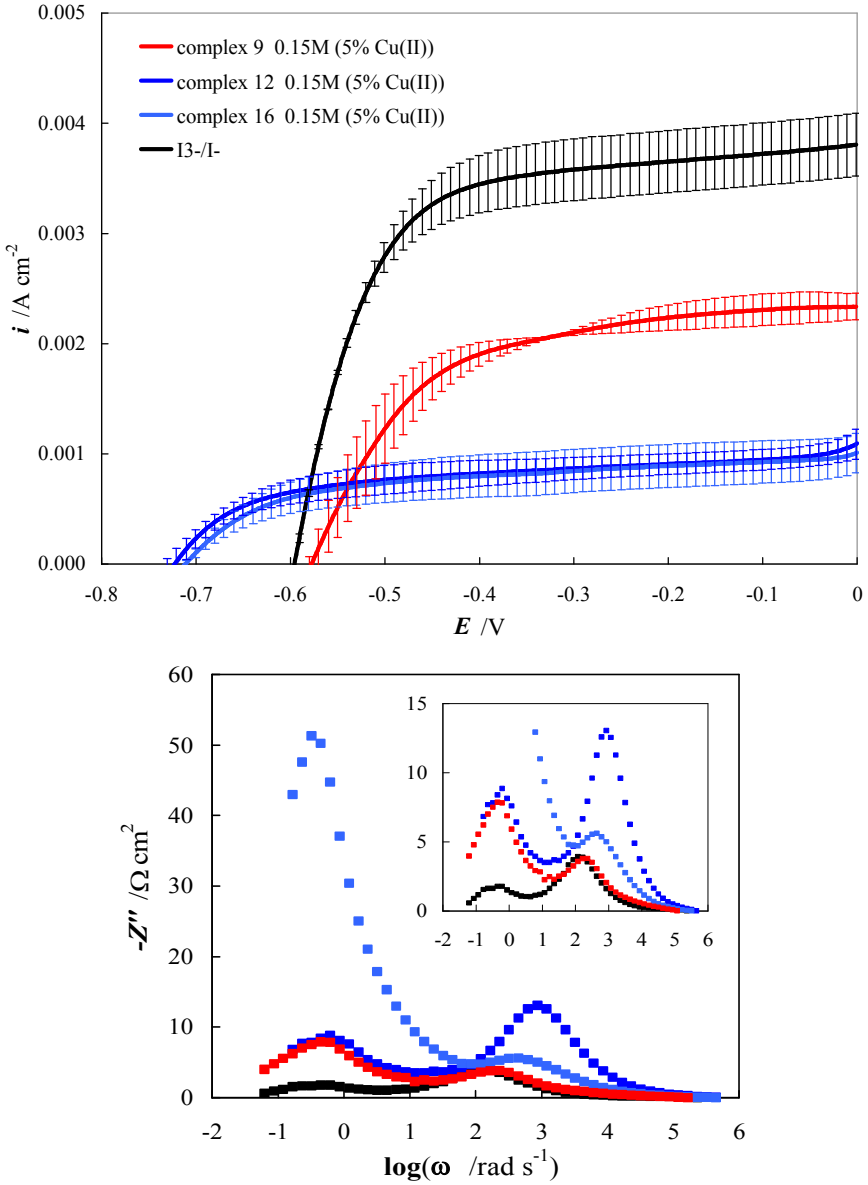

Figure 62 Top: synopsis of *iE* characteristics of the DSSCs under illumination reported in Table 18. Bottom: synopsis of imaginary impedance traces recorded for the same solar cells at their V_{oc}; inset: magnification.

Electrochemical impedance spectroscopy, EIS, was a useful technique to go into more details in the operation of a DSSC thanks to its intrinsic capability to separate the different electrochemical processes (characterized by diverse timescale) that all together determine the *iE* characteristic of a device. Models and equivalent circuits, ECs, based on transmission lines able to accurately reproduce the impedance spectrum of the entire DSSC in a broad range of experimental conditions (*i.e.* at different bias potentials, from open circuit to short circuit) have been developed in the years,

particularly thanks to the work of Prof. J. Bisquert and his co-workers [130]. A suitable equivalent circuit able to model a complete solar cell includes (Figure 63):

1) a series ohmic resistance, R_s, accounting for contact and transport resistances of transparent conducting oxide, TCO;

2) a parallel R_{TCO}-C_{TCO} connection that accounts for the uncovered underling TCO where direct recombination of the oxidized redox mediator could occur;

3) a transmission line that accounts for the TiO_2 and TiO_2/eletrolyte interphase; it is constituted by r_t in series with a parallel r_r-c_μ that, respectively, models the electron transport resistance R_t (=r_tL, with L is thickness of the mesoporous TiO_2 film), the charge transfer resistance R_r (=r_rL) related to the recombination reaction by oxidized form of the mediator at the TiO_2 interface and the chemical capacitance C_μ (=$c_\mu L$) of the TiO_2 standing for the change of electron density as a function of Fermi level of the semiconductor;

4) a impedance of diffusion, Z_d, accounting for the mass transport of redox mediators into the electrolyte;

5) a parallel R_{Pt}-C_{Pt} connection that models the counterelectrode (platinum, in this model) interphase, accounting for the charge transfer resistance, R_{Pt}, of the regeneration reaction of the mediator and the capacitance, C_{Pt}, at the interface with the electrolyte.

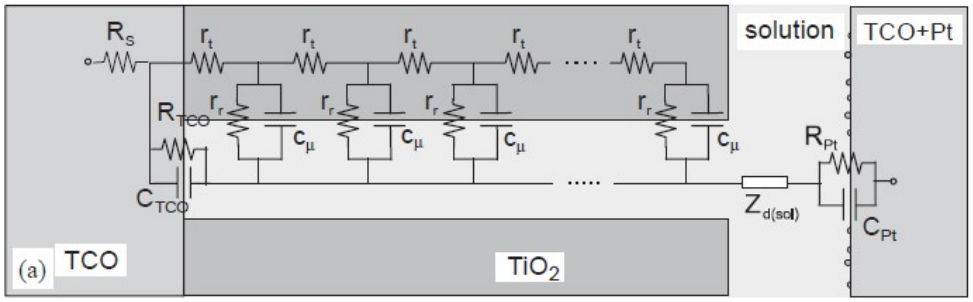

Figure 63 Equivalent circuit (employing a transmission line for modeling the complex interface of the mesoporous TiO_2 semiconductor permeated by the electrolyte) proposed by Bisquert for a complete solar cell. From ref. [130].

According to the experimental conditions (*i.e.* the applied external potential) some part of the complete EC can be neglected, so resulting in a more simplified circuit. A useful simplified EC largely employed in this work (Figure 64) can be obtained neglecting the series R_t and the R_{TCO}-C_{TCO} parallel when the TiO_2 is in the conductive state (sufficiently high negative potential, around V_{oc} value); in this conditions R_{TCO}>>R_r and so the recombination will occur only at the TiO_2-electrolyte interface, and R_t could be also neglected considering that R_t <<R_s.

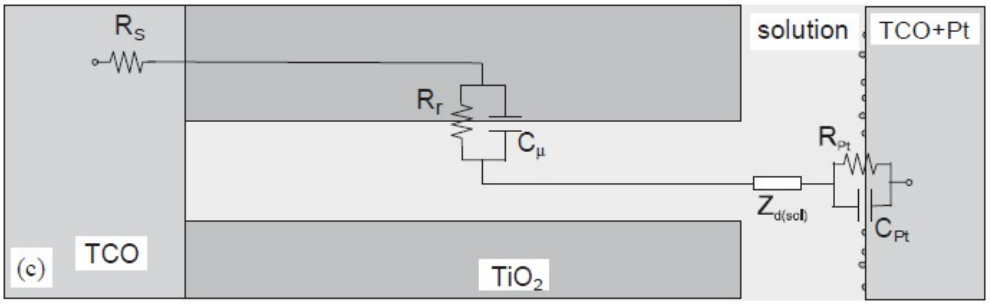

Figure 64 Simplified EC exploitable when TiO_2 is sufficiently conductive (*i.e.* at the more negative applied potentials, near the V_{oc} value). From ref. [130].

The EC in Figure 64 corresponds to at most three semi-circles in a Nyquist diagram. The first one (at higher frequencies) corresponds to the mediator regeneration reaction taking place at the cathode interface, being generally characterized by the higher characteristic frequency, $\varpi=(R_{count}C_{count})^{-1}$, or conversely the *smaller time constant*, $\tau= R_{count}C_{count}$; for sake of generality from now on R_{count} stands for the charge transfer resistance for the ET at the counterelectrode interface and, similarly, C_{coun} stands for the capacitance of the cathode/electrolyte interface. In some cases, when the ET is characterized by a very fast rate constant (hence a very small R_{count}), this first semi-circle can not be observed.

The semi-arch at middle frequencies accounts for the charge transfer resistance of the recombination reaction occurring at the TiO_2/electrolye interface; similarly to the previous case it is possible to define a recombination characteristic frequency, $\varpi= (R_rC_\mu)^{-1}$, that also correspond to the frequency at which the imaginary component of the impedance, Z'', reaches its maximum value: $\varpi= (R_rC_\mu)^{-1}=\varpi_{Z'' \, max}$ (note that ϖ is the angular frequency, in rad s^{-1}, and not the "common" frequency, f, in Hz). According to this definition in a $-Z''$ *vs* log ϖ plot, the higher the $\varpi_{Z'' \, max}$ frequency the faster the ET rate; this is a very useful indication, from a qualitative point of view, to compare at first sight different processes.

The last semi-circle, localized at the lower frequencies, is attributable to the impedance of diffusion, Z_d, that takes into account the mass transport problems of the redox species into the electrolyte. In some literature works this specific impedance element was classified as a "finite-length impedance" to distinguish it from the more classical semi-infinite Warburg element, Z_w or simply W. To be more precise the here discussed Z_d element is only one of the two possible elements developed to described finite-length diffusion phenomena; it correspond to a finite-length diffusion in presence of so called *transmissive boundary*. For further details see for example [124].

After this very brief, but necessary, introduction on the exploitation of EIS technique for the study of DSSCs it is maybe possible to well understand the important role played by this electrochemical technique in the rationalization of the photovoltaic performances of these devices.

From the comparison of EIS spectra recorded for the four cells of Table 18 and Figure 62 it was possible to see that no significant charge transfer resistance for the cathodic reaction was recorded for all copper-based electrolyte, confirming the high performances of PEDOT electrode toward reduction of copper complexes (see also the previous section dedicated to the study of ET kinetics). Only the impedance of diffusion (at lower frequencies) and the charge recombination process was visible. The first process evidenced a neatly higher mass transport resistance for copper complexes (in particular for **16**) respect to the iodine-based system due to the significantly higher steric hindrance of the complexes.

However much more interesting was the analysis of the recombination process because it was able to explain the significantly different performances of complex **9** with respect to the two structurally related **12** and **16**. The electron lifetime in the titanium dioxide, $\tau_{e\text{-}(TiO2)}$, evaluated by EIS analysis at V_{oc} was more than doubled, going from *ca.* 2 ms for the 2,9-dimethyl-substituted mediators **12** and **16** to *ca.* 5 ms of the 2-mesityl-substituted phenanthroline electrolyte (Table 18), suggesting that with the latter species the parasitic charge recombination process was, somehow, drastically reduced, allowing a more efficient generation of photocurrent. Considering the comparable dye regeneration kinetics of **9** and **12**, previously determined via TAS (Figure 60), the net difference in the electron lifetime should not be attributable to a faster dye regeneration (and hence the consequent reduce dye^+/e^- recapture) but to a more hampered back-electron transfer involving the Cu(II) centres derived from **9**. This hypothesis was in good agreement with the lower dark current recorded for **9** respect to **12** and **16** in the first part of the polarization curve (see gallery, Figure G 23); in any case the dark current observed with **9** was slightly lower than that observed with the iodide-based electrolyte.

Considering the promising performances of the Cu(I) electron mediator **9** an optimization of the electrolyte composition was performed before going on with the study. A total of nine different formulations were prepared and tested, resulting from all the possible permutations obtained combining three different concentration of redox species (0.10 M, 0.15 M and *ca.* 0.2 M) with three different Ox/Rd molar ratio (5%, 10% and 15%). Results of the screening (Figure G 24) indicated that, as expected, the increase of the total amount of electroactive species led to an increase of the photocurrent, but at the same time to a progressive net decrease in V_{oc}. On the other hand a progressive decrease of the oxidized form of the mediator resulted in improved photovoltages. As a consequence only slight variation of the overall cell efficiency was obtained.

The “optimized” composition of electrolyte based on Cu(I) complex **9** adopted for the subsequent tests was: 0.1 M total concentration of redox mediator with 5% of oxidized form.

Bi-component electrolytes: effect of a comediator

Combining the TAS results with both the EIS data (*i.e.* $\tau_{e-(TiO2)}$) and *iE* curves (*i.e.* i_{sc}) it is possible to say with good reason that the lower performance of cells equipped with complex **9** respect to the benchmark I_3^-/I^- should be attributable to the too sluggish dye regeneration. Starting from this consideration diverse two-component electrolytes were formulated combining the Cu(I) and Cu(II) mesityl-based complexes with faster comediators. Implementation of fast comediators (like phenothiazine or Fe-based complexes) in a solution of the main mediator was already reported in literature with Co(II) tris-bipyridyl complexes and led to a considerable increase of the photocurrent [131], [132], [133]. Obviously the choice of the comediator must consider its half-wave potential to be intermediate between that of the dye and of the main Cu-based mediator, in order to ensure the exoergonicity of both the heterogeneous and homogeneous electron transfer with the adsorbed dye and the main mediator, respectively.

For our scope two Fe-based complexes of general formula tris(4,4'-R_2-2,2'-bipyridyl)iron(II) have been added with a Cu(I)/Fe(II) molar ratio of 10; in particular for R=methoxy, $[Fe(dmo\text{-}bpy)_3][PF_6]_2$, $E_{1/2}$=0.36 V *vs* $Fc^+|Fc$, while for R=*tert*-butyl, $[Fe(dtb\text{-}bpy)_3][PF_6]_2$, $E_{1/2}$=0.44 V *vs* $Fc^+|Fc$. Given that the Ru(III) regeneration by Cu(I) is slow, the addition of a kinetically faster couple having a small reorganization energy, like the Fe(II)/Fe(III) complexes, allowing for a faster Ru(III) reduction, should result in an increased electron collection efficiency, leading to an improved PCE.

Tests on the bi-component electrolytes are shown in Figure 65 and the corresponding photovoltaic parameter are listed in Table 19. It is well evident that in all cases the presence of Fe(II) comediators brought down both V_{oc} and *FF* but, especially for $[Fe(dtb\text{-}bpy)_3][PF_6]_2$, a net increase in photocurrent was observed reaching a value comparable with that of the benchmark iodide-based electrolyte. Moreover a 1.2% PCE was reached to be compared to 1.7% of the I_3^-/I^- reference cell.

Table 19 Main photovoltaic parameters employing bi-component electrolytes (complex 9/Fe(II)-comediator) in solar cells (active area 0.25 cm^2) sensitized with [Ru(dcbpy)$_2$(dnbpy)][PF$_6$]$_2$ dye [a], and sandwiched with a PEDOT-modified FTO cathode.

entry	electrolyte [b]	i_{sc} /mA cm^{-2}	*FF*	V_{oc} /V	*PCE*	$\tau_{e-(TiO2)}$ /ms [c]
1	**9** optim [d]	2.0	0.64	0.60	0.9	6
2	**9** optim + 0.01 M [Fe(dmo-bpy)$_3$]$^{2+}$	2.7	0.49	0.55	0.8	11
3	**9** optim + 0.01 M [Fe(dtb-bpy)$_3$]$^{2+}$	4.0	0.51	0.51	1.2	10
4	**9** optim + 0.01 M [Fe(dtb-bpy)$_3$]$^{2+}$ + 0.1 M tbpy	1.7	0.69	0.62	0.8	6
5	I_3^-/I^-	3.8	0.66	0.60	1.7	8

[a-c] Refer to the related footnotes of Table 18. [d] Formulated with complex **9** and its oxidized form generated *in-situ* through $NOBF_4$; total complex concentration 0.1 M with 5% of Cu(II) species.

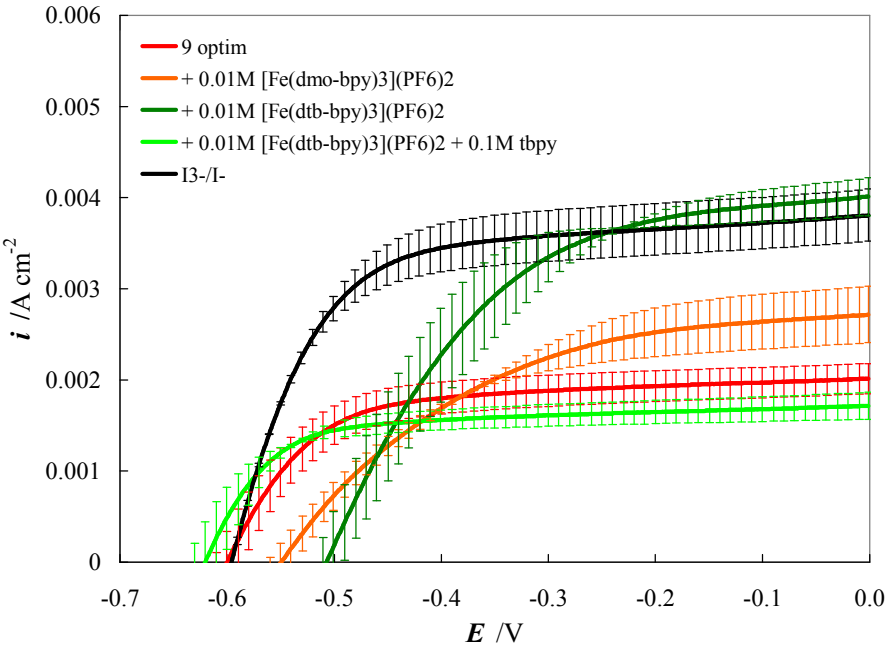

Figure 65 Normalized *iE* characteristics of DSSCs reported in Table 19, employing the "optimized" electrolyte employing Cu(I) complex 9 as such and in 10:1 molar ratio mixture with Fe(II)-based comediators.

A dipper investigation was performed recording photoaction spectra (Figure 66), and performing TAS (Figure 66) and EIS (Table 19) measurements. Transient absorption spectroscopy allowed to verify that, with respect to the simpler case of complex **9** as unique component of electrolyte (Figure 60), the addition of 10% mol/mol of Fe(II)-based mediator brought a slight acceleration of the Ru(II) recovery, particularly in the fast part of the decay, resulting in a half-life of 79 ns in the case of [Fe(dtb-bpy)$_3$]$^{2+}$ and of 43 ns in the case of [Fe(dmo-bpy)$_3$]$^{2+}$. In all case the dye

regeneration maintained still slower than in presence of iodide ions (half-life *ca.* 15 ns). The superior dye regeneration capability offered by the methoxy derivate could be explained by the higher driving-force and, possibly, by the stronger electronic coupling with the adsorbed dye molecules due to the absence of the sterically hindred *tert*-butyl groups presented in the [Fe(dtb-bpy)$_3$]$^{2+}$ comediator.

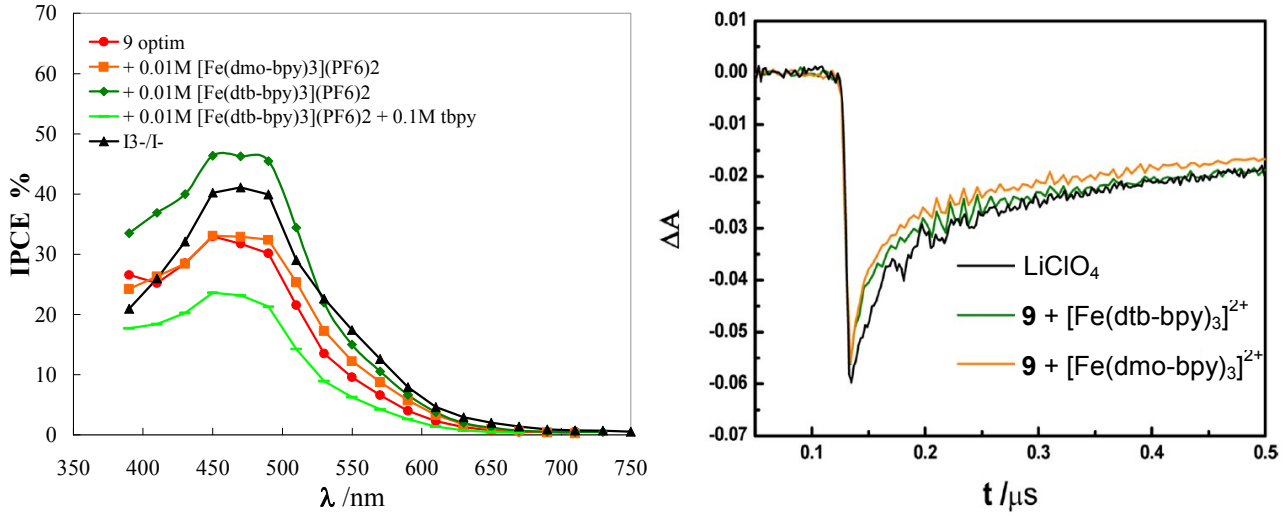

Figure 66 Left: synopsis of photoaction spectra of the DSSCs of Figure 65. Right: 490 nm recovery of Ru(II) dye in the presence of inert electrolyte (black line), and of the two di-component electrolytes (with [Fe(dtb-bpy)$_3$]$^{2+}$, green line, and [Fe(dmo-bpy)$_3$]$^{2+}$, orange line). λ_{exc} = 532 nm, excitation energies *ca.* 5 mJ cm^{-2} pulse^{-1}.

Instructive is that the faster regeneration did not correspond neither to the higher IPCE or to the best cell efficiency, suggesting that both recombination by Fe(III) species and the homogeneous Cu(I)/Fe(III) electron transfer played a crucial role in determine the overall cell performances. In particular the [Fe(dtb-bpy)$_3$]$^{3+/2+}$ couple possesses both a larger driving force for the oxidation of Cu(I) (*ca.* 0.44 eV), which could lead to a faster regeneration of Fe(II), and bulky *tert*-butyl chains, which may contribute to decouple Fe(III) from the TiO_2 surface; both characteristics were instrumental in decreasing the efficiency of electron recapture involving Fe(III) and electrons trapped in the TiO_2 resulting in the higher IPCE (up to 50%) and the best PCE.

As a further modification the addition of the common tbpy additive to the [Fe(dtb-bpy)$_3$]$^{2+}$/**9** bi-component electrolyte was also tested (Figure 65 and Figure 66). Unfortunately the resulting deep decrease in the photocurrent was not compensated by the expected improvement in V_{oc}. The adverse effect was ostensibly related to a decreased efficiency of the electron injection as a consequence of the upward shift of the TiO_2 conduction band induced by tbpy that reduced the driving-force of the process.

Solar cells sensitized with the benzothiadiazole-based dye G3

As seen in the previous subchapter one (or even the more important) drawback of copper complexes as redox mediators in solar cells sensitized with the cationic dye [Ru(dcbpy)$_2$(dnbpy)][PF$_6$]$_2$ was the

inefficient dye regeneration reaction which in turn favoured the charge recombination by Cu(II) complex and the back-electron transfer involving the dye^+ species, so negatively affecting the photovoltage and the photogenerated current respectively and, as a final consequence, limiting the overall cell efficiency. The ineffective dye structure could be counted among the causes of such a slow dye recovery; in fact for example the molecular structure of the tris-bipyridyl Ru(II) sensitizer could hamper the electronic coupling with the bulky Cu(I) complexes and hence slowing down the ET and/or disfavouring the electron/hole separation due to a poorly oriented dipole moment considering the quite low performances observed also with the iodide-based reference electrolyte.

Starting from this consideration a second series of measurements focalized on the promising complex **9** was planned employing a dye with a completely different chemical nature characterized by a neatly better polarized structure. The work was performed, again, in collaboration with Prof. Carlo A. Bignozzi and Prof. Stefano Caramori, and thanks to the additional hospitality of Ing. Michele Manca at Istituto Italiano di Tecnologia in Arnesano (LC). Also considering the recent literature showing remarkable results by the combination of organic dyes with iodine-free electrolytes (one example for all others, the actual new record over 14% [134]) the dye chosen for this second series of measurements was a fully-organic molecule named G3 published for the first time few months ago by the research group of Prof. Gian Paolo Suranna [135]. It was the results of the efforts devoted to produce an efficient but sufficiently easy-to-prepare dye, focusing the attention on the sustainability of its synthetic pathway and so limiting, for example, the chemical complexity of the molecule. G3 is a benzothiadiazole-based sensitizer (Figure 67) with the classical donor-π-acceptor architecture bearing two branched 2-ethylhexyl chains on the bulky triphenylamine terminal group that could, in principle, reduce parasitic charge recombination reactions by oxidized form of the mediator at photoanode. Moreover the high dipolar nature of the sensitizer was expected to improve the electron/hole separation, reducing back-electron transfer, and to facilitate the dye regeneration step which were particularly problematic in DSSCs with the Ru(II) dyes.

First step was to verify whether the improved dye regeneration expected by the highly polarized architecture of G3 actually occurred; this study was carried out through transient absorption spectroscopy study on sensitized thin transparent TiO_2 photoanodes in contact with different reducing mediators (*i.e.* complex **9**, **12** and I^-) employing the same experimental set-up previously described (Figure 59) was exploited.

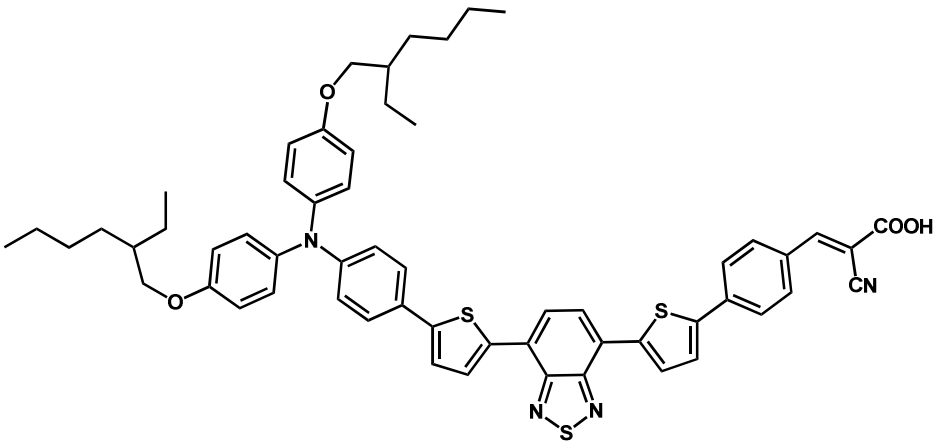

Figure 67 Chemical structure of G3 dye.

The transient absorption differential spectrum (Figure 68) of $G3^+$ dye cation (formed after laser excitation at 532 nm of G3 dye loaded on the TiO_2 film and the subsequent electron injection into the conduction band of the metal oxide) recorded into an inert solution of ACN and $LiClO_4$ 0.1 M was in good agreement with the spectrum dye dissolved in THF solution. TA differential spectrum was characterized by two intense bleaching of the charge transfer bands centred around 390 and 550 nm for the free-dye, and two positive bands due to the absorption of the dye^+ species. Three net isosbestic points are observed. The intense absorption of the dye cation at wavelengths longer than *ca.* 700 nm could be attributed to hole localization on the triphenylamine donor group relatively far from the TiO_2 surface. The amplitude weighted lifetime of dye cation, $\tau_{2/3}$ (*i.e.* the time at which one third of the original intensity is still maintained), was around 1180 ns and quite independent on the wavelength chosen for its evaluation.

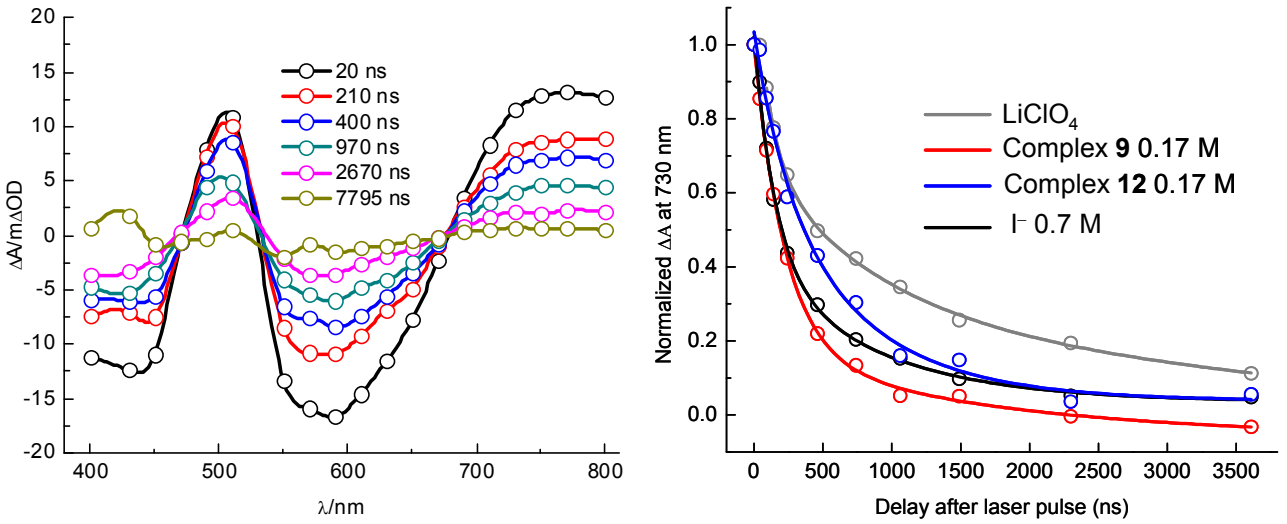

Figure 68 Left: TA differential traces of G3 dye loaded on transparent TiO_2 film in a blank ACN solution (with Li^+ 0.1 M). Right: transient recovery at 730 nm of loaded G3 dye in inert solution (gray line) and in presence of the three reducing agents. Fits to the kinetics traces were reported for sake of clarity. λ_{exc} = 532 nm; excitation energies *ca.* 1-2 mJ cm^{-2} $pulse^{-1}$.

After addition of reduced form of redox mediators (*i.e.* **9**, **12** and I^-) a significant decrease of dye cation lifetime was invariably observed accordingly with the dye regeneration reaction $dye^+ + Med_{Rd} \rightarrow dye + Med_{Ox}$. Just at first sight the situation is extremely better than with Ru(II) dye, with $\tau_{2/3}$ around 300 ns for both I^- and **9**. To avoid any interference by bleaching of mediators (λ_{max} at 445 and 455 nm for **9** and **12** respectively) the regeneration efficiency, η_{reg}, for the three mediators was evaluated at 730 nm (Figure 68). η_{reg} was calculated according to expression

$$\eta_{reg} = \frac{k_{reg}}{k_{reg} + k_{rec}}$$

where $k_{reg}=1/\tau_{2/3,reg}-1/\tau_{2/3,rec}$ and $k_{rec}=1/\tau_{2/3,rec}$ (where subscript "rec" stands for recombination).

Complex **9** revealed a regeneration efficiency of the G3 dye (at 2/3 of the starting signal) of around 70%, comparable with that calculated for the iodide-based solution. This is a remarkable result considering the neatly lower concentration (*ca.* four times), the significant higher steric hindrance and the lower driving force of Cu(I) complex **9** respect to iodide (*i.e.* $E_{1/2}$=0.28 V and –0.02 V *vs* $Fc^+|Fc$ for I_3^-/I^- and Cu^{2+}/Cu^+ couples respectively). Despite the aforementioned higher heterogeneous ET rate constant of complex **12** respect to **9** evaluated with GC electrode, bis(neocuproine)copper(I) was significantly less efficient in the dye regeneration reacting only with less than half of the molecules of the photogenerated oxidized dye during the $\tau_{2/3}$ period, being η_{reg} around 45%. However this could be tentatively attributed to its minor reducing capacity respect to the analogue complex **9**.

Considering the remarkable dye regeneration kinetics with the novel complex **9**, a series of DSSCs were assembled to evaluate the photovoltaic performances of the G3/copper-electrolyte couple and compared them once again with those of both neocuproine-based and iodide-based electrolytes (Table 20).

Table 20 Detailed formulation of the four electrolytes tested with G3 dye.

entry	electrolyte	composition [a]
1	9/21	complex **9** 0.17 M; complex **21** 0.017 M tbupy 0.25 M
2	12/22	complex **12** 0.17 M; complex **22** 0.017 M tbupy 0.25 M
3	I^-/I^{3-} equim	complex I^- 0.17 M; complex I_3^- 0.017 M tbupy 0.25 M
4	I^-/I^{3-} optim	DMPII [b] 0.8 M; LiI 0.2 M; 0.007 M I_2 tbupy 0.5 M

[a] All electrolytes were prepared in ACN with $LiClO_4$ 0.1 M. [b] DMPII is 1,2-dimethyl-3-propylimidazolium iodide.

It is useful to remember that this has been the first time that a benzothiadiazole organic dyes was coupled with a copper-based electrolyte; the higher semplicity of this condensed heteroaromatic core respect to the cyclopentadithiophene scaffold employed in the only other published work [65], able to reach considerable photovoltaic efficiencies, coud be a springboard for the development of effective iodide-free DSSCs.

Contrary to the previous study with Ru(II) dye, in this second series of measurements the Cu(II) counterpart necessary to formulate the mesityl-based and the neocuproine-based electrolytes were directly added into the solution employing the synthesized complexes **21** and **22** respectively. As shown in Table 20 photovoltaic performances of the **9/21** and **12/22** electrolytes were compared with two different iodide-based reference systems, which mainly differed for the iodide content: *i*) **I^-/I_3^- equim** was formulated with an amount of I^- and I_3^- equal to that of Cu(I) and Cu(II) respectively, to have a more direct comparison with the copper-based systems exhibiting a lower solubility; *ii*) **I^-/I_3^- optim** was prepared with a significantly higher amount of iodide (*i.e.* 1 M), to exploit the full potential of the dye.

The main photovoltage features, at 1 sun illumination, are listed in Table 21 and the related *iE* curves are reported in Figure 69. The most interesting result was the capability of the novel **9/21** electrolyte, especially when combined with Pt-based cathode, to even exceed the permormance of the equimolar iodide-based electrolyte, **I^-/I_3^- equim**, reaching photon-to-current efficiency up to 4.4%.

Table 21 Main photovoltaic parameters of solar cells (active area 0.16 cm^2) sensitized with G3 dye, and sandwiched with a Pt- or PEDOT-modified FTO cathode; spacer *ca.* 50 µm. Irradiation of 100 mW cm^{-2} simulated AM 1.5G sunlight.

electrolyte	cathode	i_{sc} /mA cm^{-2}	*FF*	V_{oc} /V	*PCE*	τ /ms [a]
9/21	Pt	9.3	0.66	0.72	4.4	6.1
9/21	PEDOT	8.2	0.67	0.76	4.2	5.4
12/22	Pt	3.8	0.59	0.86	1.9	4.2
I^-/I^{3-} equim	Pt	8.7	0.70	0.70	4.2	4.7
I^-/I^{3-} optim	Pt	15.4	0.67	0.72	7.4	30

[a] From EIS measurements at V_{oc}. For trend at other potentials see figures in main text.

Unexpectly cells filled with **9/21** electrolyte and equipped with PEDOT-coated cathode showed slightly worst photovoltaic features (and comparable *FF*) than those assembled with Pt, notwithstanding the better electron transfer promoted by the conducting polyemer film. To explain this anomaly a series of symmetical cells have been prepared coupling both Pt-Pt and PEDOT-PEDOT electrodes. Charge transfer resistance calculated by fitting of the EIS spectra at E=0 V (see gallery, Table G 2) with an Randles equivalent circuit (Figure 52) constituted by a R_{series} in series with a $C_{CE}[R_{CE}W]$ parallel, was dramatically lower for cells employing the electrodeposited PEDOT film (R_{CE}≈2 Ω cm^2 for **9/21**) than in cells based on sputtered Pt (R_{CE}≈20 Ω cm^2), so supporting the above referred findings. On the other hand EIS analysis evidenced that PEDOT substrates suffered for a *ca.* 50% higher series resistance than the metallic counterparts, mainly attributable to a higher sheet resistance and a worst resistance for the electrical connections. As a result of the two opposed effect, the overal resistance effective in DSSCs, R_{CE} + R_{series}, could be assumed comparable for cells equipped with the two cathodic substrates, this being in agreement with the same value of *FF* exhibited from both DSSCs filled with **9/21** electrolyte employing Pt and PEDOT as counter electrode (Table 21).

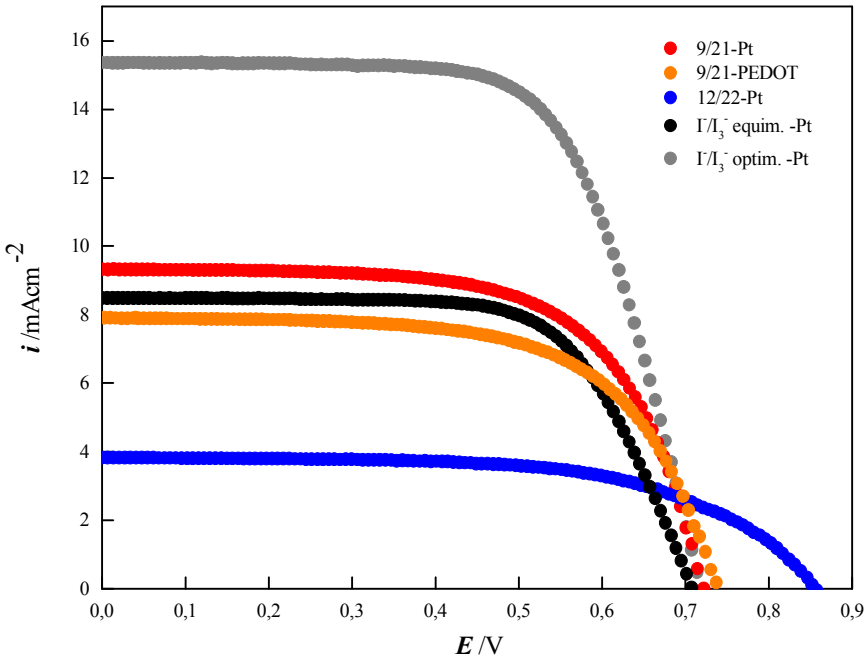

Figure 69 Normalized *iE* characteristics under 1 sun illumination for solar cells (active area 0.16 cm^2) reported in Table 21 sensitized with G3 dye, filled with the copper-based electrolytes and employing Pt or PEDOT cathode.

Moreover as a confirmation of the remarkable higher performances of the novel mesityl-based electron shuttle respect to the literature neocuproine-based benchmark, **9/21** electrolyte exhibited PCE more than twice that obtained with the **12/22** electrolyte. The net discrepancy derived mainly from the high photocurrent as a consequence of the faster dye regeneration kinetics **9** respect to **12**, as suggested by TAS and confirmed by the high photocurrent (up to 9 mA cm^{-2}, at 1 sun illumination); accordingly higher capacitance of the photoanode, C_{meas}, was recorded for **9/21** respect to **12/22** electrolyte (Figure 70). The inadeguate photovoltage features of cells filled with **12/22** electrolyte could be also attributed to the joint effect of the significantly high values of R_{CE} (one order of magnitude higher than with **9/21**, as calculated by symmetrical cells) and, most of all, a detrimentally huge value of diffusion resistance.

A quite deep study of the photoelectrode/solution interface was performed by recording impedance spectra of DSSCs under illumination at different bias potentials and extrapolating the related R_{ct} and C_{μ} values (Figure G 25 and Figure 70, respectively). The potential actually sensed by photoanode, E_{corr}, was firstly evaluated for each value of the applied potential, E_{appl}, subtracting from the last the voltage drop at the total series resistance given by the contacts, the conducting glass, the charge transfer at the counter-electrode, and the electrolyte diffusion resistances.

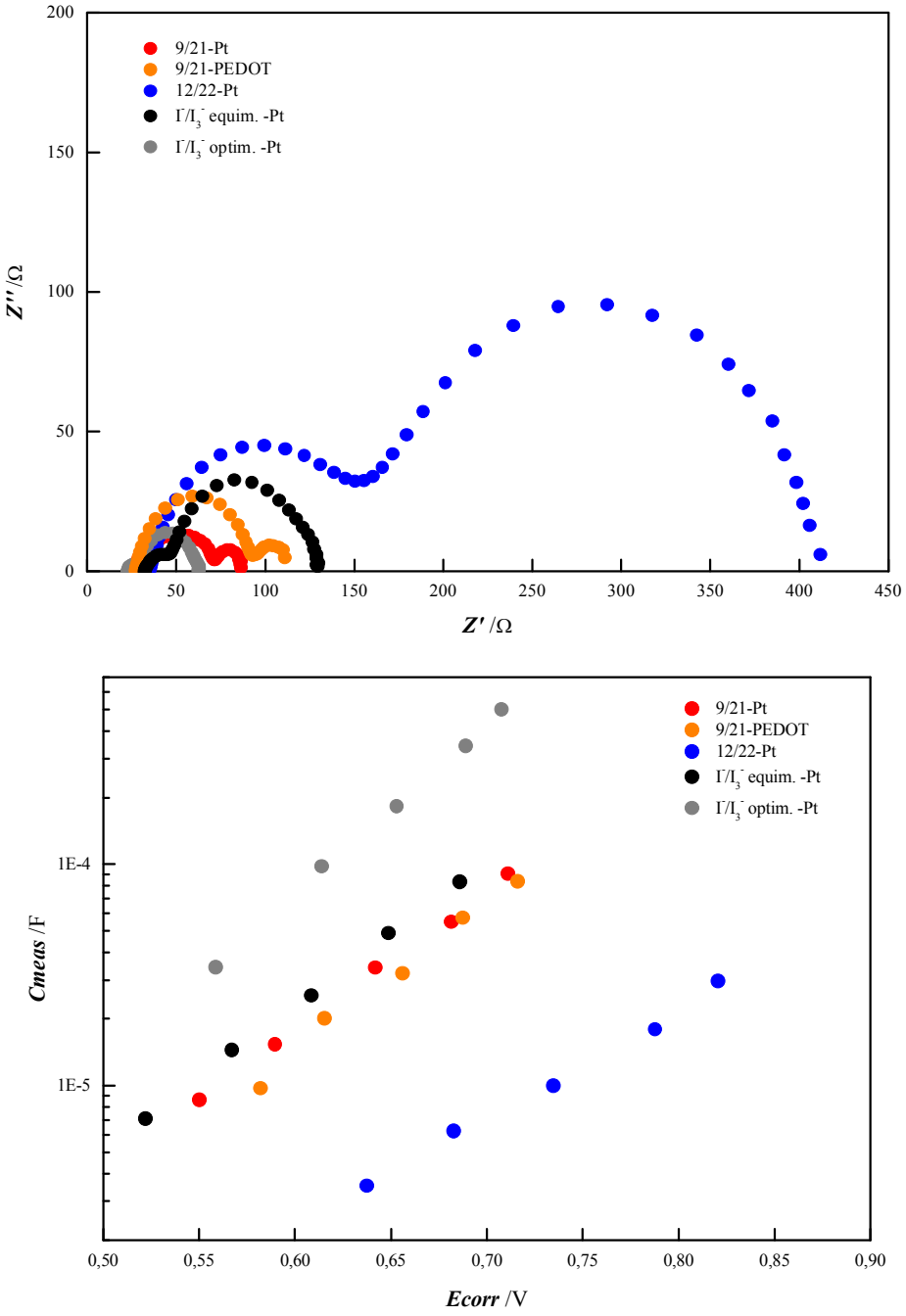

Figure 70 Up: synopsis of Nyquist spectra at V_{oc} of the DSSCs of Figure 69. Down: potential dependence of the chemical capacitance of the photoanode, C_{meas}, calculated by EIS measurements. 1 sun illumination.

The different slope of C_{meas} *vs* E_{corr} for the different electrolytes indicated that interaction of electrolyte with TiO_2 surface modify the distribution of trap states in the semiconductor [136]. In particular an upward shift of the conduction band edge, E_{CB}, of TiO_2 was straightforwardly identified in the case of **12/22** electrolyte, partially accounting for its higher V_{oc} and the poor i_{sc}. On the contrary **I^-/I_3^- optim** showed the lower E_{CB}, whereas **I^-/I_3^- equim** and **9/21** electrolytes showed almost the same position.

Considering that electrolytes differently interacts with photoanode, to properly interpret R_{ct} values and the electron lifetime in TiO_2, τ, the density of charge (reflecting the chemical capacitance, C_μ)

should be taken as the reference (Figure 71). **9/21** electrolyte exhibited higher charge recombination resistance than the counterpart **12/22**, which could be reflected in the remarkable better performance. The faster recombination reaction with **12/22** could be tentatively attributed to the low efficient dye regeneration by Cu(I) species that, as a consequence, promotes the dye recombination. According with the comparable photovoltaic features, the R_{ct} values were similar for **9/21** and **I^-/I_3^- equim** electrolyte, while a neatly higher resistance was recorded for the best performing optimized iodide-based reference cell. Similar trends were detected also from the plot of τ_{e-} *vs* C_{meas}. The higher electron lifetime observed in the cell filled with **9/21**-based electrolyte, respect to **12/22**, made supposable a better suppression of the parasitic dark current.

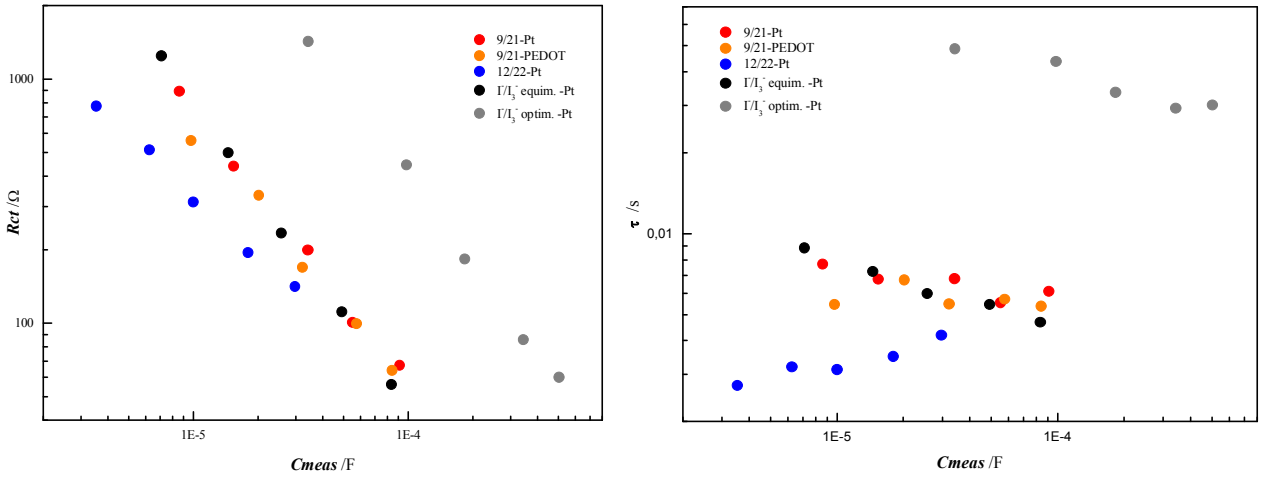

Figure 71 Charge transfer resistance (left) and electron lifetime (right) as a function of the chemical capacitance obtained from impedance spectroscopy, for solar cells of Table 21.

The better performance of the **I^-/I_3^- optim** electrolyte clearly indicated that the major drawback of **9/21** electron shuttles (and, in general, of similar copper-based systems) is the limited solubility in ACN. Such limitation reduced the charge collection, decreasing the number of dye molecules regenerated by mediator and hence limiting the i_{sc} threshold.

Summarizing

The broad study focused on the homoleptic bis(1,10-phenthroline)copper complexes for the development of effective redox mediators alternative to the much common I_3^-/I^- redox couple (far from being an ideal electron shuttles) has gone well beyond the mere formulation of different electrolytes for dye-sensitized solar cells.

In fact it has started with the design and synthesis of a wide ensamble of differently substituted phenanthrolines and their related copper complexes, in order to obtain a variagated pool of samples exploitable to rationalize how the spectroscopic and, mainly, electrochemical features of the complexes are affected by ligand substituents.

In particular the crucial role played by steric effects of substituents functionalizing the 2 and 9 internal positions of phenanthroline moieties in controlling the half-wave potential of the metal-centred ET process has been clearly identified and rationalized figuring a sort of "kiss-lock enclosure" mechanism. The structural effects induced by the same substituents on the geometry of the complexes drastically affect also the heterogeneous constant rate of the complexes, even if in this case a clear and complete rationalisation is still lacking nothwithstanding a lot of parameters have been taken into consideration.

The optical absorption of Cu(I) complexes, characterized by a broad MLCT band around 355-475 nm (in ACN), is mainly affected in term of both intensity and positions by substituents in 4 and 7 external positions; however the nature and the number of internal functionalities can also modulate the molar absorption coefficient of the complexes.

The resulting "structure *vs* activity" maps not only contributed to improve the knowledge of this important class of compounds (objects of partial or even poor studies, mainly from an electrochemical point of view), but was preparatory to the final aim of the project, it is the identification of new copper-based complexes that could efficiently substitute iodine-based electrolytes. The complexity and the multi-variable nature of the problem has made necessary, in particular, a good knowledge of the electrochemical properties of these complexes and an equally good understanding of how to tune their thermodynamic and kinetics features in order to overcome the numerous dichotomies that affect the operation of a DSSC and, hence, to propose effective redox mediators.

A lot of efforts have been focused to draft the aforementioned "maps"; after that a restricted ensemble of cautious chosen complexes was selected to be tested in DSSCs. In this way correlations between electrochemical features and photovoltaic performance have been identified, potentially useful also for further studies.

However the most exciting results have been obtained with the novel Cu(I) compound [Cu(2-mesityl-4,7-dimethyl-1,10-phenanthroline)$_2$]$^+$, **9**, and its oxidized form [Cu(2-mesityl-4,7-dimethyl-1,10-phenanthroline)$_2$]$^{2+}$, **21**. Acetonitrile-based electrolytes formulated with these two species were remarkable, more than doubling the performances of the unique literature example of effective copper-based redox couple, [Cu(2,9-dimethyl-1,10-phenanthroline)$_2$]$^{2+/+}$. The neat supremacy of the mesityl-architecture respect to the neocuproine one was confirmed in combination with two completely different sensitizers: [Ru(dcbpy)$_2$(dnbpy)][PF$_6$]$_2$ and G3 molecule, a fully-organic D-π-A dye with a benzothiadiazole core.

The Ru(II) dye resulted a not optimal choice, probably due to its chemical structure that in some how limits significantly the electron transfer rate with the Cu(II) mediator resulting into a too slow

dye regeneration reaction and in a scarse charge collection efficiency. Confirming this hypothesis, the combination with faster Fe-based comediators neatly improved the overall cell performances generating photocurrents comparable with those obtained with a control cell filled with a commercial iodide-based electrolyte.

However the coupling of the **9**/**21**-based electrolyte (in 10:1 molar ratio) with the highly polarized organic G3 dye resulted in a remarkable photon-to-current conversion efficiency of 4.4% (under 1 sun AM 1.5G illumination) that even excided that of an equimolar I_3^-/I^- electrolyte, $\mathbf{I_3^-/I^-}$ **equim**. The high PCE was mainly attributed to the high efficient dye regeneration (up to 70% during the half-life $\tau_{2/3}$ period), as confirmed by transient absorption spectroscopy studies.

The best PCE reached an absolute value that is less than the actual 7% record efficiency reported by Bai *et al.* [65], but in relative terms our new sufficiently easy-to-prepare mesityl-based couple is potentially able to double this record, so opening the way to copper complexes as new potentially competitors even of the more performing (tris-diimine)cobalt systems. The main limitation of the copper complexes is related with their lower solubility respect to iodide ions; this reduces the charge collection and hence limits the i_{sc} threshold.

For these reasons further development will surely concern the sythesis of more soluble species changing for example the counteranion, passing from the current PF_6^- to the organic bis(trifluoromethylsulfonyl)imide, $TFSI^-$, or the screening of other already synthesized copper complexes in search of a potentially more performig redox mediators.

Gallery

Pyrid-2-yl tetrazolate dye family

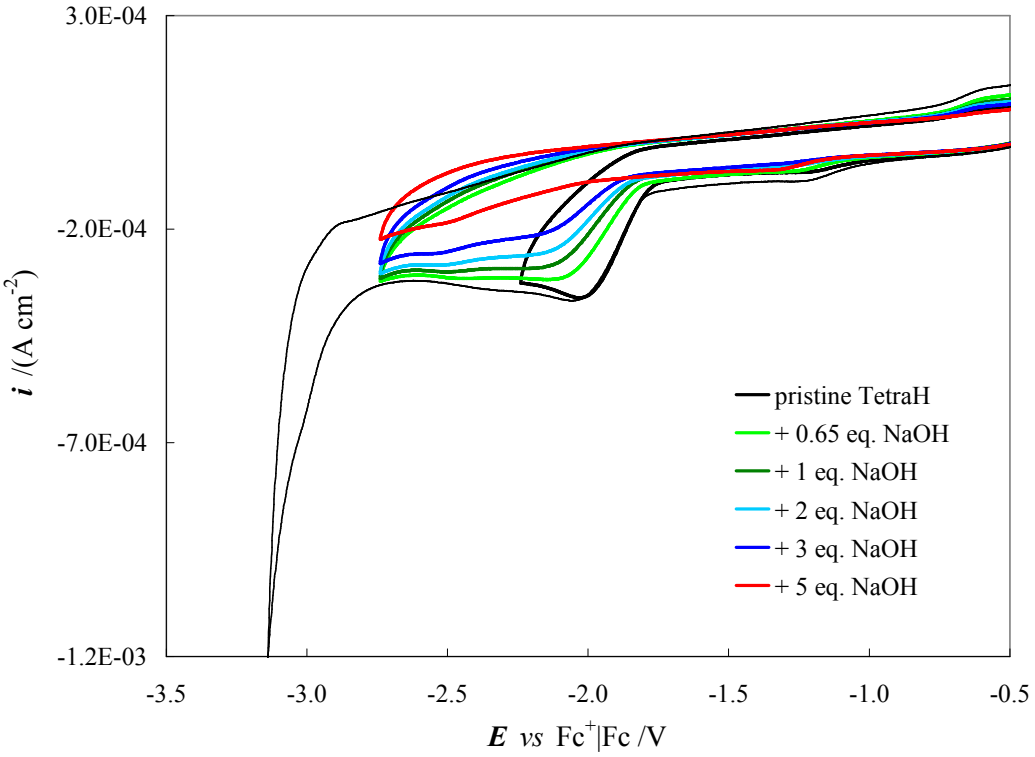

Figure G 1 Synopsis of cyclovoltammograms of TetraH ligand (black lines) during subsequent additions of NaOH solution (in DMF). Concentration ca. 0.001 M in DMF and TBAPF6 0.1 M, scan rate potential 0.2 V s–1. GC electrode.

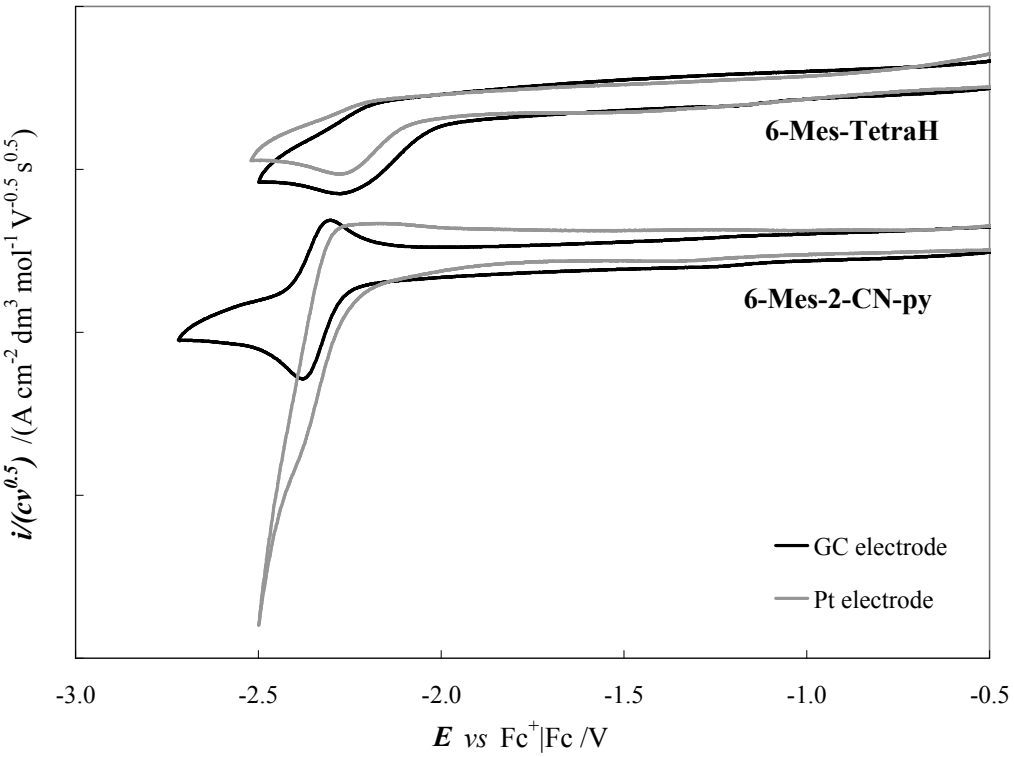

Figure G 2 Normalized cyclovoltammograms of 6-Mes-TetraH ligand (top) and of its precursor 6-mesityl-2-pyridinecarbonitrile (bottom) on GC and Pt electrode. Concentration *ca.* 0.001 M in DMF and $TBAPF_6$ 0.1 M, scan rate potential 0.2 V s^{-1}.

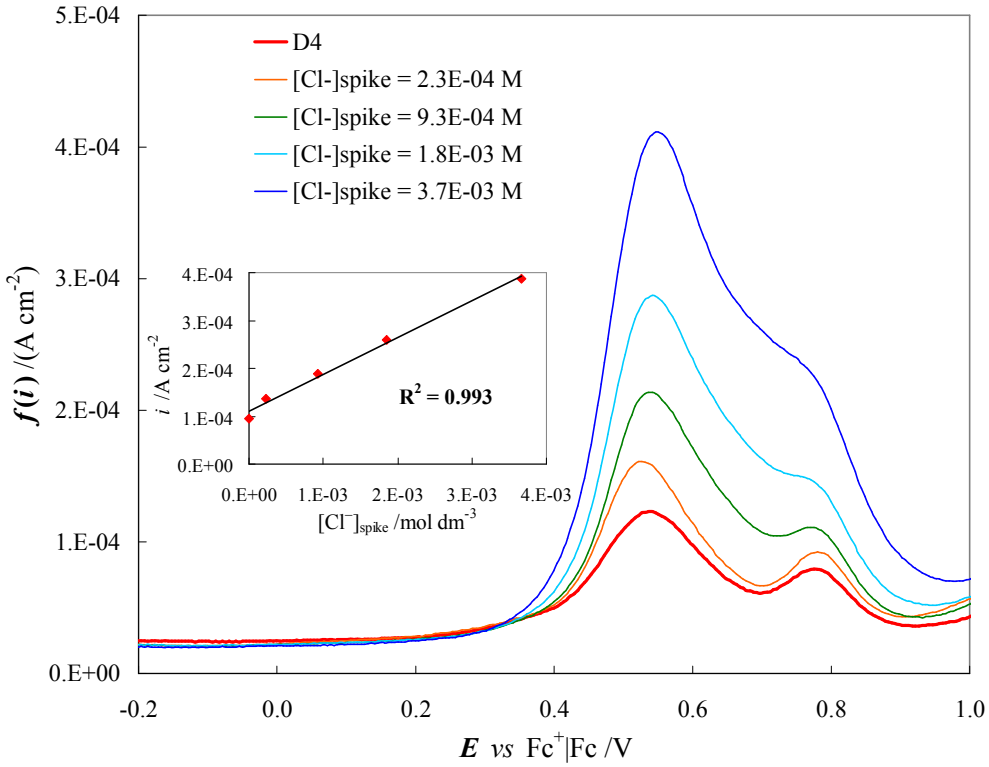

Figure G 3 DPV patterns of pristine D4 solution *ca.* $9 \cdot 10^{-4}$ M (thick red line) and after addition of known volume of a TBACl mother solution in DMF (thin lines). GC electrode; working medium DMF with $TBAPF_6$ 0.1 M. Potential scan rate 0.05 V s^{-1}. Inset: calibration plot for the added Cl^-.

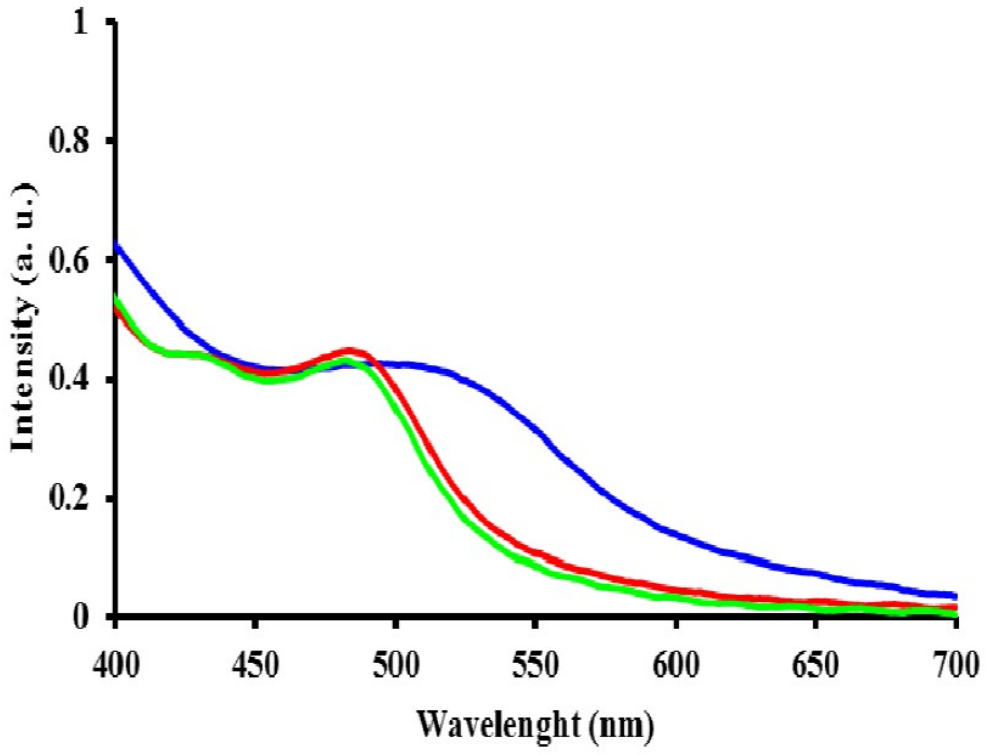

Figure G 4 Absorption spectra of D3 dye (red line) and D3 dye with CDCA (green line) adsorbed on a transparent TiO_2 electrode. Spectrum of adsorbed N719 (blue line) is also reported for comparison. From ref. 96.

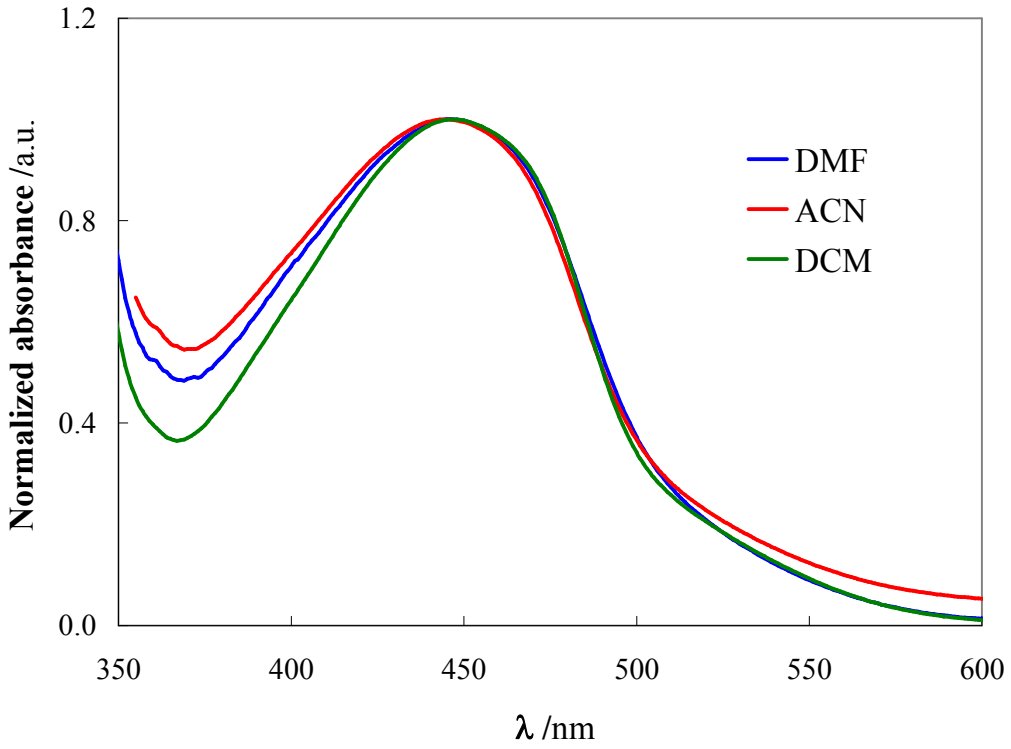

Figure G 5 Normalized electronic absorption spectra for Cu(I) complex 9 in solvents of decreasing polarity.

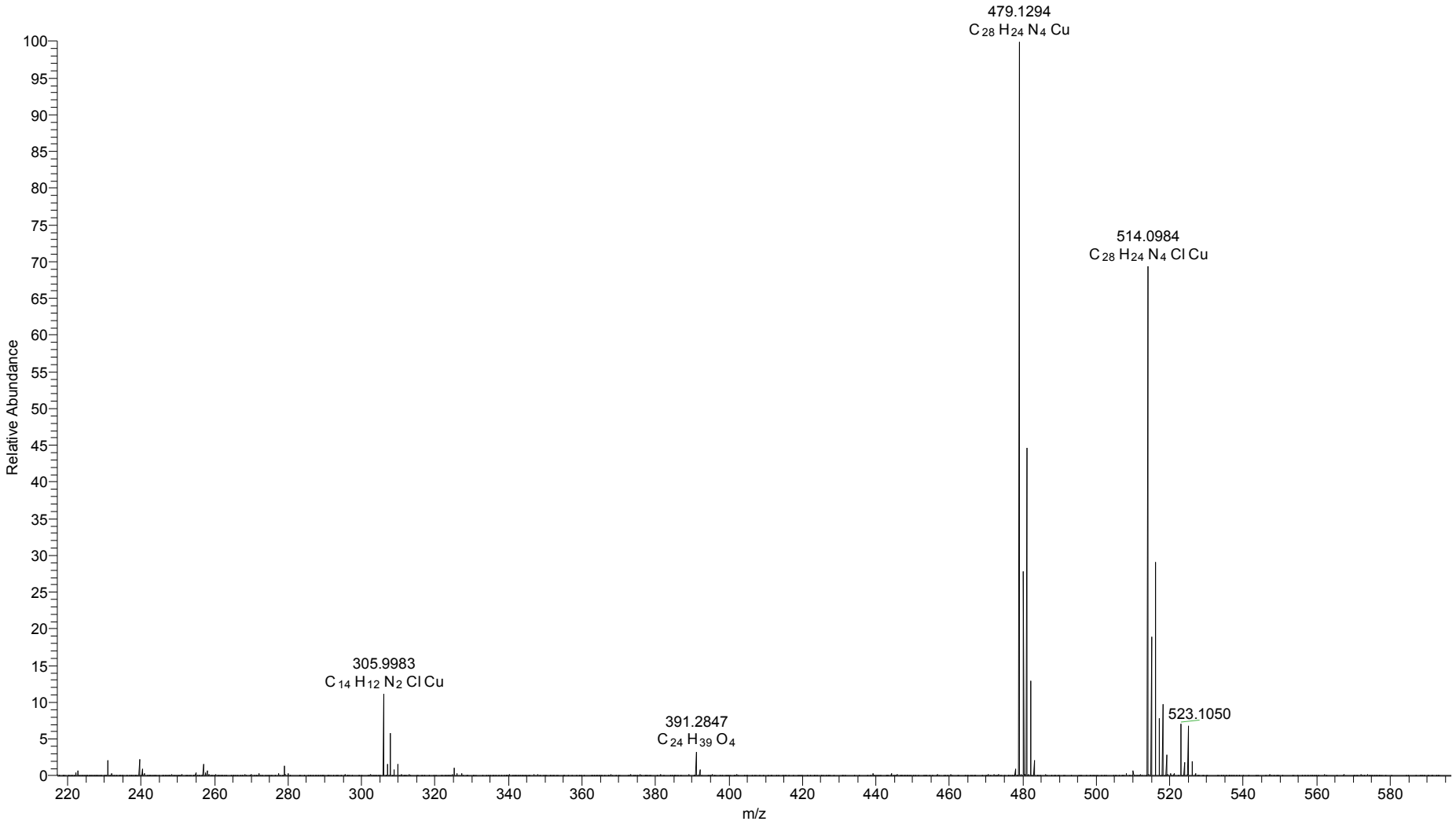

(See following page for the caption)

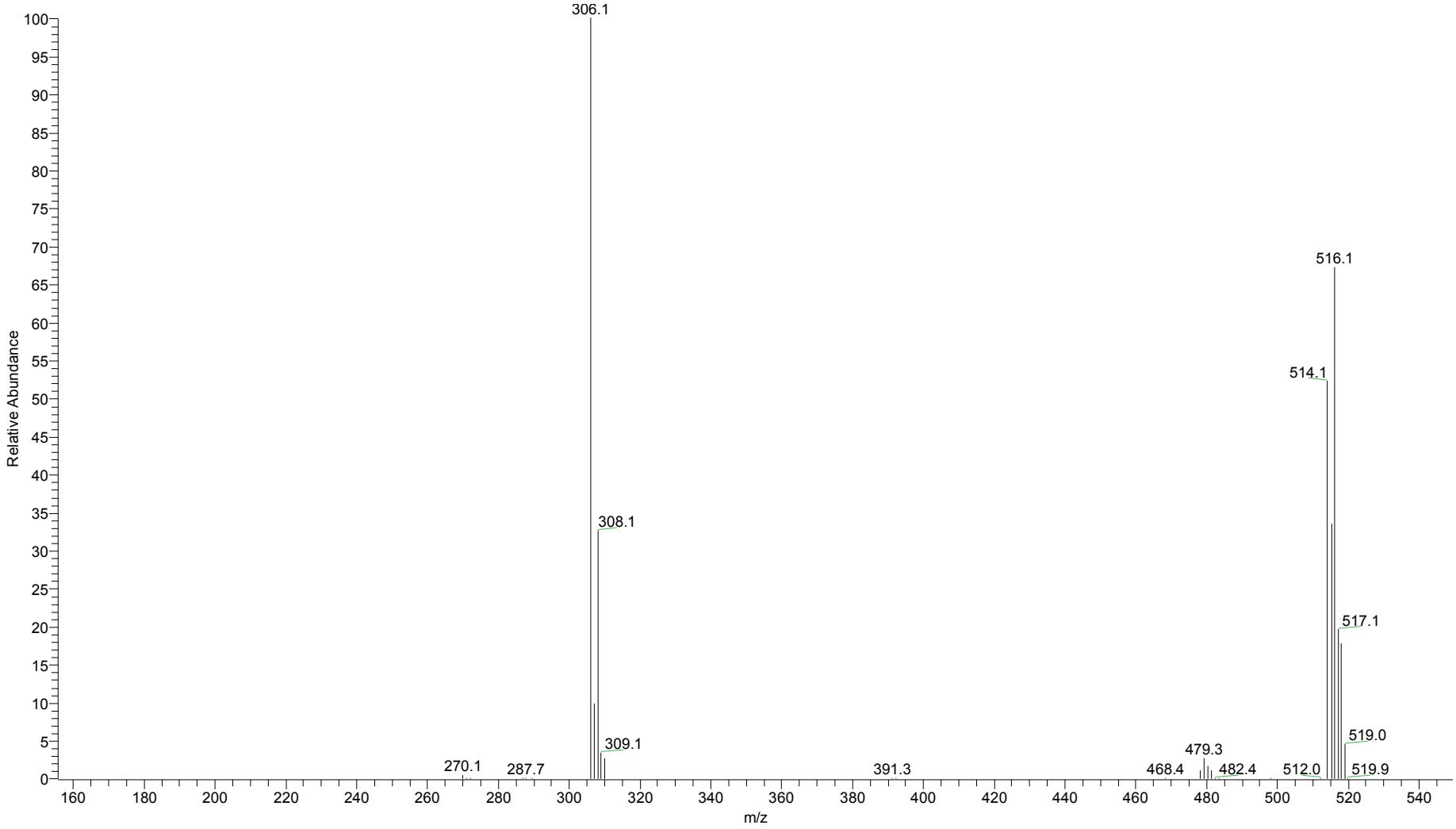

Figure G 6 Top (previous page): ESI(+)-FTICR mass spectrum of Cu(II)-complex 22 dissolved in ACN. Empirical formula are assigned to the main peaks. Bottom (this page): MS^2 spectrum of the precursor peaks m/z = 514/516/518 corresponding to the isotopic cluster of the complex. The principal fragment ion is related to the loss of one phenanthroline ligand. (They was kindly provided by Dr. Stefano Chiaberge, Mass Spectrometry Lab (CHIFIS), Renewable Energy and Environmental R&D, ENI-Donegani, Novara)

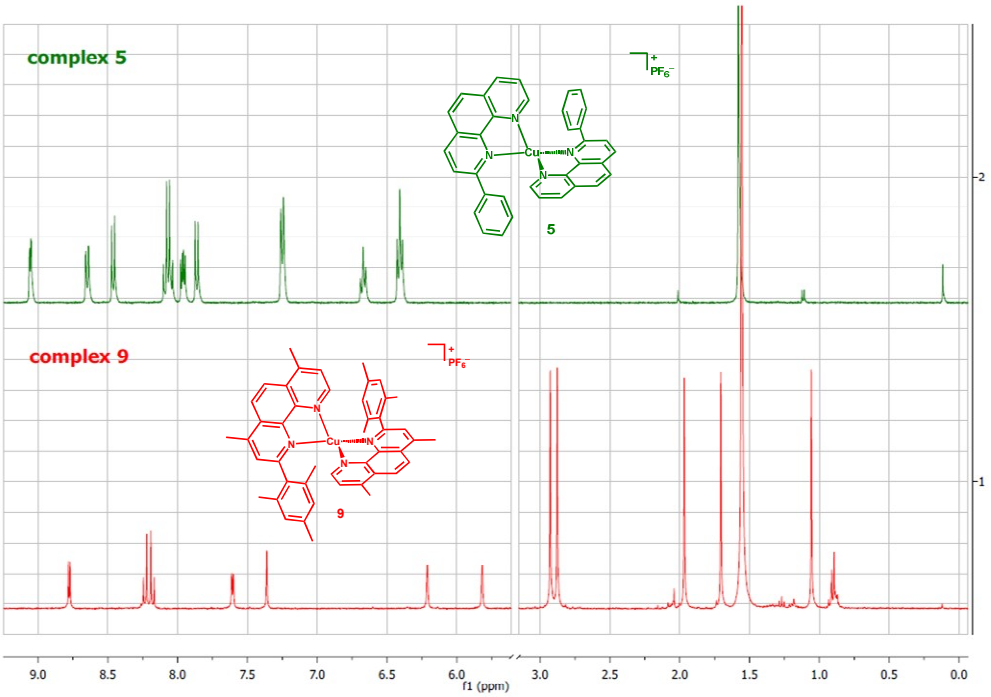

Figure G 7 ^{1}H-NMR spectra at r.t. for complex 5 (up) and 9 (down) in CD_2Cl_2 clearly showing the free rotation of the phenyl groups in 5 (*i.e.* the two homotopic aromatic hydrogens of phenyl ring at 7.25 ppm and 6.40 ppm) and the blocked conformation of the two mesityl rings in 9 (see, for example, the two singlet at 6.21 ppm and 5.82 ppm for the constitutional heterotopic aromatic hydrogens of the mesityl).

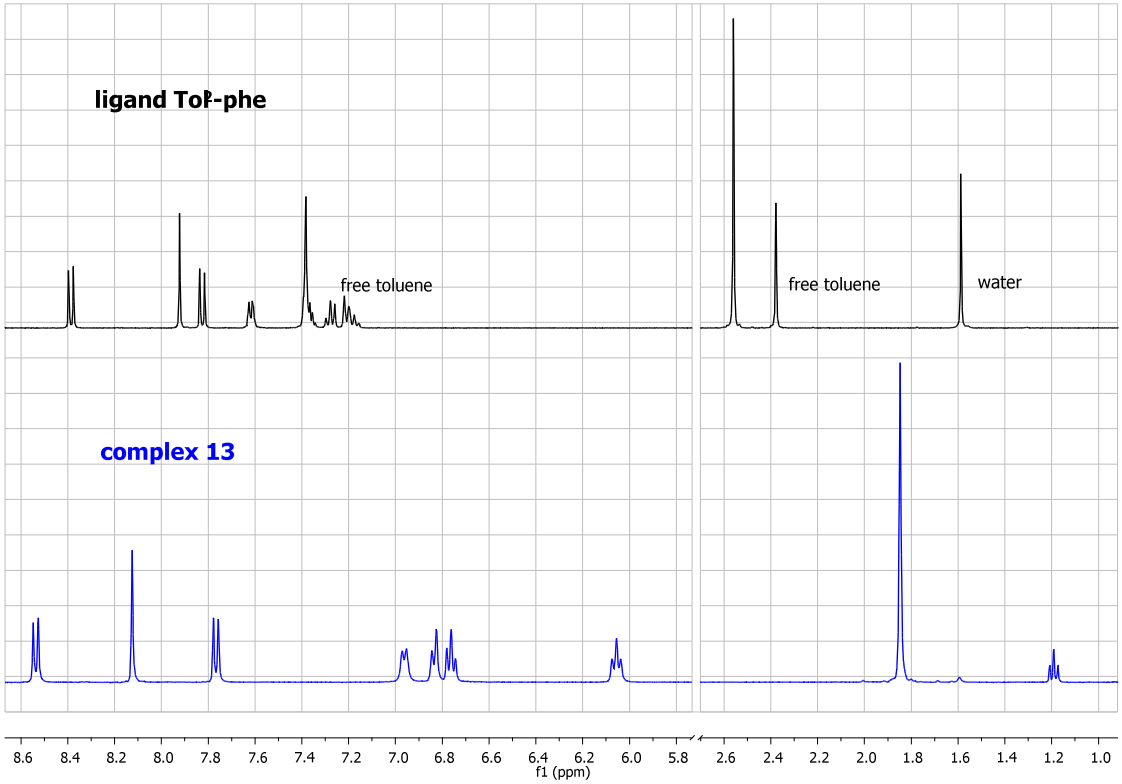

Figure G 8 ^{1}H-NMR spectra at r.t. for the ligand Tol_2-phe (up) and its related complex 13 (down) in CD_2Cl_2 They evidence the free rotation of the tolyl rings in the ligand and their "freezed" conformations after complexation.

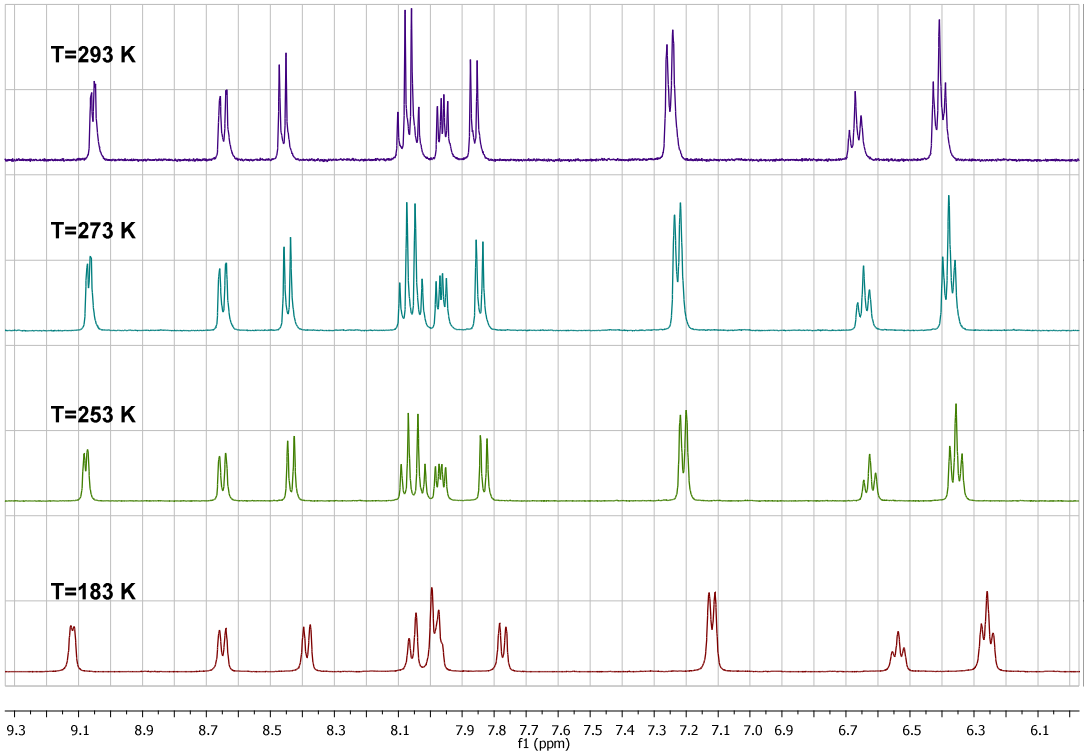

Figure G 9 VT ^{1}H-NMR study of the complex 5 in CD_2Cl_2.

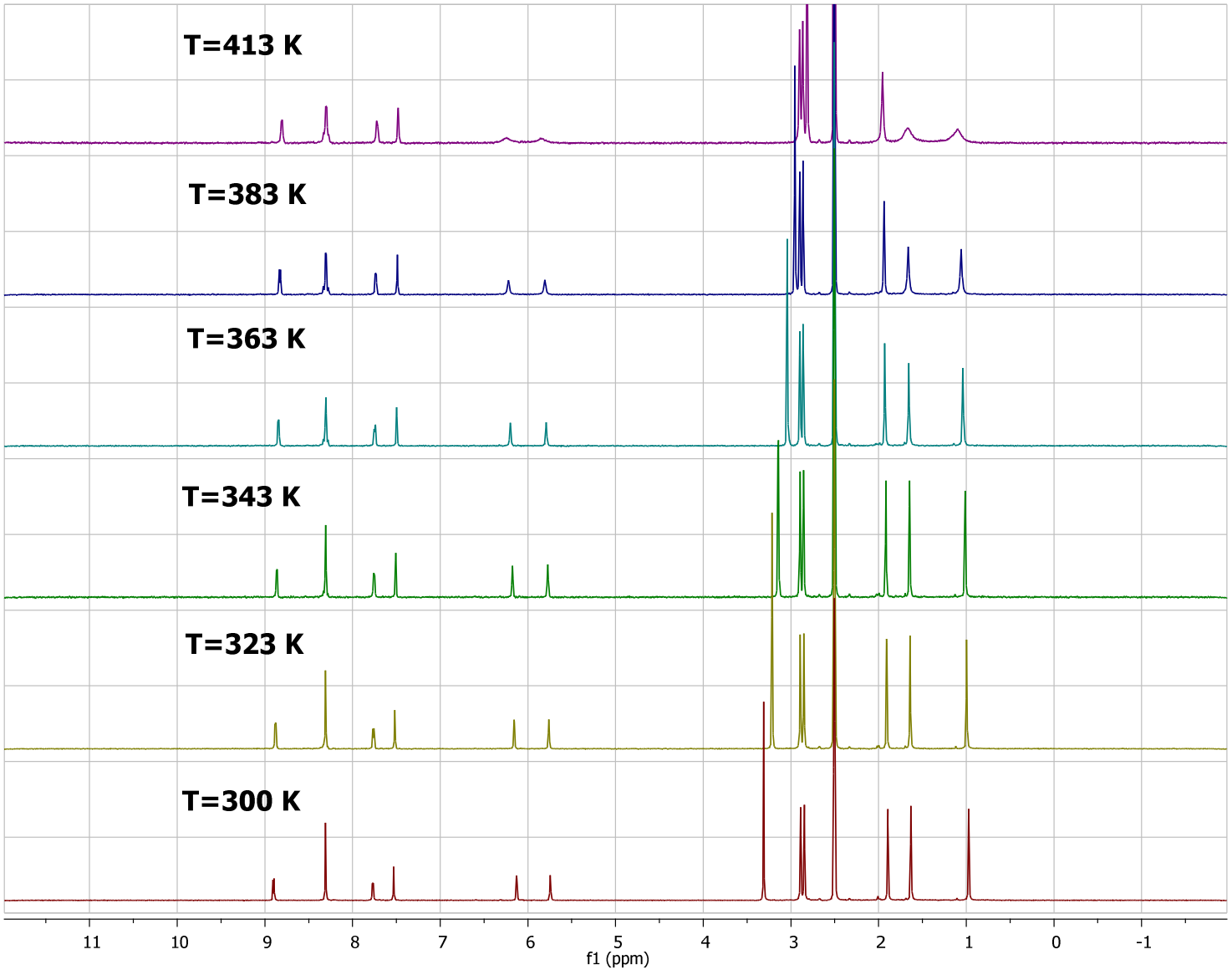

Figure G 10 VT ^{1}H-NMR in d_6-DMSO of complex 9. (Signal at 3.30 ppm at T=300 K is attributed to water residue; signals centred around *ca.* 2.50 ppm are of the solvent).

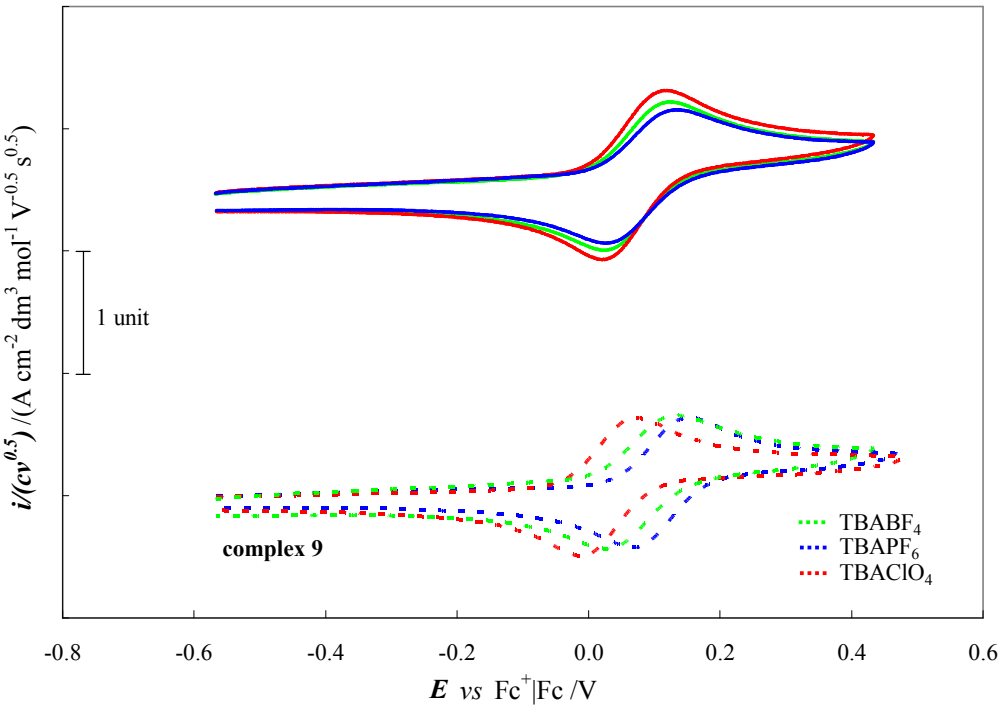

Figure G 11 Top: synopsis of normalized cyclovoltammograms of complex 9 (blue continuous line), 9-BF_4 (light green continuous line), and 9-ClO_4 (red continuous line), recorded in DCM with TBABF_4 0.1 M supporting electrolytes. Bottom: for sake of comparison CVs patterns of complex 9 in DCM with three different supporting electrolytes are also reported. In all cases a GC electrode was employed and the ohmic drop was compensated by positive feedback technique.

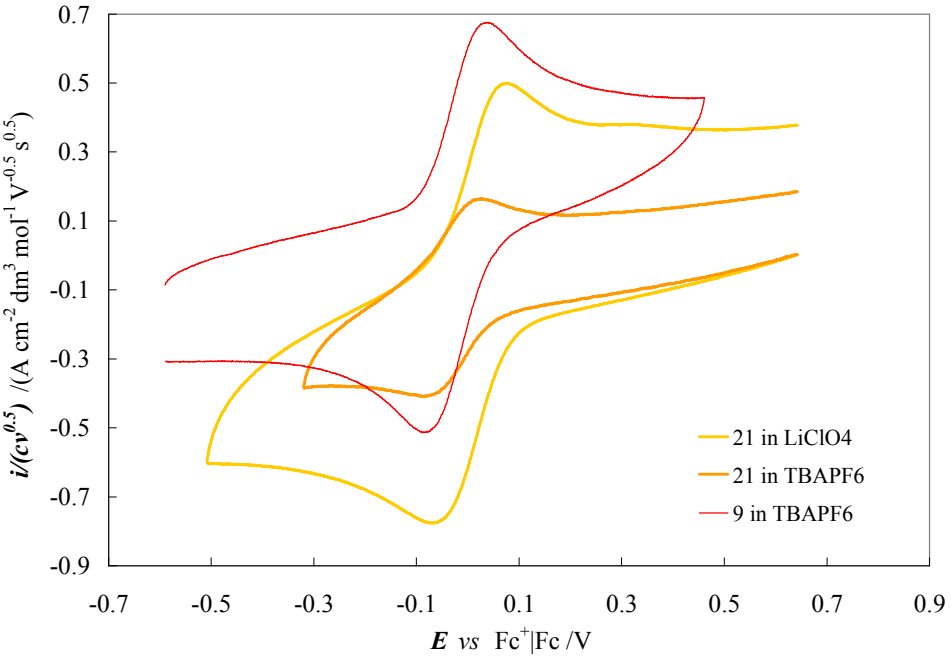

Figure G 12 Synopsis of normalized cyclovoltammograms of the complex 9 (red thin line) and its oxidized form, 21, dissolved in ACN with two different supporting electrolytes 0.1 M: TBAPF_6 (orange thick line) and LiClO_4 (yellow thick line). Complex concentrations 0.001 M; scan rate potential 0.2 V s^{-1}; GC electrode.

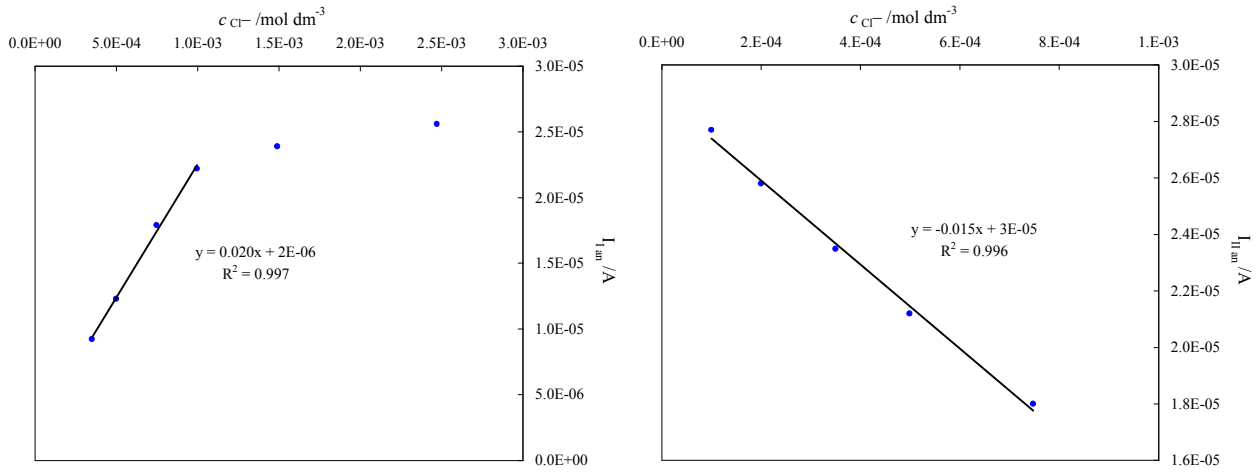

Figure G 13 Increase (left) and decrease (right) of peak currents for the first (left) and second (right) oxidation peak of Figure 48, at 0.2 V and 0.34 V *vs* $Fc^+|Fc$ respectively, after subsequent additions of chloride ions to a solution of complex 12 in ACN with $TBAPF_6$ 0.1M. GC electrode; scan rate potential 0.2 V s^{-1}.

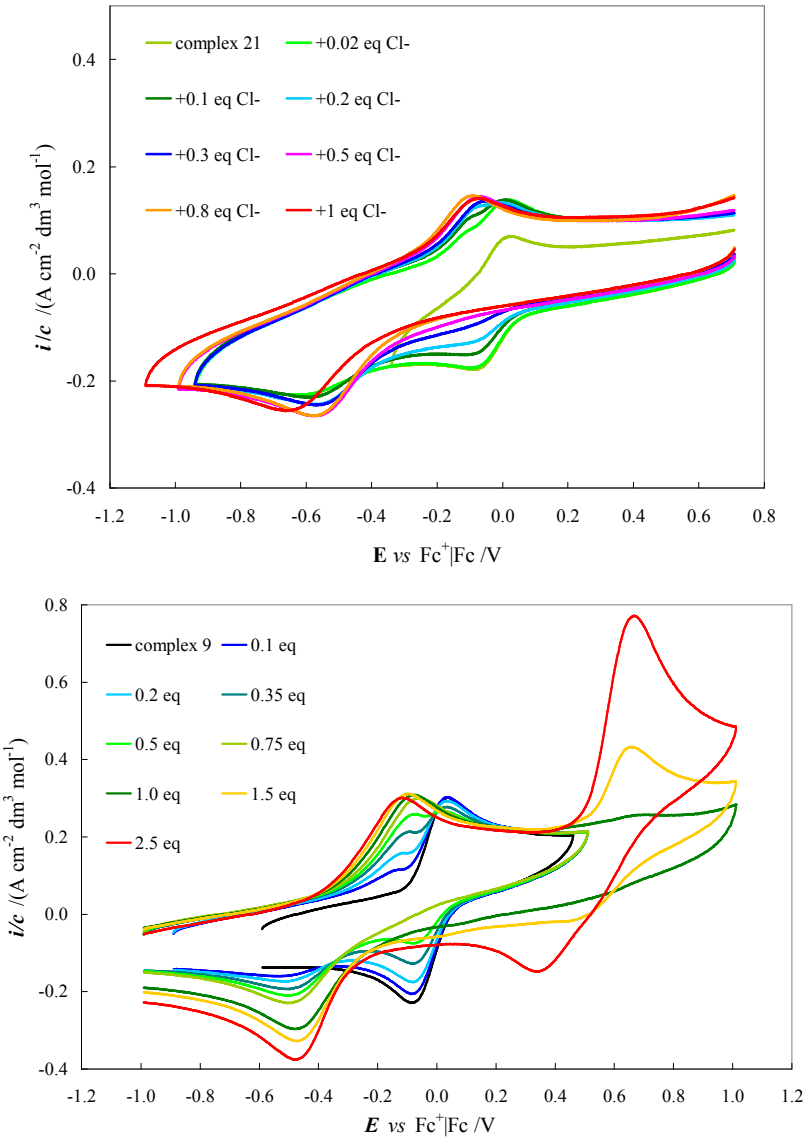

Figure G 14 Addition of Cl^- to a solution (ACN + $TBAPF_6$ 0.1 M) of Cu(II) complex 21 (up) and of its Cu(I) counterpart, 9 (down). Sample concentration *ca.* 0.001 M. GC electrode; scan rate potential 0.2 V s^{-1}.

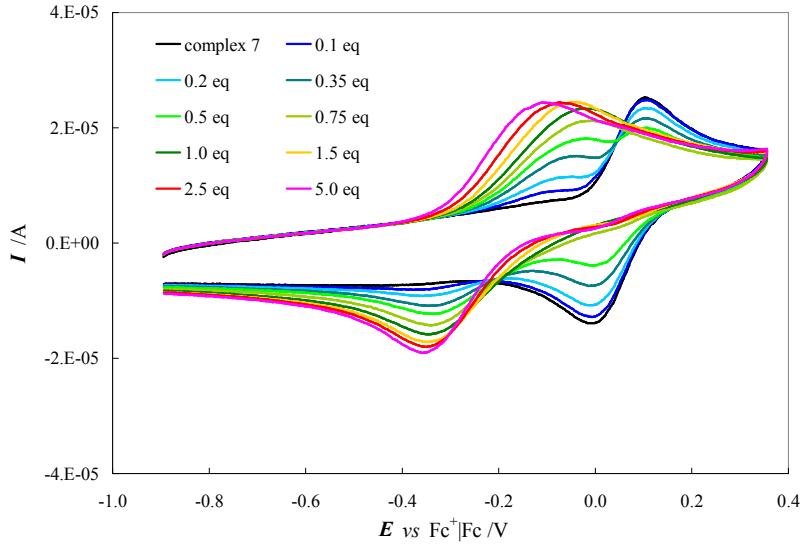

Figure G 15 Addition of Cl^- to a solution (ACN + $TBAPF_6$ 0.1 M) of Cu(I) complex 7. Sample concentration *ca.* 0.001 M. GC electrode; scan rate potential 0.2 V s^{-1}.

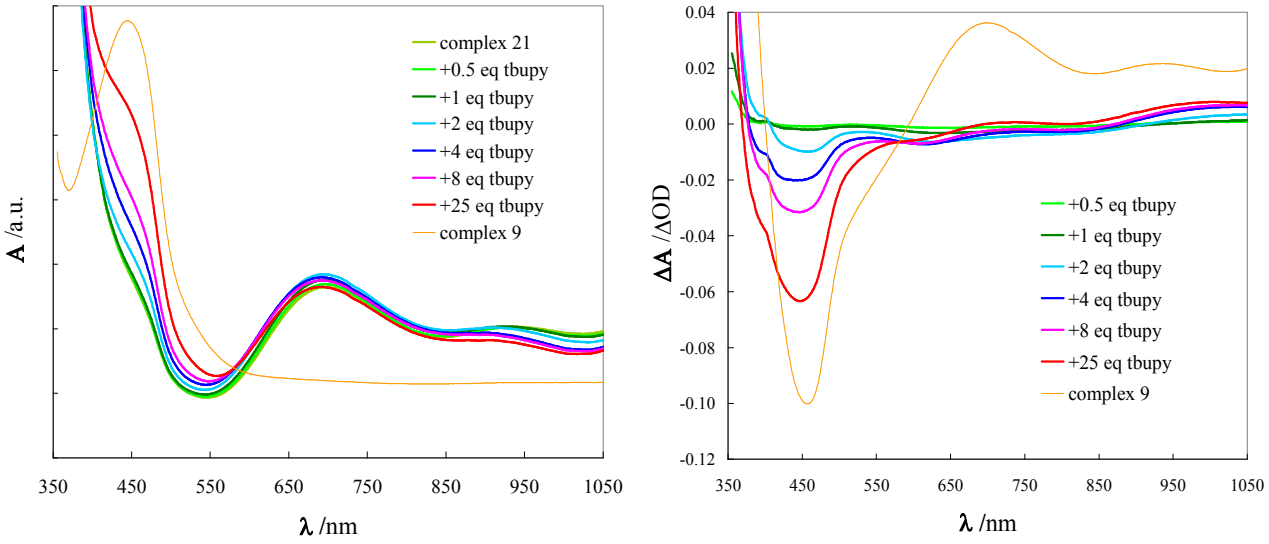

Figure G 16 Synopsis of visible spectra (left) and related differential patterns (right) of the complex 21 in ACN at increasing concentration of tbupy. For sake of comparison the spectrum of the Cu(I) complex 9 is also reported (orange thin line).

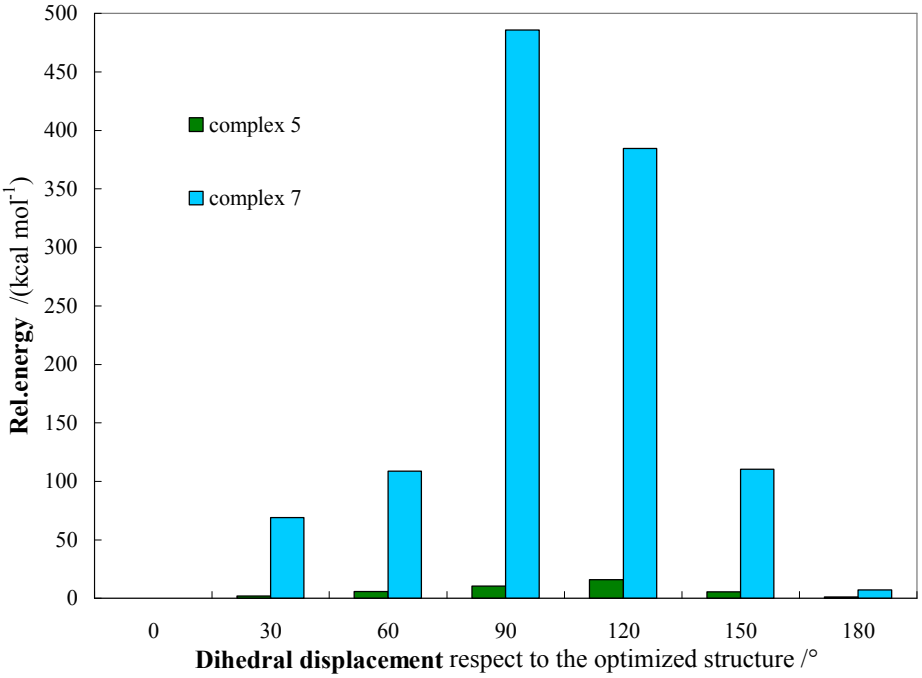

Figure G 17 Relative energy variation as a function of the dihedral angle of one of the two aromatic substituents (in position 2 of the phenanthroline) evaluated respect to the optimized structures of complex 5 and 7. DFT-B3LYP, 6-31G*.

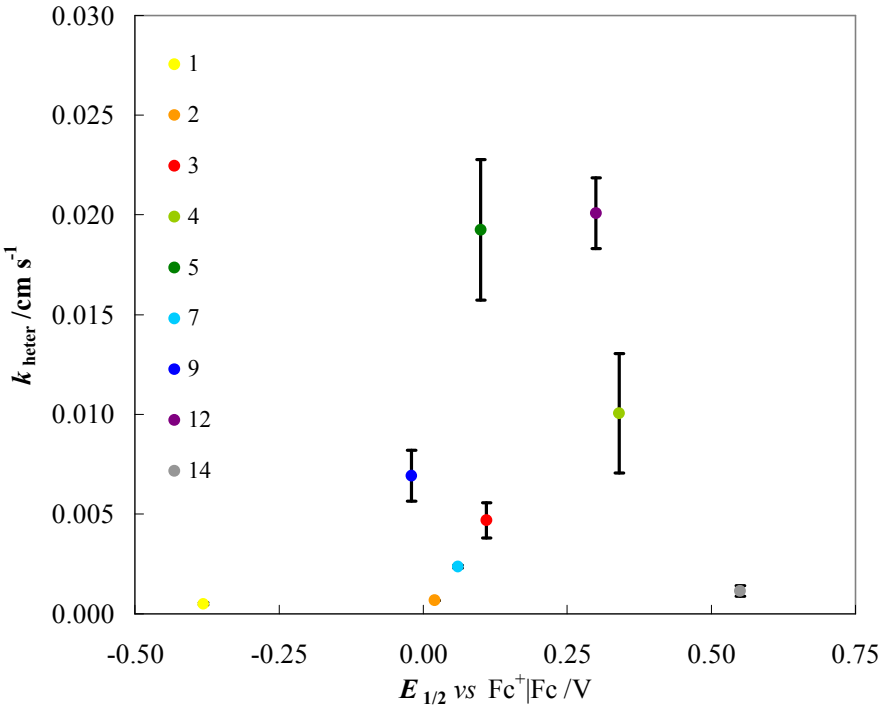

Figure G 18 Graph of k_{heter} as a function of the $E_{1/2}$ of the ensemble of Cu(I) complexes of Table 16.

Table G 1 Collection of experimental and theoretical dihedral angles for some Cu(I) complexes.

complex	R';R'';R'''	k_{heter} (error) /cm s^{-1} [a]	experimental dihedral angle /° [b]	theoretical dihedral angle /° [c]
1	H; H; H	$4.9 \cdot 10^{-4}$ ($5 \cdot 10^{-5}$)	90	–
3	H; H; *n*-Bu	$4.7 \cdot 10^{-3}$ ($9 \cdot 10^{-4}$)	–	82
4	H; H; *t*-Bu	$1.0 \cdot 10^{-2}$ ($3 \cdot 10^{-3}$)	78	88
5	H; H; Ph	$1.9 \cdot 10^{-2}$ ($4 \cdot 10^{-3}$)	75	70
7	H; H; Mesityl	$2.36 \cdot 10^{-3}$ ($7 \cdot 10^{-5}$)	–	83
9	CH_3; H; Mesityl	$6.9 \cdot 10^{-3}$ ($1 \cdot 10^{-3}$)	78	–
12	H; CH_3; CH_3	$2.0 \cdot 10^{-2}$ ($2 \cdot 10^{-3}$)	77[d]	83
14	H; Cl; Cl	$1.1 \cdot 10^{-3}$ ($3 \cdot 10^{-4}$)	75	–

[a] Defined in eq. 2; from averaged R_{ct} value. [b] From single crystal X-ray diffraction. [c] From optimized geometry, DFT-B3LYP level with 6-31G* basis set. [d] From literature [J. A. Rusanova, O. V. Kozachuk, V. V. Semenaka. V. V. Dyakonenko, Bis(2,9-dimethyl-1,10-phenanthroline)-copper(I) pentacyanidonitrosoferrate(II), A*cta Cryst.* E69 (2013), m684–m685]

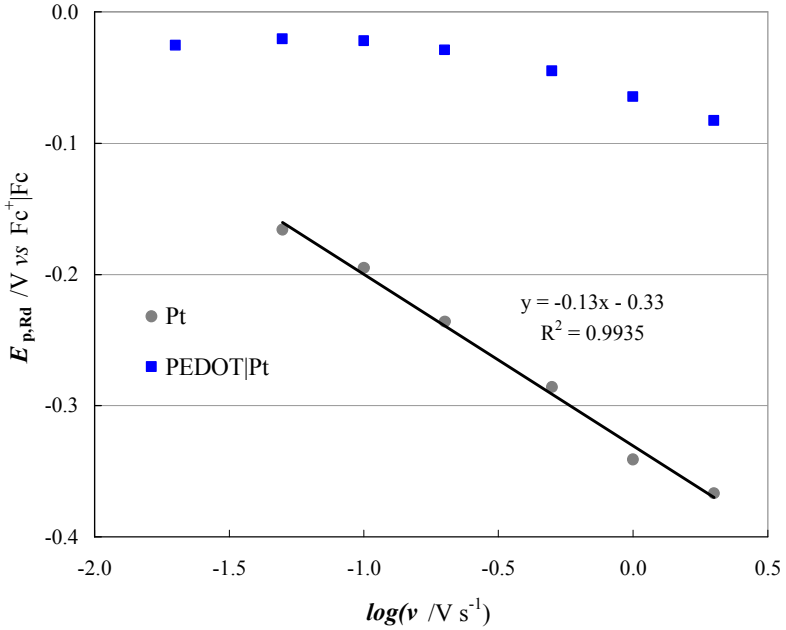

Figure G 19 Variation of reduction peak potential, $E_{p,Rd}$, with the scan rate potential for complex 21 in ACN with $LiClO_4$ 0.1 M on Pt and PEDOT-modified Pt electrode. Data were corrected for the ohmic drop in solution.

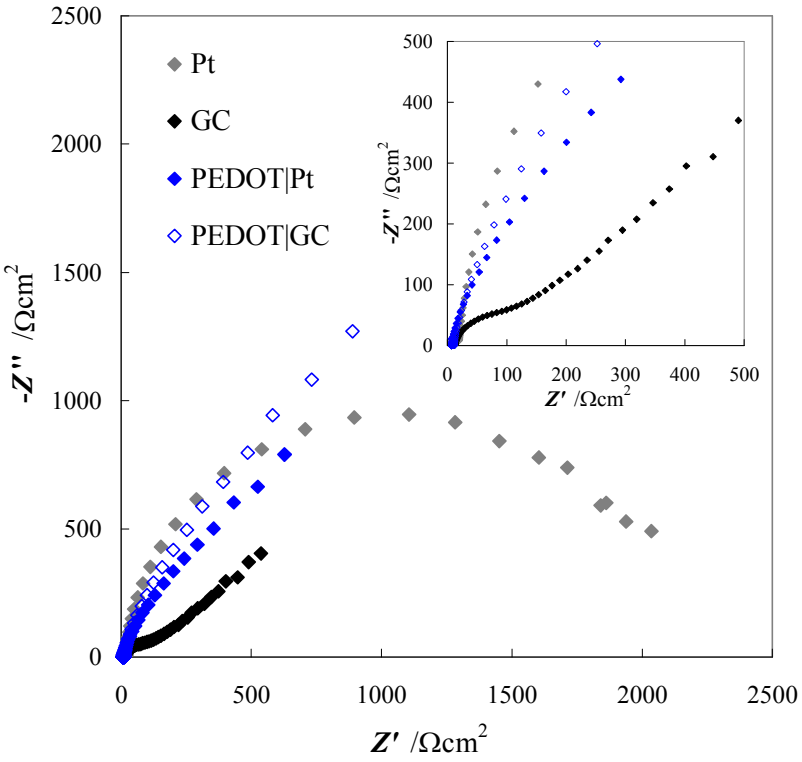

Figure G 20 Nyquist plots of Figure 56. Inset: magnification of the high frequency region.

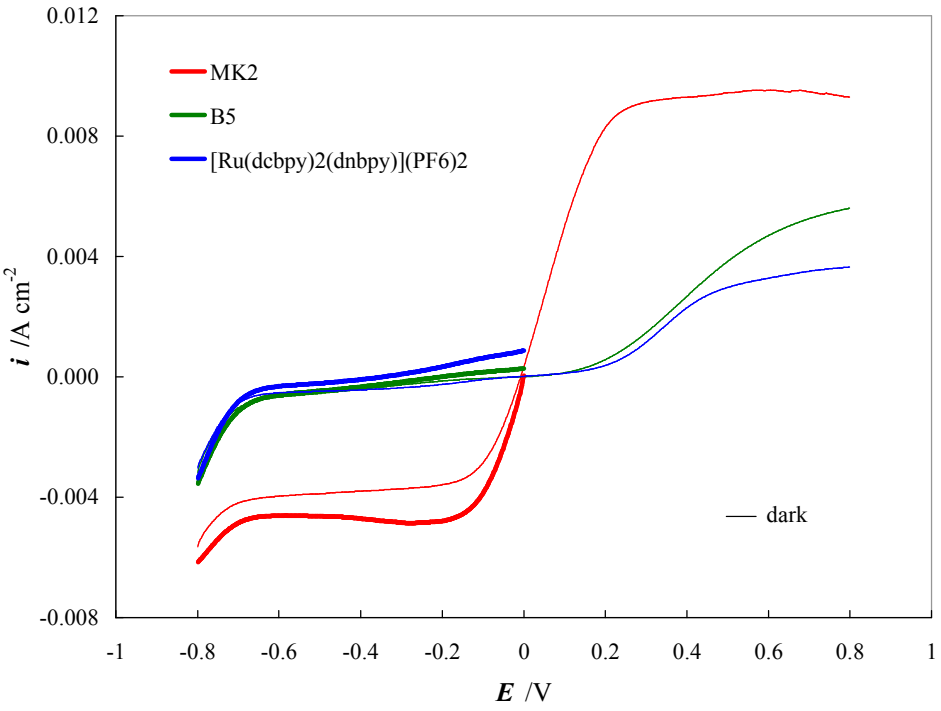

Figure G 21 Normalized *i-E* curves of DSSCs employing bilayer photoanodes (compact TiO_2 underlayer and mesoporous TiO_2 overlayer) sensitized with different dyes under 90 mW cm^{-2} AM 1.5G illumination (thick lines) and in the dark (thin lines). Electrolyte composition: 0.2 M solution of mediator 12 (0.01 Ox/Rd molar ratio) in ACN with $LiClO_4$ 0.1 M. Scan rate potential: 0.005 V s^{-1}.

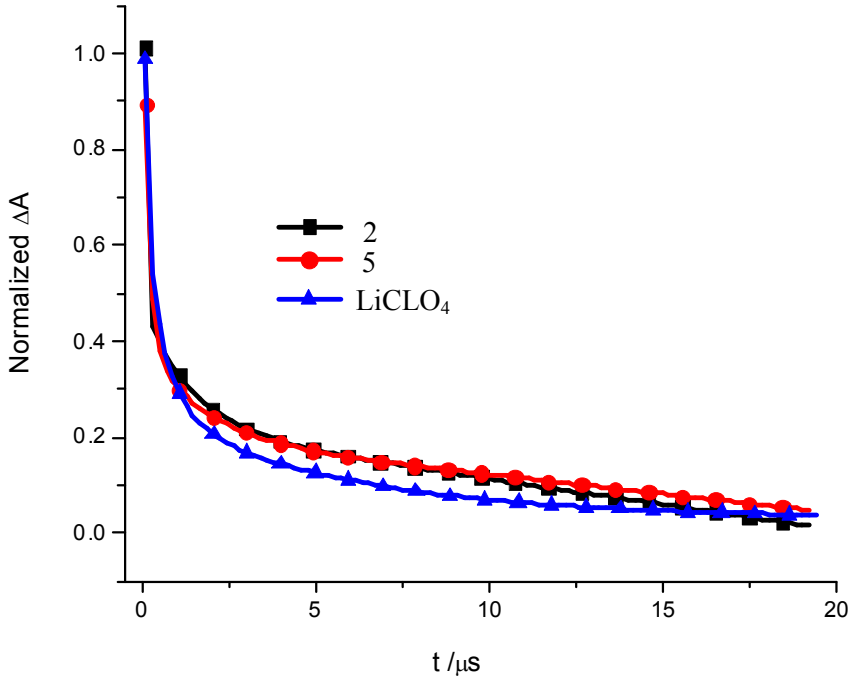

Figure G 22 Transient recovery monitored at 570 and 590 nm in the presence of complex 2 (black line) and 5 (red line) respectively. For sake of comparison trace for the inert electrolyte (blue line) is also reported. Contrary to Figure 60 here fits to the kinetics traces were reported for sake of clarity, given the very noisy traces resulting from exceedingly strong absorption by the copper based electrolytes. λ_{exc} = 532 nm.

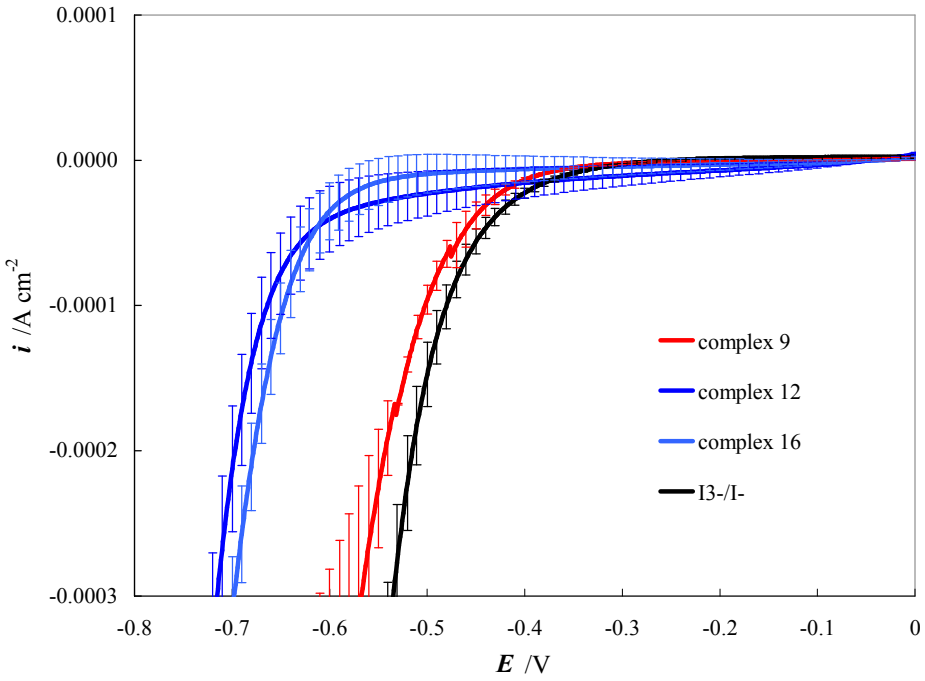

Figure G 23 Normalized dark current traces for DSSCs of Figure 62. Cu-electrolytes: 0.15 M with 5% Cu(II).

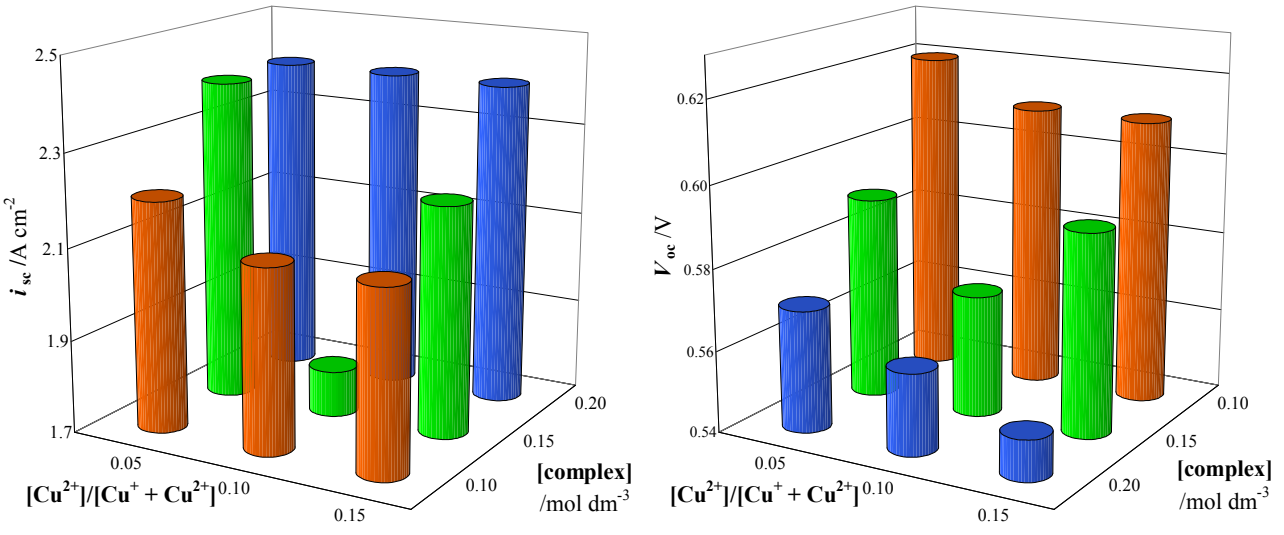

Figure G 24 Graphs reporting the dependence of i_{sc} (left) and V_{oc} (right) of DSSCs by the composition of the electrolyte based on the Cu(I) complex 9; Ox/Rd molar ratio of the copper complexes and the total concentration of Cu(I) were considered in the optimization. Solvent ACN with $LiClO_4$ 0.1 M; Ru(II) dye, under 90 mW cm^{-2} AM 1.5G illumination.

Table G 2 Fitted parameters[a] from EIS spectra for Pt-Pt and PEDOT-PEDOT symmetrical cells (active area 1 cm^2); E = 0 V.

electrolyte	cathode	R_{series} /Ω	R_{CE} /Ω	10^5 C_{CE} / F	R_{diff} / Ω
9/21	Pt	21	9.8	4.05	12.8
9/21	PEDOT	37	0.82	232	14.2
12/22	Pt	39	61	1.28	164
12/22	PEDOT	53	4.4	500	223
I^-/I^{3-} equim	Pt	30	11	2.24	11.2
I^-/I^{3-} equim	PEDOT	55	8.2	$1.90\cdot10^2$	11.5
I^-/I^{3-} optim	Pt	26	0.82	3.58	2.05
I^-/I^{3-} optim	PEDOT	53	0.61	$5.02\cdot10^3$	2.38

[a] Using the classical Randles equivalent circuit. R_{CE} and C_{CE} values from fitting have been divided and multiplied, respectively, for a factor of 2 accounting for the symmetry of the cell.

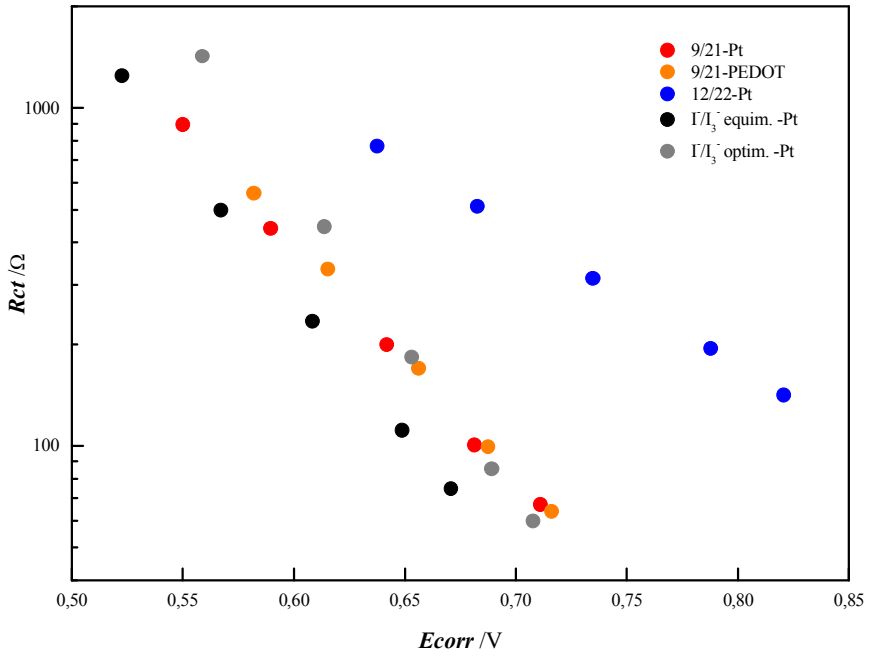

Figure G 25 Potential dependence of charge transfer resistance, R_{ct}, calculated by EIS measurements for solar cell sensitized (active area 0.16 cm^2) with G3 dye and filled with copper-based and iodide-based electrolytes (Figure 69). Two different cathodes have been compared; 1 sun illumination.

Experimental details

General information

^{1}H NMR, proton decoupled ^{13}C NMR spectra and bidimensional experiments (not reported here) were recorded at 400 MHz (T = 300 K, unless otherwise stated) on a Bruker Avance-400 instrument. Chemical shifts (δ) for ^{1}H spectra are expressed in ppm relative to internal Me_4Si as standard. Signals were abbreviated as s, singlet; d, doublet; dd, doublet of doublets; t, triplet; q, quartet; m, multiple; br, broad signal. Mass spectra were obtained with a FT-ICR Mass Spectrometer APEX II & Xmass software (Bruker Daltonics) 4.7 Magnet and Autospec Fission Spectrometer (FAB ionization).

Electrochemical measurements (CV, DPV, linear scan voltammetry and EIS) were performed using different Autolab PGSTAT-series potentiostats/galvanostats (EcoChemie, The Netherlands) managed by a PC with GPES or NOVA software. Experiments (except obviously for DSSCs or analogue two-electrode devices) were carried out in a small three-electrode cell (containing from 2 to 4 cm^3 of the working solution) including: (i) as working electrode, a Teflon-embedded glassy carbon GC disk (Amel, surface 0.071 cm^2), (ii) a Pt sheet as counter-electrode and (iii) an aqueous saturated calomel electrode (SCE) as operating reference one inserted into a jacket filled with a solution of the same electrolyte used in the cell and ensuring contact with the working solution via a glass joint, in order to prevent water and chloride leakage in the working cell. The recorded potentials have been subsequently referred to the reference redox couple $Fc^+|Fc$ (ferricenium|ferrocene) added as external standard (*ca.* 1×10^{-3} M) at the end of each measures.

For CV measurements an instrumental compensation of the resistance (*i.e.* positive feedback) was carefully performed in order to minimize the ohmic drop between the working and reference electrode. The working solution was well deareated by bubbling nitrogen before each measure starts and blowing it over the surface of the solution during the scans.

The staircase CVs were performed with a 0.001 V step potential and at potential scan rate usually ranging between 0.02 and 2 V s^{-1}.

Experimental parameters for DPV was: 5 s of equilibration time at the start potential, 0.05 s modulation time, 0.05 V modulation amplitude, 0.1 s interval time, 0.005 V step potential (*i.e.* 0.05 V s^{-1} scan rate).

Electrochemical impedance spectroscopy, EIS, measurements (also on DSSC devices) were performed applying a sinusoidal voltage (amplitude 0.01 V) superimposed to the constant bias potential opportunately tuned; frequencies from 100 MHz to 50 mHz.

Polarization curves for DSSCs (and symmetrical cells) were recorded at a sufficiently slow scan rate potential, from 5 to 20 mV s^{-1}. Photoelectrochemical measurements under AM 1.5G 0.1 (or 0.09) W cm^{-2} illumination generated by an ABET sun simulator.

Transient absorption spectroscopy was performed using a home-assembled apparatus; the detail characteristics have been described in paper [76].

TiO_2 photoanodes for the fabrication of solar cells were prepared employing commercially available (Dyesol) transparent titania paste 18NR-T (for measurements with Ru(II) dye) and 30NR-D (with G3 sensitizer), deposited on cleaned FTO substrates by the doctor blading method; after sintering, the thickness of TiO_2 films were about 10 μm. For more details see reference [76].

All reagents, solvents, and chemicals for electrochemical measurements (*i.e.* supporting electrolytes) were purchased from Sigma-Aldrich and were used without further purification.

8-Oxyquinolate dye family

Synthesis and characterization

For detailed synthetic procedures (thermal and microwave-assisted ones), characterization of complexes **D1** and **D2** (*i.e.* by ^{1}H-NMR and mass spectrometry results) and experimental procedures for voltammetric and photoelectrochemical measurements please refer to our published work [80].

Pyrid-2-yl tetrazolate dye family

Synthesis and characterization

2-cyano-4-iodopyridine, **I-1**

The commercially available 2-cyano-4-chloropyridine precursor (0.727 mmol, 1 eq) was dissolved in dry ACN (2 ml) in a MW vial under Ag, equipped with a magnetic stir bar. 10 eq of NaI (preventively dried at 100°C in vaccum for *ca.* 30 min) were added and finally acetyl chloride (1.5 eq) was syringed into the vessel cooled at –10°C. The vial was filled with Ar and then it was put into a microwave reactor for 3 hours at 80°C (modality dynamic). After that it was cooled to r.t. and treated with potassium carbonate (3 ml of a 10% w/v aqueous solution), sodium sulfite (3 ml of a 5% w/v aqueous solution) and, finally, sodium thiosulphate (3 ml of a saturated aqueous solution). After addition of DCM (20 ml) the two phases were separated; the acqueous layer was extracted with DCM (3 x 10 ml) and the combined organic phases were then dried, filtred and evaporated at reduced pressure. The yellow/orange liquid was subjected to flash chromatograpy (SiO_2; eluent: from Hex:EtOAc 1:1 to pure EtOAc). The first eluted species was the desired product which

resulted, after dryness, as a whitish solid. ^{1}H-NMR (400 MHz, CD_2Cl_2) δ (ppm): 8.38 (d, *J*= 5.1 Hz, 1H), 8.11 (d, *J*= 1.5 Hz, 1H), 7.98 (dd, *J*= 5.1 Hz, *J*= 1.5 Hz, 1H). MS (FAB^+) *m/z*: 231.

2-cyano-4-(ethynylphenyl)pyridine, **I-2**

The most effective synthesis was reported (entry 4 of Table 5). **I-1** (0.166 mmol, 1 eq) was suspended in water (4 ml) into a round-bottom flask equipped with a stir bar filled with Ar. After the addition of phenylacetylene (1.5 eq) an homogeneous yellowish solution was obtained; CuI (0.01 eq), N,N-diisopropylethylamine (DIPEA, 1.5 eq) and, finally, tetrakis(triphenylphosphine)palladium(0) catalyst (0.005 eq) was added. Reaction mixture was stirred at r.t. for 24 hours; after that it was extracted with EtOAc and the aqueous layer were extracted again with EtOAc (3 x 15 ml) and the combined organic phases were then dried, filtred and evaporated at reduced pressure. The yellowish solid was purified by flash chromatograpy (SiO_2; eluent: from Hex:EtOAc 95:5 to 8:2). The second eluted species was the desired product.
^{1}H-NMR (400 MHz, CD_2Cl_2) δ (ppm): 8.72 (d, *J*= 5.0 Hz, 1H), 7.81 (s, 1H), 7.63 (m, 3H), 7.47 (m, 3H). MS (FAB^+) *m/z*: 205.

2-cyano-4-(1'-ethynylpyrenyl)pyridine, **I-3**

Phase 1: 1-bromopyrene (1.07 mmol, 1 eq), $PdCl_2(PPh_3)_2$ (0.06 eq), CuI (0.03 eq) and PPh_3 (0.03 eq) were inserted in a two-neck round-bottomed flask under Ar. Ethynyltrimethylsilane (1 eq) and triethylamine (10.7 mL) were added. The reaction mixture was heated at reflux at 70°C overnight.
The solution was allowed to cool at room temperature and the solvent was evaporated. DCM was then added and the solution was washed wit H_2O. The crude product was purified by column chromatography (SiO_2, Hex:DCM, 9:1) to obtain, at a quantitative yield, the pure 1-(trimethylsilylethynyl)pyrene.
Phase 2: 1-(trimethylsilylethynyl)pyrene (1 eq) was dissolved in a mixture of methanol and $CHCl_3$ (18 mL each). K_2CO_3 (4 eq) was added and the reaction mixture was stirred overnight at room temperature. The solvent was evaporated, DCM was added and the solution was washed with H_2O. The organic phase was dried over Na_2SO_4, filtered, and the solvent was evaporated. The crude product was purified by column chromatography (SiO_2, Hex:EtOAc, 8:2) to obtain the deprotected 1-ethynylpyrene (88% yield).
Phase 3: Into a round-bottom flask equipped with a stir bar the cyano intermediate **I-1** (1 eq) was dissolved in 3 ml of dry DMF; then CuI (0.01 eq), $PdCl_2(PPh_3)_2$ (0.02 eq), triphenylphosphine (0.02 eq), triethylamine (0.11 ml) and, finally, 1-ethynylpyrene (1 eq) were added. The mixture was refluxed for about 18 hours. After concentration the crude was redissolved in DCM and washed with water (3 times); the organic phase was dried over Na_2SO_4, filtered, and the solvent was evaporated. Finally the crude product was purified by flash chromatography (SiO_2, Hex:DCM, 8:2).

^{1}H-NMR (400 MHz, $CDCl_3$) δ (ppm): 8.77 (d, *J*= 4.8 Hz, 1H), 8.58 (d, *J*= 8.8 Hz, 1H), 8.32-8.18 (m, 6H), 8.12-8.08 (m, 2H), 7.95 (s, 1H), 7.75 (dd, *J*= 5.2 Hz, *J*= 1.3Hz, 1H).

2-cyano-4-(4'-(N,N-dimethylamino)phen-1'-yl)pyridine, **I-4**

Into a round-bottom flask equipped with stir bar the commercially available boronic acid (2.18 mmol, 1 eq) was partially dissolved in a mixture of 30 ml of dry DMF and 18 ml of anhydrous THF under Ar; after addition of the commercially available 4-chloro-2-cyanopyridine (1 eq) and sodium carbonate (2 eq) the solution became dark. After 1 hour, under Ar, the catalyst $Pd(PPh_3)_4$ (0.02 eq) was added to the reaction mixture and refluxed at *ca.* 80°C for 24 hours. The solvent was concentrated under reduced pression; the crude was then redissolved in DCM and after addition of H_2O the two phases were separated. Organic layer was extracted with water (three times) and the combined organic phases were then dried, filtred and evaporated at reduced pressure. The crude was purified by flash chromatograpy (SiO_2; eluent Hex: EtOAc 7:3). The desired product was obtained collecting the fourth eluted species.

^{1}H-NMR (400 MHz, $CDCl_3$) δ (ppm): 8.65 (d, *J*= 5.3 Hz, 1H), 7.88 (s, 1H), 7.66 (dd, *J*= 5.3 Hz, *J*= 1.9 Hz, 1H), 7.60 (d, *J*= 7.5 Hz, 2H), 6.88 (d, J_1 = 7.5 Hz, 2H), 3.08 (s, 6H).

2-cyano-4-(thien-2'-yl)pyridine, **I-5**

Into a round-bottom flask equipped with stir bar filled with N_2 the intermediate **I-1** (0.611 mmol, 1 eq) was dissolved in dry toluene. Then LiCl (4.5 eq), $PdCl_2(Ph_3)_2$ (0.03 eq) and 2-(tri-*n*-butylstannyl)thiophene (1.5 eq) were added in series. The mixture was refluxed for 24 hours (since after half an hour the solution became dark). After it was cooled down a r.t. 10 ml of NaOH 1 M solution was added; then the mixture was extracted with EtOAc (three times), the resulting combined organic phases were dried, filtred and evaporated at reduced pressure. After flash chromatograpy (SiO_2; eluent Hex: EtOAc 7:3) the product was isolated in pure form as a white solid.

^{1}H-NMR (400 MHz, $CDCl_3$) δ (ppm): 8.69 (d, *J*= 5.2 Hz, 1H), 7.89 (d, *J*= 1.7 Hz, 1H), 7.68 (dd, *J*= 5.2 Hz, *J*= 1.8 Hz, 1H), 7.59 (dd, *J*= 3.7 Hz, *J*= 1.0 Hz, 1H), 7.54 (dd, *J*= 5 Hz, *J*= 1.0 Hz, 1H), 7.21 (t, *J*= 5 Hz, *J*= 3.7 Hz, 1H). MS (FAB^+) *m/z*: 187.

2-cyano-6-mesityl-pyridine, **I-6**

Into a Schlenk flask equipped with stir bar the commercially available 2,4,6-trimethylphenyl boronic acid (1.64 mmol, 1 eq) was dissolved in 3.2 ml of 1,2-dimethoxyethane under Ar; after that the commercially available 6-bromo-2-cyanopyridine (1 eq) and barium hydroxyde (1.5 eq) was added. Finally, after some minutes the catalyst $Pd(PPh_3)_4$ (0.02 eq) was added and the reaction mixture was heated at *ca.* 80°C for 20 hours. After it was cooled down to the room temperature the

crude was diluted with a 1:1 mixture of DCM and H_2O (*ca.* 70 ml) and the two phases were then separated. Organic layer were treated with brine (2 x 20 ml) and water (2 x 20 ml); the combined organic phases were then dried with Na_2SO_4, filtred and evaporated at reduced pressure. The crude was purified by flash chromatograpy (SiO_2; eluent Hex: EtOAc 8:2). The desired product was obtained as the first eluted species as white solid.

^{1}H-NMR (400 MHz, d_6-DMSO to be compared to **6-Mes-TetraH**) δ (ppm): 8.14 (d, *J*= 3.8 Hz, 1H), 8.03 (dd, *J*= 7.8 Hz, *J*= 0.8 Hz, 1H), 7.67 (dd, *J*= 7.8 Hz, *J*= 0.8 Hz, 1H), 6.97 (s, 2H), 2.31 (s, 3H), 1.94 (s, 6H).

General procedure for the synthesis of 5-(4'-R-pyrid-2'-yl)-1*H*-tetrazoles

In a round-bottom flask the proper 4-R-2-cyanopyridine (or 1-isoquinolinecarbonitrile) was dissolved/suspended in water (eventually mixed with a small aliquotas of a low-boiling organic solvent) and reacted with NaN_3 (1.1 eq) and $ZnBr_2$ (1 eq); the resulting mixture was refluxed for 24 hours. After it was cooled down to the room temperature, finely chopped NaOH (2.5 eq) was added and stirred for some minutes allowing precipitation of $Zn(OH)_2$ and solubilization of tetrazole in its deprotonated form. The solid was filtred off and the alkaline solution was acidified adding few drops of HCl 37% (or its diluted solution) until a precipitate was formed (around pH 3-5); it was collected by filtration, washed with water and small drops of EtO_2, and finally dried under vacuum with mild heating (40-50°C).

Characterization of the molecules 5-(pyrid-2'-yl)-1*H*-tetrazole (**TetraH**), 5-(4'-chloro-pyrid-2'-yl)-1*H*-tetrazole (**Cl-TetraH**) and 5-(4'-phenyl-pyrid-2'-yl)-1*H*-tetrazole (**Ph-TetraH**) was already published [96], [97] and so will not be reported here again.

5-(4'-iodo-pyrid-2'-yl)-1*H*-tetrazole, **I-TetraH**

^{1}H-NMR (400 MHz, $CDCl_3$) δ (ppm): 8.79 (d, *J*= 1.4 Hz, 1H), 8.39 (d, *J*= 5.2 Hz, 1H), 7.91 (dd, *J*= 5.2 Hz, *J*= 1.4 Hz, 1H). MS (FAB^+) *m/z*: 274.

5-(4'-(4''-(N,N-dimethylamino)phen-1''-yl)pyrid-2'-yl)-1*H*-tetrazole, (***p*-Me$_2$N)Ph-TetraH**

^{1}H-NMR (400 MHz, $CDCl_3$) δ(ppm): 8.96 (s, 1H), 8.49 (d, *J*= 6.6 Hz, 1H), 7.95 (dd, *J*= 6.5 Hz, 1H), 7.88 (d, *J*= 8.8 Hz, 2H), 6.90 (d, *J*= 8.8 Hz, 2H), 3.20 (s, 6H). MS (FAB^+) *m/z*: 267.

5-(4'-(thien-2''-yl)pyrid-2'-yl)-1*H*-tetrazole, **Th-TetraH**

^{1}H-NMR (400 MHz, d_6-DMSO at T=353K) δ (ppm): 8.52 (br, 1H), 8.34 (br, 1H), 7.91 (d, *J*= 3.2 Hz, 1H), 7.80 (d, *J*= 4.9 Hz, 2H), 7.27 (t, *J*= 4.9 Hz, 1H). MS (FAB^+) *m/z*: 230.

5-(6'-(2'',4'',6''-trimethylphen-1''-yl)pyrid-2'-yl)-1*H*-tetrazole, **6-Mes-TetraH**

^{1}H-NMR (400 MHz, d_6-DMSO; partially broad signals) δ (ppm): 8.07 (m, 2H), 7.26 (d, 1H), 6.78 (s, 2H), 2.26 (s, 3H), 1.78 (br, 6H). Better resolution at T=353K, δ (ppm): 8.07 (d, *J*= 4.1 Hz, 2H), 7.27 ppm (t, *J*= 4.0 Hz, 1H), 6.83 (s, 2H), 2.29 (s, 3H), 1.81 (s, 6H).

5-(isoquinol-1'-yl)-1*H*-tetrazole, **TetraH-Isoquin**

^{1}H NMR (400 MHz, d_6-DMSO) δ (ppm): 9.38 (d, *J*= 8.1, 1H), 8.7 (d, *J*= 5.5 Hz, 1H), 8.17-8.14 (m, 2H), 7.93-7.87 (m, 2H).

Synthesis of Ru(II) complexes

The detailed two-step procedure employed to synthesize **D3-D6** dyes have been previously published in our papers together with ^{1}H-NMR spectra of the complexes [96], [97]. So here I report only the characterization of the unpublished **D6** complex.

MS (FAB^+) *m/z*: 862 (Figure 72). ^{1}H-NMR data are not reported due to the low solubility of the complex.

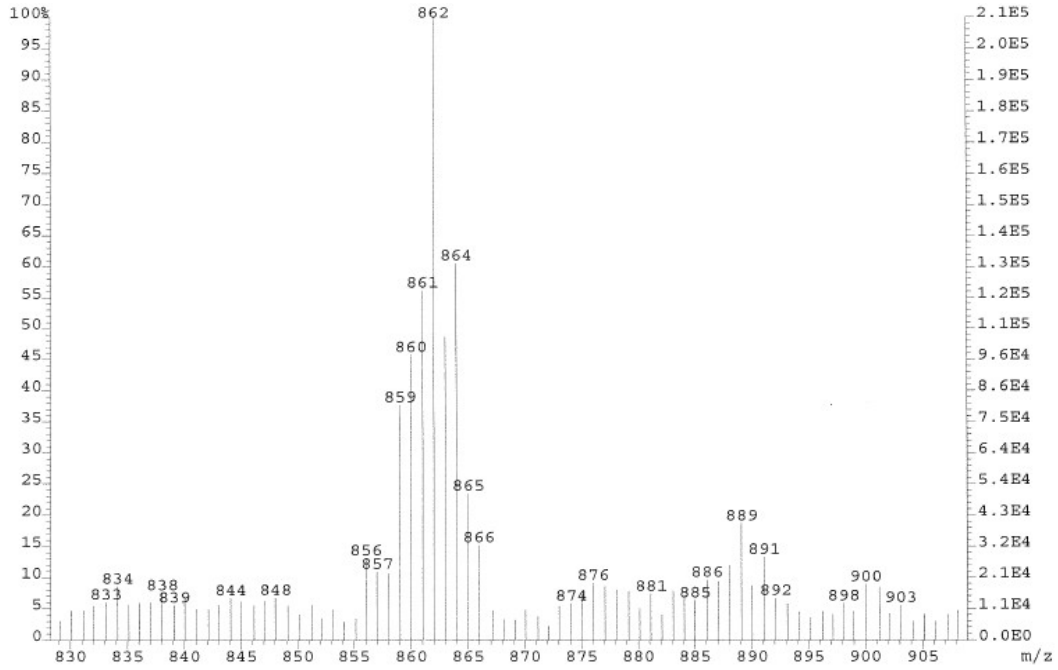

Figure 72 Magnification of the FAB^+ mass spectrum of complex D6 corresponding to its isotopic cluster.

$Cu^{(I)/(II)}$-based redox mediators

Synthesis and characterization

General procedure for the synthesis of phenanthroline ligands, **pathway A** (Table 10)

When the lithium derivate was not available, like for 2-methylphenyl lithium or the analogue 2,4,6-trimethylphenyl lithium, it was prepared under Ar according to the following procedure.

The desired bromo-arene (20 mmol, 1 eq) was dissolved in degassed dry EtO_2 (65 ml) and cooled at –78°C under an Ar atmosphere. *Tert*-butyl lithium (1.7 M in pentane) was carefully dropped (2.2

eq). When addition was completed the stirred solution was maintained at –78°C for 30 minutes and then it was let warmed up to r.t. over 30 minutes. In the case of mesityl lithium the solid product was filtred under Ar, washed with some Et_2O and then directly added, under Ag, into the flask containing the solution of phenanthroline. For 2-methylphenyl lithium the product was liquid, so a it was concentrated (to *ca.* 15-20 ml) before the addition to the phenanthroline solution.

Nucleophilic aromatic substitution of the phenanthroline (or of the 4,7-dimethyl analogue) was performed dissolving the heteroaromatic substrate (9.5 mmol, 1 eq) in dry toluene (220 ml). At 0°C the desired lithium derivate (up to 2.5 eq for disubstitutions) was slowly added to a well stirred solution; at the end of the addition a dark violet solution was obtained. After some minutes the mixture was let warmed up to r.t. and stirred overnight.
Reaction was quenched adding water; then the two layers were separated, and the aqueous one was exctracted with DCM (two times, 220 ml). The combined organic phases were dried with Na_2SO_4, and filtred into a round-bottom flask containing activated MnO_2 (32 eq, previously warmed under vaccum at 160°C for at least 4 hours, and then let to warm at r.t. under vacuum). After *ca.* 18 hours the mixture was filtered on celite, washing with toluene and DCM; finally the filtrate was concentrated under reduced pressure and the crude was purified by chromatography using neutral Al_2O_3 and as eluent, generally speaking, a mixture of toluene:DCM of progressive increased polarity, up to pure DCM). The simmetrical product was eluted first than the monosubstituted phenanthroline.

2-*n*-butyl-1,10-phenanthroline, ***n*-Bu-phe**

^{1}H-NMR (400 MHz, $CDCl_3$) δ (ppm): 9.26 (dd, *J*= 4.3, 1.4 Hz, 1H), 8.27 (dd, *J*= 8.0, 1.4 Hz, 1H), 8.19 (d, *J*= 8.2 Hz, 1H), 7.80 (d, *J*= 8.8 Hz, 1H), 7.76 (d, *J*= 8.8 Hz, 1H), 7.64 (dd, *J*= 8.0, 4.3 Hz, 1H), 7.57 (d, *J*= 8.2 Hz, 1H), 3.34-3.18 (m, 2H), 1.94-1.86 (m, 2H), 1.59-1.44 (m, 2H), 1.00 (t, *J*= 7.4 Hz, 3H).

2-*t*-butyl-1,10-phenanthroline, ***t*-Bu-phe**

^{1}H-NMR (400 MHz, $CDCl_3$) δ (ppm): 9.22 (dd, *J*=4.3, 1.6 Hz, 1H), 8.17 (dd, *J*=8.0, 1.6 Hz, 1H), 8.13 (d, *J*=8.5 Hz, 1H), 7.73 (d, *J*=8.3 Hz, 1H), 7.69 (d, *J*=8.3 Hz, 1H), 7.67 (d, *J*=8.5 Hz, 1H), 7.55 (dd, *J*=8.0, 4.3 Hz, 1H), 1.61 (s, 9H).

2-phenyl-1,10-phenanthroline, **Ph-phe**

^{1}H-NMR (400 MHz, $CDCl_3$) δ (ppm): 9.28 (dd, *J*= 4.3, 1.4 Hz, 1H), 8.37 (d, *J*= 7.5 Hz, 2H), 8.34 (d, *J*= 8.4 Hz, 1H), 8.29 (dd, *J*= 8.0, 1.4 Hz, 1H), 8.14 (d, *J*= 8.4 Hz, 1H), 7.86 (d, *J*= 8.8 Hz, 1H),

7.81 (d, *J*= 8.8 Hz, 1H), 7.67 (dd, *J*= 8.0, 4.3 Hz, 1H), 7.58 (t, *J*= 7.5 Hz, 2H), 7.50 (t, *J*= 7.5 Hz, 1H).

2-(*o*-tolyl)-1,10-phenanthroline, **Tol-phe**

^{1}H-NMR (400 MHz, CD_2Cl_2) δ (ppm): 9.18 (dd, *J*= 8.2 Hz, *J*= 4.6 Hz, 1H), 8.36 (d, *J*= 8.2 Hz, 1H), 8.33 (dd, *J*= 8.2 Hz, *J*= 4.6 Hz, 1H), 7.93(d, *J*=4.6 Hz, 1H), 7.88 (d, *J*= 4.4 Hz, 1H), 7.81 (d, *J*= 8.1 Hz, 1H), 7.70-7.67 (m, 1H), 7.61 (d, *J*= 8.2 Hz, 1H), 7.42-7.31 (m, 3H), 2.50 (s, 3H).

2-mesityl-1,10-phenanthroline, **Mes-phe**

^{1}H-NMR (400 MHz, $CDCl_3$) δ (ppm): 9.35 (dd, *J*= 8.2 Hz, J= 4.6 Hz, 1H), 8.47 (d, *J*= 8.2 Hz, 1H), 8.36 (d, *J*= 8.2 Hz, 1H), 7.96 (d, *J*=8.0 Hz, 1H), 7.90 (d, *J*=8.0 Hz, 1H) 7.78-7.76 (m, 1H), 7.59 (d, *J*= 8.1 Hz, 1H), 6.87 (s, 2H), 2.36 (s, 3H), 1.96 (s, 6H).

2-phenyl-4,7-diformyl-1,10-phenanthroline, **Ph-4,7-Form$_2$-phe**

^{1}H-NMR (400 MHz, $CDCl_3$) δ (ppm): 10.69 (s, 1H), 10.64 (s, 1H), 9.55 (d, *J*= 4.3 Hz, 1H), 9.18 (d, *J*= 9.6 Hz, 1H), 9.14 (d, *J*= 9.6 Hz, 1H), 8.52 (s, 1H), 8.39 (d, *J*= 7.4 Hz, 2H), 8.07 (d, *J*= 4.3 Hz, 1H), 7.60 (t, *J*= 7.4 Hz, 2H), 7.54 (t, *J*= 7.4 Hz, 1H).

2-mesityl-4,7-dimethyl-1,10-phenanthroline, **Mes-4,7-Me$_2$-phe**

^{1}H-NMR (400 MHz, $CDCl_3$) δ (ppm): 9.08 (d, *J*= 4.5 Hz, 1H), 8.11 (d, *J*= 9.3 Hz, 1H), 8.06 (d, *J*= 9.3 Hz, 1H), 7.44 (d, *J* = 4.5 Hz, 1H), 7.41 (s, 1H), 6.93 (s, 2H), 2.84 (s, 3H), 2.83(s, 3H), 2.34 (s, 3H), 2.09 (s, 6H).

2-mesityl-4,7-di(*p*-tolyl)-1,10-phenanthroline, **Mes-4,7-Tol$_2$-phe**

^{1}H-NMR (400 MHz, CD_3CN) δ (ppm): 9.12 (d, *J*= 4.5 Hz, 1H), 8.36 (d, J= 7.5 Hz, 2H), 8.06 (d, J = 9.3 Hz, 1H), 8.02 (d, J = 9.3 Hz, 1H), 7.96 (s, 1H), 7.56 (t, J = 7.5 Hz, 2H), 7.48 (d, J = 4.5 Hz, 1H), 7.47 (t, J = 7.5 Hz, 1H), 2.87 (s, 3H), 2.82 (s, 3H).

2,9-di(*o*-tolyl)-1,10-phenanthroline, **Tol$_2$-phe**

^{1}H-NMR (400 MHz, CD_2Cl_2) δ (ppm): 8.39 (d, *J*= 8.1 Hz, 2H), 7.92 (s, 2H), 7.83 (d, *J*= 8.1 Hz, 2H), 7.62 (d, J= 8.1 Hz, 2H), 7.38-7.34 (m, 4H), 7.30-7.26 (m, 2H), 7.22-7.16 (m, 2H), 2.56 (s, 6H).

2,9-dimesityl-1,10-phenanthroline, **Mes$_2$-phe**

^{1}H-NMR (400 MHz, CD_2Cl_2) δ (ppm): 8.36 (d, *J*= 10.8 Hz, 2H), 7.91 (s, 2H), 7.59 (d, *J*= 10.8 Hz, 2H), 6.99 (s, 4H), 2.37 (s, 6H), 2.09 (s, 12H).

Procedure for the synthesis of 2-methyl-1,10-phenanthroline, **pathway B** (Table 10)

Me-phe synthesis was performed following a reported procedure [105]. It started with the addition of acrolein (2.31 mmol, 1.66 eq) to a stirred solution of the commercially available 8-aminoquinoline (1 eq) and NaI (0.01 eq) in H_2SO_4 70% (4 eq) at *ca.*110°C. After 1 hour the dark

solution was cooled to r.t., poured into 1 M Na_2CO_3 and extracted with DCM (for 3 times). The combined organic phases were extracted with HCl 37% (five times), the acid solution was then neutralized (3 M NaOH and 1 M Na_2CO_3) and, finally, extracted with DCM (three times). The crude brown dense liquid obtained by solvent evaporation at reduced pressure was then purified via recrystalization in DCM/pentane.

^{1}H NMR (400 MHz, CD_3CN) δ (ppm): 8.92 (s, 1H), 8.69 (d, *J* = 8.2 Hz, 1H), 8.61 (d, *J* = 8.3 Hz, 1H), 8.17 (d, *J* = 9.0 Hz, 1H), 8.13 (d, *J* = 9.1 Hz, 1H), 7.91 (m, 1H), 7.88 (d, *J* = 8.3 Hz, 1H), 2.15 (s, 3H).

Procedure for the synthesis of 2,9-diiodo-1,10-phenanthroline, **pathway C** (Table 10)

The preparation of the diiodo derivate was obtained following exactly the already reported pathway [106].

^{1}H-NMR (400 MHz, $CDCl_3$) δ (ppm): 8.32 (d, *J*= 8.4 Hz, 4H), 8.38 (d, *J*= 8.4 Hz, 4H), 8.01 (s, 4H).

Synthesis of Cu(I) complexes

The desired phenanthroline (0.459 mmol, 2 eq) was dissolved, under N_2, in dry DCM (2.3 ml) and that dropped into a stirred DCM solution (4.7 ml) of Cu(I) precursor $[Cu(ACN)_4]^+$ (1 eq). The solution, which instantaneously the solution turned red, was stirred for about 30-60 min. After evaporation of the solvent, the desired complex was precipitated from DCM/diethyl ether (or diisopropyl ether) to give the colour complex that was, finally, dried under vacuum. In some cases crystals suitable for X-ray diffraction analysis were obtained.

[Cu(1,10-phenanthroline)$_2$][PF_6], **1**

^{1}H-NMR (400 MHz, CD_3CN) δ (ppm): 8.95 (br, 2H), 8.72 (br, 2H), 8.21 (br, 2H), 7.96 (br, 2H). MS (FAB^+) *m/z*: 423.

[Cu(2-methyl-1,10-phenanthroline)$_2$][PF_6], **2**

^{1}H NMR (400 MHz, CD_3CN) δ (ppm): 8.92 (s, 1H), 8.69 (d, *J* = 8.2 Hz, 1H), 8.61 (d, *J* = 8.3 Hz, 1H), 8.17 (d, *J* = 9.0 Hz, 1H), 8.13 (d, *J* = 9.1 Hz, 1H), 7.91 (m, 1H), 7.88 (d, *J* = 8.3 Hz, 1H), 2.15 (s, 3H).

[Cu(2-*n*-butyl-1,10-phenanthroline)$_2$][PF_6], **3**

^{1}H-NMR (400 MHz, MeOD) δ (ppm): 9.06 (d, *J* =4.1 Hz, 2H), 8.79 (d, *J* =7.8 Hz, 2H), 8.69 (d, *J* =8.3 Hz, 2H), 8.23 (d, *J* =9.0 Hz, 2H), 8.20 (d, *J* =9.0 Hz, 2H), 8.00 (dd, *J* =7.8, 4.1 Hz, 2H), 7.93 (d, *J* =8.3 Hz, 2H). 2.78-2.64 (m, 4H), 1.48 -1.22 (m, 4H), 0.69-0.48 (m, 4H), 0.22 (t, *J* = 7.4 Hz, 6H).

[Cu(2-*t*-butyl-1,10-phenanthroline)$_2$][PF_6], **4**

^{1}H-NMR (400 MHz, CD_2Cl_2) δ (ppm): 8.84 (dd, *J*=4.6 Hz, *J*= 1.2 Hz, 2H), 8.63 (dd, *J*=8.1 Hz, *J*= 1.0 Hz, 2H), 8.58 (d, *J*=8.7 Hz, 2H), 8.13-8.08 (m, 6H), 7.87 (m, 2H), 1.32 (s, 18H).

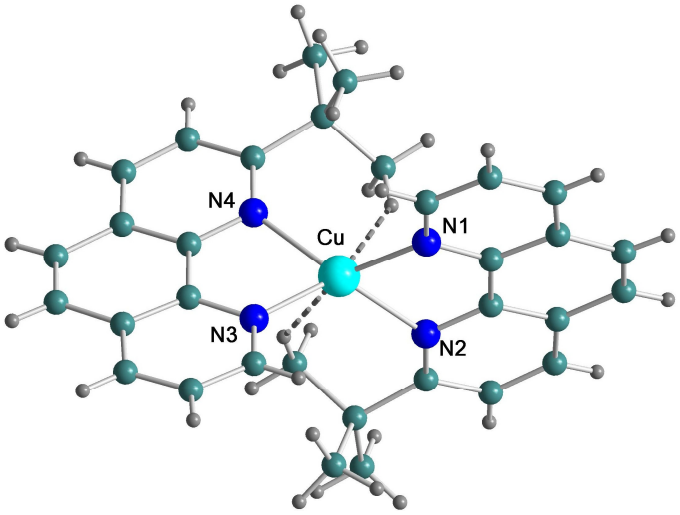

Figure 73 Perspective view of the [Cu(2-*t*-butyl-1,10-phenanthroline)$_2$]$^+$ cation; from X-ray diffraction. Dashed lines identify weak Cu--H interactions at distances shorter than the sum of van der Waals radii of the two atoms. I have started a series of DFT calculation to try to better identify such rare interaction; to date we can tentativelly attribute it to an anagostic interaction.

[Cu(2-phenyl-1,10-phenanthroline)$_2$][PF_6], **5**

^{1}H-NMR (400 MHz, MeOD) δ (ppm): 9.19 (d, *J* =4.3 Hz, 2H), 8.78 (d, J =8.0 Hz, 2H), 8.57 (d, J =8.3 Hz, 2H), 8.17 (d, J =8.9 Hz, 2H), 8.11(d, J =8.9 Hz, 2H), 8.05 (dd, J =8.0, 4.3 Hz, 2H), 7.92 (d, J =8.3 Hz, 2H), 7.27 (d, J =7.4 Hz, 4H), 6.64 (t, J =7.4 Hz, 2H), 6.38 (t, J =7.4 Hz, 4H).

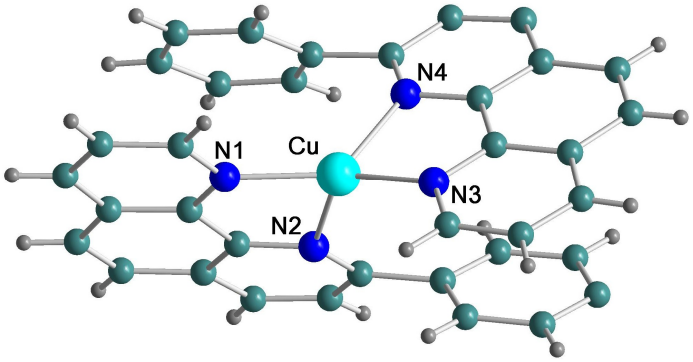

Figure 74 Perspective view of the [Cu(2-phenyl-1,10-phenanthroline)$_2$]$^+$ cation; from X-ray diffraction.

[Cu(2-*o*-tolyl-1,10-phenanthroline)$_2$][PF_6], **6**

^{1}H-NMR (400 MHz, CD_2Cl_2) δ (ppm): 8.94 (d, *J* =4.4 Hz, 2H), 8.54 (m, 4H), 8.05 (d, *J* =8.9 Hz, 2H), 8.02 (d, *J* =9 Hz, 2H), 7.89 (dd, *J* =4.7 Hz, 2H), 7.74 (d, *J* =8.2 Hz, 2H), 6.56 (d, *J* =6.8 Hz, 2H), 6.42 (d, *J* =7.5Hz, 2H), 6.35 (d, *J* =7.4 Hz, 2H), 6.06 (d, *J* =7.4 Hz, 2H), 1.85(s, 6H).

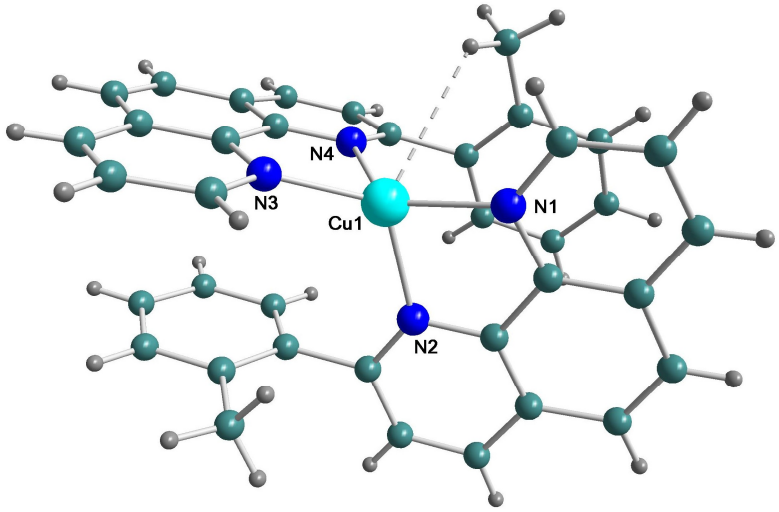

Figure 75 Perspective view of the [Cu(2-*o*-tolyl-1,10-phenanthroline)$_2$]$^+$ cation; from X-ray diffraction. Cu--H interaction is reported in dashed line. See caption of Figure 73 for more details.

[Cu(2-mesityl-1,10-phenanthroline)$_2$][PF$_6$], **7**

^{1}H NMR (400 MHz, CD_3CN) δ (ppm): 9.04 (dd, *J* = 4.8 Hz, *J* = 1.5 Hz, 2H), 8.60 (m, 4H), 8.11 (d, *J* = 8.9 Hz, 2H), 8.06 (d, *J* = 8.9 Hz, 2H), 7.88 (dd, *J* = 8.2 Hz, *J* = 4.7 Hz, 2H), 7.59 (d, *J* = 8.2 Hz, 2H), 6.12 (s, 2H), 5.79 (s, 2H), 1.95 (s, 6H; partially covered by solvent signals), 1.69 (s, 6H), 1.00 (s, 6H).

[Cu(4,7-dimethyl-1,10-phenanthroline)$_2$][PF$_6$], **8**

^{1}H NMR (400 MHz, CD_3CN) δ (ppm): 8.79 (br, 2H), 8.37 (br, 2H), 7.77 (br, 2H). 2.91 (br, 6H). MS (FAB$^+$) *m/z*: 479.

[Cu(2-mesityl-4,7-dimethyl-1,10-phenanthroline)$_2$][PF$_6$], **9**

^{1}H NMR (400 MHz, CD_2Cl_2) δ (ppm): 8.78 (d, *J*= 4.6 Hz, 2H), 8.25 (d, *J*= 7.2 Hz, 2H), 8.18 (d, *J*= 7.2 Hz, 2H) 7.61 (d, *J*= 4.6 Hz, 2H), 7.36 (s, 2H), 6.21 (s, 2H), 5.82 (s, 2H), 2.93 (s, 6H), 2.88 (s, 6H), 1.97 (s, 6H), 1.71 (s, 6H), 1.06 (s, 6H). MS (FAB$^+$) *m/z*: 715.

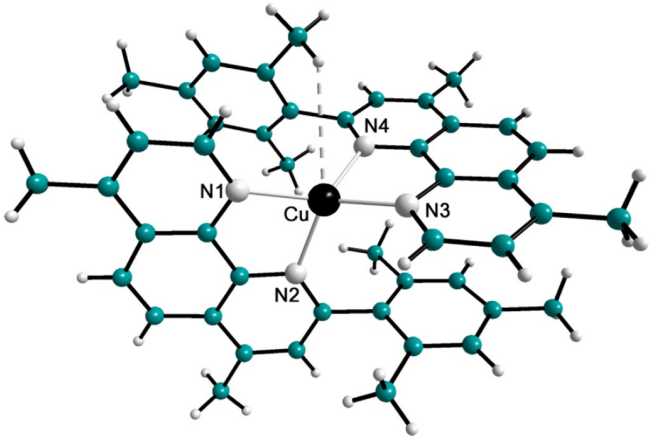

Figure 76 Perspective view of the [Cu(2-mesityl-4,7-dimethyl-1,10-phenanthroline)$_2$]$^+$ cation; from X-ray diffraction. Ref. [76]

[Cu(2-phenyl-4,7-formyl-1,10-phenanthroline)$_2$][PF$_6$], **10**

^{1}H-NMR (400 MHz, CD_3CN) δ (ppm): 10.78 (s, 2H), 10.63 (s, 2H), 9.46 (s, 2H), 9.28 (s, 2H), 9.23 (s, 2H), 8.52 (s, 2H), 8.39 (s, 2H), 7.30 (d, *J*= 7.1 Hz, 4H), 6.67 (t, *J*= 7.1 Hz, 2H), 6.46 (t, *J*= 7.1 Hz, 4H).

[Cu(2-mesityl-4,7-di(*p*-tolyl)-1,10-phenanthroline)$_2$][PF$_6$], **11**

^{1}H-NMR (400 MHz, MeOD) δ (ppm): 9.18(d, *J*= 5.0 Hz, 2H), 8.18 (d, *J*= 9.6 Hz, 2H), 8.13 (d, *J*= 9.6 Hz, 2H) 7.95 (d, *J*= 5.0 Hz, 2H), 7.83 (d, *J*= 6.9 Hz, 4H), 7.73 (d, *J*= 6.1 Hz, 4H), 7.70 (d, *J*= 6.9 Hz, 4H), 7.66 (s, 1H), 7.66 (d, *J*= 6.1 Hz, 4H), 1.92 (s, 6H), 1.82 (s, 6H), 1.30 (s, 6H), 1.15 (s, 6H), 1.13 (s, 6H).

[Cu(2,9-dimethyl-1,10-phenanthroline)$_2$][PF$_6$], **12**

^{1}H-NMR (400 MHz, CD_2Cl_2) δ (ppm): 8.52 (d, *J*= 8.3 Hz, 4H), 8.07 (s, 4H), 7.79 (d, *J*= 8.2 Hz, 4H), 2.47 (s, 12H).

[Cu(2,9-di-*o*-tolyl-1,10-phenanthroline)$_2$][PF$_6$], **13**

^{1}H-NMR (400 MHz, CD_2Cl_2) δ (ppm): 8.54 (d, *J* =8.0 Hz, 4H), 8.12 (s, 4H), 7.77 (d, *J* =8.1 Hz, 4H), 6.96 (d, *J* =7.3 Hz, 4H), 6.83 (d, *J* =7.8 Hz, 4H), 6.76 (t, *J* =7.2 Hz, 4H), 6.06 (t, *J* =7.3 Hz, 4H), 1.85 (s, 12H).

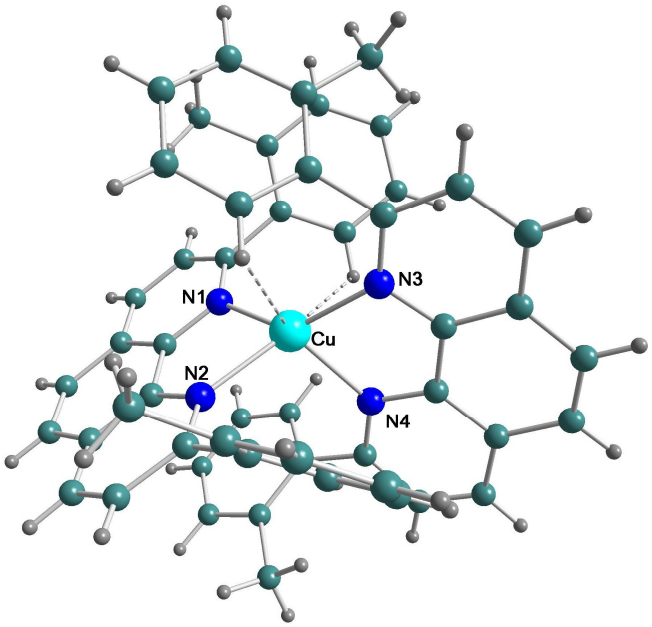

Figure 77 Perspective view of the [Cu(2,9-di-*o*-tolyl-1,10-phenanthroline)$_2$]$^+$ cation; from X-ray diffraction. Cu--H interactions are reported in dashed line. In this molecule aromatic hydrogens (instead of aliphatic ones in 4 and 6) are involved in the possible anagostic interaction. See caption of Figure 73 for more details.

[Cu(2,9-dichloro-1,10-phenanthroline)$_2$][PF$_6$], **14**

^{1}H-NMR (400 MHz, MeOD) δ (ppm): 8.85(d, *J*=8.6 Hz, 4H), 8.31(s, 4H), 8.11 (d, *J*=8.6 Hz, 4H).

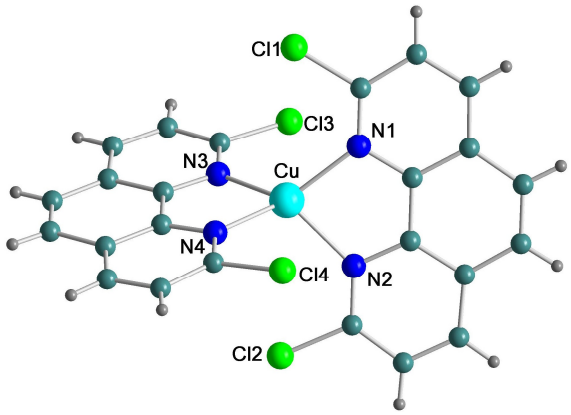

Figure 78 Perspective view of the [Cu(2,9-dichloro-1,10-phenanthroline)$_2$]$^+$ cation; from X-ray diffraction.

[Cu(2,9-diiodo-1,10-phenanthroline)$_2$][PF_6], **15**

^{1}H-NMR (400 MHz, $CDCl_3$) δ (ppm): 8.46 (d, *J*=8.4 Hz, 4H), 8.43 (d, *J*=8.4 Hz, 4H), 8.22 (s, 4H).

[Cu(2,9-dimethyl-4,7-diphenyl-1,10-phenanthroline)$_2$][PF_6], **16**

^{1}H-NMR (400 MHz, MeOD) δ (ppm): 8.12 (s, 4H), 7.91 (s, 4H), 7.71 (m, 8H), 7.64 (m, 12H).

Synthesis of Cu(II) complexes, **pathway C** (Scheme 7)

$CuSO_4 \cdot 5H_2O$ (0.092 mmol, 1 eq) was dissolved in small volume of water (3 ml) and then added dropwise to a stirred solution of the ligand (2 eq) dissolved in ACN (8 ml). After 1 hour ACN was removed under vacuum and 8-10 ml of water was added in order to obtain a transparent green/light blue solution. An aqueous solution of $NaPF_6$ (2.3 eq, in 1 ml H_2O) was added; the fine precipitate, that was istantaneously formed, was filtrated after 2 hours, washed with water and EtO_2, and dried under vaccum.

Complexes were characterized by UV-VIS-NIR spectroscopy and via cyclic voltammetry. In the last case their cathodic and anodic patterns were compared with that of the corresponding Cu(I) complex; for complex **21** mass spectra was also recorded (ESI$^+$ FTICR MS, *m/z*=357.643).

Synthesis of Cu(II) complexes, **pathway D** (Scheme 7)

$CuCl_2 \cdot 2H_2O$ (0.234 mmol, 1 eq) was dissolved in the minimum amount of ethanol and then added dropwise to a stirred solution of the ligand (2 eq) dissolved, in turns, into the minimum amount of ethanol, istantaneously producing a fine green precipitate. After 30 minutes the solid was filtrated and redissolved in *ca.* 40 ml of EtOH/H_2O mixture (1:2 v/v). Similarly to **pathway C**, an aqueous solution of $NaPF_6$ (2.3 eq, in 3 ml H_2O) was added; the fine precipitate, that was istantaneously formed, was filtrated after 2 hours, washed with water and Et_2O, and dried under vaccum.

Complexes were characterized by UV-VIS-NIR spectroscopy and via cyclic voltammetry; for complex **22** mass spectrum was also recorded (ESI$^+$ FTICR MS, *m/z*=514.096).

References

[1] R. A. Kerr, How urgent is climate change?, *Science* 318 (2007) 1230-1231.

[2] International Energy Agency, *Technology Roadmap: Solar Photovoltaic Energy*, ed. 2014.

[3] A. Kojima, K. Teshima, Y. Shirai, T. Miyasaka, Organometal halide perovskites as visible-light sensitizers for photovoltaic cells, *J. Am. Chem. Soc.* 131 (2009) 6050-6051

[4] G. E. Eperon, S. D. Stranks, C. Menelaou, M. B. Johnston, L. M. Herz, H. J. Snaith, Formamidinium lead trihalide: a broadly tunable perovskite for efficient planar heterojunction solar cells, *Energy Environ. Sci.* 7 (2014) 982.

[5] J. H. Noh, S. H. Im, J. H. Heo, T. N. Mandal, S. I. Seok, Chemical management for colorful, efficient, and stable inorganic–organic hybrid nanostructured solar cells, *Nano Lett.* 13 (2013) 1764.

[6] S. D. Stranks, G. E. Eperon, G. Grancini, C. Menelaou, M. J. P. Alcocer, T. Leijtens, L. M. Herz, A. Petrozza, H. J. Snaith, Electron-hole diffusion lengths exceeding 1 micrometer in an organometal trihalide perovskite absorber, *Science* 342 (2013) 341.

[7] J.-H. Im, C.-R. Lee, J.-W.Lee, S.-W. Park, N.-G. Park, 6.5% efficient perovskite quantum-dot-sensitized solar cell, *Nanoscale* 3 (2011) 4088.

[8] H.-S. Kim, C.-R. Lee, J.-H. Im, L.-B. Lee, T. Moehl, A. Marchioro, S.-J. Moon, R. Humphry-Baker, J.-H, Yum, J. E. Moser, M. Gratzel, N.-G. Park, Lead iodide perovskite sensitized all-solid-state submicron thin film mesoscopic solar cell with efficiency exceeding 9%, *Sci. Rep.* 2 (2012) 591.

[9] J. Burschka, N. Pellet, S.-J. Moon, R. Humphry-Baker, P. Gao, M. K. Nazeeruddin, M. Graetzel, Sequential deposition as a route to high-performance perovskite-sensitized solar cells, *Nature* 499 (2013) 316.

[10] M. M. Lee, J. Teuscher, T. Miyasaka, T. N. Murakami, H. J. Snaith, Efficient hybrid solar cells based on meso-superstructured organometal halide perovskites, *Science* 338 (2012) 643.

[11] J. M. Ball, M. M. Lee, A. Hey, H. J. Snaith, Low-temperature processed meso-superstructured to thin-film perovskite solar cells, *Energy Environ. Sci.* 6 (2013) 1739.

[12] G. E. Eperon, V. M. Burlakov, P. Docampo, A. Goriely, H. J. Snaith, Morphological control for high performance, solution-processed planar heterojunction perovskite solar cells, *Adv. Funct. Mater.* 24 (2014) 151.

[13] G. Niu, X. Guo, L. Wang, Review of recent progress in chemical stability of perovskite solar cells, *J. Mater. Chem. A* 3 (2015) 8970-8980.

[14] B. O'Regan, M. Graetzel, A low-cost, high-efficiency solar cell based on dye-sensitized colloidal TiO2 films, *Nature* 353 (1991) 737-740.

[15] J. Moser, Notiz über Verstärkung photoelektrischer Ströme durch optische Sensibilisirung, *Monatsh. Chemie* 8 (1887) 373.

[16] H. Gerischer, H. Tributsch, Electrochemical studies on the spectral sensitization of zinc oxide single crystals, *Phys. Chem.* 72 (1968) 437-445.

[17] D. Duonghong, N. Serpone, M. Graetzel, Integrated systems for water cleavage by visible light; sensitization of titanium dioxide particles by surface derivatization with ruthenium complexes, *Helv. Chim. Acta* 67 (1984) 1012-18.

[18] J. Desilvestro, M. Graetzel, L. Kavan, J. Moser, J. Augustynski, Highly efficient sensitization of titanium dioxide, *J. Am. Chem. Soc.* 107 (1985) 2988-2990.

[19] M. K. Nazeeruddin, E. Baranoff, M. Graetzel, Dye-sensitized solar cells: A brief overview, *Solar Energy* 85 (2011) 1172-1178.

[20] M. Graetzel, Advances in sensitized mesoscopic solar cells, *Accounts Chem. Res.* 42 (2009) 1788-1798.

[21] Y. Chiba, A. Islam, Y. Watanabe, R. Komiya, N. Koide, L. Han, Dye-sensitized solar cells with conversion efficiency of 11.1%, Jpn. *J. Appl. Phys.* 45 (2006) L638.

[22] A. Yella, H.-W. Lee, H. N. Tsao, C. Yi, A. K. Chandiran, M.K. Nazeeruddin, E. W.-G. Diau, C.-Y. Yeh, S. M Zakeeruddin, M. Graetzel, Porphyrin-sensitized solar cells with cobalt (II/III)–Based Redox Electrolyte Exceed 12 Percent Efficiency, *Science* 334 (2011) 629-634.

[23] S. Mathew, A. Yella, P. Gao, R. Humphry-Baker, B. Curchod, N. Ashari-Astani, I. Tavernelli, U. Rothlisberger, M. K. Nazeeruddin, M Graetzel, *Nat. Chem.* 6 (2014) 242-247.

[24] J. Wu, Z. Lan, J. Lin, M. Huang, Y. Huang, L. Fan, G. Luo, Electrolytes in Dye-Sensitized Solar Cells, *Chem. Rev.* 115 (2015) 2136−2173.

[25] C.-L. Chen, H. Teng, Y.-L. Lee, In situ gelation of electrolytes for highly efficient gel-state dye-sensitized solar cells, *Adv. Mater.* 23 (2011) 4199-4204.

[26] J. Burschka, A. Dualeh, F. Kessler, E. Baranoff, N. Cevey, C. Yi, M. Nazeeruddin, M. Graetzel, Tris(2-(1*H*-pyrazol-1-yl)pyridine)cobalt(III) as p-type dopant for organic semiconductors and its application in highly efficient solid-state dye-sensitized solar cells, *J. Am. Chem. Soc.* 133 (2011) 18042-18045.

[27] Z. Yu, F. Li, L. Sun, Recent advances in dye-sensitized photoelectrochemical cells for solar hydrogen production based on molecular components, *Energy Environ. Sci.* 8 (2015) 760-775.

[28] K. S. Joya, Y. F. Joya, K. Ocakoglu, R. van de Kro, Water-splitting catalysis and solar fuel devices: artificial leaves on the move, *Angew. Chem. Int. Ed.* 52 (2013) 10426-10437.

[29] A. Listorti, B. O'Regan, J. R Durrant, Electron transfer dynamics in dye-sensitized solar cells, *Chem. Mater.* 23 (2011) 3381-3399.

[30] M. Graetzel, Recent advances in sensitized Mesoscopic Solar Cells, *Accounts Chem. Res.* 42 (2009)788-1798.

[31] K. Hara, T. Sato, R. Katoh, A. Furube, Y. Ohga, A. Shinpo, S. Suga, K. Sayama, H. Sugihara, H. Arakawa, Molecular Design of Coumarin Dyes for Efficient Dye-Sensitized Solar Cells, *J. Phys. Chem. B* 107 (2003) 597-606.

[32] Lei Zhang, J, M. Cole, Anchoring groups for dye-sensitized solar cells, *ACS Appl. Mater. Interfaces* 7 (2015) 3427-3455.

[33] G. C. Vougioukalakis, A. I. Philippopoulos, T. Stergiopoulos, P. Falaras, Contributions to the development of ruthenium-based sensitizers for dye-sensitized solar cells, *Coordin. Chem. Rev.* 255 (2011) 2602-2621.

[34] M. K. Nazeeruddin, A. Kay, I. Rodicio, R. Humphry-Baker, E. Muller, P. Liska, N. Vlachopoulos, M. Grätzel, *J. Am. Chem. Soc.* 115 (1993) 6382-6390.

[35] M. K. Nazeeruddin, P. Pechy, M. Grätzel, *Chem. Commun.* (1997) 1705-1706.

[36] M. K. Nazeeruddin, P. Pechy, T. Renouard, S.M. Zakeeruddin, R. Humphry- Baker, P. Comte, P. Liska, L. Cevey, E. Costa, V. Shklover, L. Spiccia, G.B. Deacon, C. A. Bignozzi, M. Graetzel, *J. Am. Chem. Soc.* 123 (2001) 1613-1624.

[37] M. Graetzel, DSC-IC 3, April 23^{th}-25^{th}, Nara, Japan, 2009.

[38] A. R. Andersen, J. Halme, T. Lund, M. I. Asghar, P. T. Nguyen, K. Miettunen, E. Kemppainen, Oo Albrektsen, Charge transport and photocurrent generation characteristics in dye-solar cells containing thermally degraded N719 dye molecules, *J. Phys. Chem. C* 115 (2011) 15598-15606.

[39] T. Bessho, E. Yoneda, J.H. Yum, M. Guglielmi, I. Tavernelli, H. Imai, U. Rothlisberger, M. K. Nazeeruddin, M. Grätzel, New paradigm in molecular engineering of sensitizers for solar cell applications, *J. Am. Chem. Soc.* 131 (2009) 5930-5934.

[40] T. Bessho, E. C. Constable, M. Graetzel, A. H. Redondo, C. E. Housecroft, W. Kylberg, K. Nazeeruddin, M. Neuburger, S. Schaffner, An element of surprise-efficient copper-functionalized dye-sensitized solar cells, *Chem. Commun.* (2008) 3717-371.

[41] E. C. Constable, A. H. Redondo, C. E. Housecroft, M. Neuburger, S. Schaffner, Copper(I) complexes of 6,6'-disubstituted 2,2'-bipyridine dicarboxylic acids: New complexes for incorporation into copper-based dye sensitized solar cells (DSCs), *Dalton Trans.* (2009) 6634-6644.

[42] Y.-J. Yuan, Z.-T. Yu, J.-Y. Zhang, Z.-G. Zou, A copper(i) dye-sensitised TiO2-based system for efficient light harvesting and photoconversion of CO_2 into hydrocarbon fuel, *Dalton Trans.* 41 (2012) 9594-9597.

[43] A. Colombo, C. Dragonetti, D. Roberto, A. Valore, P. Biagini, F. Melchiorre, A simple copper(I) complex and its application in efficient dye sensitized solar cells, *Inorg. Chim. Acta* 407 (2013) 204-209.

[44] N. Robertson, Cu^{I} versus Ru^{II}: Dye-sensitized solar cells and beyond, *Chem. Sus. Chem.* 1 (2008) 977-979.

[45] S. Ito, S. M. Zakeeruddin, R. Humphry-Baker, P. Liska, R. Charvet, P. Comte, M. K. Nazeeruddin, P. Pechy, M. Takata, H. Miura, S. Uchida, M. Graetzel, High efficiency of dye-sensitized solar cells based on metal-free indoline dyes, *J. Am. Chem. Soc.* 126 (2004) 12218-12219.

[46] S. Ito, H. Miura, S. Uchida, M. Takata, K. Sumioka, P. Liska, P. Comte, P. Pechy, M. Graetzel, High-conversion-efficiency organic dye-sensitized solar cells with a novel indoline dye, *Chem. Commun.* (2008) 5194-5196.

[47] G. Zhang, H. Bala, Y. Cheng, D. Shi, X. Lv, Q. Yu, P. Wang, High efficiency and stable dye-sensitized solar cells with an organic chromophore featuring a binary π-conjugated spacer, *Chem. Commun.* (2009) 2198-2200.

[48] N. Koumura, Z.-S. Wang, S. Mori, M. Miyashita E. Suzuki, K. Hara, Alkyl-functionalized organic dyes for efficient molecular photovoltaics, *J. Am. Chem. Soc.* 128 (2006) 14256-14257.

[49] G. Schlichthorl, S. Huang, J. Sprague, A. Frank, Band edge movement and recombination kinetics in dye-sensitized nanocrystalline TiO_2 solar cells: a study by intensity modulated photovoltage spectroscopy, *J. Phys. Chem. B* 101 (1997) 8141-8155.

[50] I. R. Perera, A. Gupta, W. Xiang, T. Daeneke, U. Bach, R. A. Evans, A. C. Ohlin, L. Spiccia, Introducing manganese complexes as redox mediators for dye-sensitized solar cells, *Phys. Chem. Chem. Phys.* 16 (2014) 12021-12028.

[51] T. W. Hamann, R. A. Jensen, A. B. F. Martinson, H. Van Ryswykac, J. T. Hupp, Advancing beyond current generation dye-sensitized solar cells, Energy Environ. Sci., 1 (2008) 66-78.

[52] J. N. Clifford, E. Palomares, M. K. Nazeeruddin, M. Gratzel, J. R. Durrant, *J. Phys. Chem. C* 111 (2007) 6561-6567.

[53] G. Boschloo, E. A. Gibson, A. Hagfeldt, Photomodulated voltammetry of iodide/triiodide redox electrolytes and its relevance to dye-sensitized solar cells, *J. Phys. Chem. Lett.* 2 (2011) 3016-3020.

[54] A. J. Bard, L. R. Faulkner, *Electrochemical methods: Fundamental and Applications*, 2nd ed., Wiley, New York, 2001.

[55] Z. S. Wang, K. Sayama, H. Sugihara, Efficient eosin Y dye-sensitized solar cell containing Br^-/Br_3^- electrolyte, *J. Phys. Chem. B* 109 (2005) 22449-22455.

[56] G. Oskam, B. V. Bergeron, G. J. Meyer, P. C. Searson, Pseudohalogens for dye-sensitized TiO_2 photoelectrochemical cells, *Phys. Chem. B* 105 (2001) 6867-6873.

[57] T. Daeneke, T.-H. Kwon, A.B. Holmes, N.W. Duffy, U. Bach, L. Spiccia, *Nat. Chem.* 3 (2011) 211-215.

[58] T.C. Li, A.M. Spokoyny, C. She, O.K. Farha, C.A. Mirkin, T.J. Marks, T.J. Hupp, *J. Am. Chem. Soc.* 132 (2010) 4580-4582.

[59] I. R. Perera, A. Gupta, W. Xiang, T. Daeneke, U. Bach, R. A. Evans, C. A.Ohlin, L. Spiccia, Introducing manganese complexes as redox mediators for dye-sensitized solar cells, *Phys. Chem. Chem. Phys.* 16 (2014) 12021-12028.

[60] S. M. Feldt, E. A. Gibson, E. Gabrielsson, L. Sun, G. Boschloo, A. Hagfeldt, Design of organic dyes and cobalt polypyridine redox mediators for high-efficiency dye-sensitized solar cells, *J. Am. Chem. Soc.*, 132 (2010) 16714-16724.

[61] D. F. Zhou, Q. J. Yu, N. Cai, Y. Bai, Y. H. Wang, P. Wang, Efficient organic dye-sensitized thin-film solar cells based on the tris(1,10-phenanthroline)cobalt(II/III) redox shuttle, *Energy Environ. Sci.*, 4 (2011) 2030-2034.

[62] H. N. Tsao, C. Yi, T. Moehl, J. H. Yum, S. M. Zakeeruddin, M. K. Nazeeruddin, M. Grätzel, Cyclopentadithiophene bridged donor–acceptor dyes achieve high power conversion efficiencies in dye-sensitized solar cells based on the tris-cobalt bipyridine redox couple, *ChemSusChem*, 4 (2011) 591-594.

[63] S. Hattori, Y. Wada, S. Yanagida, S. Fukuzumi, Blue copper model complexes with distorted tetragonal geometry acting as effective electron-transfer mediators in dye-sensitized solar cells, *J. Am. Chem. Soc.* 127 (2005) 9648-9654.

[64] M. Brugnati, S. Caramori, S. Cazzanti, L. Marchini, R. Argazzi, C. A. Bignozzi, Electron transfer mediators for photoelectrochemical cells based on Cu(I) metal complexes, *Int. J. Photoenergy* (2007) 80756/1-80756/10.

[65] Y. Bai, Q. Yu, N. Cai, Y. Wang, M. Zhang, P. Wang, High-efficiency organic dye-sensitized mesoscopic solar cells with a copper redox shuttle, *Chem. Comm.* 47 (2011) 4376-4378.

[66] M. Freitag, Q. Daniel, M. Pazoki, K. Sveinbjörnsson, J. Zhang, L. Sun, A. Hagfeldt, G. Boschloo, High-efficiency dye-sensitized solar cells with molecular copper phenanthroline as solid hole conductor, *Energ. Environ. Sci.*, 8 (2015) 2634-2637.

[67] B. M. Klahr, T. W. Hamann, Performance enhancement and limitations of cobalt bipyridyl redox shuttles in dye-sensitized solar cells, *J. Phys. Chem. C* 113 (2009) 14040-14045.

[68] S. Ito, Investigation of dyes for dye-sensitized solar cells: ruthenium-complex dyes, metal-free dyes, metal-complex porphyrin dyes and natural dyes, in *Solar Cells - Dye-Sensitized Devices*, Prof. Leonid A. Kosyachenko (Ed.), 2011, InTech.

[69] S. A. Sapp, C. M. Elliott, C. Contado, S. Caramori, C. A. Bignozzi, Substituted polypyridine complexes of cobalt(II/III) as efficient electron-transfer mediators in dye-sensitized solar cells, *J. Am. Chem. Soc.* 124 (2002) 11215–11222.

[70] J. Spivack, O. Siclovan, S. Gasaway, E. Williams, A. Yakimov, J. Gui, Improved efficiency of dye sensitized solar cells by treatment of the dyed titania electrode with alkyl(trialkoxy)silanes, *Sol. Energ. Mat. Sol. C.* 90 (2006) 1296-1307.

[71] P. G. Bomben, K. D. Thériault, C. P. Berlinguette, Strategies for optimizing the performance of cyclometalated ruthenium sensitizers for dye-sensitized solar cells, *Eur. J. Inorg. Chem.* (2011) 1806-1814.

[72] C. Dragonetti, A. Valore, A. Colombo, D. Roberto, V. Trifiletti, N. Manfredi, M.M. Salamone, R. Ruffo, A. Abbotto, A new thiocyanate-free cyclometallated ruthenium complex for dye-sensitized solar cells: Beneficial effects of substitution on the cyclometallated ligand, *J. Organomet. Chem.* 714 (2012) 88-93.

[73] A. Abbotto, C. Coluccini, E. Dell'Orto, No. Manfredi, V. Trifiletti, M. M. Salamone, R. Ruffo, M. Acciarri, A. Colombo, C. Dragonetti, S. Ordanini, D. Roberto, A.Valore, Thiocyanate-free cyclometalated ruthenium sensitizers for solar cells based on heteroaromatic-substituted 2-arylpyridines, *Dalton Trans.* 41 (2012) 11731-11738.

[74] K.-L. Wu, H.-C. Hsu, K. Chen, Y. Chi, M.-W. Chung, W.-H. Liu, P.-T. Chou, Development of thiocyanate-free, charge-neutral Ru(II) sensitizers for dye-sensitized solar cells, *Chem. Commun.* 46 (2010) 5124-5126.

[75] K.-L. Wu , W.-P. Ku , S.-W. Wang, A. Yella , Y. Chi, S. H. Liu, P.-T. Chou, M. K. Nazeeruddin, M. Grätzel, Thiocyanate-free Ru(II) sensitizers with a 4,4'-dicarboxyvinyl-2,2'-bipyridine anchor for dye-sensitized solar cells, *Adv. Funct. Mat.* 23 (2013) 2285-2294.

[76] A. Colombo, C. Dragonetti, M. Magni, D. Roberto, F. Demartin, S. Caramori, C.A. Bignozzi, Efficient copper mediators based on bulky asymmetric phenanthrolines for DSSCs, *ACS Appl. Mater. Interfaces* 6 (2014) 13945-13955.

[77] D. B. Rorabacher, Electron transfer by copper centers, *Chem. Rev.* 104 (2004) 651-697.

[78] N. Armaroli, Photoactive mono- and polynuclear Cu(I)–phenanthrolines. A viable alternative to Ru(II)–polypyridines?, *Chem. Soc. Rev.* 30 (2001) 113-124.

[79] H.C. Zhao, J.P. Harney, Y.-T. Huang, J.-Ho Yum, Md K. Nazeeruddin, M. Graetzel, M.-K. Tsai, J. Rochford, Evaluation of a ruthenium oxyquinolate architecture for dye-sensitized solar cells, *Inorg. Chem.* 51 (2012) 1-3.

[80] C. Dragonetti, A. Valore, A. Colombo, M. Magni, P. Mussini, D. Roberto, R. Ugo, A. Valsecchi, V. Trifiletti, N. Manfredi, A. Abbotto, Ruthenium oxyquinolate complexes for dye-sensitized solar cells, *Inorg. Chim. Acta* 405 (2013) 98-104.

[81] X.-H. Wu, S. Wang, Y. Guo, Z.-Y. Xie, L. Han, Z.-H. Jiang, Enhanced energy conversion efficiency of La^{3+}-modified nanoporous TiO_2 electrode sensitized with a ruthenium complex, *Chin. J. Chem.* 26 (2008) 1939-194.

[82] G. Gritzner, J. Kuta, Recommendations on reporting electrode potentials in nonaqueous solvents, *Pure Appl. Chem.* 56 (1984) 461-466.

[83] Z. P. Yung, M. Alafandy, K. Boutakhrit, J.-M. Kauffmann, J. Arcos, Electrochemical oxidation of 8-hydroxyquinoline and selective determination of Tin(II) at solid electrodes, *Electroanalysis* 8 (1996) 25-29.

[84] M. C. Stevic, L. M. Ignjatovic, G. Ciric-Marjanovic, S. M. Stanisic, D. M. Stanković, J. Zima, Voltammetric behaviour and determination of 8-hydroxyquinoline using a glassy carbon paste electrode and the theoretical study of its electrochemical oxidation mechanism, *Int. J. Electrochem. Sci.* 6 (2011) 2509-2525.

[85] Y. Liu, A. Hagfeldt, X. Xiao, S. Lindquist, Investigation of influence of redox species on the interfacial energetics of a dye-sensitized nanoporous TiO_2 solar cell, *Sol. Energy Mater. Sol. Cells* 55 (1998) 267-281.

[86] M. Graetzel, Conversion of sunlight to electric power by nanocrystalline dye-sensitized solar cells, *J. Photochem. Photobiol. A* 164 (2004) 3-14.

[87] J. S. Mihina, R. M. Herbst, The reaction of nitriles with hydrazoic acid: synthesis of monosubstituted tetrazoles, *J. Org. Chem.* 15 (1950) 1082-1092; and referencees herein.

[88] H. Singh, A. S. Chawla, V. K. Kapoor, D. Paul, R. K. Malhotra, Medicinal chemistry of tetrazoles, *Prog. Med. Chem.* 17 (1980) 151-183.

[89] E.-S. M. Sherif, Comparative study on the inhibition of iron corrosion in aerated stagnant 3.5 wt. % sodium chloride solutions by 5 phenyl-1*H*-tetrazole and 3-Amino-1,2,4-triazole, *Ind. Eng. Chem. Res.* 52 (2013) 14507-14513.

[90] Z. P. Demko, K. B. Sharpless, Preparation of 5-substituted 1H-tetrazoles from nitriles in water, *J. Org. Chem.* 66 (2001) 7945 -7950.

[91] D. Amantini, R. Beleggia, F. Fringuelli, F. Pizzo, L. Vaccoro, TBAF-catalyzed synthesis of 5-substituted 1*H*-tetrazoles under solventless conditions, *J. Org. Chem.* 69 (2004) 2896-2898.

[92] A. C. Bissember, M. G. Banwell, Microwave-assisted trans-halogenation reactions of various chloro-, bromo-,trifuloromethanesulfonyloxy- and nonafluorobutanesulfonyloxy-substituted quinolines, isoquinolines, and pyridines leading to the corresponding iodinated heterocycles, *J. Org. Chem.* 74 (2009) 4893-4895.

[93] H. Huang, H. Liu, H. Jiang, K. Chen, Rapid and efficient Pd-catalyzed sonogashira coupling of aryl chlorides, *J. Org. Chem.* 73 (2008) 6037-6040.

[94] N. Inoue, O. Sugimoto, K.-I. Tanji, Palladium-catalyzed coupling reaction of haloheteroaromatic compounds in water, *Heterocycles* 72 (2007) 665-671.

[95] S. J. Vella, J. Tiburcio, J. W. Gauld, S. J. Loeb, Push-pull [2]pseudorotaxanes. Electronic control of threading by switching ON/OFF an intramolecular charge transfer, *Org. Letters* 8 (2006) 3421-3424.

[96] C. Dragonetti, A. Colombo, M. Magni, P. Mussini, F. Nisic, D. Roberto, R. Ugo, A. Valore, A. Valsecchi, P. Salvatori, M. G. Lobello, F. De Angelis, Thiocyanate-free ruthenium(II) sensitizer with a pyrid-2-yltetrazolate ligand for dye-sensitized solar cells, *Inorg Chem*. 52 (2013) 10723−10725.

[97] A. Colombo, C. Dragonetti, M. Magni, D. Meroni, R. Ugo, G. Marotta, M. G. Lobello, P. Salvatori F. De Angelis, New thiocyanate-free ruthenium(II) sensitizers with different pyrid-2-yl tetrazolate ligands for dye-sensitized solar cells, *Dalton Trans.* 44 (2015) 11788-11796.

[98] S. Stagni, A. Palazzi, S. Zacchini, B. Ballarin, C. Bruno, M. Marcaccio, F. Paolucci, M. Monari, M. Carano, A. J. Bard, A new family of ruthenium(II) polypyridine complexes bearing 5-aryltetrazolate ligands as systems for electrochemiluminescent devices, *Inorg. Chem.* 45 (2006) 695-709.

[99] K. Hu, M. E. Niyazymbetov, D. H. Evans, Nucleophilic aromatic substitution by paired electrosynthesis: reactions of methoxy arenes with 1*H*-Tetrazoles, *Tetrahedron Lett.* 36 (1995) 7027-7030.

[100] M. E. Niyazymbetov, Z. Rongfeng, D. H: Evans, Oxidation potential as a measure of the reactivity on anionic nucleophiles. Behaviour of different calsses of nucleophiles, *J. Chem. Soc., Perkin. Trans.* 2 (1996) 1957-1961.

[101] S. Arnaboldi, A. Gennaro, A. A. Isse, P. R. Mussini, The solvent effect on the electrocatalytic cleavage of carbon-halogen bonds on Ag and Au, *Electrochimica Acta* 158 (2015) 427-436.

[102] A. A. Isse , P. R. Mussini , A. Gennaro, New insights into electrocatalysis and dissociative electron transfer mechanisms: the case of aromatic bromides, *Phys. Chem. C*, 113 (2009) 14983-14992.

[103] C. O. Dietrick-Buchecker, P. A. Marnot, J. P. Sauvage, Direct synthesis of disubstituted aromatic polyimine chelates, *Tetrahedron Lett.* 23 (1982) 5291-5294.

[104] S. Jakobsen, M. Tilset, A rapid synthesis of asymmetric alkyl and aryl-2,9-disubstituted 1,10-phenanthrolines, *Tetrahedron Lett.* 52 (2011) 3072-3074.

[105] P. Belser, S. Bernhard, U. Guerig, Synthesis of mono and dialkylsubstituted 1,10-phenanthrolines, *Tetrahedron* 52 (1996) 2937-2944.

[106] S. Toyota, C. R. Woods, M. Benaglia, J. S. Siegel, Synthesis of unsymmetrical 2,8- and 2,9-dihalo-l,10-phenanthrolines and Derivatives, *Tetrahedron Lett.* 39 (1998) 2697-2700.

[107] G. J. Kubas, Tetrakis(acetonitrile)copper(I)-hexafiuorophosphate, *Inorg. Synth.* 19 (1979) 90-92.

[108] A. K. Ichinaga, J. R. Kirchhoff, D. R. McMillin, C. O. Dietrich-Buchecker, P. A. Marnot, J.-P. Sauvage, Charge-transfer absorption and emission of $Cu(NN)_2^+$ systems, *Inorg. Chem*. 26 (1987) 4290-4292.

[109] C. T. Cunningham, K. L. H. Cunningham, J. F. Michalec, D. R. McMillin, Cooperative substituent effects on the excited states of copper phenanthrolines, *Inorg. Chem.* 38 (1999) 4388-4392.

[110] M. Magni, A. Colombo, C. Dragonetti, P. Mussini, Steric *vs* electronic effects and solvent coordination in the electrochemistry of phenanthroline-based copper complexes, *Electrochimica Acta* 141 (2014) 324-330.

[111] G. Shul, M., Weissmann, D. Bélanger, Electrochemical formation of ultrathin electroactive film on a glassy carbon electrode from 1,10-phenanthroline in acidic electrolyte, *Langmuir* 30 (2014) 6612-6621; and references herein.

[112] B. R. James, R. J. P. Williams Oxidation-reduction potentials of some copper complexes, *J. Chem. Soc.* (1961) 2007-2019.

[113] M. Ruthkosky, F. N. Castellano, G. J. Meyer, Photodriven electron and energy transfer from copper phenanthroline excited states, *Inorg Chem.* 35 (1996) 6406-6412.

[114] D. H. Igo, R. C. Elder, W. R. Heineman, EXAFS solid-state spectroelectrochemistry: effects of supporting electrolyte on the electrochemical and structural behavior of $Cu(bcp\text{-}s)^{2-}$ (bcp-s =

2,9-dimethyl-4,7-diphenyl-1,10-phenathroline disulfonic acid), *J. Electroanal. Chem.* 314 (1991) 45-47.

[115] A. Cinquantini, G. Opromolla, P. Zanello, Electrochemistry of the $[Cu(Hdpa)_2]^{2+/+}$couple (Hdpa = di-2-pyridylamine), *J. Chem. Soc. Dalton Trans.* (1991) 3161-3163.

[116] I. M. Kolthoff, J. J. Lingane, *Polarography*, Interscience, New York, 1952.

[117] C. Hansch, A. Leo, R.W. Taft, A survey of Hammett substituent constants andresonance and field parameters, *Chem. Rev.* 91 (1991) 165-195.

[118] P. Zanello, *Inorganic Electrochemistry Theory, practice and application*, The Royal Society of Chemistry, 2003.

[119] K. Srivastava, D. Srivastava, M. Kumari, S. Khare, J. Prasad, EPR spectral and redox properties of some 2,9-dimethyl-1,10-phenanthroline copper(II) complexes, *J. Indian Chem. Soc.* 82 (2005) 824-828.

[120] M. K. Kashif, J. C. Axelson, N. W. Duffy, C. M. Forsyth, C. J. Chang, J. R. Long, L. Spiccia, U. Bach, A new direction in dye-sensitized solar cells redox mediator development: in situ fine-tuning of the cobalt(II)/(III) redox potential through Lewis base interactions, *J. Am. Chem. Soc.* 134 (2012) 16646-16653.

[121] C. R. Goldsmith , R. T. Jonas , A. P. Cole , T. D. P. Stack, A Spectrochemical walk: single-site perturbation within a series of six-coordinate ferrous complexes, *Inorg. Chem.* 41 (2002) 4642-4652.

[122] R. S. Nicholson, Theory and application of cyclic voltammetry for measurement of electrode reaction kinetics, Anal Chem. 37 (1965) 1351-1355.

[123] M.E. Orazem, B. Tribollet, *Electrochemical impedance spectroscopy*, ECS, Wiley.

[124] A. Lasia, *Eletrochemical impedance spectroscopy and its applications, modern aspect of electrochemistry*, B.E. Conway, J. Bockris, R.E. White, Edts., Kluwer Academic/Plenum Publishers, New York, 1999, Vol. 32, p. 143-248.

[125] E. Barsoukov, J. R. Macdonald, *Impedance spectroscopy. Theory, experiment and applications*, 2nd edition, Wiley.

[126] Master thesis M. Magni, *La spettroscopia di impedenza elettrochimica: un utile strumento per lo studio dei polimeri conduttori e della scissione elettrochimica del legame carbonio-alogeno*, A.A. 2011/2012.

[127] J. E. B. Randles, Kinetics of rapid electrode reactions, *Discuss. Faraday Soc.*, 1 (1947) 11-19.

[128] F.Hao, P.Dong, Q. Luo, J. Li, J. Lou, H. Lin, Recent advances in alternative cathode materials for iodine-free dye-sensitized solar cells, *Energy Environ. Sci.* 6 (2013) 2003-2019.

[129] S. Yun, A. Hagfeldt, T. Ma, Pt-free counter electrode for dye-sensitized solar cells with high efficiency, *Adv. Mater.* 26 (2014) 6210-6237.

[130] F. Fabregat-Santiago, J. Bisquert, G. Garcia-Belmonte, G. Boschloo, A. Hagfeldt, Influence of electrolyte in transport and recombination in dye-sensitized solar cells studied by impedance spectroscopy, *Sol. Energ. Mater. Solar C.* 87 (2005) 117-131.

[131] C. A. Bignozzi, R. Argazzi, R. Boaretto, E. Busatto, S. Carli, F. Ronconi, S. Caramori, The role of transition metal complexes in dye sensitized solar devices, *Coord. Chem. Rev.* 257 (2013) 1472-1492.

[132] S. Cazzanti, S Caramori, R. Argazzi, C. M. Elliott, C. A. Bignozzi, Efficient non-corrosive electron-transfer mediator mixtures for dye-sensitized solar cells, *J. Am. Chem. Soc.* 128 (2006) 9996-9997.

[133] S. Caramori, J. Husson, M. Beley, C. A. Bignozzi, R. Argazzi, P. C. Gros, Combination of cobalt and iron polypyridine complexes for improving the charge separation and collection in Ru-(terpyridine)$^{2-}$ sensitised solar cells, *Chem. Eur. J.* 16 (2010) 2611-2618.

[134] K. Kakiage, Y. Aoyama, T. Yano, K. Oya, J. Fujisawab, M. Hanaya, *Chem. Comm.* (2015) DOI: 10.1039/c5cc06759f.

[135] R. Grisorio, L. De Marco, C. Baldisserri, F. Martina, M. Serantoni, G. Gigli, G. P. Suranna, Sustainability of organic dye-sensitized solar cells: the role of chemical synthesis, *Sustainable Chem. Eng.* 3 (2015) 770-777.

[136] J. Bisquert, Chemical capacitance of nanostructured semiconductors: its origin and significance for nanocomposite solar cells, *Phys. Chem. Chem. Phys.* 5 (2003) 5360-5364.

Heteroleptic Luminescent Cu(I) Complexes

Introduction

State of the art for luminescent Cu(I) complexes for light emitting devices

In the last two/three decades organic electroluminescent devices have attracted intensive attention of both academia and industry. They are efficient, thin and flexible, so optimum for the fabrication of light-weight, low-consumption and smart electronic devices, many of which have already penetrated in our everyday life like display of smartphones and notepads, or in monitors and televisions.

Nowadays the two main technologies available and object of careful studies all over the world are organic light emitting diodes, OLEDs, and light-emitting electrochemical cells, LECs. The simplest configuration of an organic light emitting diode, invented by Tang and VanSlyke in 1987 [1] employing the fluorescent properties of tris(8-oxyquinolate)Al(III) complex, consists of a single layer of an organic semiconductor sandwiched between two electrodes, an anode and a cathode. After application of a bias across the two electrodes holes and electrons are injected into the active layer from the anode and the cathode interface respectively; when holes and electrons meet in the bulk of the organic layer, they may combine to form excitons that in turn partially recombine giving rise to the light emission; this is the so-called electroluminescence process. Conversely stable and efficient state-of-the-art OLEDs are based on a multi-stack architecture assembled in high-vacuum conditions necessary for evaporation/sublimation of the active components. To avoid such expensive fabrication LEC technology was developed. In fact a LEC device can be easily prepared via solution-based technologies such as spin-coating, printing or slot-die coating. Lee and co-workers [2] firstly demonstrated that ionic transition metal complexes (iTMC) simply sandwitched in between two electrodes can lead to effective electroluminescent devices; the combined ionic and electronic conduction properties of this material enable the fabrication of single component devices (Figure 79) with air-stable electrode materials, reducing the need of a rigorous encapsulation.

As briefly outlined, transition metal complexes played important role in the development and optimization of both kind of electroluminescent devices. A quite net distinction can be done, according to the specific devices in which you are interested; neutral metal complexes are preferred in OLED fabrication (due to their superior emission characteristics and the lack of mobile counteranions which negatively effect the device performances) while, as explicitly just said, ionic ones are employed in LEC technology.

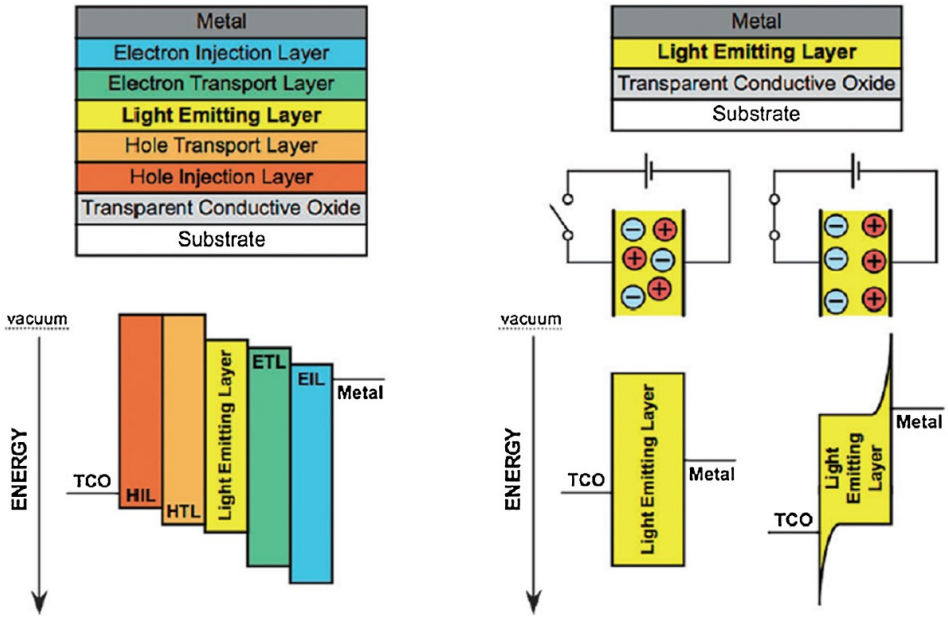

Figure 79 (a) Schematic representation of a state-of-the-art OLED. (b) A state-of-the-art LEC. From ref. [3].

Despite the final aims, emitters based on the quite abundant and relatively cheap first-row transition metals have gained increasing interest respect to the more precious Pt-group elements or rare metals (like Os, Ru and Re) in view of a widespread diffusion of "luminescent" technology. Among the 3d-block elements, copper surely holds a prominent place due to its peculiar spectroscopic properties, allowed by its d^{10} electronic configuration. In fact contrary to the other first-row metal analogues the d^{10} metal ions lack of non-emissive low-lying d-d metal centred (MC) levels that would quench luminescent excited states by thermal equilibrium or energy transfer.

As a direct consequence, among the two more common oxidation states Cu(I) and Cu(II), d^9 cupric complexes do not have any interest in this field because their MC absorption band (localized in the Vis-near IR region) deactivates via ultra fast non-radiative pathways that make the emission quantum yield, Φ_{em}, nothing.

The first, and also largely investigated, Cu(I) complexes belong to the homoleptic family $[Cu(N\hat{}N)_2]^+$ where the diimine chelating ligands are substituted 1,10-phenanthrolines [4], [5], so the same kind of complexes that have been subjected of the intensive study in the first section of this thesis. However, in recent years, attention has largely been focused on heteroleptic complexes of general formula $[Cu(N\hat{}X)(P\hat{}P)]^+$ due to their greatly enhanced emission performances where P^P represents a bisphosphine ligand, while X could be a nitrogen (*i.e.* phenanthroline ligand) [6], [7], [8] ,[9], [10] or also a phosphorus atom (*i.e.* amidophosphine ligand) [11], [12].

After first experiments by McMillin and co-workers started in 70's [6], [7], $[Cu(N\hat{}N)(P\hat{}P)]^+$ complexes have been largely neglected until the discovery that in the presence of suitably tailored diimines the complexes exhibited intense green emission [8] attributable to MLCT excited states. The first example [8], $[Cu(neocuproine)(POP)]^+$ with Φ_{em}=0.15 and a lifetime of 14.3 μs (in

deaerated DCM), allowed to understand the crucial role of (alkyl) substituents in the 2 and 9 positions of the phenanthroline in combination with a chelating P^P bisphosphine (instead of two individual phosphines). Moreover the increased luminescent performance of the heteroleptic complex respect to the homoleptic bis(diimine) analogue was attributed to the high-energy MLCT that disfavours non-radiative deactivation pathways.

This milestone paper largely contributed to design the ideal prototype of Cu(I) luminophore, and thanks to a variety of subsequent studies (as an example [13]), this image was progressively confirmed. Two characteristics are mandatory for any ideal Cu(I) luminophore: *i*) *structural rigidity*, to limit the degree of freedom of the ligands itself and any conformational rearrangements of the complex geometry that can act as non-radiative deactivation pathways detrimental for emission quantum yield, and ii) *steric protection* of the metal center against nucleophilic attack (*e.g.* coordinating solvent molecules) that can lead to the formation of pentacoordinate excited complex (*i.e.* exciplex) that deactivates via non-emissive deactivation pathway .

Starting from this milestone paper, a lot of different $[Cu(N^N)(P^P)]^+$ systems have been proposed and employed as emitters in both OLEDs and LECs [14], [15]. Particular interest has been given to pyridyl-azolates [15], and in particular 5-(pyrid-2-yl)-tetrazolates [16], [17], for the development of even *neutral Cu(I)* luminescent complexes [18], [19], suitable for OLED applications due to the lack of mobile anions and their increase volatility (respect to charged analogues) that makes them more suitable for thermal vacuum deposition.

Aim of the work

As largely evidenced in literature work, sterically hindered ligands played a crucial role in inducing the proper level of structural rigidity necessary to minimize the distortion in the excited state of transition-metal complexes and properly protecting the metal center from nucleophilic attack (*e.g.* of solvent), both resulting in less favourable non-radiative deactivation pathways. From a certain point of view, the role of ligands in this field is analogue to the purpose done in the previous bigger part of my PhD project focused on the development of Cu-based complexes employable as electron shuttles in dye sensitized-solar cells. In this sense copper and bulky phenanthrolines have constituted the link between the two main projects of the thesis.

In the previous part the insertion of sufficiently bulky phenanthrolines in the coordination sphere of copper complexes have been investigated to affect the electrochemical properties (and, even, the optical absorption ones) of the resulting complexes with the final aim to be able to tune both their oxidability and their electron transfer kinetics. In this new project the employment of sterically demanding chelating ligands has been aimed to design and synthesize novel Cu(I)-based

luminophores (*i.e.* fluorophores and/or electro-luminophores), in which a rigid geometry and conformation is mandatory to ensure a good emission quantum efficiency. More in details the project has concerned the synthesis of a family of *Cu(I) complexes,* [Cu*(N^N)(P^P)]*$^{+}$, (Figure 80) where:

- N^N chelating ligand is a *1,10-phenanthroline* functionalized in 2 and 9 positions with substituents with different electronic effect and of progressive sterical hindrance;
- P^P chelating ligand is a *bisphosphine* characterized by a rigid xanthene core and two sterically hindered phenyl pendants on each phosphorus atoms (*i.e.* Xanthphos).

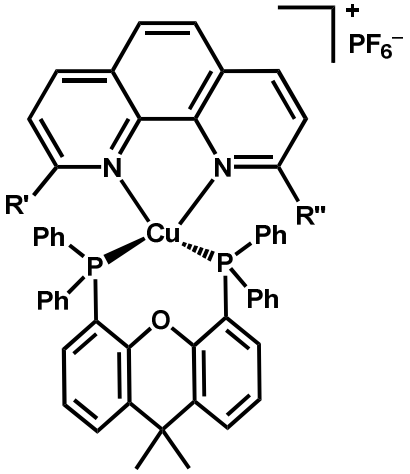

Figure 80 General structure for the family of cationic heteroleptic Cu(I) complexes, [Cu(N^N)(P^P)]$^{+}$.

It is important to notice that both ligands have a planar scaffold constituted by rigid condensed rings in order to reduce at a minimum the conformational degrees of freedom that, acting as non-radiative rotational energy relaxation pathways, could bring to considerable loss of emission quantum efficiency.

Finally the employment of the slightly toxic, relatively cheap and quite abundant copper metal, instead of the classical but also expensive and rare third-row transition metals, allowed to continue along the "sustainability" pathway that acts as a thread of this PhD thesis.

Very preliminary results will be also presented for the innovative project devoted to the synthesis of new *heteroleptic neutral Cu(I) complexes* of general formula [Cu(N^N)(P^P)] which should guarantee better performances, as evidenced by literature, and easier application in solid state photoemission devices such as OLEDs, due to the absence of the counteranions and their increased volatility.

Results and discussion

Synthesis and very preliminar characterizations

The main idea in the preparation of heteroleptic complexes, to avoid formation of multi-component mixtures and/or massive complexation of the metal in homoleptic species, is to firstly react the metal with the more sterically hindered ligands (that ideally can not allowed the formation of a stable homoleptic complex) and then, after a certainly period of time, to add the second less bulky ligand.

[Cu(R',R''-phenanthroline)(P^P)]$^+$ complexes

According to this general rule and inspired by literature [20] the one-pot, two-step procedure descibed in Scheme 9 was employed for the preparation of [Cu(N^N)(P^P)]$^+$ complexes. It started with the addition to a Cu(I) precursor solution in dichloromethane of the chelating bis-phosphine 4,5-bis(diphenylphosphino)-9,9-dimethylxanthene, shortly named Xantphos; after 1 hour the solution of the desired substituted 1,10-phenanthroline was dropped and reacted for additional 1 hour. The pure product was obtained from a simple recrystallization. The synthesis of the phenantholines employed here were all previously described in the related section in the previous "Dye-Sensitized Solar Cells, DSSCs" chapter of this thesis.

All complexes **L1**-**L5**[8] resulted stable at room temperature even when dissolved in common organic solvents like acetonitrile, ACN, and dichloromethane, DCM; in fact no additional proton peaks were observed after around 24-48 h, the time necessary to exploit a quite complete NMR study, including ^{1}H, ^{13}C, ^{31}P, and different bidimensional experiments. The only exception was **L5**; in this case the complex seemed to be less stable probably already in the solid state (the yellow needles formed during recrystallization seemed to partially turn toward light orange during the first minutes of the essication under vaccum) and in solution as confirmed by the presence of three signals attributable to the homoleptic bis(2,9-diiodo-phenanthroline)Cu(I) complex (the complex **15** of the previous chapter). The comparison with the proton integrals of the main heteroleptic product allowed to estimate a homo/hetero molar ratio of less than 0.1. The instability of **L5** could be tentatively attributed to the extremely bulkiness of iodide atoms that could bring to a partial conversion of the kinetically stable heteroleptic complex into the two thermodynamically more stable homoleptic species (monomeric form for N^N and, probably, dimeric form for the P^P ligand).

[8] For sake of curiosity: "L" used in the identification of the complexes stands for "luminophore".

Interestingly from the structural point of view, the analysis of ^{1}H-NMR spectra clearly evidenced that, similarly to bis(2-mesityl-4,7-R_2-phenanthroline)Cu(I) homoleptic complexes (R= H for **7**, and Me for **9**), in **L1**, and even in **L3,** the mesityl rings are "freezed" in a specific conformation. This could limit the non-radiative dectivation pathways. On the contrary **L2** was characterized by a highly fluxional geometry as demonstrated by the very broad signals of the tolyl and phenyl rings in the ^{1}H-NMR spectrum recorded at 300 K. Through VT-NMR experiments more defined peaks were obtained at lower temperatures (down to 183 K).

Scheme 9 Synthetic pathways for the preparation of heteroleptic [Cu(N^N)(P^P)][PF_6] complexes, L1-L5.

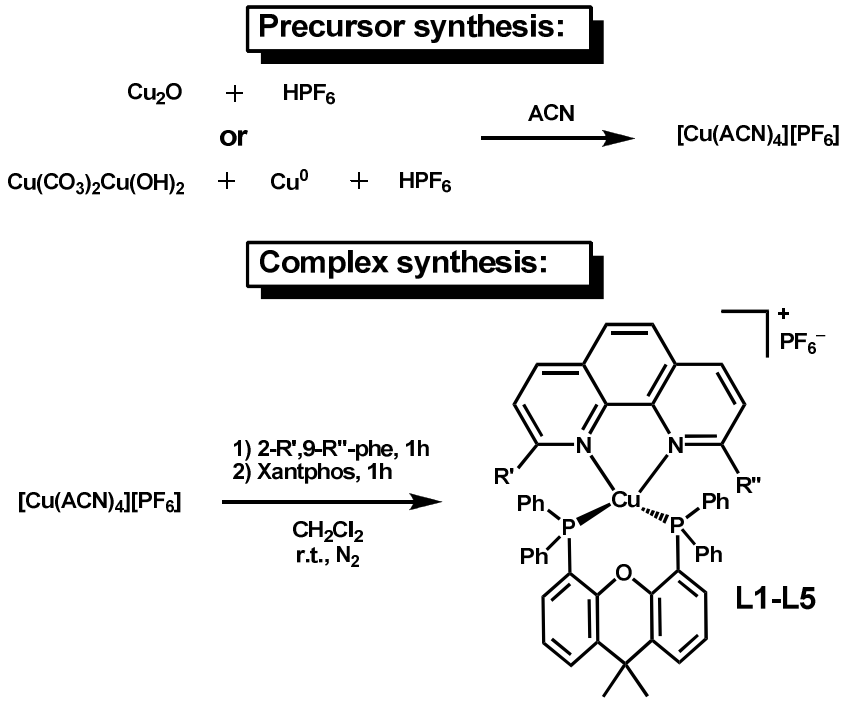

entry	complex name	R'	R''	yield[a]
1	L1	Mesityl	H	89
2	L2	*o*-Tolyl	H	71
3	L3	Mesityl	Mesityl	79
4	L4	Cl	Cl	68
5	L5	I	I	72

[a] Evaluated on the isolated product.

To date only partial and preliminary characterization was performed for the five Cu(I) complexes. Due to the instability of complex **L5** it was excluded by the series of measurements reported below. The UV-Vis spectra (Table 22) showed a broad low-intensity absorption band attributable to a MLCT electronic transition centred between 390 and 420 nm, affected by solvatochromic effect (see Figure 81 for **L1** compound), and a very intense and sharp ligand centred absorption around 275 nm. The considerable 15 nm red shift of the charge transfer band recorded for the dichloro

derivate, **L4**, accounted for the electron withdrawing nature of the chlorides that can induce a stabilization of LUMO orbital. This hypothesis is substained by theoretical calculations performed on similar $[Cu(N^N)(P^P)]^+$ complexes which showed the absence of any contribution by the bisphosphine ligand in LUMO orbital [21].

Table 22 Optical absorption data of Cu(I) complexes L1-L4 in dichloromethane.

complex	λ_{max} /nm	10^3 ε /dm^3 mol^{-1} cm^{-1}
L1	272	40.9
	393	3.07
L2	275	44.6
	391	3.52
L3	270	36.9
	390 sh	1.96
L4	277	43.1
	418	3.04

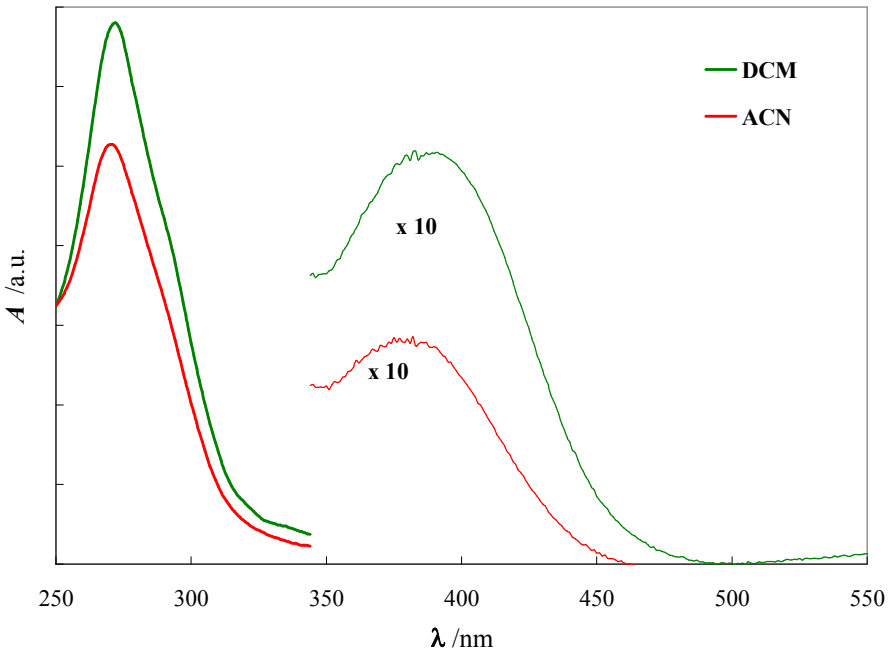

Figure 81 UV-VIS spectra of L1 complex in dichloromethane (green line) and acetonitrile (red line).

The expected high similarity between optical absorption features of **L1** and **L2** are also confirmed by cyclic voltammetry measurements (Figure 82). CVs in DCM clearly evidenced a chemically reversible oxidation process attributed to a Cu^{2+}/Cu^{+} electron transfer that differed by about 60 mV between the two complexes; its electrochemical quasi-reversible character suggested that the coordination sphere around the copper atom was not significantly changed after the electron transfer, coherently with the quite sterically congested environment generated by the phenyls and the mesityl. Accounting for the extraordinary increased luminescent properties of complex **L3** in

solution respect to its two analogues **L1** and **L2** (see below), it will be interesting to verify whether **L3** compound will also exhibit an higher electrochemical reversibility.

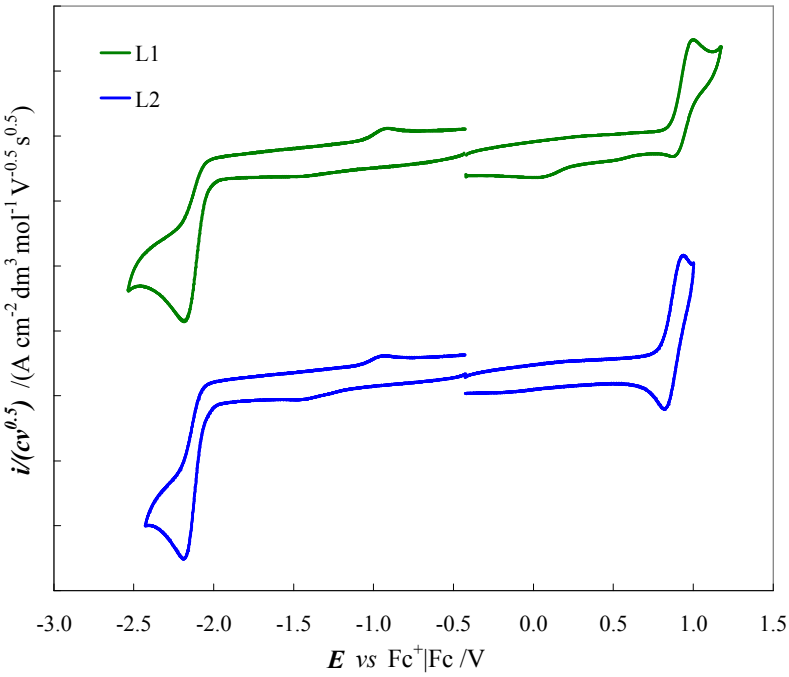

Figure 82 Synopsis of normalized cyclovoltammograms of heteroleptic Cu(I) complexes L1 (green) and L2 (blue) on GC electrode (geometric area 0.071 cm^2). Sample concentration around $1 \cdot 10^{-3}$ M in DCM and $TBAPF_6$ 0.1 M; potential scan rate 0.2 V s^{-1}. Ohmic drop compensated by electronic positive feedback.

The cathodic window showed a unique electrochemical process tentatively ascribed to a ligand-based ET; in this case the process occurred at quite exactly the same potential in both **L1** and **L2**, according to the high similarity between ligands. The electron transfer was clearly electrochemically reversible and it became chemically reversible only at high potential scan rates (around 1-2 V s^{-1}) suggesting a competition between the back-ET and a chemical follow-up reaction involving the electrogenerated anion.

However the most interesting and intriguing result obtained after this preliminary characterizations, was, without a doubt, the emission properties shown by the more sterically hindered **L3** complex.

From a qualitative analysis the simple irradiation of solid samples with a 366 nm laboratory lamp (Figure 83) allowed to detect the emissive nature of all complexes except for **L5**. However after the dissolution of Cu(I) complexes in non-degassed DCM the emission was quenched for all samples except for the more congested **L3**.

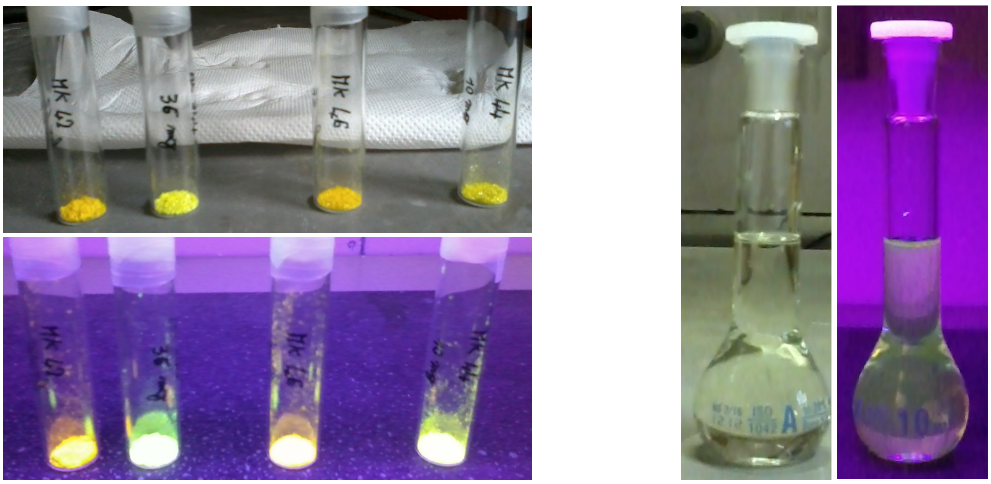

Figure 83 On the left: pictures of the solid Cu(I) complexes under natural light (top) and under 366 nm irradiation (bottom). From left to right: L1, L3, L2 and L4. On the right: comparison of a L3 solution dissolved in aerated DCM without or with a 366 irradiation.

Starting from these results a series of preliminary quantitative analyses have been performed in collaboration with Prof. J. A. Gareth Williams at Durham University. Data on the emission properties of complexes in both degassed DCM solution and in solid state at room temperature are collected in Table 23.

The much better luminescence performance of the heteroleptic Cu(I) complex bringing the di-mesityl phenanthroline ligand was fully confirmed in solid state but, even more, in solution. In solid state it had a maximum emission at 542 nm characterized by a lifetime, τ, of 24 μs, two-times longer than its two best competitors (*i.e.* **L1** and **L2**). Even more exciting is the comparison of both lifetime and emission quantum yield measured in solution; complex **L3** not only doubled the lifetime of **L1** and **L2** in aerated solution, but in degassed dichloromethane it reached a valuable 20.5 μs value which is ten-fold longer than the values recorded for the two analogues. A similar comparison also applies for emission quantum yield; a very remarkable Φ_{lum}=0.40 was measured, almost three-times the value of the first performing [Cu(2,9-dimethyl-1,10-phenanthroline)(POP)]$^+$ luminophore [8], and neatly better than the record for the cationic family of luminophores with the general formula [Cu(N^N)(P^P)] obtained in 2007 by Armaroli and co-worker [9]. On the other hand it is still below the 70% efficiency obtained with a neutral Cu(I) imidophosphine disolved in benzene [12].

It is possible to notice the smaller difference between solid state and solution lifetimes for **L3**; this is consistent with a higher level of rigidity and thus smaller distortion in the excited state for this luminophore (respect to the others). Similar consideration goes for the emission maxima (Figure 84) suggesting a quite self-consistency of the data. Finally, according to the previous statement, a small Stoke shift for **L3** was also detected between absorption and emission band.

Table 23 Collection of data for emission in solution (DCM) and in solid state for Cu(I) complexes L1-L4, at room temperature.

complex	in solution			in solid state	
	λ_{max} /nm	τ /µs [a,b]	Φ_{lum} x 10^2 [c]	λ_{max} /nm	τ /µs [b]
L1	611	4.7 (0.35)	6.4	597	12.7
L2	630	2.8 (0.36)	2.8	570	12.0
L3	553	20.5 (0.71)	40	542	24.0
L4	607	0.33 (0.20)	0.54	553	12.4

[a] In degassed solution, with values in aerated solution shown in parenthesis. [b] The lifetime of **L3** in degassed solution and lifetimes in solid state measured using multichannel scaling following excitation with a xenon flashlamp at 420 nm; all other values measured by time-correlated single photon counting, TCSPC, following excitation using a 405 nm laser diode. [c] In degassed solution, measured using $[Ru(bpy)_3]Cl_2$ as the standard.

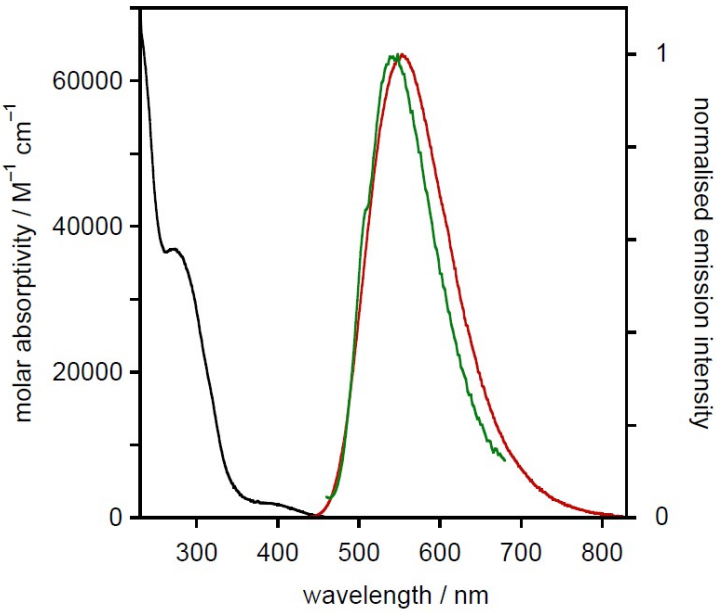

Figure 84 Synopsis of the absorption (black line) and normalized emission spectra (red= in solution; green=in solid state) for the more promising L3 Cu(I) luminophore.

Toward neutral complexes: the case of [Cu(6-Mes-Tetra)(P^P)]

Attempts to synthesize deprotonable chelating agents for the development of heteroleptic neutral Cu(I) complexes brought to think about the tetrazole ring as part of the ligand, considering both the very interesting recent literature [16], [18], [19], and the expertise acquired during the preparation of Ru(II) dyes (see dedicated chapters in the previous section).

The target ligand was identified in 5-(6-mesityl-pyrid-2'-yl)-1*H*-tetrazole, **6-Mes-TetraH**. The novelty respect to previous reports has been the insertion of the bulky mesityl ring next to the coordinated pyridyl nitrogen in order to hopefully further reduce the conformational degrees of freedom of the related complexes, and hence to complementary increase the photon emission quantum efficiency.

The synthesis of such sterically hindered pyridyltetrazole (carried out in the context of the Marta Trifilò's bachelor degree thesis) required the functionalization of the free position immediately adjacent to the heteroatom of the pyridine ring with the bulky mesityl moiety. The direct arylation of inactivated C-6 through the lithium-chemistry (the same employed for the preparation of substituted 1,10-phenathrolines in the previous section of the thesis) revealed impracticable due to the interference of the reacting –CN group which can be subjected to a nucleophilic attack. So we decided to activate the C-6 atom through a C-Br bond that then can be subjected to a classical Pd-catalyzed cross-coupling reaction. Attempts to synthesize the precursor 6-Br-2-cyanopyridine failed by reacting with Br_2 both the pristine cyanopyridine and its Pd-complex [22], [Pd(dichloro-bis(2-cyanopyridyl)] (isolated and characterized for the first time, see experimental section).

To save time the desired brominated precursor was purchased; it was subjected to the Suzuky cross-coupling reaction with the commercially available 2,4,6-trimethylphenyl boronic acid (Scheme 10), and after fast purification via SiO_2 flash chromatography the intermediate 6-mesityl-2-cyanopyridine, **I-6**, was obtained with 49% yield as a white solid. The desired **6-Mes-TetraH** was finally synthesized through the already described pathway (Table 4). Experimental details have been already reported in the previous chapter of the thesis.

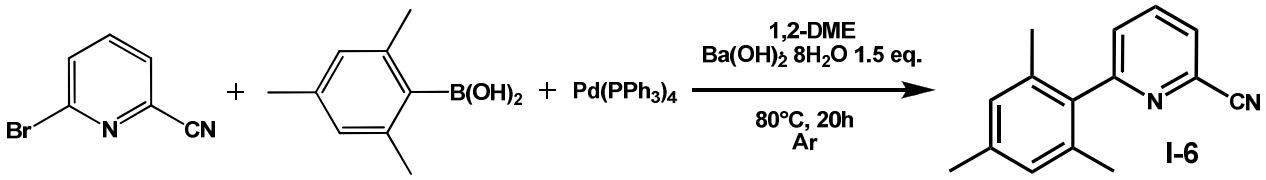

Scheme 10 Schematic procedure for the synthesis of I-6 intermediate.

Attempts to prepare the corresponding heteroleptic Cu(I) complex [Cu(6-Mes-Tetra)(Xantphos)] were done following, essentially, the same procedure employed for the cationic heteroleptic analogues (Scheme 9) with an additional step for the deprotonation of tetrazole derivate. More solvating DMF was also used instead of CH_2Cl_2; unfortunately to date no definitive data confirming the correct nature of the isolated products can be given. However the fluorescent properties (Figure 85) observed for the solid obtained at the end of the synthetic procedure seemed to be promising.

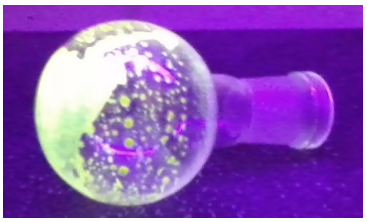

Figure 85 Picture of the potential complex [Cu(6-Mes-Tetra)(Xantphos)] under 366 nm lamp.

Experimental details

General information

Apparatus and reagents

^{1}H NMR, proton decoupled ^{13}C NMR, ^{31}P NMR spectra and bidimensional experiments (not reported here) were recorded at 400 MHz (T = 300 K) on a Bruker Avance-400 instrument. Chemical shifts (δ) for ^{1}H spectra are expressed in ppm relative to internal Me_4Si as standard; for ^{31}P spectra the standard is H_3PO_4 80% in water. Signals were abbreviated as s, singlet; d, doublet; dd, doublet of doublets; t, triplet; q, quartet; sept, septet; m, multiple; br, broad signal. Cyclic volammetries were recorded as already described in the experimental section of the previous chapter.

Synthesis and characterization

Phenanthrolines, 6-mesityl-pyridinecarbonitrile (**I-6**) and 5-(6'-mesityl-pyrid-2'-yl)-1*H*-tetrazole used as ligands were obtained according to the procedure report above in the previous chapter.

^{31}P-NMR at r.t. (300 K) for **L1**-**L5** complexes showed a relativelly broad signal (see below) for the phosphorus atoms of the coordinated bisphosphine (*i.e.* Xantphos) if compared with the sharp septet of the $PF6^{-}$ anion; this suggested a fluxional equilibrium that, in any case, did not affect the stability of the complexes (except for the peculiar case of **L5**, as just discussed).

General procedure for the synthesis of heterolptic Cu(I) complexes, **L1**-**L5**

A xantphos (0.100 mmol, 1.05 eq) solution in dry DCM (*ca.* 10 ml) was added into a well stirred solution of $[Cu(ACN)_4][PF_6]$ (1 eq) in dry DCM (*ca.* 10 ml). No colour change occurred. After 1 hour a solution (2.5 ml, dry DCM) of the proper phenanthroline (1.05 eq) was added dropwise; a bright yellow solution was formed and it was stirred for 1 hour. The solution was concentrated at reduced pressure and than the product was isolated as yellow/orange solid through recystallization in DCM/*iso*-propyl ether.

[Cu(2-mesityl-1,10-phenanthroline)(4,5-bis(diphenylphosphino)-9,9-dimethylxanthene)][PF_6], **L1**

^{1}H NMR (400 MHz, CD_2Cl_2) δ (ppm): 8.61 (d, *J* = 8.2 Hz, 1H), 8.51 (d, *J* = 8.1 Hz, 1H), 8.21 (d, *J* = 8.8 Hz, 1H), 8.16 (d, *J* = 8.8 Hz, 1H), 7.72 (d, *J* = 7.8 Hz, 2H), 7.62 (d, *J* = 8.2 Hz, 1H), 7.34 (d, *J* = 4.6 Hz, 1H), 7.29 (m, 2H), 7.21 (m, 3H), 7.07 (m, 8H), 6.94 (t, *J* = 7.6 Hz, 4H), 6.86 (q, *J* = 6.4 Hz, 4H), 6.42 (m, 4H), 6.32 (m, 2H), 2.65 (s, 3H), 2.08 (s, 3H), 1.45 (s, 3H), 1.22 (s, 6H).

^{31}P-NMR (161 MHz, CH_2Cl_2) δ (ppm): –12.8 (br s, 2P), –144.3 (sept, 1P).

[Cu(2-*o*-tolyl-1,10-phenanthroline)(4,5-bis(diphenylphosphino)-9,9-dimethylxanthene)][PF_6], **L2**

^{1}H NMR (400 MHz, CD_2Cl_2) δ (ppm): 8.54 (d, *J* = 8.2 Hz, 1H), 8.44 (d, *J* = 8.1 Hz, 1H), 8.13 (d, *J* = 8.8 Hz, 1H), 8.07 (d, *J* = 8.8 Hz, 1H), 7.68 (m, 3H), *ca.* 7.4-6.4 (various br peaks, 31H), 1.71 (s, 3H). (6H of the two xantphos methyls were not clearly visible at r.t).

^{31}P-NMR (161 MHz, CH_2Cl_2) δ (ppm): –12.0 (br s, 2P), –144.3 (sept, 1P).

[Cu(2,9-dimesityl-1,10-phenanthroline)(4,5-bis(diphenylphosphino)-9,9-dimethylxanthene)][PF_6], **L3**

^{1}H NMR (400 MHz, CD_2Cl_2) δ (ppm): 8.49 (d, *J* = 8.2 Hz, 1H), 8.29 (d, *J* = 8.3 Hz, 1H), 7.86 (d, *J* = 8.7 Hz, 1H), 7.73 (d, *J* = 8.7 Hz, 1H), 7.62 (d, *J* = 8.2 Hz, 3H), 7.48 (d, *J* = 8.2 Hz, 1H), 7.34 (t, *J* = 7.6 Hz, 2H), 7.20 (t, *J* = 7.6 Hz, 2H), 7.08 (t, *J* = 7.7 Hz, 6H), 6.92 (t, *J* = 7.8 Hz, 4H), 6.78 (s, 2H), 6.46 (m, 4H), 6.38 (m, 6H), 6.31 (s, 2H), 2.34 (s, 3H), 2.09 (s, 3H), 2.05 (s, 3H), 1.94 (s, 6H).

^{31}P-NMR (161 MHz, CH_2Cl_2) δ (ppm): –14.8 (br s, 2P), –144.4 (sept, 1P).

[Cu(2,9-dichloro-1,10-phenanthroline)(4,5-bis(diphenylphosphino)-9,9-dimethylxanthene)][PF_6], **L4**

^{1}H NMR (400 MHz, CD_3CN) δ (ppm): 8.48 (d, *J* = 8.5 Hz, 2H), 7.97 (s, 2H), 7.73 (d, *J* = 8.5 Hz, 4H), 7.45-6.85 (broad signals , 24H), 2.13 (bs, 6H).

^{31}P-NMR (161 MHz, CH_2Cl_2) δ (ppm): –11.9 (br s, 2P), –144.5 (sept, 1P).

[Cu(2,9-diiodo-1,10-phenanthroline)(4,5-bis(diphenylphosphino)-9,9-dimethylxanthene)][PF_6], **L5**

^{1}H NMR (400 MHz, CD_2Cl_2) δ (ppm): 8.13 (d, *J* = 8.3 Hz, 2H), 8.02 (d, *J* = 8.3 Hz, 2H), 7.86 (s, 2H), 7.65 (dd, *J* = 7.7 Hz, *J* = 1.4 Hz, 2H), 7.33 (m, 8H), 7.26 (t, *J* = 7.5 Hz, 4H), 7.23 (t, *J* = 5.6 Hz, 2H), 7.18 (m, 2H), 7.11 (t, *J* = 7.6 Hz, 8H), 1.71 (s, 6H).

^{31}P-NMR (161 MHz, CH_2Cl_2) δ (ppm): –12.9(br s, 2P), –144.8 (sept, 1P).

Synthesis of the intermediate complex [$PdCl_2$(2-cyano-pyridine)$_2$]

Reaction was performed according to a literature procedure [23]. $PdCl_2$ (0.282 mmol, 1 eq) was placed in a round-bottom flask equipped with magnetic stirrer and 2-cyanopyridine (2 eq) in 2.5 ml acetonitrile was added. The reaction was carried out at r.t. for 24 h; then the yellow precipitate was crystallized from acetone.

^{1}H-NMR (400 MHz, d_6-DMSO) δ (ppm): 8.77 (d, *J*= 4.8 Hz, 1H), 8.07 (m, 2H), 7.76 (d, *J*= 6.0 Hz, 1H).

References

[1] C. W. Tang, S. A. VanSlyke, Organic electroluminescent diodes, *Appl. Phys. Lett.* 51 (1987) 913-915.

[2] J. K. Lee, D. S.Yoo, E. S. Handy, M. F. Rubner, Thin film light emitting devices from an electroluminescent ruthenium complex, *Appl. Phys. Lett.* 69 (1996) 1686-1688.

[3] S. B. Meier, D. Tordera, A. Pertegas, C. Roldan-Carmona, E. Ortì, H, J. Bolink, Light-emitting electrochemical cells recent progress and future prospects, *Materials Today* 17 (2014) 217-223.

[4] M. T. Miller, P. K. Gantzel, T. B. Karpishin, A highly emissive heteroleptic Copper(I) bis(phenanthroline) complex: $[Cu(dbp)(dmp)]^+$ (dbp = 2,9-Di-*tert*-butyl-1,10-phenanthroline; dmp = 2,9-Dimethyl-1,10-phenanthroline), *J. Am. Chem. Soc.* 121 (1999) 4292-4293.

[5] Y. Leydet, D. M. Bassani, G. Jonusauskas, N. D. McClenaghan, Equilibration between three different excited states in a bichromophoric Copper(I) polypyridine complex, *J. Am. Chem. Soc.* 129 (2007) 8688-8689.

[6] M. T. Buckner, D. R. McMillin, Photoluminescence from copper(I) complexes with low-lying metal-to-ligand charge transfer excited states, *J. Chem. Soc. Chem. Commun.* (1978) 759-761.

[7] R. A. Rader, D. R. McMillin, M. T. Buckner, T. G. Matthews, D. J. Casadonte, R. K. Lengel, S. B. Whittaker, L. M. Darmon, F. E. Lytle, Photostudies of 2,2'-bipyridine bis(triphenylphosphine)copper(1+), 1,10-phenanthroline bis(triphenylphosphine)copper(1+), and 2,9-dimethyl-1,10-phenanthroline bis(triphenylphosphine)copper(1+) in solution and in rigid, low-temperature glasses. Simultaneous multiple emissions from intraligand and charge-transfer states, *J. Am. Chem. Soc.* 103 (1981) 5906-5912.

[8] D. G. Cuttell, S. M. Kuang, P. E. Fanwick, D. R. McMillin, R. A. Walton, Simple Cu(I) complexes with unprecedented excited-state lifetimes, *J. Am. Chem. Soc.*, 124 (2002) 6-7.

[9] N. Armaroli, G. Accorsi, M.Holler, O. Moudam, J.-F. Nierengarten, Z. Zhou, R. T. Wegh, R. Welter, Highly luminescent Cu^I complexes for light-emitting electrochemical cells, *Adv. Mater.* 18 (2006) 1313-1316.

[10] K. Saito, T. Arai, N. Takahashi, T. Tsukuda, T. Tsubomura, A series of luminescent Cu(I) mixed-ligand complexes containing 2,9-dimethyl-1,10-phenanthroline and simple diphosphine ligands, *Dalton Trans.* (2006) 4444-4448.

[11] S. B. Harkins, J. C. Peters, A highly emissive Cu_2N_2 diamond core complex supported by a $[PNP]^-$ ligand, *J. Am. Chem. Soc.* 127 (2005) 2030-2031.

[12] A. J. M. Miller, J. L. Dempsey and J. C. Peters, Long-lived and efficient emission from mononuclear amidophosphine complexes of copper, *Inorg. Chem.* 46 (2007) 7244-7246.

[13] N. Armaroli, Photoactive mono- and polynuclear Cu(I)–phenanthrolines. A viable alternative to Ru(II)–polypyridines?, *Chem. Soc. Rev.* 30 (2001) 113-124.

[14] Q. Zhang, Q. Zhou, Y. Cheng, L. Wang, D. Ma, X. Jing, F. Wang, Highly efficient electroluminescence from green-light-emitting electrochemical cells based on Cu^{I} complexes, *Adv. Funct. Mat.* 16 (2006) 1203-1208.

[15] Y. Chi, B. Tong, P.-T. Chou, Metal complexes with pyridyl azolates: Design, preparation and applications, *Coord. Chem. Rev.* 281 (2014) 1–25.

[16] C. Femoni, S. Muzzioli, A. Palazzi, S. Stagni, S. Zacchini, F. Monti, G. Accorsi, M. Bolognesi, N. Armaroli, M. Massi, G. Valenti, M. Marcaccio, New tetrazole-based Cu(I) homo- and heteroleptic complexes with various P^P ligands: synthesis, characterization, redox and photophysical properties, *Dalton Trans*. 42 (2013) 997-1010.

[17] C. Han, Y. Zhao, H. Xu, J. Chen, Z. Deng, D. Ma, Q. Li, P. Yan, A simple phosphine–oxide host with a multi-insulating structure: high triplet energy level for efficient blue electrophosphorescence, *Chem. Eur. J.* 17 (2011) 5800-5803.

[18] Claudia Bizzarri, C. Strabler, J. Prock, B. Trettenbrein, M. Ruggenthaler, C.-H. Yang, F. Polo, A. Iordache, P. Bruggeller, L. De Cola, Luminescent dinuclear Cu(I) complexes containing rigid tetraphosphine ligands, *Inorg. Chem.* 53 (2014) 10944-10951.

[19] L. Bergmann, J. Friedrichs, M. Mydlak, T. Baumann, M. Nieger, S. Bräse, Outstanding luminescence from neutral copper(I) complexes with pyridyl-tetrazolate and phosphine ligands, *Chem.Commun.* 49 (2013) 6501-6503.

[20] A. C. Hernandez-Perez, A. Vlassova, S. K. Collins, Toward a visible light mediated photocyclization: Cu-based sensitizers for the synthesis of [5]helicene, *Org. Lett.* 14 (2012) 2988-2991.

[21] X.-L. Chen, R. Yu, Q-K. Zhang, L-J. Zhou, X.-Y. Wu, Q. Zhang, C.-Z. Lu, Rational design of strongly blue-emitting cuprous complexes with thermally activated delayed fluorescence and application in solution-processed OLEDs, *Chem. Mater.* 25 (2013) 3910-3920.

[22] S. Paraskewas, Chlorination and bromination of pyridinepalladium(II) chloride complex, *Synthesis* (1980) 378-379. (German language)

[23] A. Krogul, J. Skupinska, G. Litwinienko, Catalytic activity of $PdCl_2$ complexes with pyridines in nitrobenzene carbonylation, *J. Mol. Catal. A-Chem.* 337 (2011) 9-16.

Ringrazio tutti coloro che nel corso di questi tre anni mi hanno aiutato e fatto crescere professionalmente (e non solo):

Alessia, Adriana e Arianna,
che hanno inziato me, un povero elettrochimico, al mondo della sintesi

Pasquale,
per la sua grandissima disponibilità e
per avermi insegnato molto sulle tecniche NMR

Infine un saluto generale a tutti i ragazzi e ragazze del laboratorio,
tra cui Marta, Giulia, Rachele, Ilaria, Federico, Eleonora, Valentina, Mattia ecc..

Un grazie particolare va, infine, a Serena!!!!!!!